VOLUME 38 MAY 1960 NUMBER 5

Canadian Journal of Physics

Editor: H. E. DUCKWORTH

Associate Editors:

L. G. ELLIOTT, *Atomic Energy of Canada, Ltd., Chalk River*
J. S. FOSTER, *McGill University*
G. HERZBERG, *National Research Council of Canada*
L. LEPRINCE-RINGUET, *Ecole Polytechnique, Paris*
B. W. SARGENT, *Queen's University*
G. M. VOLKOFF, *University of British Columbia*
W. H. WATSON, *University of Toronto*
G. A. WOONTON, *McGill University*

Published by THE NATIONAL RESEARCH COUNCIL

OTTAWA CANADA

CANADIAN JOURNAL OF PHYSICS

Under the authority of the Chairman of the Committee of the Privy Council on Scientific and Industrial Research, the National Research Council issues THE CANADIAN JOURNAL OF PHYSICS and five other journals devoted to the publication, in English or French, of the results of original scientific research. Matters of general policy concerning these journals are the responsibility of a joint Editorial Board consisting of: members representing the National Research Council of Canada; the Editors of the Journals; and members representing the Royal Society of Canada and four other scientific societies.

EDITORIAL BOARD

Representatives of the National Research Council

I. McT. Cowan, *University of British Columbia*
A. Gauthier, *University of Montreal*
H. G. Thode (Chairman), *McMaster University*
D. L. Thomson, *McGill University*

Editors of the Journals

D. L. Bailey, *University of Toronto*
T. W. M. Cameron, *Macdonald College*
H. E. Duckworth, *McMaster University*
Léo Marion, *National Research Council*
J. F. Morgan, *Department of National Health and Welfare, Ottawa*
R. G. E. Murray, *University of Western Ontario*
J. A. F. Stevenson, *University of Western Ontario*

Representatives of Societies

D. L. Bailey, *University of Toronto*
Royal Society of Canada
T. W. M. Cameron, *Macdonald College*
Royal Society of Canada
H. E. Duckworth, *McMaster University*
Royal Society of Canada
Canadian Association of Physicists
P. R. Gendron, *University of Ottawa*
Chemical Institute of Canada
D. J. Le Roy, *University of Toronto*
Royal Society of Canada
J. F. Morgan, *Department of National Health and Welfare, Ottawa*
Canadian Biochemical Society
R. G. E. Murray, *University of Western Ontario*
Canadian Society of Microbiologists
J. A. F. Stevenson, *University of Western Ontario*
Canadian Physiological Society

Ex officio

Léo Marion (Editor-in-Chief), *National Research Council*
J. B. Marshall (Administration and Awards), *National Research Council*

Manuscripts for publication should be submitted to Dr. H. E. Duckworth, Editor, Canadian Journal of Physics, Hamilton College, McMaster University, Hamilton, Ontario.
For instructions on preparation of copy, see **NOTES TO CONTRIBUTORS** (back cover).

Proof, correspondence concerning proof, and orders for reprints should be sent to the Manager, Editorial Office (Research Journals), Division of Administration and Awards, National Research Council, Ottawa 2, Canada.

Subscriptions, renewals, requests for single or back numbers, and all remittances should be sent to Division of Administration and Awards, National Research Council, Ottawa 2, Canada. Remittances should be made payable to the Receiver General of Canada, credit National Research Council.

The journals published, frequency of publication, and subscription prices are:

Canadian Journal of Biochemistry and Physiology	Monthly	$9.00 a year
Canadian Journal of Botany	Bimonthly	$6.00 a year
Canadian Journal of Chemistry	Monthly	$12.00 a year
Canadian Journal of Microbiology	Bimonthly	$6.00 a year
Canadian Journal of Physics	Monthly	$9.00 a year
Canadian Journal of Zoology	Bimonthly	$5.00 a year

The price of regular single numbers of all journals is $2.00.

Canadian Journal of Physics

Issued by THE NATIONAL RESEARCH COUNCIL OF CANADA

VOLUME 38 MAY 1960 NUMBER 5

THE FREEZING POINTS OF HIGH PURITY METALS AS PRECISION TEMPERATURE STANDARDS

VI. THERMAL ANALYSES ON FIVE SAMPLES OF LEAD WITH PURITIES GREATER THAN 99.999+%[1]

E. H. MCLAREN AND E. G. MURDOCK

ABSTRACT

An investigation has been made of the freezing and melting temperatures of five samples of high purity lead (supplier's analyzed impurity contents < 0.7 to < 4 p.p.m.) including zone refined metal. Using the induced freezing technique, plateaux of essentially constant ($< \pm 0.0001°$ C) temperature with durations of over 1 hour are readily obtained on the cooling curves of these samples. A standard deviation in plateau temperature (liquidus point) of $\pm 0.0001°$ C was obtained from a series of 30 induced freezes on a particular sample. The pressure effect on the freezing temperature of lead was found to be 0.0080° C for 1 atmosphere. A value of 327.426° C (Int. 1948) was determined for the standard liquidus point of pure lead.

The liquidus points of the samples were intercompared with a precision of about 0.0002° C, and alloy melting ranges were examined following different types of freezing with and without overnight anneals near the solidus temperature. Alloy melting range parameters were found to be useful in the selection of the samples of highest purity and at the same time showed that an uncertainty of 0.002° C in the above value of the liquidus point of pure lead may exist because of residual impurity contents in the purest samples that were examined.

INTRODUCTION

An investigation of the freezing and melting temperatures of five samples of high purity lead has been carried out to determine the suitability of this transition as a thermometric fixed point and to examine the usefulness of precision resistance thermometry to discriminate among samples of high purity lead.

MATERIAL

Table I lists the origin, grade, and form of the lead metal as received, and Table II shows the chemical analyses supplied by the sources. Since the lead-rich portions of the respective binary phase diagrams for these analyzed impurity solutes appear to be reasonably well established, estimates, listed in Table III, were made of the expected lowerings of the liquidus and solidus from that of pure element and the associated alloy melting ranges for the samples.

[1]Manuscript received January 27, 1960.
Contribution from the Division of Applied Physics, National Research Council, Ottawa, Canada.
Issued as N.R.C. No. 5634.

TABLE I

Identification of the lead samples

Sample	Origin	Grade	Form
Pb.3	The Consolidated Mining and Smelting Co.,	High Purity No. 50	Bar, 2.5×2.5×25 cm
Pb.4	Trail, B.C., Canada	High Purity (ZR-2) No. 186 (Zone Refined)	Bar, 2.5×2.5×25 cm
Pb.5	American Smelting and Refining Co., South Plainfield, N.J., U.S.A.	Special High Purity Lot HPL No. 7	Bar, 1.2 triangular section ×25 cm
Pb.6	Philipp Bros. (Canada) Ltd., Montreal 25, Que., Canada	Zone Refined (Japanese)	Bar, 1.2×1.0×30 cm
Pb.7	Associated Lead Manufacturers Ltd., Middlesex, England.	Special High Purity No. HPEL/2	Small bars

TABLE II

Impurity contents of the lead samples supplied by the sources

	Weight, p.p.m.							
Sample	Bi	Cu	Tl	Ag	Sb	Fe	Mg	Mo
Pb.3	0.1	0.1	<0.3	0.1	<0.1			
Pb.4	0.1	0.1	<0.3	0.1	<0.1			
Pb.5	<1	<1		<1		<1		
Pb.6*		tr.		v.w.		tr.	tr.	tr.
Pb.7	<1	<1	<1	<0.5				

NOTE: tr., trace; v.w., very weak.
*Qualitative spectrochemical analysis only.

TABLE III

Estimated alloy melting ranges

		Estimated change from pure element (°C)				
Impurity	Slope,* °C/p.p.m.	Pb.4	Pb.3	Pb.6	Pb.7	Pb.5
	Of liquidus	In liquidus				
Cu	−0.0023	−0.00023	−0.00023	tr.	−<0.0023	−<0.0023
Bi	−0.00044	−0.00004	−0.00004	—	−<0.00044	−<0.00044
Ag	−0.00092	−0.00009	−0.00009	v.w.	−<0.00046	−<0.00092
Sb	−0.00067	−<0.00007	−<0.00007	—	—	—
Tl	+0.000088	+<0.000026	+<0.000026	—	+<0.00009	—
Estimated liquidus depression		<0.0003	<0.0003	—	<0.0031	<0.0037
	Of solidus*	In solidus				
Cu	−0.0200	−0.0020	−0.0020	tr.	−<0.0200	−<0.0200
Bi	−0.00066	−0.00007	−0.00007	—	−<0.0007	−<0.0007
Ag	−0.0230	−0.0023	−0.0023	v.w.	−<0.0115	−<0.0230
Sb	−0.0021	−<0.00021	−<0.0021	—	—	—
Estimated solidus depression		<0.0046	<0.0046	—	<0.0322	<0.0437
Estimated melting range		<0.0043	<0.0043	—	<0.03	<0.04

*Phase diagrams, Metals Handbook (1948); Pb–Tl, Hansen (1958). These estimates assume that the liquidus and solidus are linear with composition: the solidus for Pb–Cu and Pb–Ag are more likely to be convex (possibly retrograde) with respect to the base of the diagram.

EXPERIMENTAL

The apparatus and techniques used in these thermal analyses have been described previously* (McLaren, Parts I–V, 1957*a*, *b*; 1958*a*, *b*; McLaren and Murdock 1960). Samples of about 1750 g contained in high purity graphite crucibles under dry nitrogen atmospheres were used. This investigation includes an examination of the alloy melting ranges of the samples following different types of freezing with and without overnight anneals near the solidus temperature and a precision intercomparison of their liquidus points.

A. Thermal Survey

Figure 1 shows typical cooling curves that were obtained when a sample of high purity lead (Pb.3) solidifies under different rates and types of freezing.

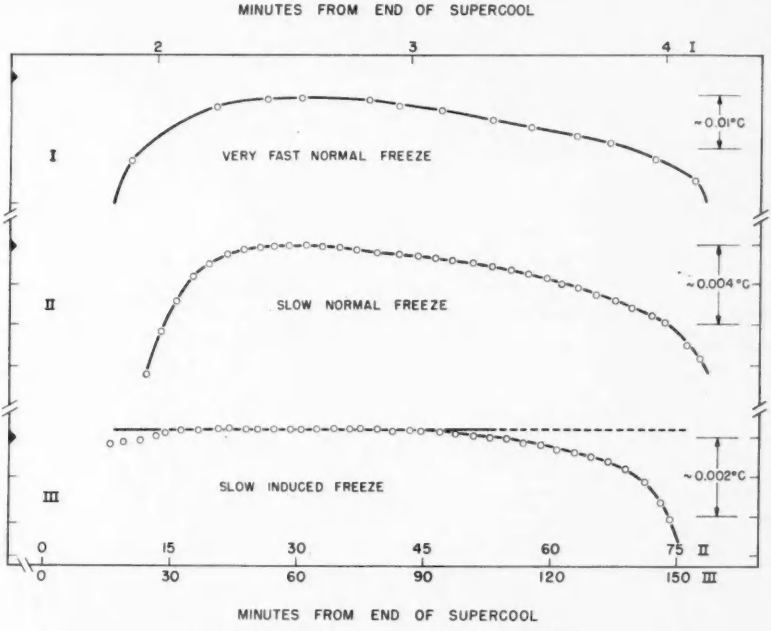

FIG. 1. Typical freezing curves on high purity lead.

The very fast normal freezes are made by extracting the melts from the furnace and allowing solidification to take place in room air; on slow induced and slow normal freezes the melts remain in the slowly cooling furnace block and on nucleation are, respectively, either assisted or not (by the induced freezing technique, see McLaren, Part II, 1957*b*) to overcome a slow recalescence. A variable supercooling of up to 0.14° C was found on solidifying the high purity lead in this experimental arrangement. The plateaux of nearly constant temperature found on the cooling curves of slow induced freezes provide, as

*Reference to preceding papers in this series is made by Part number and date of publication.

did similar plateaux on the induced freezing curves of high purity zinc, cadmium, and indium, an excellent index for a precision temperature standard.

In order to assess the thermal effects of dissolved chemical impurities in the five samples of high purity lead, alloy melting ranges were gauged following different types of freezing and varying amounts of solid anneal near the melting temperatures. Table IV gives the approximate durations and transformation conditions for several series of heating curves from which estimates of the alloy melting ranges were made: samples were annealed at 320±5° C.

TABLE IV

Transformation conditions for the thermal survey

Transformation	Type	Designation	Figure	Prior freeze duration	Solid anneal, hr	Melting duration, hr
Melt	After very fast normal freeze	c_1	2	4 min	2	2
Melt	After very fast normal freeze with overnight anneal	c_2	3	4 min	17	2
Melt	After slow induced freeze	g_1	4	2 hr	2	2
Melt	After slow induced freeze with overnight anneal	g_2	5	2 hr	17	2

Two types of derived curves (see McLaren and Murdock, Part V, 1960) were determined from these melting curves for each melting: type *a*, inverse-rate histograms of % duration against a melting temperature interval and type *b*, incremented % duration against minimum melting range. The type *b* derived curves are shown in Figs. 2–5 inclusive.

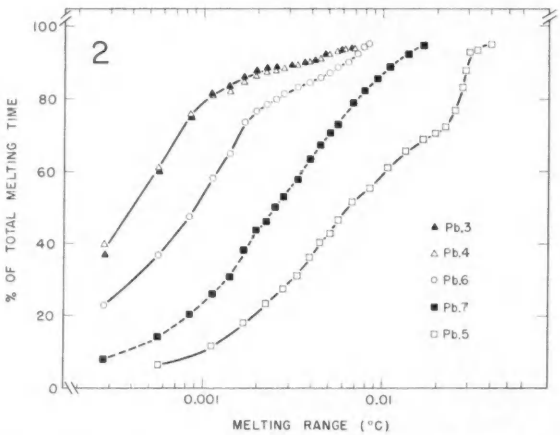

FIG. 2. Fraction of the total melting time spent in given melting ranges following very fast normal freezes with 2-hr solid anneals: derived from 'c_1' curves.

FIG. 3. Fraction of the total melting time spent in given melting ranges following very fast normal freezes with 17-hr solid anneals: derived from 'c_2' curves. FIG. 4. Fraction of the total melting time spent in given melting ranges following slow induced freezes with 2-hr solid anneals: derived from 'g_1' curves. FIG. 5. Fraction of the total melting time spent in given melting ranges following slow induced freezes with 17-hr solid anneals: derived from 'g_2' curves.

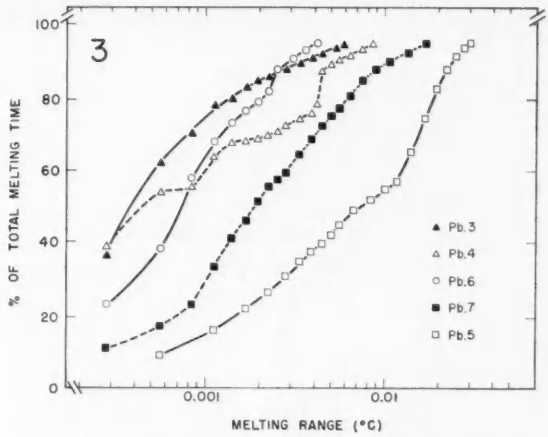
3
% OF TOTAL MELTING TIME
100
80
60
40
20
0
0.001
0.01
MELTING RANGE (°C)
Pb.3
Pb.4
Pb.6
Pb.7
Pb.5

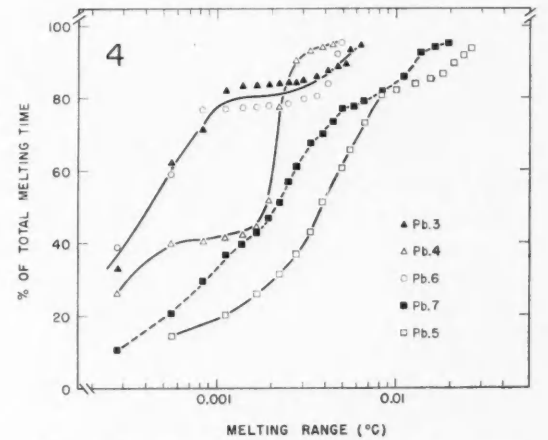
4
% OF TOTAL MELTING TIME
100
80
60
40
20
0
0.001
0.01
MELTING RANGE (°C)
Pb.3
Pb.4
Pb.6
Pb.7
Pb.5

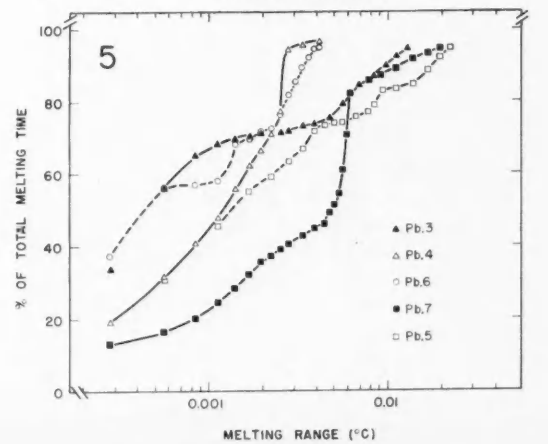
5
% OF TOTAL MELTING TIME
100
80
60
40
20
0
0.001
0.01
MELTING RANGE (°C)
Pb.3
Pb.4
Pb.6
Pb.7
Pb.5

FIGS. 3–5.

From the type *a* histograms the temperature widths at the 1% level of the total melting time were determined both for the over-all sample and, where found, the width at this level of any prominent core revealed on the melting curve; from the type *b* plots melting ranges for both 50% and 90% durations were determined. Table V summarizes the values of these melting range parameters that were made on all the samples. Consideration of these alloy melting range measurements will be deferred until after presentation of the

TABLE V

Alloy melting range comparisons

Transformation type	Ingot	Pb.4	Pb.3	Pb.6	Pb.7	Pb.5
		Melting width (°C) at 1% level from inverse curves				
c_1	w*	0.0019	0.0019	0.0029	0.0067	0.0069
	W	0.0019	0.0019	0.0040	0.0067	0.0175
c_2	w	0.0012	0.0029	0.0042	0.0064	0.0072
	W	0.0043	0.0029	0.0042	0.0064	0.0140
g_1	w	0.0020	0.0014	0.0008	0.0036	0.0083
	W	0.0028	0.0050	0.0047	0.0108	0.0083
g_2	w	0.0028	0.0019	0.0006	0.0061	0.0089
	W	0.0028	0.0046	0.0039	0.0061	0.0089
		Melting range (°C) for 50% duration				
c_1		0.0004	0.0004	0.0007	0.0020	0.0072
c_2		0.0004	0.0004	0.0009	0.0025	0.0064
g_1		0.0020	0.0004	0.0004	0.0022	0.0039
g_2		0.0014	0.0004	0.0004	0.0050	0.0014
		Melting range (°C) for 90% duration				
c_1		0.0036	0.0036	0.0060	0.012	0.030
c_2		0.0050	0.0033	0.0028	0.010	0.024
g_1		0.0028	0.0053	0.0047	0.013	0.022
g_2		0.0026	0.0097	0.0033	0.011	0.018
Table III (estimate)		<0.0043	<0.0043	—	<0.03	<0.04

NOTE: w., grain cores; W., over-all sample.

results of the liquidus point intercomparison because it is not possible to decide which of the samples of high purity lead is the purest solely on the basis of narrow alloy melting range.

B. Intercomparison of Liquidus Points

(a) Pressure Effects on the Freezing Temperature

The effects of the external nitrogen pressure over the melts and the immersion pressure in the liquid metal on the plateau freezing temperature were experimentally determined in order that accurate corrections could be applied in temperature calculations at the lead point: these results are shown in Fig. 6. The increase in the freezing temperature of lead for 1 atm gas pressure over the melt was 0.0080° C. An immersion of about 10 cm (of the mid-point of the sensing element of a Meyers thermometer) was required before the measured temperatures agreed within 0.0001° C of the variation deduced from the Clausius–Clapeyron relation using the above measured gross pressure effect and a liquid density at the freezing point of 10.6 g/cc (Liquid Metals Handbook

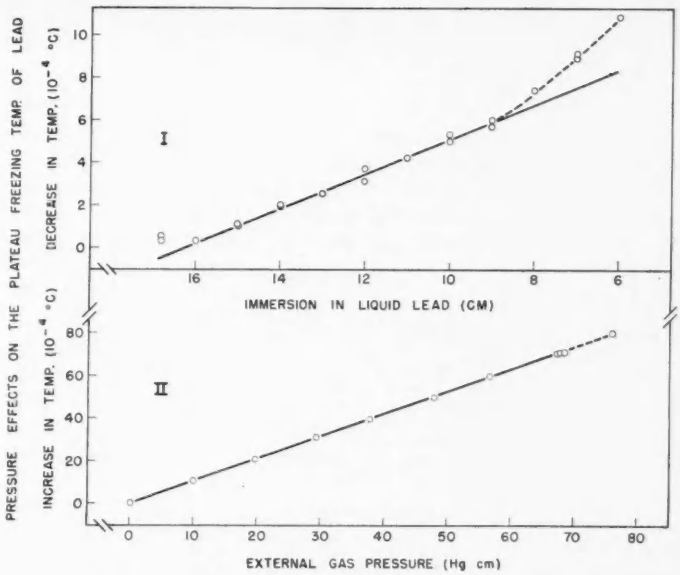
PRESSURE EFFECTS ON THE PLATEAU FREEZING TEMP OF LEAD
DECREASE IN TEMP. (10^{-4} °C)
INCREASE IN TEMP. (10^{-4} °C)
I
II
IMMERSION IN LIQUID LEAD (CM)
EXTERNAL GAS PRESSURE (Hg cm)

FIG. 6. Pressure effects on the plateau freezing temperature of lead.

1952). This expected variation of 0.0000819° C per centimeter is shown as the solid line in curve I of Fig. 6.

(b) Freezing Temperature Comparison

A careful intercomparison of the plateau freezing temperatures obtained on slow (~3 hours) induced freezes on the five samples of lead was carried out: the temperature of four samples were compared to that of sample Pb.4 using the measuring scheme that is regularly employed for precision temperature intercomparisons (see McLaren, Part III, 1958*a*). The fully corrected zero current resistances at the liquidus points of a single Meyers thermometer, S155, at 15 cm mid-point immersion corrected to 1 atm dry nitrogen pressure

TABLE VI

Intercomparison of plateau temperatures

Mean date	Sample	No. of freezes	Ratio R_{Pb}/R_{TP} Mean	$10^8\times$ std. dev.	Reproducibility (equivalent 10^{-4}°C) Std. dev.	Spread	Plateau temp. rel. to Pb.4, °C	Liquidus depression from Table III, °C
14.9.59	Pb.3	10	2.24182546	±36	±1.2	3.9	+0.00012	<0.0003
	Pb.4	10	2504	±26	±0.9	2.7	0.0	<0.0003
20.9.59	Pb.6	10	2.24181749	±30	±0.8	2.9	−0.0021	—
	Pb.4	10	2503	±47	±1.3	5.0		
25.9.59	Pb.7	5	2.24181402	±68	±1.9	4.6	−0.0031	<0.0031
	Pb.4	5	2521	±18	±0.5	1.1		
30.9.59	Pb.5	5	2.24181436	±56	±1.6	3.6	−0.0030	<0.0037
	Pb.4	5	2531	±24	±0.7	1.6		
(All freezes)	Pb.4	30	2.24182511	±36	±1.0	5.0		

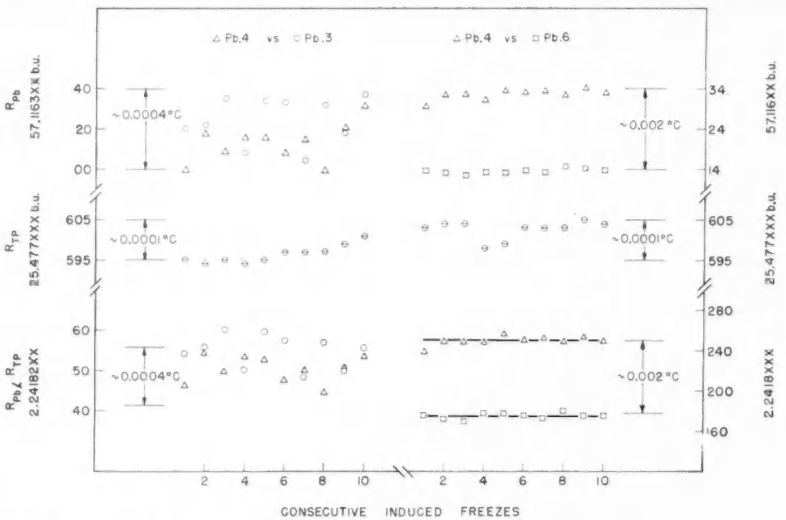

FIG. 7. Intercomparison of plateau freezing temperatures of Pb.3 and Pb.6 with Pb.4: R_{TP} and R_{Pb}, zero current fully corrected resistances of the thermometer at the triple point of water and the lead point respectively.

over the melts were determined. Measurements at the triple point of water (triple cell 29) were made before and after the measurements at the freezing points of the lead samples and the average R_{TP} was used to determine R_{Pb}/R_{TP} ratios. Figure 7 gives the results of comparing samples Pb.3 and Pb.6 against Pb.4, 10 determinations being made on each sample. Table VI summarizes the measurements that were made on all the samples.

(*c*) *Freezing Temperature of Lead*

A value of 327.4258° C (Int. 1948) was determined for the standard liquidus point of sample Pb.4.

DISCUSSION

(a) Purest Sample

An inspection of Figs. 2–5 together with a consideration of the values of the melting range parameters in Table V afford the means to appraise differences in the effects of dissolved impurity solutes among the samples. These results show that samples Pb.4, Pb.3, and Pb.6 are clearly purer than the remaining two samples because they melt over distinctly narrower ranges following different types of freezing with and without the overnight solid anneals. On the other hand it is difficult to distinguish among the three purest samples on the basis of melting range alone. Evidence of strong coring can be seen on melting curves of all these samples which is variously dependent on prior thermal history, e.g. Pb.4, c_2; Pb.3, g_1, g_2; Pb.6, g_1, g_2. This coring is the result of considerable impurity segregation on freezing and shows that all the samples

contain residual impurity solutes in sufficient concentration to have associated alloy melting ranges that can be readily detected by the resistance thermometer.

Further evidence of significant impurity segregation in all these samples may be deduced from Fig. 8, which shows a selection of the front ends of melting curves determined on the samples. Similar structures were found on the melting curves of samples of high purity tin (McLaren and Murdock, Part V, 1960) and were thought to be associated with gross impurity segregations in the ingots because they were not observed on the melting curves of the purest samples.

In the absence of a purer sample of lead that could be shown to have a narrower transition range that would be invariant with rate of freezing and amount of solid anneal, it is only possible to estimate which of these three samples is most likely to be the purest one. The liquidus points of Pb.4 and Pb.3 are nearly identical and were found to be about 0.002° C higher than that of Pb.6. The problem thus reduces to deciding whether the liquidus points of Pb.4 and Pb.3 lie closer to that of pure element than does the liquidus point of Pb.6.

From Tables II and III it may be inferred that the three samples would melt in a temperature range bounded by the Pb–Tl liquidus and the Pb–Ag solidus. The following factors weigh in favor of samples Pb.4 and Pb.3 having liquidus points closer than that of Pb.6 to the liquidus point of pure element.

(i) From Table V it appears that sample Pb.4 generally had narrower over-all melting ranges than Pb.6.

(ii) Reasonable agreement was found between the measured liquidus depressions (Table VI) and alloy melting ranges (Table V) and the values of these quantities that were estimated from known phase diagrams and the supplied chemical analyses.

(iii) Sample Pb.6 showed a greater amount of coring (W/w . . . . . g_1, g_2, Table V) following slow freezing: this must be attributed to a segregation of slightly solid-soluble solutes such as Cu and Ag. This observation is substantiated by the qualitative spectrochemical analysis which indicates the presence of a trace of copper and silver in this sample. It is also significant that only 1 p.p.m. Cu would depress the liquidus about 0.002° C.

(iv) For the liquidus points of Pb.4 and Pb.3 to be raised by 0.002° C from that of pure element would require the presence of 23 p.p.m. Tl, an amount nearly 100 times greater than their analyzed thallium contents.

(b) Thermometric Standard

The reproducibilities of the liquidus points of these samples of high purity lead are comparable with that of any fixed temperature point on the International Temperature Scale. Alloy melting range parameters may be used to select samples of lead that would have liquidus points within 0.001° C of pure element: samples with an over-all width at the 1% level of the total melting time on inverse melting curves of $\leqslant$ 0.002° C following fast and slow freezing would meet this requirement.

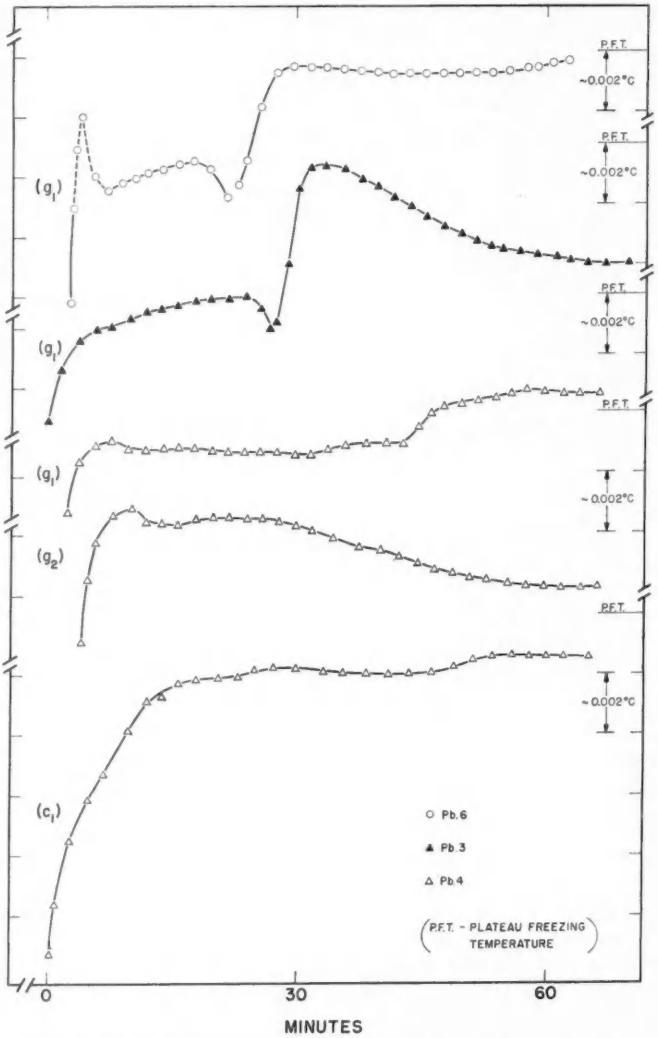

FIG. 8. Portions of melting curves showing anomalous front end structures: types (see Table IV) of melting curves are indicated.

The cadmium point (321.032° C Int. 1948) has three slight advantages over the lead point as a fixed temperature standard: samples are already available that have liquidus points within 0.001° C of pure element (McLaren, Part IV, 1958*b*); a smaller supercooling (0.03° C for cadmium compared with up to 0.14° C for lead) decreases the amount of initial dendritic freezing which

possibly could interfere with the smooth interface coring that is responsible for the plateau temperatures; and cadmium has a larger (1.7 times) latent heat of fusion per cubic centimeter, which assists in the ready attainment of steady plateaux of long durations on induced freezes in simple block furnaces. Interpolation errors arising in the use of the lead point as a fixed point in the quadratic calibration of resistance thermometers would be similar to those found for the cadmium point and discussed by McLaren (1959).

CONCLUSIONS

This investigation has shown that the liquidus point of high purity lead (327.426° C Int. 1948) may be used as a reliable precision fixed-temperature point and has an experimental realization that is comparable in simplicity and ease of attainment to the freezing temperatures of the pure metals previously studied. The resistance thermometer has been shown to have the sensitivity required to discriminate among samples of nominal 99.9999% purity lead on the basis of narrow alloy melting range.

ACKNOWLEDGMENT

The authors are grateful to the Consolidated Mining and Smelting Co., Trail, B.C., for supplying samples Pb.3 and Pb.4.

REFERENCES

HANSEN, M. 1958. Constitution of binary alloys (McGraw-Hill Book Co. of Canada, Ltd., Toronto).
LIQUID METALS HANDBOOK. 1952. (U.S. Government Printing Office, Washington, D.C.), p. 40.
McLAREN, E. H. 1957*a*. Can. J. Phys. **35**, 78.
——— 1957*b*. Can. J. Phys. **35**, 1086.
——— 1958*a*. Can. J. Phys. **36**, 585.
——— 1958*b*. Can. J. Phys. **36**, 1131.
——— 1959. Can. J. Phys. **37**, 422.
McLAREN, E. H. and MURDOCK, E. G. 1960. Can. J. Phys. **38**, 100.
METALS HANDBOOK. 1948. (The American Society for Metals, Cleveland, Ohio).

THE WHITE TIN → GREY TIN TRANSITION IN TIN–MERCURY ALLOYS[1]

R. W. SMITH[2]

ABSTRACT

The effect of the addition of mercury on the linear rate of white tin (β) → grey tin (α) transformation in a number of dilute tin-binary alloys has been examined. Rates of transformation at −78° and −25° C are shown for binary alloys of zone-refined tin and aluminum, arsenic, bismuth, germanium, indium, lead, antimony, and zinc, and also for a number of commercially pure tins. The resultant rates of all of these upon further alloying with 0.6 at.% Hg are likewise given. At −78° C, the addition of mercury always produces a very low transformation rate, approximately 4×10^{-4} mm/hr. However, at −25° C, an increase in rate is observed in certain cases.

The results are discussed and a theory is developed to account for them and also to predict the effect of mercury on the $\beta \rightarrow \alpha$ transition in any tin-binary system.

1. INTRODUCTION

In a recent study of the $\alpha \rightleftarrows \beta$ transition in tin–mercury alloys (Smith 1959), it was shown that the introduction of mercury into pure tin yields transformation data valuable in understanding the general characteristics of this classic phase change. The rate of conversion of white tin into the grey allotrope was considerably reduced and by an amount which was virtually independent of the mercury content of the alloy. Also, the rates of transformation in alloys of zone-refined tin and mercury were found to be similar to that in one made from a less pure tin. A mechanism was proposed to account for these observations based on the fact that mercury is mobile well below the transition temperature. The following experiments were devised to verify and extend this postulate.

2. EXPERIMENTAL PROCEDURE AND RESULTS

A number of non-mercurial alloys were first prepared from zone-refined tin and certain metallic additions.* Then 0.6 at.% mercurial alloys were made from one half of each. All were cold-rolled to a thickness of 1 mm, cut into $0.1\times0.15\times3.0$ cm strips and annealed in argon at 200° C for 1 hour. Each specimen was then fixed at one end to a metric scale and, after inoculation with grey tin at the other end, sealed in a glass tube to be maintained at the test temperature.

When a grey tin wart had established itself across a specimen's entire cross section, the further progress of the phase boundary was determined by accu-

[1]Manuscript received December 2, 1959.
Contribution from the Department of Metallurgical Engineering, University of Toronto, Toronto, Ontario.

[2]Present address: Department of Physical Metallurgy, University of Birmingham, England.

*Vulcan extra pure tin (99.998%) was zone-refined to a purity of 99.9999% Sn (as indicated by $\beta \rightarrow \alpha$ transformation rates and analysis). The mercury used in these tests was 'Analar Reagent' (>99.999% Hg) and the other additions were the purest commercially obtainable.

rately checking its position against the scale at regular intervals. It was important that the position of a particular interface be determined in a few seconds to prevent change in the specimen's temperature. A graphical plot of interface position against time gave an accurate estimate of the rate of transformation. This method of rate determination had been found to be the most convenient of a number tried (Smith, to be published).

Two temperatures were employed, −25° C, using a refrigerator, and −78° C, obtained by surrounding the specimen tubes with solid carbon dioxide. Four specimens of each material were tested at both temperatures, except in the case of tin–germanium, where the confusion incident upon spontaneous nucleation required more.

The transformation rates for zone-refined tin, three commercially pure tins, and a number of alloys are shown in Table I. No values are given for the tin–lead alloy at −25° C since its linear transformation was immeasurably small over the 60-day period of the test.

3. DISCUSSION

One of the most significant points to note from the results is that the introduction of mercury into tin alloys will always produce a reduction in the rate of $\beta \rightarrow \alpha$ transformation when maintained at −78° C, whilst exposure at −25° C may in some cases result in a rate increase. Also, the reductions in rate at −78° C are usually drastic and all to approximately the same final value, 4×10^{-4} mm/hr. Such a $\beta \rightarrow \alpha$ transformation rate is only brought about in pure tin by the addition of a relatively large amount of a potent transformation inhibitor, e.g. lead. Explanation of these observations must be associated with the melting point of mercury, −38.8° C.

The $\beta \rightarrow \alpha$ transformation of a tin–mercury alloy requires the decomposition of any existing precipitates of $HgSn_{12}$* and the rejection of mercury at the $\alpha-\beta$ phase boundary.† At −78° C, diffusion is slow and rejected mercury is solid. This results in considerable hindrance to the movement of an $\alpha-\beta$ interface and so impedes transformation, predominantly intergranular at this temperature (Bornemann and Gela 1953; Smith, to be published).

It is not so directly obvious why alloying with mercury resulted in widely different transformation rates at −25° C, only producing an increase over the original value in certain cases. However, from an examination of the following cases, it is proposed to supply the reason.

(a) Transformation of White Tin Containing Only Mercury, at −25° C

As a small region of grey tin forms in the white tin matrix, mercury is rejected at the interface (Ewald and Tufte 1958, 1959). If possible, this mercury will combine with adjacent white tin, presumably to form $HgSn_{12}$. Further transformation will require this compound to decompose, again liberating mercury. Thus in the steady state, a cross section through a $\beta \rightarrow \alpha$ interface would reveal the white tin matrix, possibly with free regions of $HgSn_{12}$,

*$HgSn_{12}$ is a hexagonal compound formed in white tin when mercury is present in excess of 0.2 at.% (Groen 1954).

†Mercury is insoluble in grey tin (Ewald and Tufte 1958, 1959).

TABLE I

The linear rate of $\beta \rightarrow \alpha$ transformation in zone-refined tin and certain dilute alloys*

Material	Transformation at −78° C				Transformation at −25° C			
	Without Hg		With 0.6 at.% Hg		Without Hg		With 0.6 at.% Hg	
	Rate, mm/hr	r.m.s. deviation, ±mm/hr	Rate, mm/hr	r.m.s. deviation, ±mm/hr	Rate, mm/hr	r.m.s. deviation, ±mm/hr	Rate, mm/hr	r.m.s. deviation, ±mm/hr
Zone-refined tin (99.9999% Sn)	1.31×10^{-1}	0.06×10^{-1}	7.8×10^{-4}	1.3×10^{-4}	2.18	0.06	4.5×10^{-1}	0.2×10^{-1}
Pure tin 1 (99.998% Sn)†	1.19×10^{-1}	0.01×10^{-1}	4.5×10^{-4}	1.4×10^{-4}	9.8×10^{-1}	0.5×10^{-1}	4.3×10^{-1}	0.3×10^{-1}
Pure tin 2 (99.996% Sn)‡	1.03×10^{-1}	0.03×10^{-1}	3.6×10^{-4}	0.9×10^{-4}	1.03	0.07	4.2×10^{-1}	0.3×10^{-1}
Pure tin 3 (99.988% Sn)§	6.0×10^{-2}	0.1×10^{-2}	6.0×10^{-4}	2.2×10^{-4}	7.4×10^{-3}	1.0×10^{-3}	3.9×10^{-1}	0.3×10^{-1}
Zone-refined tin + 0.45 at.% Al	3.35×10^{-2}	0.05×10^{-2}	4.0×10^{-4}	1.6×10^{-4}	5.5×10^{-1}	0.2×10^{-1}	3.4×10^{-1}	0.4×10^{-1}
Zone-refined tin + 0.15 at.% As	5.39×10^{-2}	0.06×10^{-2}	2.4×10^{-4}	0.7×10^{-4}	4.9×10^{-1}	0.2×10^{-1}	2.8×10^{-1}	0.1×10^{-1}
Zone-refined tin + 0.03 at.% Bi	6.4×10^{-2}	0.4×10^{-2}	3.8×10^{-4}	1.0×10^{-4}	5.3×10^{-4}	2.7×10^{-4}	9.0×10^{-2}	0.9×10^{-2}
Zone-refined tin + 1.2 at.% Ge	2.4×10^{-2}	0.3×10^{-2}	2.7×10^{-4}	1.0×10^{-4}	2.2×10^{-2}	0.2×10^{-2}	4.7×10^{-1}	0.1×10^{-1}
Zone-refined tin + 0.02 at.% In	9.0×10^{-2}	0.7×10^{-2}	6.5×10^{-4}	0.9×10^{-4}	6.5×10^{-1}	0.5×10^{-1}	5.0×10^{-1}	0.2×10^{-1}
Zone-refined tin + 0.02 at.% Pb	7.9×10^{-4}	3.2×10^{-4}	4.2×10^{-4}	1.6×10^{-4}	—	—	4.5×10^{-1}	0.3×10^{-1}
Zone-refined tin + 0.07 at.% Sb	1.02×10^{-1}	0.04×10^{-1}	2.3×10^{-4}	1.1×10^{-4}	8.0×10^{-1}	0.6×10^{-1}	8.8×10^{-2}	0.3×10^{-2}
Zone-refined tin + 0.2 at.% Zn	3.2×10^{-3}	0.3×10^{-3}	2.8×10^{-4}	0.5×10^{-4}	3.7×10^{-2}	0.2×10^{-2}	2.1×10^{-1}	0.1×10^{-1}

*J. H. Becker (J. Appl. Phys. **29**, 7, 1110 (1958)) reports $\beta \rightarrow \alpha$ transformation rates at −30° C for Vulcan tin and a number of dilute tin-rich alloys of compositions similar to some of those listed above. Becker's results for Vulcan tin and a tin–arsenic alloy agree closely, whilst a rate of 0.1±0.05 mm/hr is reported for a 0.1 at.% antimony alloy.

†Extra pure tin (supplied by Vulcan Detinning Co., Sewaren, N.J., U.S.A.).

‡Spectroscopically pure tin (supplied by Johnson, Matthey & Co. Ltd., London, England).

§Chempur tin (supplied by Metals and Alloys Co. Ltd., Toronto, Canada).

a layer of $HgSn_{12}$, then a layer of mercury, and finally the grey tin matrix. Since the mercury layer can only have a limited width, pockets of free mercury will also appear in the grey tin. Transformation can be pictured as the transference of tin atoms from the β-matrix, through the layers of $HgSn_{12}$ and mercury, to the grey tin lattice for depositions. Such a transformation path is energetically more difficult than direct diffusion from $\beta \rightarrow \alpha$ and so a reduction in transformation rate is therefore to be expected when mercury is alloyed with pure tin.

(b) Transformation of White Tin When Soluble Additions Are Present, Together with Mercury, at −25° C

During the very early stages of transformation, the conditions described in (*a*) would exist at an α–β interface. Continued transformation would result in the mercury layer becoming saturated with the other solutes originally present in the white tin. (Most elements have only a very limited solubility in mercury at −25° C and are insoluble in grey tin.) Thus a solute-rich layer would gradually form between the $HgSn_{12}$ and the mercury. Accordingly, diffusion of tin atoms across the boundary region is further impeded and a lower transformation rate is observed than in (*a*).

(c) Transformation of White Tin Containing Mercury and Also Other Solutes Present as Local Precipitates, at −25° C

Initial transformation will follow (*b*) until the mercury layer becomes saturated and the localized precipitates in the white tin are no longer attacked. These particles will present local barriers to diffusion but, between them, the β-matrix will gradually dissolve away to be deposited as grey tin. This process will eventually result in the particles becoming completely detached from the β-surface. Hence only a slightly smaller transformation rate is to be expected when compared with that of pure tin and mercury alone.

(d) Transformation of White Tin Containing Mercury and Grey-Tin-Soluble Additions, at −25° C

Grey tin would only be expected to dissolve an appreciable amount of those elements which possess its own diamond cubic structure, e.g. germanium. However, a diamond cubic element would have only low solubility in tetragonal tin and thus it would be energetically favorable for any such solute appearing in the $HgSn_{12}$–mercury interface to be taken up by the mercury and deposited on the grey tin. Such practice would tend to an increase in the rate of transformation over (*c*).

These cases may be summarized thus: The solute properties tending to make the $\beta \rightarrow \alpha$ transformation rate of a ternary tin–mercury alloy approach that of zone-refined tin and mercury are a localized dispersion in white tin, high solubility in mercury at −25° C, and a similar structure to that of grey tin.

As yet only a prediction has been made of the transformation rate at −25° C of a ternary tin–mercury alloy. How this value differs from that observed in the binary alloy in the absence of mercury will depend on the particular solute and also on its concentration. Any decrease results from the reduced ease with which tin atoms diffuse through the mercury-rich phase

boundary region. An increase in transformation rate is effected through mercurial rearrangement of the solute which originally caused so much hindrance to the advance of an $\alpha-\beta$ interface.

The data shown in Table I agrees with the predictions. The rates of transformation of the 'pure' tins reflect the purity of each. Of the metallic additions to the zone-refined tin, only antimony, bismuth, and indium have any appreciable solid solubility in white tin at room temperature (Hansen 1958). That of zinc is only 2 at.% at the eutectic temperature and is probably very small at room temperature. However, the expected tendency for a very low transformation rate at $-25°$ C in the tin–indium–mercury alloy, is more than offset by indium's high solubility in mercury, 68.9 at.% at 10° C. The other metallic additions have very small or negligible solubilities in mercury below room temperature. The rather high rate of transformation in the alloy containing mercury and germanium is presumably due to the latter's solubility in grey tin and that it may also act as a deposition center.

Thus it is seen that the results of this study are in close agreement with the theory developed herein.

ACKNOWLEDGMENTS

The work described in this paper forms a part of the wider program of research into the grey tin $\rightleftharpoons$ white tin transformation in zone-refined material carried out in the Metallurgical Engineering Department of the University of Toronto. The author is grateful to the National Research Council for financial assistance and to Dr. L. M. Pidgeon, Head of the Department, for his interest throughout the course of this work. The staff and research students are to be thanked for their helpful discussions.

REFERENCES

BORNEMANN, A. and GELA, T. 1953. Final Report, Contract No. DA-36-039-SC-15393, Signals Corps Project 2005 – MO8 – Metals, U.S. Army.
EWALD, A. W. and TUFTE, O. N. 1958. J. Appl. Phys. **29**, 7, 1007.
——— 1959. J. Phys. Chem. Solids, **8**, 523.
GROEN, L. G. 1954. Nature, **174**, 836.
HANSEN, M. 1958. Constitution of binary alloys (McGraw-Hill Book Co., Inc., New York).
SMITH, R. W. 1959. Can. J. Phys. **37**, 1079.
——— To be published.

ON THE GEOMETRY OF RADIO REFLECTIONS FROM AURORA[1]

P. A. Forsyth

ABSTRACT

By assuming that auroral radio reflections are produced by volume scattering in clouds of ionization having the same spatial configuration as the visible auroral structures, and by taking into account the radar pulse duration and antenna beam width, it is possible to predict the probability of echo occurrence as a function of range and azimuth. This echo distribution is quite similar to that observed experimentally even when "aspect sensitivity" of the individual scatterer is neglected. Unfortunately, the optical evidence is not sufficiently extensive to permit precise calculations to be made, nor the radio evidence to permit detailed comparisons, but previous estimates of the shape of the scattering structures that have been based on the azimuthal echo distribution without regard to the factors discussed here are likely to be seriously in error.

INTRODUCTION

Although the reflection of radio waves from auroral ionization has been observed regularly for more than 10 years, there is no general agreement concerning the nature of the reflection mechanism. Soon after the first observations it was noted that for stations in north middle latitudes radar echoes could be obtained only from auroral displays that occurred several hundred kilometers to the north of the radar station, that is, from auroral displays that were located at low elevation angles as seen visually from the radar station. This characteristic of the radar reflections still awaits a completely satisfactory explanation. The first attempt to provide such an explanation was made by Herlofson (1947), who suggested that the reflection process was specular and that reflections would occur only when the direction of incidence of the radio waves was accurately normal to the auroral structures, which, in turn, are known to lie along the earth's magnetic field lines. At first, this explanation was accepted enthusiastically by most researchers, but as more experimental evidence was accumulated it became necessary to reject the specular reflection process in favor of a less rigid geometric control that has come to be known as "aspect sensitivity". Booker (1956) suggested that the observed aspect sensitivity could result from the diffraction pattern produced by long thin ionic inhomogeneities aligned with the magnetic field. Kaiser (1956) in England and Forsyth and Vogan (1957) in Canada concluded independently that the observed degree of aspect sensitivity could result from simple scattering by prolate spheroids having a ratio of length to diameter of about three or four to one. In this work the usual experimental evidence is the distribution in range and azimuth of the density of occurrence of radar echoes as seen from a single radar station. For stations such as Saskatoon (52.1° north, 106.6° west) the echo occurrence shows a strong tendency to peak in the approximate direction of magnetic north and at distances of 600 to 800 kilometers. This

[1]Manuscript received December 7, 1959.
Contribution from the Institute of Upper Atmospheric Physics, University of Saskatchewan, Saskatoon, Saskatchewan.

paper grew out of an attempt to arrive at a more accurate estimate of the degree of aspect sensitivity involved in auroral radio reflections by taking into consideration some of the known characteristics of visible aurora. As the work progressed it became apparent that echo distributions approximating closely to those observed experimentally could be derived without recourse to the "aspect sensitive" scattering structures and that the statistical characteristics of visible aurora are not known at the present time with sufficient accuracy to arrive at a meaningful estimate of the shape of the scattering structures by this method. Even though these echo distributions can be calculated only crudely, it is felt that it is worth while to present them at this time because they depend critically on factors that have been almost completely ignored in previous attempts at quantitative analysis of the observed distributions.

CALCULATION OF ECHO PROBABILITY DISTRIBUTIONS

There is still some uncertainty concerning the extent to which the radio reflections can be associated with visible auroral displays, but there seems to be no doubt that at least a significant fraction of the radar echoes observed at, say, Saskatoon are produced by ionization associated with auroral structures that could, under the proper conditions, be observed visually. What evidence there is on the subject suggests that the auroral echoes tend to come from the more well-defined auroral forms. One feature of these forms is a characteristic configuration in space. They frequently extend for many hundreds and perhaps even thousands of kilometers in the east–west direction (Störmer 1936), some 30 or 40 kilometers in the vertical direction (Currie and Weaver 1955), and only about a kilometer or perhaps less in the north–south direction. The first basic assumption used in the computations is that the echo-producing auroral ionization has the same configuration as the auroral luminosity. The second assumption is that the reflection process is a non-coherent, volume effect. Another way of stating this assumption is to say that many scatterers are involved, and at least some of the scatterers are separated by several wavelengths. No specific assumption is made about the size or shape of the scatterers.

A wide variety of radar parameters have been used to investigate aurora. Pulse durations varying from about ten to several hundred microseconds have been used. Aside from the usual expectation that the radar sensitivity increases with increasing pulse duration, relatively little attention has been paid to this important parameter in making comparisons between data obtained with different radars. If, however, the auroral ionization has the spatial configuration outlined above, then the distribution of echoes in range and azimuth should depend markedly on both the pulse duration and antenna radiation beam width of the radar. Two situations are illustrated in Fig. 1, which shows a plan view of the radar location in relation to two auroral forms. In Fig. 1(*a*) the auroral structure is located well to the north of the radar and the direction of travel of the incident radio waves is nearly normal to the length of the auroral form. If the range increment dR corresponds to the pulse duration T, of the radar (i.e. $dR = cT/2$) then the volume of auroral ionization

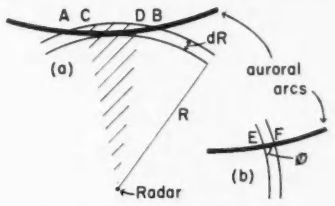

FIG. 1. Plan view of area surrounding a radar station, illustrating the geometric factors that enter the calculation.

that can simultaneously contribute to the echo is proportional to the length AB. In Fig. 1(b) the radio wave front makes an appreciable angle ϕ with the length of the auroral structure and the corresponding volume is proportional to the much shorter length EF. Actually, in order to determine the distribution in azimuth of the echoes it is necessary to use a directive antenna (i.e. an antenna of limited beam width). In this case, a further restriction on the simultaneous scattering volume may arise. In Fig. 1(a) is sketched an antenna beam width of 20° for which the scattering volume would be proportional to CD rather than to AB. This simple approach has been followed in the calculations on which this paper is based.

The computation of the scattering volume as a function of range and azimuth was carried out for Saskatoon, initially for the assumption that all auroral forms were parallel and roughly aligned with the lines of geomagnetic latitude. The volume parameter x (corresponding to EF in Fig. 1(b)), was calculated for about sixty field points in a region representing one (the eastern) half of the radar coverage. For this calculation the following approximate expression was used,

$$x = R\,(\sin^2\phi + 2dR/R)^{\frac{1}{2}} - R\sin\phi,$$

where the symbols have the meaning indicated in Fig. 1. The quantity x, according to the initial assumption, should be proportional to the power reflected by the auroral form. There are some conditions under which the probability of observing an echo may be proportional to this quantity raised to some fractional power, but for the present purpose, it seemed wisest to assume the more usual simple proportionality between echo power and echo detectability. In general, there are two segments, x, which contribute to the scattering volume. Whenever the centers of these two segments lay within an azimuth sector of 20° the larger figure, $2x$, was used to compute the echo probability. This procedure is equivalent to assuming an antenna beam width of 20°. Although the use of a specific value detracts from the generality of the treatment, some antenna beam width must be assumed and 20° seems fairly representative of those that have been used. This value was used also throughout the computation to restrict the volume in the manner indicated in Fig. 1(a).

Similarly, some range dependence must be assumed. The particular range dependence chosen corresponds to that frequently found for v.h.f. radars.

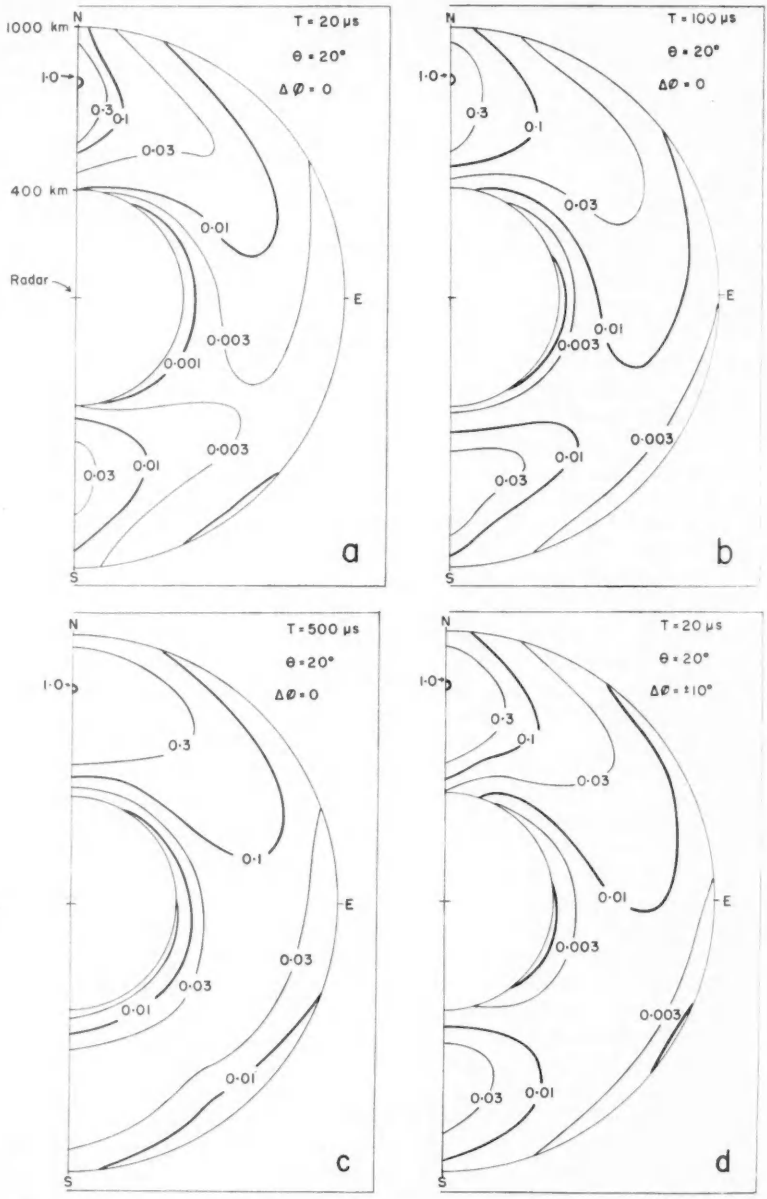

FIG. 2. Contour maps for the neighborhood of Saskatoon showing the calculated distributions of echo occurrence for a number of different radar pulse durations (T) and constant antenna beam width (θ). The maps (a), (b), and (c) assume that all the auroral arcs are parallel while (d), (e), and (f) are smoothed for variability of arc orientation.

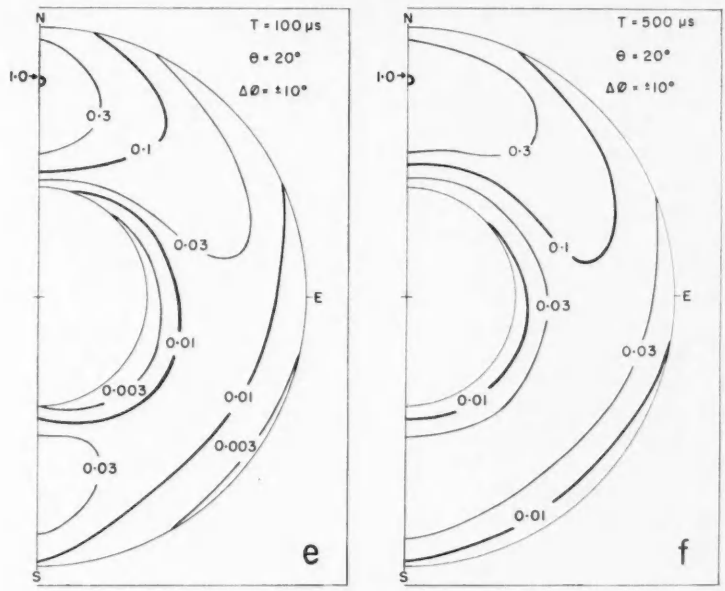

FIG. 2.

The radar sensitivity was assumed to be proportional to 0.04, 1.0, 1.0, and 0.2 at ranges of 400, 600, 800, and 1000 kilometers respectively, and zero at ranges appreciably greater or less than these values.

Finally, the distribution of density of occurrence of visual aurora must be taken into account. This distribution must, of course, be specific to the location of the radar, in this case Saskatoon. The values used were those given by Vestine (1944). Once again, the use of these particular values might be questioned as being inaccurate, but no more reliable information is at hand. The probability of echo occurrence for each field point was calculated by multiplying together the factors representing the scattering volume, the radar sensitivity, and the occurrence of visible aurora. In Figs. 2(*a*), 2(*b*), and 2(*c*) are plotted contours of the probability of echo occurrence for the region surrounding Saskatoon for three different pulse durations, 20, 100, and 500 microseconds corresponding to range increments of 3, 15, and 75 kilometers respectively.

The assumption that all auroral structures are parallel provides an instructive example, but is not in accord with the observations. Jensen and Currie (1953) found that at Saskatoon auroral arcs tended to have directions that varied through about $\pm 10°$ about the mean direction. In order to take account of this variability the value of ϕ for each field point was varied through $\pm 10°$ about the value used for the first computation and the average resulting value for x was used. The resulting echo probability distributions, smoothed in this way for variability in direction of the auroral forms, are plotted in Figs. 2(*d*), 2(*e*), and 2(*f*). The same three values of pulse duration were used for these calculations.

DISCUSSION

The most striking feature of the echo occurrence graphs of Fig. 2 is the very strong concentration in the northward direction. The concentration is even more marked than is usually encountered in experimental investigations. It should be noted that while the north direction in these graphs was referred to earlier as being coincident with the geomagnetic meridian, it should be taken more precisely as the normal to the mean local orientation of the auroral forms. For Saskatoon, Jensen and Currie (1953) found that this mean orientation changed seasonally through more than 25°, a factor that could contribute to the width of the observed distribution.

Variation with Latitude

One of the strongest arguments in favor of the existence of aspect sensitive scattering structures is based on radar observations made at College, Alaska. There, even though the location is close to the maximum of the auroral zone, radar echoes are obtained most frequently from aurora well to the north of the station. An approximate calculation of the kind carried out for Saskatoon was also carried out for College. The curvature of the lines of geomagnetic latitude in the neighborhood of College differs slightly from the curvature in the neighborhood of Saskatoon but for the calculation this slight difference was ignored and the values of x calculated for Saskatoon were used. College is not only farther north geomagnetically than Saskatoon, but in that area the auroral zone is farther south. The geomagnetic latitude of College was taken as 64° and that of the auroral zone as 67°. (The corresponding figures for Saskatoon were 60.5° and 69°.) The calculation was carried out only for the 100-microsecond pulse duration with smoothing for variability of direction of auroral forms. The results are shown in the form of a contour diagram in Fig. 3, where it may be seen that there is still a strong concentration of predicted echo occurrence in the northern direction.

Azimuthal Distribution

Another way of studying the relative occurrence of echoes is to examine the variation of echo occurrence as a function of azimuth angle for constant range. Several curves derived in this way for a range of 700 kilometers are shown in Fig. 4. The results of the three calculations carried out for $T = 100$ microseconds; unsmoothed and smoothed for Saskatoon and smoothed for College are shown. Also shown is a histogram of the experimental distribution found at Saskatoon in an earlier investigation by Currie, Forsyth, and Vawter (1953). For that investigation, using a frequency of 56 Mc/s, the pulse duration was only 16 microseconds and the antenna beam width was about 45°, much wider than that used for the calculation. Both these factors should tend to sharpen the distribution in the northern direction, but it is seen that the observed distribution is much wider than the calculated distribution.

The simplest way in which the computed distributions could be modified to agree more closely with the observed distribution is to increase the degree of smoothing, that is, to assume a greater variability in orientation of auroral structures. While the evidence of Currie and Weaver is probably valid for most

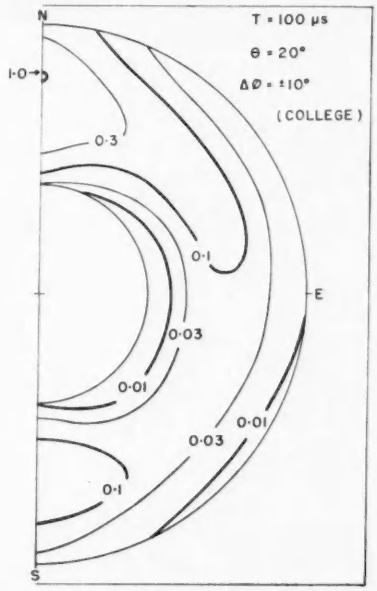

FIG. 3. Contour map of echo distribution in the neighborhood of College, Alaska, calculated for the radar parameters of Fig. 2(*e*).

extended auroral formations, large local deviations in orientation frequently occur, particularly for the more active forms of aurora. It may be that this is the reason that auroral radar echoes seem to be preferentially associated with the more active auroral forms. A recent study by Lyon (1960) has shown that for a radar beam directed at an angle of 45° from the geomagnetic meridian the echoes occur most frequently during the period of breakup of the visible aurora, the period in which the quiet arcs break up into bands and then into the rayed forms. In particular, there seems to be a tendency for the echoes to be produced

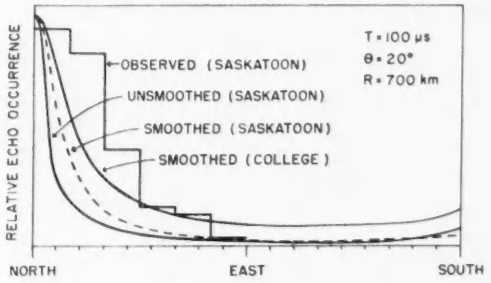

FIG. 4. Comparison of various distributions of echo occurrence with azimuth for constant range (700 km).

most frequently by the so-called "curl" form first discussed by Webster (1957) and later by Gartlein (1959). It might be noted that if the scattering volume effects discussed in this paper are important then the results of Lyon's investigation are entirely reasonable. In Fig. 5, which again shows a plan view of the area around the radar station, this time including two auroral curl forms, it may be seen that for certain combinations of pulse duration and antenna beam width the azimuthal distribution of echo occurrence could be modified by the appearance of curl forms. The probability of echo occurrence for a form at the azimuth of (*b*) would be increased relative to that of the simple form in Fig. 1, resulting in an increase in the width of the distribution. At the same time it may be noticed by comparing Figs. 5(*a*) and 5(*b*) that this effect will only

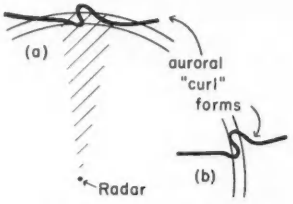

FIG. 5. Plan view of area surrounding a radar station, illustrating the effect of the occurrence of "curl" forms on the echo distribution.

modify the width of the peak in the distribution. As long as the extent of the auroral form is substantially greater in the east–west direction than it is in the north–south direction, then the northern peak in echo occurrence will persist, even for stations located under the auroral zone. It would be necessary to locate a radar well to the north of the auroral zone in order to cause this northern peak to disappear.

Frequency Dependence

The experimental evidence concerning the frequency dependence of the azimuthal distribution of echoes is confusing. In the earlier work at Saskatoon using 56 Mc/s and 106 Mc/s the higher frequency radar had the longer pulse duration and the narrower beam width. The resulting azimuthal distribution was slightly more peaked for the higher frequency. A recent investigation by Presnell *et al.* (1959) at College used frequencies of 216 Mc/s and 398 Mc/s. In this case various pulse durations were used at both frequencies and the antenna beam width was inversely proportional to frequency. The peak in the resulting azimuthal distribution is slightly sharper for the lower frequency. It is unfortunate that there seems to have been no investigation of the azimuthal distribution of echoes carried out at two or more frequencies with radars having equal pulse durations and accurately scaled antennas. On the other hand, there is ample evidence to show conclusively that the occurrence of radar echoes falls off rapidly with increasing frequency. It is reasonable to infer from this that as the radar frequency is increased, the number of effective scattering centers is reduced so that the scatterers become more widely separated in space as well

as in time. If this be the case, a larger volume of the auroral structure must contribute in order to produce a threshold echo at the higher frequencies. Thus as the frequency is increased the importance of local variations in orientation would decrease and the resulting azimuthal distribution of echoes would approximate more closely to the unsmoothed distributions of Figs. 2 and 4.

Since the treatment has made use of parameters typically associated with v.h.f. radars, some modifications would be necessary in a consideration of the distribution to be expected for a u.h.f. radar. In addition, the most recent results obtained with u.h.f. radars operating at frequencies between 400 and 500 Mc/s suggest that the assumptions of this paper may not apply to all echoes observed with these radars. Many echoes display the characteristics to be expected for reflection from ionization having the same spatial configuration as the visible aurora, but others appear to come from patches of ionization which occur within a relatively thin layer. The importance of this second type of echo relative to the first is not yet established but the present treatment could not apply directly to reflection from a horizontal layer. It may be that both of these kinds of ionic volume distribution contribute also to v.h.f. radar reflections. Some of the earlier observations could be interpreted in this way. The fact that the two distributions have not been clearly distinguished before might be due simply to the poor angular resolution that is characteristic of radars operating in the lower frequency range.

Vertical Extent of Aurora

The calculations and discussion up to this point have left out of consideration the effect of the vertical extent of the auroral forms. It seems likely that the vertical extent of the echo-producing volume is somewhat less than that of the corresponding visible form. Nevertheless, it may be instructive to consider the effect of the vertical extent of the radio-aurora, assuming it to be identical with that of the visible aurora. Clearly, the two-dimensional computations can be extended to three dimensions. For short pulse durations the echo amplitude (and hence echo occurrence) will fall off for the higher elevation angles. The elevation angle dependence that arises in this way will be much reduced for pulse durations corresponding to range increments of more than the vertical extent of the forms, say for pulse durations greater than about 300 microseconds.

Variation with Elevation Angle

There is another variation with elevation angle to be expected that is independent of the vertical extent of the auroral forms. This is due to the fact that the lower edge of an auroral form is very nearly horizontal (located at a constant height near 100 kilometers). As the elevation angle increases, the range to the 100 kilometer level decreases and the curvature of the wave front at that level increases. As a result of this increasing curvature the scattering volume of an auroral form, as seen by a radar of fixed pulse duration looking toward the north, decreases with increasing elevation angle. Other factors such as antenna beam width and auroral absorption probably affect, and may even dominate, the distribution of auroral echoes in elevation angle. Here again, few

experimental data exist, largely because of the difficulty in producing an antenna beam of small vertical dimension that is variable in elevation angle.

Continuous-Wave Experiments

Quantitative experiments using continuous-wave, as opposed to pulsed, radar systems are comparatively rare. If the approach followed in the foregoing discussion is pertinent to the natural situation, then there should be quite striking differences between the two types of system. It would be expected that the continuous-wave systems would experience a large advantage in sensitivity over the pulsed system, in addition to the usual band width advantage. The few experimental results now available, such as those of Forsyth and Vogan (1957), Collins (1958), and Collins and Forsyth (1959) tend to confirm this expectation. Some of these results were obtained with bistatic continuous-wave systems in which the transmitters were separated from the receivers by a distance of about 1000 kilometers. For bistatic systems the geometric considerations become more complex, but it is worth noting here that for these systems also there should be major differences between pulsed and continuous-wave systems. The pulsed system will have a sharp maximum of sensitivity for auroral structures located near the mid-point of the direct path from transmitter to receiver, and additional maxima for structures located well to either side of, and parallel to, the direct path. In contrast, the continuous-wave system will have a much more uniform sensitivity for structures located in various parts of the area of coverage.

CONCLUDING REMARKS

It is evident that if it is assumed that auroral radar echoes arise

(*a*) from configurations of ionization that are similar to the visually observable auroral structures, and,

(*b*) by means of volume scattering,

then many of the observed characteristics of the echoes may be explained simply. The author is well aware that the experimental support for this approach is far from conclusive. Many of the same characteristics may be explained just as convincingly, though perhaps not as simply, by various combinations of aspect-sensitive scattering centers. The existence of such scattering structures was first proposed to explain the strong northern peak in the azimuthal distribution of auroral radar echoes. It seems hardly likely that this peak is due exclusively to the combination of effects discussed in this paper, but it is very unlikely that they play no part at all in its formation. If this point of view is accepted then it is not possible to determine the aspect sensitivity of the individual scattering structures by study only of the azimuthal echo distribution.

Some method of separating the effects of aspect sensitivity from those of the volume scattering process discussed in this paper is clearly required. At first glance the small local maximum in the southern direction (see Fig. 2) for volume scattering might seem suitable. Unfortunately, this maximum tends to disappear with smoothing of the kind used to derive the distribution of Figs. 2(*d*), 2(*e*), and 2(*f*) (see also Fig. 4). For this reason, it is not likely to be easily

observed. On the other hand, for the particular case of a radar with a long pulse duration (say, more than 1 millisecond) and a very narrow beam width (one or two degrees) there might occur a local maximum in the azimuthal echo distribution for a beam direction parallel to the orientation of the auroral forms. The discovery of such a maximum would confirm the assumptions of this paper, but it would still be difficult to arrive at a quantitative evaluation of the aspect sensitivity of the scattering structures. Such an evaluation must await some more direct measurement, possibly a radar system capable of resolving an individual scattering center would also provide an indication of its shape.

REFERENCES

BOOKER, H. G. 1956. J. Atmospheric and Terrest. Phys. **8**, 204.
COLLINS, C. 1958. Can. J. Phys. **36**, 926.
COLLINS, C. and FORSYTH, P. A. 1959. J. Atmospheric and Terrest. Phys. **13**, 315.
CURRIE, B. W., FORSYTH, P. A., and VAWTER, F. E. 1953. J. Geophys. Research, **58**, 179.
CURRIE, B. W. and WEAVER, J. T. 1955. Can. J. Phys. **33**, 611.
FORSYTH, P. A. and VOGAN, E. L. 1957. J. Atmospheric and Terrest. Phys. **10**, 215.
GARTLEIN, C. W. 1959. Ann. de Geophys. **15**, 31.
HERLOFSON, N. 1947. Nature, **160**, 867.
JENSEN, R. E. and CURRIE, B. W. 1953. J. Geophys. Research, **58**, 201.
KAISER, T. R. 1956. The airglow and the aurorae (Pergamon Press, Ltd., London).
LYON, G. F. W. 1960. Can. J. Phys. **38**, 385.
PRESNELL, R. I., LEADABRAND, R. L., DYCE, R. B., SCHLOBOHM, J. C., and BERG, M. R. 1959. Unpublished.
STÖRMER, C. 1936. Geofys. Publikasjoner, **11**, 3 (12).
VESTINE, E. H. 1944. Terrestrial Magnetism and Atmospheric Elec. **49**, 77.
WEBSTER, H. F. 1957. J. Appl. Phys. **28**, 1388.

SPIN LATTICE RELAXATION IN NEODYMIUM ETHYLSULPHATE AT LIQUID HELIUM TEMPERATURES[1]

J. M. Daniels and K. E. Rieckhoff

ABSTRACT

The optical Faraday effect was used to measure instantaneous magnetization in neodymium ethylsulphate. The spin populations were disturbed by pulses of microwave power, and by adiabatic magnetization and demagnetization, and the approach to equilibrium was studied. The relaxation was found to be exponential and spin lattice relaxation times were measured, for temperatures between 1.3° K and 4.2° K, and for magnetic fields between 80 and 6000 oersted. The relaxation time was found to decrease with increasing magnetic field, and to vary with temperature approximately as $1/T^3$. No dependence of relaxation time on pulse length was found.

1. INTRODUCTION

The Faraday effect (the rotation of the plane of polarization of light passing through a material in a magnetic field) is very large, in general, in paramagnetic salts. The rotation of the plane of polarization is proportional to the magnetic moment of the salt, and for a single crystal of neodymium ethylsulphate the maximum rotation corresponding to saturation of the magnetization is about 114° per mm of path length for green mercury light (λ = 5461 Å) propagated along the optic axis (Becquerel *et al.* 1938). Thus, the Faraday rotation can be used to measure the spin temperature of a sample of one of these paramagnetic salts. It can also be used to detect changes in spin temperature (or relative populations of the spin states) under the influence of disturbing factors. For example, microwave radiation, of a frequency which produces paramagnetic resonance, alters the relative populations of the spin states, and produces a change in the Faraday rotation. This effect was predicted by Kastler (1951), a theory was given by Opechowski (1953), and the effect was verified experimentally for neodymium ethylsulphate by Daniels and Wesemeyer (1958) (see also Wesemeyer and Daniels (1958)). In the last publication, the authors used this effect to estimate the spin lattice relaxation time by the saturation method. The Faraday effect can, with suitable detection and presentation equipment, be used to measure *instantaneous* spin populations, and to follow the course of the spin populations as a function of time during the return to equilibrium from a disturbed state. It is thus a useful tool for a study of spin lattice relaxation, and this paper presents the results of such a study of neodymium ethylsulphate. Measurements were made in the temperature range 1.3° K to 4.2° K, and for fields between 80 and 6000 oersted.

2. EXPERIMENTAL PROCEDURE

The apparatus used was originally a conventional X-band paramagnetic resonance spectrometer, suitable for use at liquid helium temperatures, with a

[1]Manuscript received January 25, 1960.
Contribution from the Department of Physics, University of British Columbia, Vancouver 8, British Columbia.

transmission cavity and crystal video display. The microwave power, up to 140 mw, was supplied by a 2K39 klystron. The following modifications were made to enable the optical studies to be carried out:

(*a*) A magnet with a hole through the pole pieces parallel to the magnetic field was used.

(*b*) Two holes about 2 mm in diameter were made in the broad face of the cavity, near the center of the top of each face, to permit light to pass through the cavity and the crystal. The crystal was mounted on a removable choke plunger at the top of the cavity, as is usual.

(*c*) The cavity was immersed in liquid helium contained in a dewar vessel, and this was itself immersed in another dewar containing liquid nitrogen. The tails of these dewars were left unsilvered. A cylinder of copper foil was wrapped round the tail of the inner dewar and holes 4 mm×4 mm were cut in this to let the light pass through. Square windows of the same size were cut out of Scotch brand No. 33 electrical tape, and were stuck over the copper foil so that the inner dewar fitted tightly into the outer dewar. In this way, the path of the light was kept free of liquid nitrogen, and of nitrogen bubbles which would have introduced disturbing fluctuations into the transmitted light.

(*d*) The input coaxial line was critically coupled to the cavity, to ensure maximum power transfer. The output coaxial line was weakly coupled, and the current of the silicon–tungsten rectifier crystal was used only to monitor the tuning of the cavity and klystron.

(*e*) The modulation coils of the magnet, which are usually energized with 60-cycle alternating current to provide a field sweep, were not used for their normal function.

The light source was a General Electric mercury arc, type H100-4A. It was energized from a d-c. generator via a filter which stabilized the current in the arc, and reduced the ripple. The light passed through a collimator, a glass filter which passed the 5461 Å green mercury line, a Glan–Thompson polarizing prism, and a system of lenses to condense the light on to the sample in the cavity. The light which emerged from the cavity passed through another collimator, a Glan–Thompson prism analyzer, and was incident on the photocathode of an RCA 5819 photomultiplier. This experimental system is depicted in Fig. 1.

The photomultiplier voltages were supplied from batteries. The anode load was 10 kΩ, shunted by a 0.01 μf condenser to cut down the noise bandwidth. A galvanometer was put in series with the 10-kΩ resistor, and the voltage output from the anode circuit was connected to the Y_1 d-c. amplifier of a Cossor 1049 double beam oscilloscope. Time markers from a General-Radio 1217-A unit pulser were fed to the Y_2 plates of the oscilloscope. The trace of the oscilloscope was photographed. A Tektronix model 502 oscilloscope was used in later experiments. Before an experiment, the electrodes of the photomultiplier were prefatigued by running the photomultiplier for some 10 hours with a weak illumination on the cathode. The linearity of the recording system was then checked using the $\cos^2\theta$ transmission law for polarized light.

The neodymium ethylsulphate crystals were made from neodymium oxide

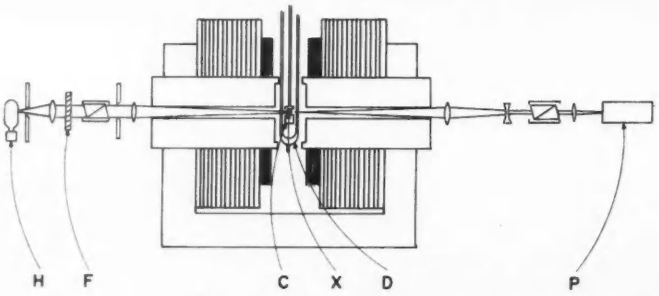

FIG. 1. Diagram of the apparatus. H, mercury arc; F, filter; C, cavity; X, crystal of neodymium ethylsulphate; D, dewar vessel; P, photomultiplier. For reasons of clarity, only one of the dewars is shown, and no attempt has been made to draw the details of the microwave cavity and its electrical connections.

supplied by the Lindsay Chemical Company. It is described as 99% pure, the impurities being 0.1% to 0.4% of each of praseodymium and samarium, and up to 0.5% of other rare earth oxides. The oxide was first converted into the sulphate by dissolving it in sulphuric acid and crystallizing. Barium ethylsulphate, freshly prepared according to Beilstein (1918), was added to the calculated amount of neodymium sulphate both in solution. The solution was filtered to remove the precipitated barium sulphate, and crystals were grown in a vacuum desiccator. The neodymium ethylsulphate was kept in a refrigerator until required. Single crystals were grown by a variety of methods, but one of the best was to leave about 10 cc of a saturated solution covered and undisturbed in a room at a fairly constant temperature for a week or two. It was usually possible to cut out a portion of one of these crystals which was sufficiently good optically for the experiments. Two faces, perpendicular to the optic axis, were cut and polished on these crystals.

When mounting a crystal in the cavity, care was taken that the hexagonal axis was parallel to the direction of propagation of light. This is necessary because the crystals are doubly refracting, and it was usually possible to adjust the orientation of the crystal so that the minimum intensity passed by the analyzer was about 1% of the maximum. This amount of ellipticity in the polarization of the emergent light can introduce errors of up to 2° in the measurement of the Faraday rotation.

The temperature of the helium bath was maintained by pumping on the liquid helium through a throttle valve. The pressure above the liquid helium was measured using a mercury and an oil manometer, and was kept constant by manual adjustment of the throttle valve. The temperature of the bath was obtained from this measured pressure.

A multivibrator, which delivered square pulses to the reflector of the klystron, was used to switch the klystron on and off. The pulse length could be varied between 8 and 124 mseconds. The multivibrator could either run free at about one cycle every 2 seconds, or could be manually triggered to give single pulses. The leading edge of the pulse was used to trigger the oscilloscope sweep. The

paramagnetic resonance line is so wide that at liquid helium temperatures 100 mw of microwave power is sufficient to saturate the spin system at all fields between about 800 and 2000 oersted.

The procedure during an experiment was more or less as follows. First the throttle valve on the helium pumping line was set, and the helium bath was allowed to come to equilibrium. Only minor adjustments of the throttle valve were needed subsequently to maintain this temperature. The alignment of the crystal was then checked. A curve of the Faraday rotation, as a function of magnetic field, was obtained by rotating the analyzer to a position of minimum

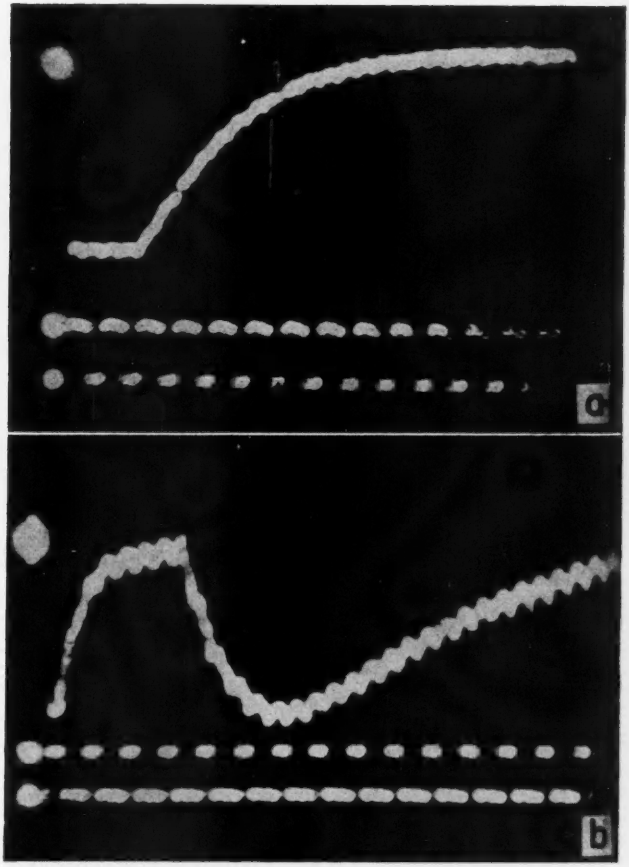

FIG. 2. Typical oscilloscope traces showing the saturation due to the microwave pulse, and the subsequent relaxation. The time markers are 1/30 sec apart. The irregularities on the trace are 60 cycle pickup from the stray light in the room. Figure 2*b* shows a trace in which the rotation is so large that the transmission through the analyzer prism passes through a minimum.

photomultiplier current for various values of magnetic field. The rotation was read off from a scale of degrees on the analyzer housing. The klystron was then switched on, and the multivibrator adjusted so that the pulses brought the klystron into tune with the cavity. Next, a value of the magnetic field was selected, and the analyzer was adjusted to some convenient position, usually 45° from the position of minimum transmission. Finally pulses of microwave power were fed into the cavity, and photographs of the oscilloscope trace were taken. This procedure was repeated for different fields and temperatures. The photographs, which were on 35-mm film, were mounted on the stage of a low power binocular microscope, with millimeter graph paper behind, and the trace was measured by visual inspection. Figure 2 shows some typical traces.

Another series of experiments was carried out without using microwave power at all. It was found that, by connecting the modulation coils of the electromagnet to a 110-v d-c. supply, the field could be changed by some 250 gauss, coming to equilibrium in about 10 mseconds. When the field is thus suddenly changed, the spin temperature is changed also, a process of adiabatic magnetization or demagnetization. This technique has the advantage that it can be used at any field, and is not confined to the region 800 to 2200 oersted in which microwaves are absorbed. It has the disadvantage, however, that the change in population, and hence rotation, which is produced is much less than can be produced by microwave absorption near resonance.

3. RESULTS

According to the phenomenological theory of relaxation, the difference in the populations of the two spin states of the Nd^{+++} ion, ν, follows an equation

$$\frac{d\nu}{dt} = -\frac{\nu-\nu_0}{\tau} - W\nu; \tag{1}$$

τ is the spin lattice relaxation time, ν_0 is the equilibrium value of ν, determined by the bath temperature, and W is a factor which is proportional both to the absorption coefficient of the crystal, and to the microwave energy in the cavity. In the presence of some radiation in the cavity, a steady state value ν_1 is reached where

$$\nu_1 = \nu_0/(1 + W\tau),$$

whence equation (1) becomes

$$\frac{d\nu}{dt} = -\frac{(\nu-\nu_1)\nu_0}{\nu_1\tau}. \tag{2}$$

Hence ν relaxes exponentially to ν_1 with a time constant $\tau\nu_1/\nu_0$. Since the Faraday rotation θ is proportional to ν, we can expect θ to relax to a value θ_1, somewhat less than the rotation θ_0 measured with no microwave power in the cavity. This relaxation should be exponential with a time constant $\tau\theta_1/\theta_0$. Experimentally, it was difficult to adjust the multivibrator so that the klystron was switched off completely during the off-period; there was usually a small radiation background in the cavity, hence this correction for background radiation is important.

The Q of the cavity was about 10,000, hence the time constant for the radiation in the cavity to come to equilibrium was about 10^{-6} sec. This is so much less than τ that radiation reaction effects are negligible, and the radiation in the cavity can be considered to be in equilibrium at all times.

The Faraday rotations, θ, obtained from the photographs, were plotted as a function of time on semilog paper. In every case, straight lines were obtained covering up to 90% of the whole decay, and the slope of these lines gave $\tau\theta_1/\theta_0$. We estimate an accuracy of $\pm 10\%$ in the final values of τ.

The first topic to be investigated was the effect of the length of the microwave pulse on the relaxation time. Speculations have been raised that in the principal mode of relaxation at low temperatures the ions give their energy to a relatively narrow band of lattice vibrations, which in turn gives its energy to the other lattice vibrations. Van Vleck (1941*a*, *b*) suggested that the observed relaxation times might depend on the rate of transfer of energy between the lattice vibrations rather than on the rate of transfer of energy between the ions and the lattice vibrations, and one criticism of almost all theories of relaxation is the assumption of thermal equilibrium among the lattice vibrations. While microwave power is being absorbed by the crystal, energy is being fed into the lattice, and there is always the possibility that when the microwave power is switched off and the system begins to relax, the lattice is in a non-equilibrium state with a consequent change in the relaxation time. Measurements were made at different temperatures and fields for pulse lengths between 8 and 124 mseconds. In no case was there found any dependence on pulse length. The result of a typical set of measurements is shown in Table I. Measurements

TABLE I

Measured relaxation times at 1.685° K and 1540 gauss, for different pulse lengths (two measured relaxation times for each pulse length)

Pulse length, msec	Relaxation time, msec	
8	145	135
17	136	162
35	155	134
63	125	166
124	147	136

were made of relaxation time as a function of field and temperature. These were possible between about 800 and 2500 gauss, outside this range the absorption of microwaves was so small that it was not possible to disturb the population of the spin level sufficiently with the power available. Since an accuracy no better than 10% is claimed for these measurements, there is no advantage in trying to present them in graphical form, as the picture would be somewhat confused. Instead we present these results as a table (Table II) and we would like to point out that the values quoted are the experimental measurements. They are in no way smoothed, and are quoted to at least one figure more than is significant, in order to give an idea of the spread of the points. We see that

TABLE II

Relaxation times as a function of temperature and magnetic field, measured by the microwave method. Times in mseconds. These are unsmoothed measured values of accuracy not more than ±10%

H, gauss / *T*, °K	780	1030	1290	1540	1790	2040	2290	2540
1.380	184	196	208	170	163	126	121	125
1.542	129	134	154	144	141	121	118	116
1.685	116	176	159	144	155	151	117	108
1.875	57	67	75	68	67	68	64	65
2.06	—	69	72	73	67	65	63	61
4.22	—	—	11	11	13	16	—	—

the values of relaxation time decrease rapidly with temperature, and that they decrease gradually with increasing magnetic field, with a broad maximum in the neighborhood of 1500 gauss.

The results of relaxation times measured by the technique of suddenly changing the applied magnetic field are shown in Fig. 3. These cover a much

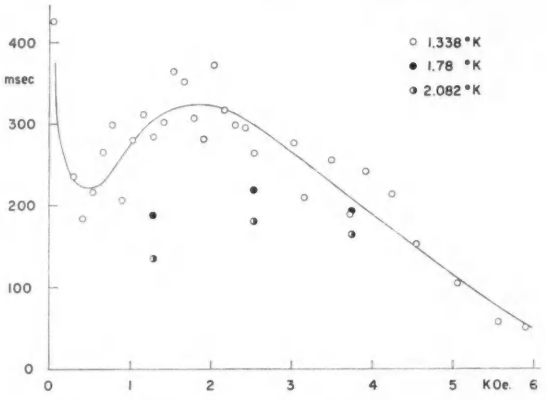

FIG. 3. Relaxation time as a function of magnetic field. The few measurements at 1.78° K and 2.082° K were done with crystal No. 2.

larger range of field, but this method is inherently less accurate than the microwave method, since the relatively small change in the field used, 250 gauss, produces a much smaller change in the Faraday rotation than can be obtained using microwaves. All the measurements made with the microwave method, and also the long series, using the change of applied field, at 1.338° K were made on the same crystal of neodymium ethylsulphate. The other results depicted in Fig. 3 were made from a different crystal, grown, however, from the same batch.

Figure 4 is a series of log–log plots of relaxation time against temperature for four chosen fields, 1290 gauss, 1540 gauss, 1790 gauss, and 2040 gauss. The values for the last three fields for the second crystal are obtained by interpola-

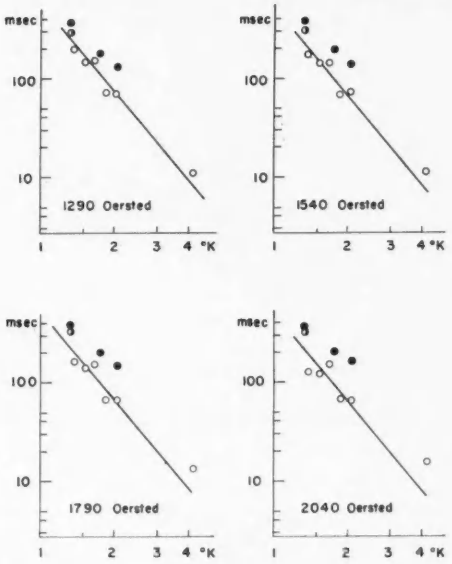

FIG. 4. Relaxation time as a function of temperature (log–log plot) for four different fields. The solid line drawn through the points has a slope of -3. Open circles, values using pulses of microwave power, taken from Table II; half open circles, values using adiabatic demagnetization corresponding to the solid curve in Fig. 3; solid circles, values using adiabatic demagnetization on crystal No. 2, obtained by interpolation from Fig. 3.

tion from Fig. 3, and should not carry much weight; however, they are significantly higher than the values for the first crystal. This is not surprising, since there is ample evidence that relaxation times are very sensitive to impurities of all kinds. The accuracy of the measurements is too poor to draw any definite conclusions about the temperature dependence of the relaxation time; the point at 4.22° K, which should carry much weight, is the least accurate of all. However, it can be said that the relaxation time varies with temperature in a manner somewhere between $\tau \propto T^{-2}$ and $\tau \propto T^{-3}$. Our results seem to favor an exponent nearer to -3 than to -2, and the lines drawn through the points in Fig. 4 have a slope -3.

Figure 5 shows a curious phenomenon, observed on one crystal which was later accidentally destroyed, and which we have not been able to repeat. It is seen that, after a long pulse of microwave power, the Faraday rotation increases to a value greater than that which corresponds to the bath temperature, and slowly returns to its equilibrium value. It seems inconceivable that the spin system should cool to a temperature below that of the bath and we suggest the following as a likely explanation. We assume that the crystal was not a single crystal and that in one part the direction of propagation of light, and the external magnetic field, were not parallel to the hexagonal axis. We assume further that the relaxation time is a function of the angle between the external

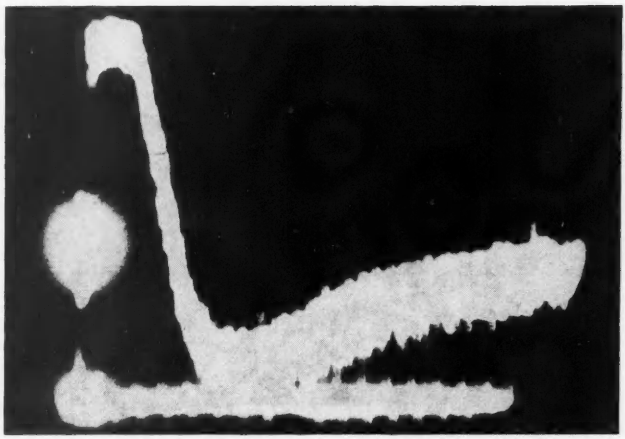

FIG. 5. The "overshoot phenomenon". Note that the overshoot occurs during the relaxation, but not during the saturation period.

field and the hexagonal axis. When the microwave power is applied, the populations of the spin levels are equalized at approximately the same rate in both parts of the crystal, since the approach to equilibrium is governed principally by the microwave field. When the microwave power is turned off, the two parts of the crystal return to equilibrium at different rates. The intensity of the light passed by the analyzer is a complicated function of time, since in at least one part of the crystal the light suffers double refraction as well as Faraday rotation. A qualitative analysis of this problem, which it is inconvenient to reproduce here, has been given by Rieckhoff (1959) and it is shown that such an "overshoot" can occur if the relaxation time is shorter in the part of the crystal which has the field parallel to the hexagonal axis.

4. CONCLUSIONS

We present these results principally as an example of a new technique for the measurement of relaxation times. So far, very few measurements have been made of relaxation time for one salt over an extensive range of fields and temperatures, except for the Dutch work on chromium potassium alum (Kramers *et al.* 1950). The methods used to measure relaxation times in the past have been (*a*) that of de Haas and du Pré (1939), in which the real and imaginary parts of the a-c. susceptibility are measured at audio frequencies; (*b*) the study of the steady state saturation of paramagnetic resonance absorption (Eschenfelder and Weidner 1953); and (*c*) the use of the strength of the paramagnetic resonance signal as an instantaneous spin temperature thermometer to follow the return to equilibrium after the spin populations have been disturbed by a pulse of microwave power (e.g. Giordmane *et al.* 1958; Davis *et al.* 1958; Bowers and Mims 1959). The first two methods do not observe the relaxation directly, being steady state methods, and there are reasons for doubting the results of the method of de Haas and

du Pré in some cases. For instance, the locus of the point which represents the magnetic susceptibility in the $\chi' \chi''$ plane should be a semicircle, and the experimental results of Benzie and Cooke (1950) show curves far from semicircular in some cases. The same criticism might be levied against the method of steady state saturation of the paramagnetic resonance signal. Just like the method of de Haas and du Pré, its interpretation rests on the assumption of the basic relaxation equation (1) and there is in this method no means of checking this equation. These results should, therefore, be interpreted with caution, as it is now known that the relaxation process is quite complicated. What is needed is a means of observing directly and instantaneously the populations of the various spin levels. This facility exists in the third method and also in our method. Unfortunately, for technical reasons, the use of paramagnetic resonance as a spin thermometer limits the measurements to certain values of magnetic field for which oscillators are available. The use of the Faraday effect is not limited to certain values of the magnetic field, however it can measure only an average of the spin populations, whereas paramagnetic resonance can measure the population differences between individual levels where the resonance absorption lines are resolved. This is an advantage where more than two spin levels are involved, and, for example, where cross pumping is to be investigated. The Faraday rotation is, unfortunately, rather small in most substances, but there is good reason to believe that with a little attention to the instrumentation it should be possible to attain an adequate signal-to-noise ratio with the arrangement that we describe. Thus we may claim that the use of the Faraday rotation is an interesting new technique for investigating paramagnetic relaxation.

The results are presented merely as measured values; it would be impossible to interpret them in terms of a theory of relaxation since there is no adequate theory at the present time. The mechanism which is believed to be responsible for the relaxation has been described by van Vleck (1940, 1941*a*, *b*). However, the agreement between this theory and experiment has always been poor, as has also been the agreement between different experiments. For example, van Vleck predicts that for chromium potassium alum, the relaxation time should vary as $1/T$ in the liquid helium range. de Vrijer and Gorter (1952) found a dependence as $T^{-2.6}$, while Kramers, Bijl, and Gorter (1950) found a dependence as T^{-3}, and Eschenfelder and Weidner (1953), who found a dependence as $1/T$, are the only workers whose results agree with van Vleck's theory. So far, no one has succeeded in verifying the predictions of van Vleck's theory with regard to the dependence on field.

We may review some of the more important assumptions of van Vleck's theory, as these give an indication of the direction in which further efforts should be directed. They are:

(i) That there is thermal equilibrium in the spin system.
(ii) That there is thermal equilibrium in the lattice.
(iii) That there is good heat contact between the lattice and the helium bath.
(iv) That the frequency spectrum of the lattice is a Debye spectrum.
(v) That spin–spin interactions play no part in the spin lattice relaxation process.

Items (ii) and (iii) have received attention from many workers, and there is still no really convincing experimental evidence on these two points. For instance, the conclusions of Eisenstein (1951) and Giordmane *et al.* (1958) on this point are in direct contradiction. Item (iv) should not be very important at low temperatures. The most serious assumption is that contained in (i) and (v). We can say generally that in concentrated paramagnetic salts the interactions are strong enough to establish thermal equilibrium in a time of the order of 10^{-6} seconds, but that this is by no means true in dilute salts, so that a distinction must be drawn between these two cases. Where there is a strong interaction between the spins, it is unreasonable to expect no influence on the relaxation time, and it is now well known that if the separation between two levels is the same as that between another two levels, there is a ready transfer of energy between systems whose state is one of the first pair, and systems whose state is one of the second pair. This produces a shortening of the relaxation time, and is the basis for the control of relaxation times in masers by "doping". In our experiments, we must remember that neodymium has two isotopes with nuclear spin different from zero: Nd143, 12.2% abundant, and Nd145, 8.3% abundant, both with spin 7/2. The ions containing these isotopes have a hyperfine structure, and the condition for a three-spin process occurs at about 800 oersted. This may explain the initial dip in the relaxation time as a function of magnetic field (Fig. 3).

We feel that the theory of relaxation is in too poor a state, and that our measurements are not sufficiently accurate to attempt any further explanation of our results.

ACKNOWLEDGMENTS

We would like to express our thanks to the National Research Council of Canada for a grant-in-aid which enabled the research described here to be carried out. One of us (K. E. R.) is also indebted to the National Research Council for a bursary during the tenure of which this work was done. We must express our thanks to Miss Marilyn S. Jay, who measured most of the photographs taken during this course of experiments.

REFERENCES

BECQUEREL, J., DE HAAS, A., and VAN DEN HANDEL, J. 1938. Physica, **5**, 753.
BEILSTEIN, F. K. 1918. Handbuch der Organischen Chemie. Vol. I (Springer-Verlag, Berlin), p. 325.
BENZIE, R. J. and COOKE, A. H. 1950. Proc. Phys. Soc. A, **63**, 201.
BOWERS, K. D. and MIMS, W. B. 1959. Phys. Rev. **115**, 285.
DANIELS, J. M. and WESEMEYER, H. 1958. Can. J. Phys. **36**, 405.
DAVIS, C. F., Jr., STRANDBERG, M. W. P., and KYHL, R. J. 1958. Phys. Rev. **111**, 1268.
EISENSTEIN, J. 1951. Phys. Rev. **84**, 548.
ESCHENFELDER, A. H. and WEIDNER, R. T. 1953. Phys. Rev. **92**, 869.
GIORDMANE, J. A., ALSOP, L. E., NASH, F. R., and TOWNES, C. H. 1958. Phys. Rev. **109**, 302.
DE HAAS, W. J. and DU PRÉ, F. K. 1939. Physica, **6**, 705.
KASTLER, A. 1951. Compt. rend. **232**, 953.
KRAMERS, H. C., BIJL, D., and GORTER, C. J. 1950. Physica, **16**, 65.
OPECHOWSKI, W. 1953. Revs. Modern Phys. **25**, 264.
RIECKHOFF, K. E. 1959. M.Sc. Thesis, University of British Columbia, Vancouver, B.C. p. 64.

VAN VLECK, J. H. 1940. Phys. Rev. **57**, 426.
——— 1941*a*. Phys. Rev. **59**, 724.
——— 1941*b*. Phys. Rev. **59**, 730.
DE VRIJER, F. W. and GORTER, C. J. 1952. Physica, **18**, 549.
WESEMEYER, H. and DANIELS, J. M. 1958. Z. Physik, **152**, 591.

TRANSISTORIZED POWER SUPPLIES FOR A MASS SPECTROMETER[1]

R. D. Russell and Frank Kollar

ABSTRACT

While a mass spectrometer itself may require a few hundred watts of regulated power for the magnet and only a few watts of regulated power for all other purposes, the regulating supplies often dissipate kilowatts. The construction of more efficient supplies using transistors and magnetic amplifiers results in substantial savings in the physical size of the supplies, the cost of their component parts, and the effort required for maintenance.

Circuits and descriptions are presented for a magnet current power supply and a filament emission control that have been used in the mass spectrometer built recently at this laboratory. These illustrate the simplicity possible with transistor-regulated supplies, as well as the savings mentioned above. The mass spectrometer is a 12-in. radius 90° instrument used at mass 250 with a 5000-volt accelerating voltage. The magnet, which supplies a field of more than 5000 gauss over an area of 800 cm^2 and across a gap of 1.9 cm, and which weighs three quarters of a ton, is supplied from a regulated supply dissipating about 50 watts. The filament emission control takes about 30 watts from the mains.

INTRODUCTION

The electronic supplies associated with mass spectrometers have shown remarkably few fundamental changes in the past fifteen years, despite the very great advances that have been made during that time in the field of applied electronics. After working for a number of years with conventional mass spectrometer electronic circuits and then for the last year with an instrument using transistors and magnetic amplifiers, the writers are completely convinced of the superiority of these more modern components in almost every mass spectrometer circuit, and of the fact that they are not more widely used now simply because most mass spectrometrists are unfamiliar with them. The object in our making these circuits available is primarily to demonstrate some of the advantages of transistor-operated power supplies in mass spectrometers.

In the construction of a mass spectrometer at this university, it was decided to use transistor regulators for both the magnet current power supply and the filament emission control. The magnet current power supply was constructed from a combination of transistor, vacuum tube, and magnetic amplifiers; the filament emission control uses only transistors. Both supplies have proved efficient, rugged, and inexpensive, and both have required negligible maintenance.

The mass spectrometer itself is a general purpose gas-source mass spectrometer, intended initially for the analysis of lead tetramethyl. It uses a copper tube having a 12-in. radius of curvature, and an accelerating voltage of 5000 v.

[1]Manuscript received January 4, 1960.
Contribution from the Geophysics Laboratory, Department of Physics, University of British Columbia, Vancouver 8, B.C.

A modified grid-ratio measuring system is used to measure the ion current intensities. This incorporates a servo voltmeter of 0.025% linearity and reproducibility. The measuring system will be described in a future publication.

THE MAGNET CURRENT SUPPLY

The magnet is constructed from a mild steel ("boiler plate") yoke with armature and pole pieces from Armco iron. The area of each pole piece is 800 cm² and the distance between them is 0.7500±.0005 inch. The reluctance of the magnetic circuit is substantially that of the air gap and therefore the magnetizing curve is linear except at very high fields. The magnet coils contain a total of 21,000 turns of No. 18½ A.W.G. copper wire having a total resistance, when connected in series, of 720 ohms. The inductance of the magnet calculated from the above figures is 2100 henrys. However, the effect of eddy currents becomes significant at frequencies higher than about 0.2 cycle per second. The impedance of the magnet is shown as a function of frequency in Fig. 1. The data for this figure was obtained at higher frequencies

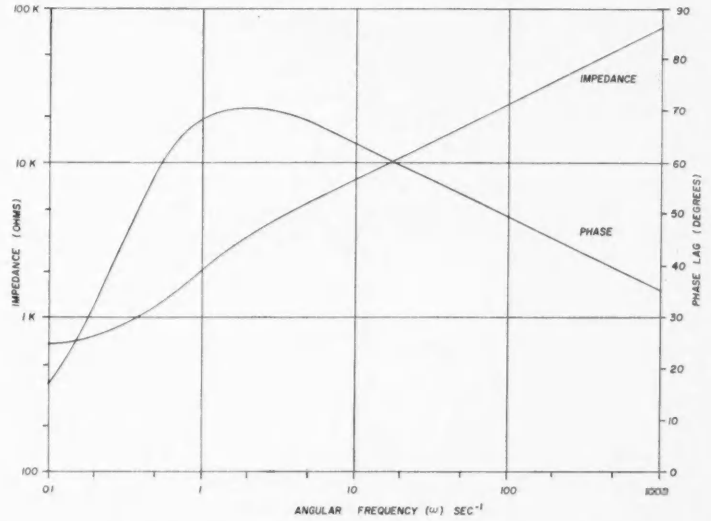

FIG. 1. Approximate impedance characteristics of the magnet measured at its terminals.

by determining the amplitude and phase of the current produced by a small sinusoidal driving voltage, and at lower frequencies by analyzing the response due to a voltage step. The characteristic applies at zero d-c. current and can be expected to be different in detail at high fields. The magnet characteristics are a dominant term in the over-all transfer function of the magnet current power supply and the knowledge of its form is necessary to obtain optimum stability and speed of response of the over-all circuit (see Savant (1958) for a general discussion of this subject).

The maximum magnet current used is 500 ma, at which current the magnet voltage is 360 v and the power dissipated is 180 w. The measured field is 5500 gauss at this current, sufficient to analyze masses to nearly 300 with the maximum accelerating voltage.

The circuit for the regulator is shown in Fig. 2. It incorporates two regulating devices, the saturable reactor which is a slow device, and the transistor

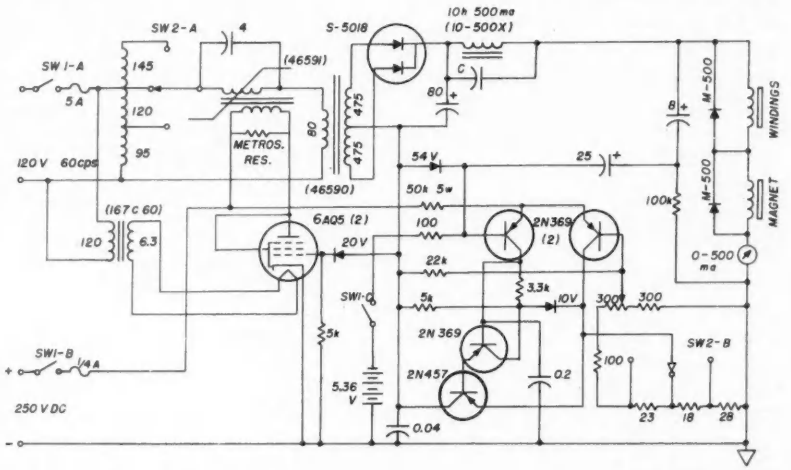

FIG. 2. Magnet current supply. Condenser values are given in microfarads, resistors in ohms. Zener diodes are identified by their breakdown voltages. Transformer and reactor numbers in parentheses are Hammond type numbers. The condenser C is chosen for minimum ripple (0.2 μf).

circuit, which has a fast response. One important function of the saturable reactor circuit is to keep the voltage across the control transistor at a suitable level. However, it also contributes significantly to the regulating action. Thus the regulation is seriously impaired if the saturable reactor is removed and the power transformer is supplied a suitable fixed input voltage by means of a variable voltage transformer (e.g. a Variac).

The supply operates as follows. The voltage of the mains is fed through an auto transformer to the primary of the power transformer connected in series with the saturable reactor. The auto transformer adjusts the supply voltage close to the optimum value for the different current ranges employed. Since the saturable reactor can itself produce changes in the transformer voltage by approximately a factor of 10, the auto transformer could probably be omitted, but the regulation would be somewhat impaired, particularly at very high and very low currents. A full wave rectifier is employed with a condenser input filter. The filtering circuit used is in the same servo loop as the saturable reactor, which has a long time constant resulting from the large inductance of the d-c. winding. A conventional LC filter introduces additional phase lags and causes a deterioration in the transient characteristics of the

over-all system. Thus the tuned 120-cycle rejection circuit shown is used to reduce ripple. The remaining ripple, the order of 1 volt, is easily handled by the transistor regulator circuit. The output from the filtered power supply is connected to the magnet windings in series with the 2N457 control transistor and a series resistor, the voltage drop across which resistor serves as a measure of the magnet current. The sum of the voltages across the control resistor and transistor regulates the bias of the triode operated 6AQ5 vacuum tubes controlling the saturable reactor current. This serves to hold the voltage drop across the control transistor to a reasonable value (about 30 volts) at all magnet current ranges, and well below the 60-volt maximum rating of the transistor. The control transistor is rated at a current of 5 amp maximum and a power dissipation of the order of 50 watts. Therefore the maximum magnet current that can be delivered by the supply is here limited to 500 ma only by the transformer, choke, and saturable reactor ratings.

Two 2N369 transistors are used as a difference amplifier, comparing a fraction of the voltage developed across the series control resistor with the 5.36 v produced by four mercury cells which serve as the basic reference. This reference voltage is high enough so that pickup and drift in the difference amplifier inputs can easily be made negligible. We feel that the use in this circuit of a very low reference voltage (50 mv) as suggested by Garwin (1958) and Garwin *et al.* (1959) would not only exaggerate problems of noise but sacrifice loop gain needlessly and therefore require additional gain in the electronic circuits increasing the problems of stability. In this circuit the mercury cells are quite stable and have a long life, and therefore seem to be a convenient reference; if the use of batteries were considered undesirable, a Zener diode would provide an excellent reference. A third 2N369 isolates the power transistor from the difference amplifier. This transistor is essentially an emitter follower, matching the a-c. and d-c. impedances of the difference amplifier to the power transistor. The 10-v Zener diode stabilizes the collector supply voltage for one transistor in the difference amplifier otherwise the gain would be greatly reduced by negative feedback. The difference amplifier is designed so that the collector voltages are almost identical at all operating currents. The 20-v Zener diode adjusts the operating point of the 6AQ5, and thereby adjusts the range of voltages across the control transistor. The 22k resistor provides some positive feedback, thereby increasing the loop gain.

The 54-v Zener diode protects the circuit against switching or other transients that might result in exceeding the voltage rating of the 2N457. The M-500 Sarkes Tarzian diodes protect the magnet windings from a voltage transient when the supply is shut off. Many diodes would be equally suitable, but in any case best results can be obtained by measuring the reverse characteristics and selecting diodes of low reverse current. The characteristics of these silicon diodes were quite variable.

In the construction of the unit, care must be taken to eliminate a-c. pickup in the inputs to the difference amplifier. In particular it was found worth while to use bifilar-wound control resistors. The transistor amplifier was built on a heat sink made from 3 in. $\times$ 2 in. $\times$ 1/8 in. aluminum channel,

4 inches long, which plugs into an octal socket. The performance of the remainder of the circuit can be easily checked by unplugging this unit and replacing it by a variable power resistor of 50–300 ohms resistance. Thus the saturable reactor circuit can be checked independently of the transistor circuit. Similarly replacing the 6AQ5 tubes by a suitable resistor permits the transistor unit to be tested independently of the saturable reactor control loop. The a-c. power for the supply is obtained from a Sola regulating transformer and the d-c. from a 250-v Sola d-c. supply. These supplies were available for other parts of the mass spectrometer; otherwise the d-c. could be obtained from a simple circuit with silicon rectifiers. The performance of the supply does not deteriorate very much if the Sola regulating transformer is not used.

A 10-v step in the input line voltage (without the a-c. Sola regulator) results in a 0.012% change in magnet current. The stability of the current is in the order of 1 part in 25,000 for variations of periods in the order of seconds or minutes, and the ripple current is less than this if the filter is reasonably well tuned so that the transistor amplifier is not overdriven. This is not only because the ripple voltage is greatly reduced by the a-c. degenerative feedback, but also because of the high coil impedance at 120 c.p.s. (see Fig. 1).

The difference amplifier transistors are individually quite temperature sensitive. The slow drift resulting from this can be minimized by arranging that the temperatures of these transistors are always equal. A further improvement in long term stability might be achieved with silicon transistors in this part of the circuit.

Power losses are quite small. At maximum current there are about 15 watts dissipated on the power transistor, 5 watts on the control resistor, 5 watts on the 6AQ5 filaments, and about 25 watts in the 6AQ5 plate circuit. The power delivered to the magnet is about 180 watts, giving an over-all efficiency of more than 75%. The cost of the electronic components was in the order of $150 not including the meter, which is a mirror scale instrument of 1% accuracy imported from Denmark at a cost of $40 and the magnet coils which were manufactured commercially at a cost of $650. The meter has, in addition to the current scale, a scale proportional to the square of the current, which is useful as a mass indicator.

A number of modifications could be considered in the design. The use of 400 cycles or higher frequency power is possible and at present we feel this would be worth while. The substitution of transistors for the 6AQ5 is an obvious change that would require only a change of resistance of the d-c. winding of the saturable reactor. Thyratron regulators could substitute for the saturable reactor, as grid-controlled rectifiers. Since the supply was built, silicon-controlled rectifiers have appeared on the market and these also seem to offer an attractive substitute for the saturable reactor. In either case the speed of response and gain of the "slow" loop could be greatly increased, and this in turn would make the filter design less critical.

THE FILAMENT EMISSION CONTROL

The circuit for this unit is shown in Fig. 3. It is a straightforward regulated power supply using a series transistor as the regulating element. This trans-

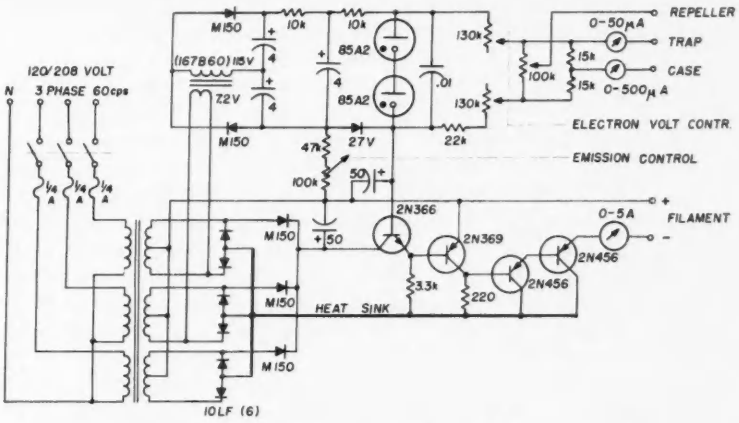

FIG. 3. Filament emission control. Component identification is the same as in Fig. 2. Three-phase transformer secondaries are 9-v center-tapped windings insulated to 5 kv. The resistance of the filament and 5A meter, including interconnecting cables, must not exceed 1 ohm, unless the secondary voltages of the three-phase transformer are increased accordingly.

istor can easily regulate the 5-amp current used at a voltage drop of less than 2.5 volts. Obviously no vacuum tube will operate at these currents and voltages and therefore this type of circuit is only possible with transistors.

A three-phase 120/208-v service was available at this laboratory, and therefore a three-phase input – six-phase output transformer was used for the filament supply to give a low ripple without additional filtering (approximately 4.5% r.m.s. in the d-c. voltage). A similar result could be obtained by using a full wave single phase rectifier with a large condenser (several tens of thousands of microfarads) or an LC filter. In some cases the large ripple of an unfiltered supply might not be considered objectionable.

The 2N456 control transistor is connected with a second similar transistor in the Darlington compound arrangement (Shea 1957) to provide a large value of current gain and therefore a sufficiently low base current (typically 0.7 ma). This pair is driven by a 2N369 voltage amplifier, which in turn is driven by a 2N366 emitter follower. The forward voltage drops across the emitter-base diodes of the latter two transistors approximately cancel and therefore at balance the error signal, which is applied between the base of the 2N366 and the emitter of the 2N369, is very nearly zero. The error voltage is the difference between the voltage developed across the 100k helipot and its series resistor, and the reference provided by the 27-v Zener diode.

In addition there are two supplies of very low power. One is a glow-tube-stabilized supply to provide the electron accelerating voltage and the trap bias in the mass spectrometer source, as well as providing current for the 27-v Zener. This supply uses the smallest available filament transformer connected backwards so that 7.2 v r.m.s. from the three-phase transformer is applied across its 6.3-v winding, the voltage developed in the primary being rectified

with silicon diodes in a simple doubler circuit. This arrangement avoids the necessity of having a second transformer insulated for the 5000-v accelerating voltage. The second supply is a low voltage three-phase silicon rectifier circuit which supplies the emitter follower. The three-phase power was available from the main transformer secondary, and using it simplified the filtering.

This supply is physically the smallest used in our mass spectrometer. The electronic units, including the two subsidiary power supplies and the required heat sinks for the power transistors and silicon rectifiers fit entirely into a chassis 2 in. × 8 in. × 10 in. This chassis floats to 5000 v when the mass spectrometer is operating and is suspended inside a somewhat larger grounded chassis, thus eliminating the possibility of corona discharges around small components and providing increased safety. The transformer is mounted on the subsidiary chassis and the meters are mounted separately on the front panel with the various controls. The supply input power is less than 30 w. The supply cost approximately $100 plus the cost of the meters.

The regulation of the supply is quite adequate, the measured r.m.s. variation in electron current being in the order of one or two parts in 10,000. The supply requires no warm-up time and exhibits remarkably little drift in view of the fact that the base current of the 2N366 shuts the 100k control helipot. The electrolytic condenser in parallel with the error signal is necessary for a well-damped system and has not caused any of the difficulties we had anticipated, perhaps because the maximum voltage across it is tens of millivolts.*

CONCLUSIONS

Certain of the regulated power supplies normally used with a mass spectrometer lend themselves well to conversion to transistor-operated circuits. Normally the actual power used by the mass spectrometer itself is very small, while the regulating supplies dissipate several kilowatts. It is to be expected that an increased efficiency would not only simplify problems of construction, but require fewer expensive components and less maintenance. Therefore it is well worth the effort to modernize the usual mass spectrometer power supplies.

Two supplies have been described in this paper, a magnet current power supply and a filament emission control. These supplies illustrate well the relative simplicity of transistor-operated mass spectrometer circuits and have now been used long enough in our mass spectrometer so that we can be confident that they will continue to work well in their present form. Although both supplies are quite adequate for our needs, they would probably have to be modified somewhat for different mass spectrometers. Certainly the regulation and stability of either could be further improved if this were necessary. Circuits we are presently designing for a second mass spectrometer differ from these primarily in using transistorized d-c.–d-c. converters at higher frequencies (hundreds of cycles per second) to utilize still smaller and less expensive components, and obtain better servo characteristics in some cases.

*We later replaced this condenser with a 4-μf condenser between base of the 2N366 and the negative side of the filament. This further improved stability and reduced ripple.

ACKNOWLEDGMENTS

The construction of the mass spectrometer whose circuits are described here was financed by the National Research Council of Canada through a grant to Prof. J. A. Jacobs. The impedance characteristics of the magnet were measured by T. J. Ulrych. The technical assistance of J. S. Stacey and P. Neukirchner is acknowledged with thanks. The manuscript was typed by Mrs. S. Maxwell.

REFERENCES

GARWIN, R. L. 1958. Rev. Sci. Instr. **29**, 223.

GARWIN, R. L., HUTCHINSON, D., PENMAN, S., and SHAPIRO, G. 1959. Rev. Sci. Instr. **30**, 105.

SAVANT, C. J., Jr. 1958. Basic feedback control system design (McGraw-Hill Book Co., Inc.).

SHEA, R. F. (*Editor*). 1957. Transistor circuit engineering (John Wiley & Sons, Inc.), p. 130.

CORRELATION STUDIES OF RADIO-AURORA, MAGNETIC, AND EARTH-CURRENT DISTURBANCES[1]

B. K. BHATTACHARYYA[2]

ABSTRACT

Correlation studies of the radar echo occurrence rate from aurora in half-hourly intervals at Ottawa, S and S_d components of the horizontal magnetic field H at Agincourt, and the disturbance diurnal variation of earth current at Crow River have been carried out. Short-time variations in auroral echo strength and moderate perturbations in H have also been correlated. The auroral echo occurrence rate seems to have a diurnal variation characteristic similar to that of H. It is found that auroral activity always precedes magnetic activity. The variation of the delay time between the two phenomena shows a local time dependence, being practically constant and quite small (0–15 minutes) before local midnight and increasing afterwards. This variation of the delay time appears to have a connection with reports of others regarding reversal of the direction of auroral ionization drift from west to east somewhere around midnight with subsequent magnetic perturbations which change from positive to negative.

No definite conclusion could be reached regarding the relationship of earth current to other factors because of a practically random variation of cross-correlation coefficients from month to month.

INTRODUCTION

The interrelationship between magnetic disturbance and auroral activity has been known for a long time. More recently, attempts have been made to establish a systematic relationship between the two phenomena with the help of visual, photographic, and radio data of aurora on the one hand, and magnetograms recording the three components of the magnetic field on the other.

Firstly, with the help of visual aurora data, striking relationships between the two phenomena have been obtained. The control of the degree of magnetic disturbances over the maximum elevation of aurora above the northern horizon at Saskatoon has been shown (Meek 1953, 1954). A relationship between the 3-hour range K index and the auroral position in the sky at Ithaca has been empirically derived (Gartlein 1944). Time sequences and spatial relations in auroral activity during magnetic bays at College Alaska have been studied in great detail (Heppner 1954). Atmospheric electric currents have been shown to be associated spatially with aurora (Stagg and Paton 1939; Heppner 1954). Very recently, evidences (Bless *et al.* 1959) have been produced to show that magnetic bays and auroras are manifestations of the same phenomena.

Secondly, photographic auroral data have been utilized to study mainly the motions of visible auroral forms. Attempts have been made to find the local time dependence of the change in the direction of motion (Meinel and Schulte 1953; Meek 1954; and Bless *et al.* 1955). Most of the studies indicate a reversal in the direction of the drift velocity from west to east near local midnight.

[1]Manuscript received February 6, 1960.
Contribution from the Division of Radio and Electrical Engineering, National Research Council, Ottawa.
Issued as N.R.C. No. 5629.
[2]National Research Council Postdoctorate Fellow.

However, this reversal of the direction of drift appears to be related more to the character of aurora and of the magnetic disturbance than to the local time (Nichols 1959).

Thirdly, from the study of radio auroral data it has been suggested that the drift motion of auroral ionization as observed by radar is probably the motion of electrons associated with the magnetic disturbance current system (Nichols 1957; Unwin 1959). Bowles (1954) has shown that these drift motions occur along the magnetic lines of force while Bullough and Kaiser (1955) have concluded that they are either eastward or westward along parallels of geomagnetic latitude. The latter workers have also found a reversal of the direction of motion from west to east between 2100 and 2200 U.T. Recent measurements by Nichols (1957), however, have disproved the observation by Bowles and convincingly indicated that the motions are generally horizontal and in the geomagnetic east–west plane. The speeds of the motions as determined by Nichols vary from 350 meters per second to about 3000 meters per second.

Since the earth currents are supposed to be normally the effect of the overhead current systems responsible for magnetic field perturbations, correlation studies of aurora, magnetic, and earth-current activities have also been attempted (Currie and Edwards 1936; Rooney 1934).

This paper is an outcome of studies made to probe the gross and detailed relationships between certain characteristics of radio aurora, variations of the horizontal magnetic field component H, and earth current.

As regards the gross effects, correlation studies are made between each pair of the following:

(*a*) the duration of radio auroral echo in half-hour periods;

(*b*) the half-hourly mean daily (S) and disturbance diurnal (S_d) variations of H; and

(*c*) the half-hourly mean disturbance diurnal variations of the earth current.

A statistical study of the occurrence rate of radio aurora and magnetic disturbance indices, the 3-hour range K index, and ΣK index for the whole day is also made.

For the study of detailed relationship, separate individual moderate magnetic disturbances are chosen and the envelopes of the individual disturbance and corresponding auroral echo, if any, have been correlated.

The radio auroral data have been obtained with the help of a 50 Mc/s radar designed for back-scatter detection of auroral echoes at Ottawa (45.4° N lat. and 75.9° W. long.) (McNamara 1958). The time duration of radar echo from aurora in half-hourly intervals throughout all days in 1958, hereinafter referred to as 'echo duration', has been determined from the photographic records taken in the form of a continuous film strip displaying range and time. The instantaneous radar echo strength has been measured from the Esterline–Angus chart records displaying the integrated echo intensity with time.

The magnetic data have been collected from the magnetograms of the Dominion Observatory of Canada taken at Agincourt (43.8° N. lat. and 79.3° W. long.) with the help of a standard photographic variometer. The half-hourly average values of the horizontal component H of the magnetic field have been scaled for all days in 1958.

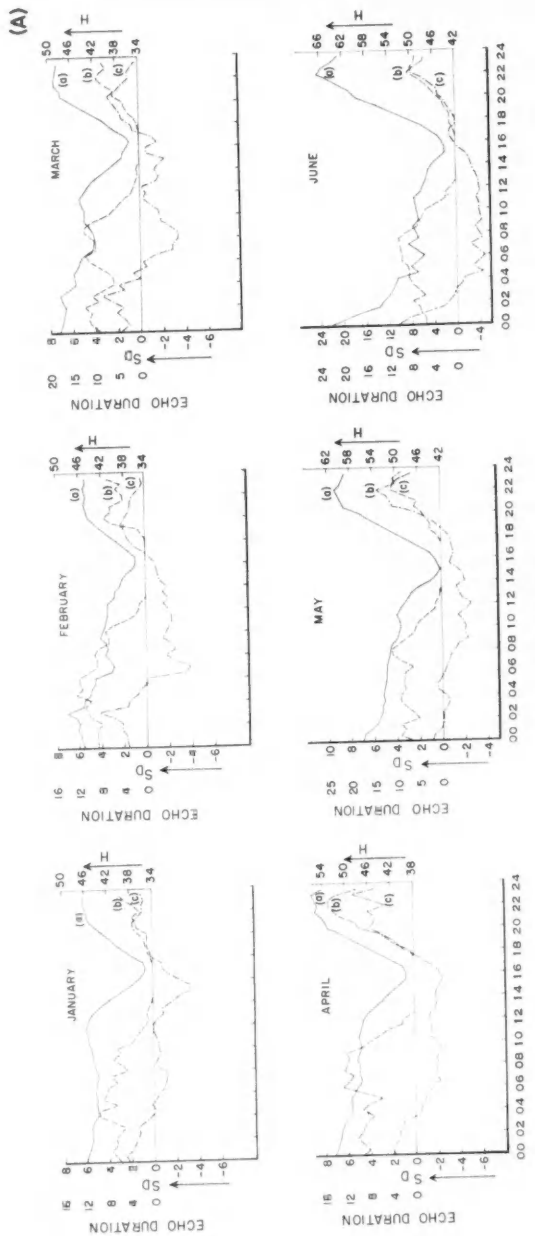
(A)
MARCH
JUNE
FEBRUARY
MAY
JANUARY
APRIL
ECHO DURATION
H
SD
(a)
(b)
(c)
UNIVERSAL TIME
00 02 04 06 08 10 12 14 16 18 20 22 24

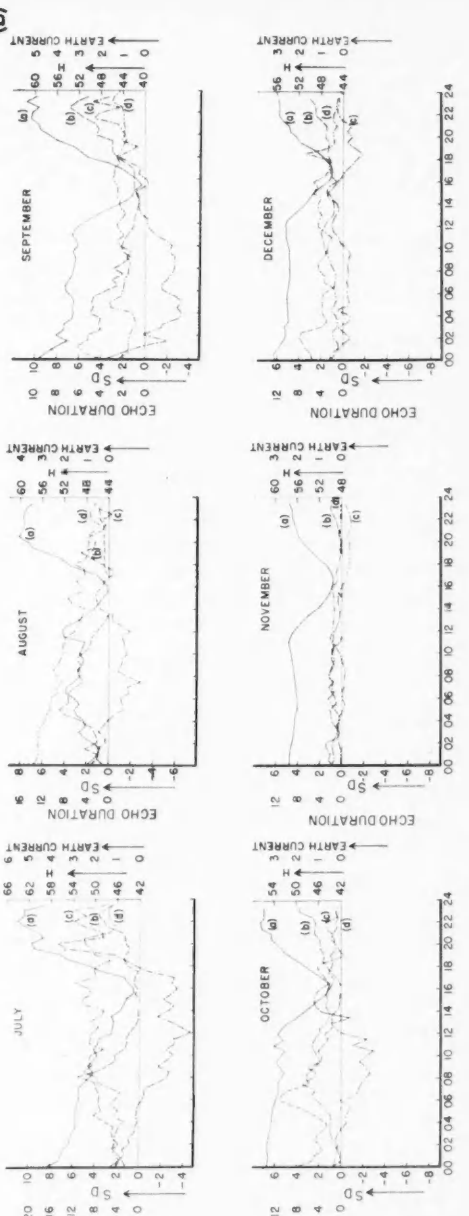

FIG. 1. Diurnal variations of echo duration and S and S_H components of horizontal magnetic field and earth current for all months in 1958. All are in arbitrary units. ——— H; – – – echo duration; ·–·–·– S_H; ····· earth current.

The earth-current records are taken at Crow River (51.5° N. lat. and 90.1° W. long.) by the Hydro-Electric Power Commission of Ontario with the help of a d-c. potentiometer connected to measure the d-c. voltage across a portion of the power transformer neutral connection to ground. The other end of the transmission line, which is 161.7 miles long, is at Ear Falls (50.6° N. lat. and 93.2° W. long.), approximately 22.5° south of west from Crow River. The half-hourly range of deviation of the earth current from the mean has been read from the chart records for all days from July to December, 1958.

DIURNAL VARIATION CURVES OF ECHO DURATION AND *H*

With the help of the data available the monthly half-hourly mean values are calculated and then plotted in Fig. 1. The following results were found from the figures.

(*a*) The diurnal minima in *H* and echo duration are conspicuous and occur around 1600 hours U.T., which is very close to the geomagnetic noon. In winter months the minima tend to occur at times later than those in summer months and in equinoxial months at an intermediate time. This is true in the case of both sets of data. In most of the months an auroral echo does not appear at all around local noon, which is close to geomagnetic noon.

(*b*) There are two maxima in both sets of curves, one is very prominent and the other quite minor. The prominent maxima occur mostly between 2200 and 2400 in both cases. This time seems always to be ahead of the geomagnetic midnight. The other maxima in case of *H* occur mostly between 0900 and 1100 and in the case of echo duration between 0500–0800 (early morning).

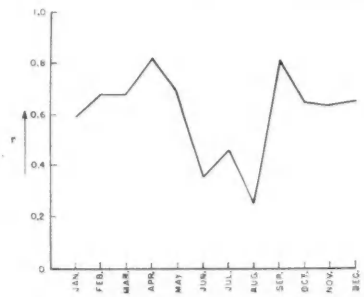

FIG. 2. Linear correlation coefficient between echo duration and *S* component of *H* for every month in 1958.

From Fig. 1 it is found that both *H* and echo duration have some strikingly similar features in their diurnal variation components. To determine an index of the dependence of one on the other, linear correlation coefficients have been calculated and plotted in Fig. 2. Except for some summer months, in particular June, July, and August, the correlation coefficient in quite high, above 60%. In the equinoxial months the correlation is highest, about 75% on the average.

DISTURBANCE DIURNAL VARIATION OF H AND ECHO DURATION

In determining the disturbance diurnal variation, magnetically quiet days are selected with the help of the 3-hour range K indices and also the magnetic data available. In the selection of quiet days, attention is paid not only to the ΣK value but also to the absence of any moderate disturbances. The number of quiet days varies from month to month, 9 in November, 6 in April and June, and 5 in the other months of the year. Then the S_d component of H is calculated for every month of the year. These have been plotted in Fig. 1.

The linear correlation coefficients between the S_d component of H and the auroral echo duration for every month of the year is then determined. The value of the correlation coefficient on the average is below 30% except for the month of August, where it is 66%. This leads to a very surprising result—that there is practically no correlation between the auroral echo duration and S_d field—a result contrary to expectation.

The possibility of some delay time between the two phenomena, which may be responsible for the above result, is then explored by calculating the maximum cross-correlation coefficients after the introduction of optimum delays in the two sets of data for every month. The coefficients and the delays thus obtained are plotted in Fig. 3 for every month in 1958. The magnitude of the cross-

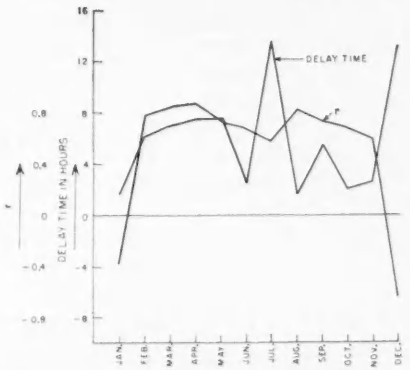

FIG. 3. Linear cross-correlation coefficients and delay times between echo duration and S_d component of H for every month in 1958.

correlation coefficient is quite high throughout most of the year, except in January when it is −38%. It is found that radar auroral activity at Ottawa always precedes the magnetic activity at Agincourt. The delay time between the two activities undergoes a seasonal change. In summer months this fluctuates very rapidly but near the equinoxes, particularly during March and April, it is more or less steady. The latter is also evident in the seasonal characteristic of the cross-correlation coefficient which is negative in mid-winter, during December and January, and decreases in magnitude in mid-summer during June and July as compared to the equinoxial months.

SHORT-TIME CORRELATION OF INDIVIDUAL MODERATE PERTURBATIONS IN *H* AND CORRESPONDING ECHOES

As already stated, the auroral activity always occurs earlier than the magnetic activity. This suggests that the disturbances in *H* are mostly the result of the intense current flowing in the auroral zone which is proportional to the number of charged particles present therein. This number again determines the radar echo strength (Moore 1952; Booker 1956). Hence a correlation between the instantaneous variations of echo strength and *H* may be expected.

In calculating this correlation we are faced with one difficulty. Whereas the radar echo strength is always positive in sign, the sign of the magnetic field perturbations in relation to the average is sometimes positive and sometimes negative. This appears to be due to the change of the direction of the drift of auroral ionization produced by incoming solar protons (Heppner 1954).

Whatever may be the cause, if magnetic field perturbations are caused by currents in the auroral zone, the instantaneous magnitudes of the negative perturbations will correlate well with the corresponding echo strength and the cross-correlation coefficient will be negative. In the case of positive perturbations the coefficients will always be positive. Hence the above coefficients between echo strength and magnitude of the magnetic perturbations have been determined. This should give information about the relation between the instantaneous intensities of individual perturbations in *H* and those of the corresponding echoes, more particularly an answer to the question regarding the cause-and-effect relationship between the two phenomena.

At Ottawa a continuous record of the integrated echo strength (both with respect to range and time) is recorded on Esterline–Angus charts (McNamara 1958). From these charts days are selected which have a number of separated echoes of moderate peak intensity and of duration about 2 hours, distributed practically all throughout the day. In spite of this selection, there is a period of about 8 hours near midday when echoes are absent because of a predominant tendency of aurora to occur at night. Each of these echoes is then scaled at intervals of 5 minutes. From the magnetograms the *H*-component at and around the time of occurrence of each radar echo is also scaled at similar intervals. Since for a time interval of 2 hours or so, the diurnal variation of the earth's magnetic field will not have any appreciable effect, no correction is made to the scaled values of *H*.

In all cases it is noted that around the times of appearance of an auroral echo there are perturbations in the *H*-component. The peak intensities of moderate perturbations do not seem to be in the same ratio as that of the corresponding peak echo intensities in most cases studied. This is not unexpected because factors determining the echo strength, such as echo range variation and the effect of the polar pattern of the radar antenna, and factors responsible for magnetic field perturbations, such as the direction of current flow in the auroral zone, are not all the same and have not identical effects on both the phenomena. Nevertheless, very high amplitude echoes are always found to accompany severe magnetic storms.

The cross-correlation coefficients are then determined with the help of two sets of scaled values for a number of days. They are practically always found to be quite high, above 65% most of the time and some above 80%. Only in a few cases are they about 50%.

An auroral echo is always found to precede the associated magnetic perturbation. The delay times obtained have been plotted against universal time for a few days in Fig. 4. In this figure the delay time between the two events has

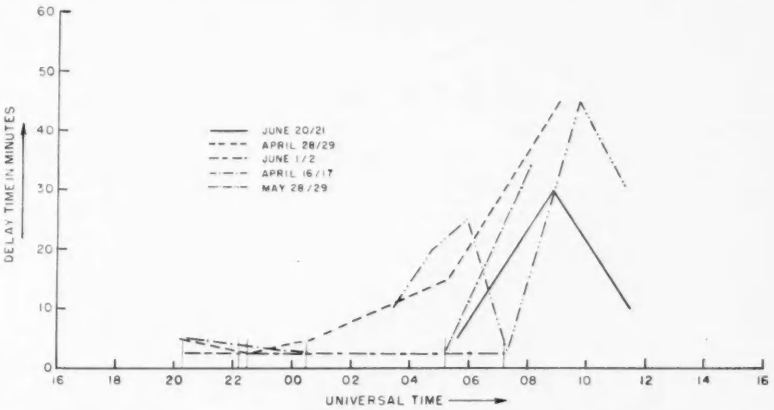

FIG. 4. Delay time between individual auroral echoes and magnetic perturbations against universal time. The thin vertical lines denote that the delay times are between 0 and 5 minutes.

been plotted against the universal time midway between the duration of the radar echo. In Fig. 4 we find that starting from the afternoon hours the delay time remains practically constant between 0 and 10 minutes until about local midnight (0500 U.T.). Thereafter the delay time tends to increase.

This variation of delay time at about the local midnight seems to be related to the change in the direction of auroral ionization drift. From both photographic and radio studies of the drifts of auroral forms and ionization referred to in the introduction, it has been found that the direction of drift before midnight is usually westward causing positive bay type perturbations in the magnetic field, whereas after midnight the direction is reversed, causing negative bay type perturbations. This may be due to a change in the polarities of the electromotive force driving the current in the auroral zone. The delay time between the auroral echo occurrence and associated magnetic perturbations may be the delay between the setting-up of the electromotive force and the full growth of the current.

AURORA AND BAYS

Statistics of auroral echo occurrence with geomagnetic bays may be summarized in the following way for the year 1958.

Magnetic elements	*H*		D		Z	
Sign of the disturbance	−	+	−	+	−	+
No. of days of disturbance	11	35	46	43	59	7
No. of days aurora recorded in radar film	9	29	35	26	50	6
% of disturbed days on which aurora occurred	82	83	76	60	85	86

The cross-correlation coefficients between two negative bays in H of duration close to 2 hours and auroral echo strengths at about the corresponding times are found to be above 80%, and the delay times between the two events are less than 5 minutes.

AURORAL ECHO DURATION AND THE 3-HOUR RANGE *K* INDEX

Correlation studies of auroral echo duration with magnetic disturbances as deduced from the chart of 3-hour range K indices in 1958 may be summarized as follows:

	Range of variations in H, gamma	K indices	Percentage of total disturbed periods auroral echo is received
(i)	>330	8, 9	79
(ii)	200–330	7	74
(iii)	120–200	6	65
(iv)	70–120	5	53
(v)	40–70	4	37
(vi)	0–40	<4	6.5

The percentage of time of the total disturbed periods is shown as a histogram in Fig. 5 against the different range of variations of H. The relation between the two appears to be exponential.

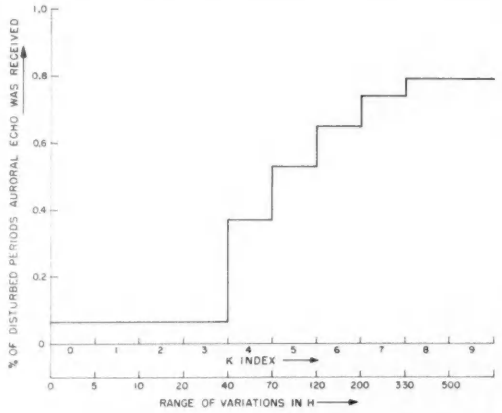

FIG. 5. Percentage of total disturbed periods on which auroral echo was received as a function of the range of variations of H.

If the days are divided into different categories according to the magnitude of ΣK for the whole day, the statistics of observations may be put in the following way:

ΣK	No. of days	Percentage of days auroral echo is received
0–10	84	1.5
10–20	149	8.36
20–30	88	21.3
>30	44	42.8

The nature of variation of the right-hand side with the ΣK values is also practically the same as shown in Fig. 5.

From the plot of percentage of time of auroral echo duration and K_{av} for every month in 1958 (Fig. 6), it is observed that there is practically a one-to-

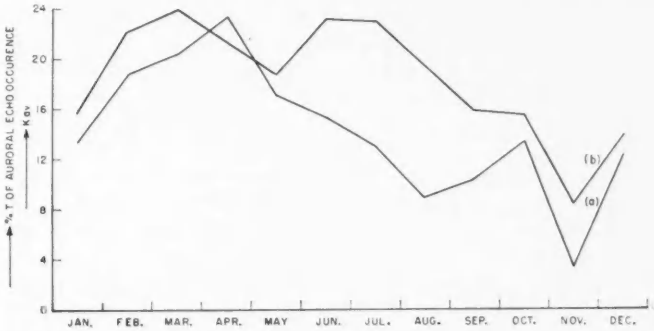

FIG. 6. Plot of percentage of time of auroral echo duration and K_{av} every formonth in 1958. (*a*) % T of auroral echo occurrence; (*b*) K_{av}

one correspondence between the two sets of curves in winter, a moderate amount of correspondence in the equinoxial months, and a poor correspondence in the summer months.

ECHO DURATION, S AND S_d VARIATION IN H, AND DISTURBANCE DIURNAL VARIATION IN EARTH CURRENT

The earth-current records obtained from Crow River – Ear Falls stations are quiescent on magnetically quiet days and so the half-hourly mean ranges of maximum deviation from the mean for a whole month will give the disturbance diurnal variation of the earth current. This variation for the months of July to December in 1958 is plotted in Fig. 1.

The atmospheric current system responsible for magnetic perturbations gives rise to earth currents by an induction process and so the earth current will appear to be related to the time derivative of the magnetic field. Since the data on the rate of change of the field at Agincourt is not available, and

it is extremely time-consuming to compute the above from the magnetograms, direct correlation studies between the disturbance diurnal variations of earth current and the magnetic field have been attempted, with expectation of a phase shift and consequent delay time between the two phenomena. The result of computation is given below:

Month	Delay time, hours	Cross-correlation coefficient
July	−3	56.37
August	−10	−55.95
September	+4	−61.64
October	0	53.88
November	+2	−63.06
December	0	53.37

In the above table the negative delay time indicates a precedence of earth-current activity over the magnetic activity and the positive one the reverse. The physical significance of these results seems to be perplexing. In particular, in the summer months of July and August, the magnetic activity seems to lag behind the earth-current activity. This may be due to some sort of complex phase shifts introduced by the intervening medium between the atmospheric and earth-current systems. Moreover, the two measurements, Crow River – Ear Falls for the earth current and Agincourt for the magnetic field, are quite far apart and so a number of hypothetical reasons may be put forward. Nevertheless, it has been found that earth-current activity is always associated with moderate and severe magnetic disturbances though the amplitudes of earth current and horizontal magnetic field are not very well correlated. In earth-current records micropulsations of small period, normally less than 5 minutes, are always present. These pulsations cannot, in most of the cases, be accounted for by the variation of the horizontal magnetic field component at corresponding times.

It is always found that the auroral activity antedates the earth-current activity. The results of the correlation study between earth-current activity and auroral echo occurrence activity are as given below:

Month	Delay time, hours	Cross-correlation coefficient
July	12	67.23
August	7	59.59
September	4½	−48.07
October	5½	49.46
November	6½	84.58
December	13½	72.49

It seems from both tables that in November, the magnetically quietest month in 1958, the cross-correlation coefficients are highest. This may be due to the least effect of extraneous disturbances on earth current in that month.

SUMMARY AND DISCUSSION

Studies in this paper have shown that auroral echo activity always antedates the magnetic activity. This appears to be the reason why the mean disturbance diurnal variation of H always lags in time behind the mean auroral echo occurrence rate. The delay time has a diurnal variation and its monthly mean value betrays a marked seasonal change.

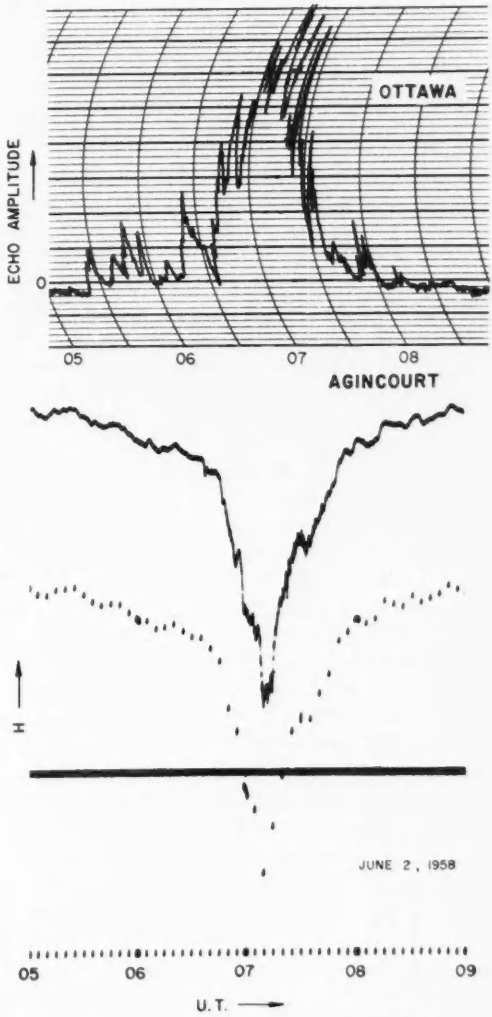

FIG. 7. An example showing development of a negative bay and a corresponding radar echo on June 2, 1958, at 06:38 U. T.

It seems, therefore, that the auroral phenomenon is the primary effect of the intrusion of solar charged particles into the upper atmosphere and this is then the origin of most of the magnetic disturbances. The latter is caused by the current flow in the auroral zone due to the drift of protons in the ionized gas with the surrounding wind, as postulated by Bless *et al.* (1959) in their study of relationship between bays and aurora. They have shown that only protons will move with the wind and they are capable of giving rise to magnetic bays. But it is not clear from their study how electrons, which have been found to move with a velocity as high as 500 m/s (Bullough and Kaiser 1955; Nichols 1957; Unwin 1959), are not effective in producing the bays. Their idealized analysis only shows that bays would have been much larger in magnitude than observed if the drift of electrons were responsible.

The close association of bays and aurora has been lately reported by many workers. At Saskatoon (52.1° N. lat. and 106.6° W. long.) in Canada Meek and McNamara (1954) have shown that 56 and 106.5 Mc/s radar echoes from aurora are associated very closely in time with positive bays whereas no such association is detected with the negative bays. Zaborshchikov and Fediakina (1957) have also made similar observations at Tiksi Bay Arctic Station (71.6° N. lat. and 128.9° E. long.) in the U.S.S.R. This has been suggested as due to the occurrence of aurora at higher angles of elevation during negative bays, and the fact that radar echoes are not normally received from aurora at high angles. The above suggestion has been supported by the report of Meek (1954) that auroral light associated with positive bays occurs at a higher geomagnetic latitude than that associated with negative bays.

In this study disappearance of auroral echoes with the onset of a negative bay has not been noticed. On the contrary, the auroral echo strength has been found to increase up to its maximum value and then decrease in a gradual and systematic fashion with the formation of a negative bay (Fig. 7). The high negative correlation coefficients between the envelopes of bays and corresponding auroral echo strengths justify our observation. The cause of this may be that at Ottawa, which is more southerly than the other two stations in geographic latitude, aurora associated with negative bays is not displaced to such high angles of elevation and the reflection of radio signals is still possible.

ACKNOWLEDGMENTS

The author is deeply indebted to Dr. A. G. McNamara for suggesting this problem and for much valuable advice and suggestions throughout the progress of the work. He is also thankful to Dr. P. M. Millman for his keen interest in the work and for his help in the preparation of the manuscript.

The author takes this opportunity to record his grateful thanks to Mr. R. G. Madill of the Dominion Observatory at Ottawa for supplying him the magnetograms of Agincourt and to Mr. R. H. Hillery for the earth-current records of Crow River.

This work has been possible due to the award of a postdoctorate fellowship to the author by the National Research Council of Canada.

REFERENCES

BLESS, R. C., GARTLEIN, C. W., and KIMBALL, D. S. 1955. Astrophys. J. **122**, 205.
BLESS, R. C., GARTLEIN, C. W., KIMBALL, D. S., and SPRAGUE, G. 1959. J. Geophys. Research, **64**, 949.
BOOKER, H. G. 1956. J. Atmospheric and Terrest. Phys. **8**, 204.
BOWLES, K. L. 1954. J. Geophys. Research, **59**, 553.
BULLOUGH, K. and KAISER, T. R. 1955. J. Atmospheric and Terrest. Phys. **6**, 198.
CURRIE, B. W. and EDWARDS, H. W. 1936. Terrestrial Magnetism and Atmospheric Elec. **41**, 265.
GARTLEIN, C. W. 1944. Trans. Am. Geophys. Union, **25**, 533.
HEPPNER, J. P. 1954. Ph.D. Dissertation, California Institute of Technology, Pasadena, Calif.
MCNAMARA, A. G. 1958. Can. J. Phys. **36**, 1.
MEEK, J. H. 1953. J. Geophys. Research, **58**, 445.
——— 1954. J. Geophys. Research, **59**, 87.
MEEK, J. H. and MCNAMARA, A. G. 1954. Can. J. Phys. **32**, 326.
MEINEL, A. B. and SCHULTE, D. H. 1953. Astrophys. J. **117**, 454.
MOORE, R. K. 1952. Trans. I.R.E., PGAP-3, 217.
NICHOLS, B. 1957. J. Atmospheric and Terrest. Phys. **11**, 292.
——— 1959. Proc. I.R.E., **47**, 245.
ROONEY, W. J. 1934. Terrestrial Magnetism and Atmospheric Elec. **39**, 103.
STAGG, J. M. and PATON, J. 1939. Nature, **143**, 941.
UNWIN, R. S. 1959. Nature, **183**, 1044.
ZABORSHCHIKOV, F. YA. and FEDIAKINA, N. I. 1957. Problemy Arktiki, **2**, 149.

HIGH-ALTITUDE COSMIC RAY MEASUREMENTS AT FORT CHURCHILL[1]

I. B. McDiarmid and D. C. Rose

ABSTRACT

Measurements with rocket-borne Geiger counters have been carried out at altitudes up to 250 km at Fort Churchill, Manitoba. The total primary cosmic ray intensity at a time near a solar maximum has been determined and compared with other measurements taken at times of high solar activity and also with other Geiger counter measurements obtained near a solar minimum. A low-energy radiation was observed whose intensity increased with altitude up to about 25% of the primary intensity at 250 km.

INTRODUCTION

Cosmic ray detectors were included in the instrument loads carried in two Defence Research Board Aerobee-Hi rockets launched in September 1959 at Fort Churchill, Manitoba (geomagnetic latitude, 69°). The major part of the rocket instrumentation consisted of electron density experiments designed to study the state of the lower ionosphere in regions where ionospheric absorption takes place. The electron density experiments were carried out by the Defence Research Board Telecommunications Establishment.

The purpose of the cosmic ray experiment was the following: to measure particle intensity changes associated with ionospheric absorption events, to determine the primary intensity at a time of high solar activity, to look for trapped radiation at altitudes around 250 km and, if possible, to obtain an estimate of the intensity of low-energy albedo radiation. The detectors employed were three Geiger counters (Nuclear Instruments D 79) surrounded by various amounts of shielding material. Table I lists the amount of shielding

TABLE I

Counter No.	Equivalent shielding, g/cm²	Minimum proton momentum, Mev/c	Intensity particles cm^{-2} sec^{-1} sterad^{-1}
1	0.45 Al	182	0.261±.005
2	1.8 Cu	257	0.214±.005
3	7.6 Pb	350	0.212±.005
Telescope	1.9 Cu	260	0.226±.014

(including the nose-cone skin) surrounding the counters and the minimum proton momentum to which the counters were sensitive. The omnidirectional geometric factor for the individual counters was 7.0 cm² for protons with momenta greater than the values listed in Table I. Counters 1 and 2 were also operated as a counter telescope inclined 45° to the rocket axis and with

[1]Manuscript received January 11, 1960.
Contribution from the Division of Pure Physics, National Research Council, Ottawa, Canada.
Issued as N.R.C. No. 5610.

a solid angle area factor of 3.1 cm² sterad. Transistorized circuitry fed both scaled and unscaled counting rates to subcarrier oscillators and these rates were monitored with the aid of telemetry equipment which was part of the ionosphere experiment.

The first rocket was fired on 17 September, 1959. Throughout the flight the condition of the ionosphere remained undisturbed and all of the instrumentation performed satisfactorily. The second rocket was fired on 20 September, 1959, after the onset of an auroral absorption event. Unfortunately, the rocket failed shortly after firing and no useful information was obtained from this flight.

RESULTS AND CONCLUSIONS

The counting rates of the four detectors flown on 17 September are shown as a function of time and altitude in Fig. 1; the altitude measurements below

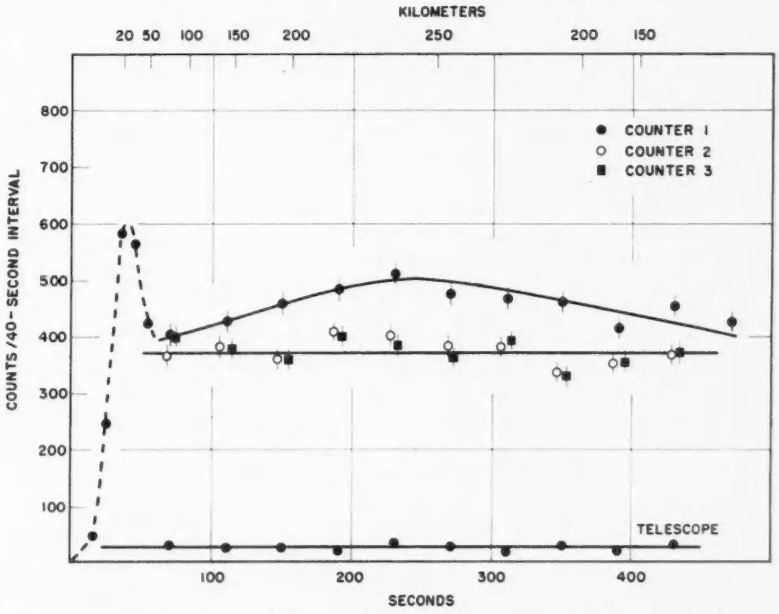

FIG. 1. Counting rates vs. time of flight and altitude. The points represent counts during 40 seconds except the points connected by the broken line which are 10-second averages normalized to counts per 40 seconds.

160 km were obtained from radar tracking data and above this the height was estimated by extrapolating the trajectory measured below 160 km. Above the Pfotzer maximum the counting rates of counters 2 and 3 and the telescope are essentially independent of altitude while counter 1 increased by about 25% between altitudes of 50 and 250 km. The particles responsible

for the increased rate in the counter with least absorber are of quite low energy. For instance if they are electrons their energy must be less than 3 Mev or they would have been detected in counter 2 with 1.8 g/cm² of absorber. The low energy of the particles and the fact that their intensity increases with altitude suggests that they are associated with the trapped radiation in the outer Van Allen layer (Van Allen and Frank 1959*a*). This would be consistent with their being electrons.

The average intensities above 60 km calculated from the measured rates assuming an isotropic distribution over one hemisphere and zero over the other are given in Table I. Apart from the low-energy altitude-dependent component already mentioned the intensities as measured by all detectors are essentially the same. This implies that there is no measurable contributions from protons with momenta less than 350 Mev/c, a value considerably above the Stormer cutoff momentum (110 Mev/c) at Fort Churchill. The absence of low-energy protons in the primary spectrum at a time near a solar maximum would be expected (Neher 1956) but if, as has been assumed by Neher, albedo radiation contributes 50% of the total intensity then the fraction of these particles with momenta less than 350 Mev/c should be detectable in the present experiment. The observed absence of low-energy particles can be used along with a reasonable assumption about the albedo energy spectrum to give an approximate upper limit of 15% for albedo relative to total intensity. Since albedo radiation is concentrated in directions near the horizontal the telescope detection efficiency is considerably less than the single counter efficiency for this radiation. Hence a further indication that the albedo intensity is small is given by the near equality of the telescope and single counter results in Table I. This agreement also implies the absence of an appreciable contribution by photons.

In Fig. 2 the intensity determined by counters 2 and 3 (with no albedo correction) is plotted along with other high-latitude measurements of the primary intensity obtained near the solar maximum; for these measurements no albedo correction was necessary. The Zurich sunspot number averaged over 12-month periods is also shown. The threshold energies of the detectors used in the various experiments differed considerably but all were less than the primary spectrum cutoff energy (at solar maximum) and hence a direct comparison is possible. Points labelled 2 and 3 are the sum of proton and α-particle intensities obtained by Meyer (1959) and McDonald (1959) with a combination Cerenkov–scintillation detector. Points 4 and 5 are interplanetary values of the primary intensity measured in Pioneer IV (Van Allen and Frank 1959*b*) and in the Soviet cosmic rocket (Vernov *et al.* 1959). The point labelled 1 was calculated by Neher (1959) from ionization chamber data near the top of the atmosphere. With the exception of the ionization chamber intensity there is fair agreement among the various values. A rough indication is also given of the expected inverse relationship between primary intensity and solar activity even though the fraction of a solar cycle covered in Fig. 2 is rather small.

It is interesting to compare the present measurements with Geiger counter

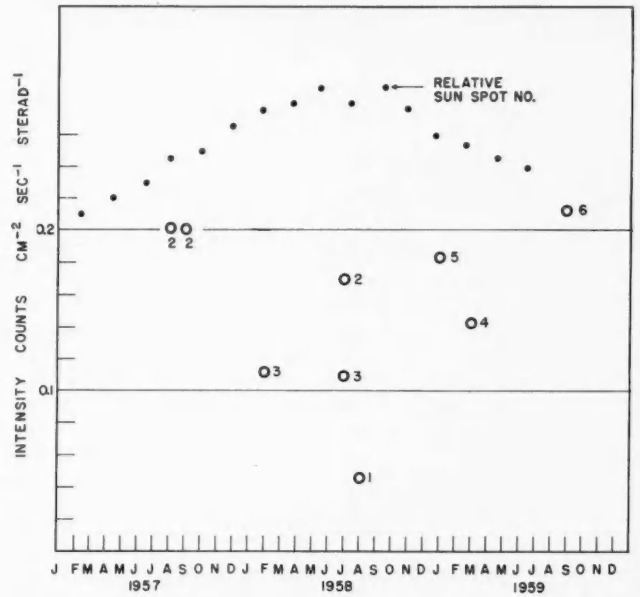

FIG. 2. Measurements of primary intensity near a solar maximum. 1, Neher (1959); 2, Meyer (1959); 3, McDonald (1959); 4, Van Allen and Frank (1959); 5, Vernov *et al.* (1959); 6, present experiment. The points due to Meyer (1959) refer to an atmospheric depth of 13.5 g/cm² and would be slightly higher if corrected to the top of the atmosphere.

measurements made at a latitude of 87° near a solar minimum by Meredith *et al.* (1955). It is found that the ratio of the measured intensities in 1952 and 1959 as determined by Geiger counters is 2.3. This ratio should be very nearly independent of albedo effects and should therefore represent the ratio of the primary intensities. Neher (1959) using ionization chamber data has given a value of 5 for the ratio of primary intensities in 1954 and 1958.

We are indebted to the Defence Research Telecommunications Establishment for the opportunity of carrying out the measurements described here. In particular, we wish to thank Dr. W. Heikkila and Mr. S. Penstone for their very considerable assistance.

REFERENCES

McDONALD, F. B. 1959. Phys. Rev. To be published.
MEREDITH, L. H., VAN ALLEN, J. A., and GOTTLIEB, M. B. 1955. Phys. Rev. **99**, 198.
MEYER, P. 1959. Phys. Rev. To be published.
NEHER, H. V. 1956. Phys. Rev. **103**, 228.
——— 1959. Preprint private communication.
VAN ALLEN, J. A. and FRANK, L. A. 1959*a*. Nature, **183**, 430.
——— 1959*b*. SUI Report No. 59-18.
VERNOV, S. N., CHUDAKOV, A. Y., VAKULOV, P. V., and LOGACHEV, Y. I. 1959. Doklady Akad. Nauk S.S.S.R. **125**, 304.

SOME OXYGEN IONS FORMED AT HIGH PRESSURES IN A MASS SPECTROMETER[1]

WM. MCGOWAN AND LARKIN KERWIN

ABSTRACT

The oxygen ions formed by electron bombardment and collision processes in the mass spectrometer at pressures of about 10^{-3} mm Hg are examined. Mass spectrum lines due to O^+, O_2^+, O_3^+, and O^{++} as well as Aston bands due to O^+, O_3^+, and O_2^{++} are found. Processes leading to these species, as well as abundances and appearance potentials, are considered.

1. INTRODUCTION

When ordinary molecular oxygen at a pressure of about 10^{-5} mm Hg is bombarded by electrons of about 50 ev, the resulting ions form a mass spectrum such as that shown in Fig. 1.

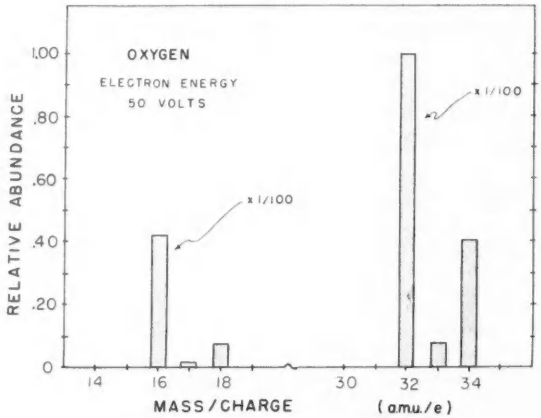

FIG. 1. Low-pressure mass spectrum of O_2.

In this spectrum, the peak at 16 may be identified as consisting of O^+ and O_2^{++}, from the reactions

$$O_2 + e = O^+ + O + 2e \qquad (A)$$

and

$$O_2 + e = O_2^{++} + 3e. \qquad (B)$$

The small peaks at 17 and 18 are isotopic variations of reaction (A) involving O^{17} and O^{18}. No other stable isotopes exist to more than 1 part in 20,000 of the

[1]Manuscript received December 14, 1959.
Contribution from the Department of Physics, Laval University, Quebec, Que.

whole (Kerwin, McElcheran, and Cottin 1957). Isotopic variations of reaction (B) which would appear at 16.5 and 17 are too rare to be identified in the usual analysis.

The peak at 32 consists of O_2^+ from the reaction

$$O_2 + e = O_2^+ + 2e \qquad (C)$$

while the small peaks at 33 and 34 are isotopic variations of (C) involving O^{17} and O^{18}. Isotopic variations at 35 and 36 are normally too rare to be detected.

These reactions are well known (e.g. Hagstrum and Tate 1941; Frost and McDowell 1958). The abundances, appearance potentials, etc. are well catalogued. In the remainder of this paper, we shall omit reference to isotopic variations, although some of these have been observed in the reactions to be discussed. At high-bombarding electron energies, a small peak may be seen at 8, as has been noted by Mattauch and Lichtblau (1939) and Hagstrum and Tate (1941). It is O^{++} from the reaction

$$O_2 + e = O^{++} + O + 3e. \qquad (D)$$

2. HIGH-PRESSURE MASS SPECTRUM

If the pressure of oxygen is raised appreciably above that used for measurements such as those shown in Fig. 1, the spectrometer filament is usually burned. However, a pure carbon filament or a thoriated iridium filament may be operated at pressures up to 10^{-2} mm Hg without suffering ill effects. Under these conditions, and for a bombarding electron energy of 100 ev, we have obtained oxygen spectra such as appears in Fig. 2. In addition to peaks at 16 and 32 we made the following observations.

Mass 8: Spur

The sharp spur sitting on top of the broad peak centered at mass 8 is O^{++} from reaction (D) mentioned above.

Mass 8: Triangle

The broad triangle at the base of peak 8 comes from the two reactions:

$$O_2^+ + O_2 = O^+ + O + O_2 \qquad (E)$$

where the O^+ produced appears principally at 8, and

$$O_2^+ + O_2 = O_2^{++} + O_2^- \qquad (F)$$

where O_2^{++} appears also principally at 8. In reactions (E) and (F), the O_2^+ is first produced by reaction (C). These broad peaks are known as Aston bands and result from ions formed by collisions which take place in or past the ion-accelerating region. They then appear to have an effective mass-to-charge ratio given to a good approximation by the expression

$$\frac{m_z}{1} = \frac{m_t^2 q_0}{q_t^2 m_0}\frac{V_1}{V} + \frac{m_t}{q_t}\left(1 - \frac{V_1}{V}\right) \qquad (1)$$

where m_0 and m_t are the masses of the initial and resulting ions, q_0 and q_t are their charges, and V_1 and V are the voltages of the point within the accelerating

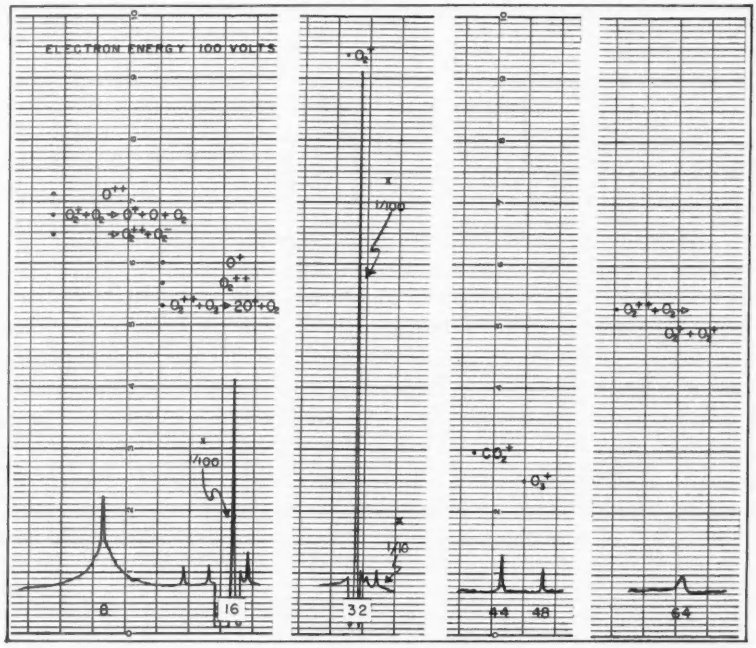

FIG. 2. High-pressure mass spectrum of O_2.

region where the collision takes place and the total accelerating voltage respectively. When the collision takes place past the accelerating region, $V_1 = V$, and the equation simplifies to

$$\frac{m_x}{1} = \left(\frac{m_t}{q_t}\right)^2 \frac{q_0}{m_0}, \tag{2}$$

which is given by Mattauch and Lichtblau (1939). The charge-invariant form of equation (1) is given by Hipple, Fox, and Condon (1946). If collisions take place at various points inside the accelerating region, then a spread of masses m_x will be observed, making up part of the high-mass side of the Aston band. The low-mass side is partially attributed to fringing field effects. The precise shape of this part of the band does not appear to have been satisfactorily explained.

Mass 48

A small peak at 48 may be identified with the ozone ion, O_3^+. This may arise in a variety of ways, for example,

$$O_2^+ + O = O_3^+. \tag{G}$$

This peak has previously been observed (Grundland 1953; Herron and Schiff 1958).

Mass 64

This peak could result from two processes: O_4^+ has been reported by Grundland (1953), who examined with a mass spectrometer the products of a discharge in oxygen. There is also the collision process,

$$O_2^{++} + O_2 = O_2^+ + O_2^+, \tag{H}$$

where, as a result of being formed after the O_2^{++} has been accelerated in the spectrometer, the O_2^+ appears as an Aston band at mass 64. The O_2^{++} is first formed from reaction (B). As will be seen, our peak is not O_4^+.

3. DISCUSSION

The reactions (D), (E), (F), and (H) postulated in Section 2 are those considered in this paper. Their assumption is based on the following considerations.

Mass 8: Spur

The mass spectrometer is fitted with an energy filter at the detecting end. When this is set to pass ions of any energy and when bombarding electrons of 100 ev are used, the peak at mass 8 appears as in Fig. 2, and is reproduced in Fig. 3*a*. When the ion energy selector is set to repel ions not having essentially all of the initial ion beam energy, the triangle disappears, leaving the spur (Fig. 3*b*). This is a sharp peak with practically no energy spread. Its relative

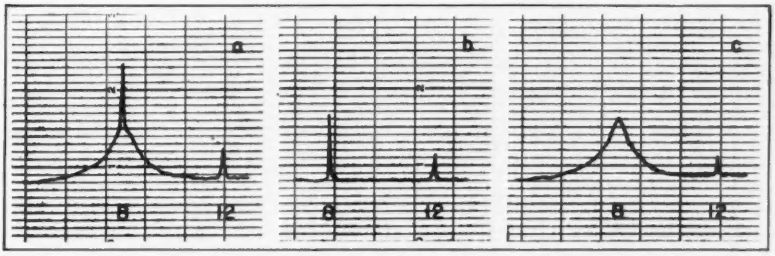

FIG. 3. Appearance of ion peak at mass 8: (*a*) low-energy barrier, high electron energy; (*b*) high-energy barrier, high electron energy; (*c*) low-energy barrier, low electron energy.

intensity of 0.1% of the O_2^+ peak does not vary with pressure, indicating a primary process, as shown in reaction (D). Hagstrum and Tate (1941) found an abundance of 0.01% for this peak. The abundance does not vary with ion energy of from 400 ev to 2000 ev.

An appearance potential curve made for the spur (Fig. 4) shows that the peak first appears at 64.9 ev, and that there are several well-defined breaks in the curve between this value and 80 ev. Now the total energy required to produce O^{++} according to reaction (D), if everything is in the ground state, is 53.8 ev (e.g. Herzberg 1944). While lack of sensitivity may have failed to disclose the onset of the reaction at this point, it is clear that an abundant reaction sets in at 64.9 ev and that several others are involved at higher energies.

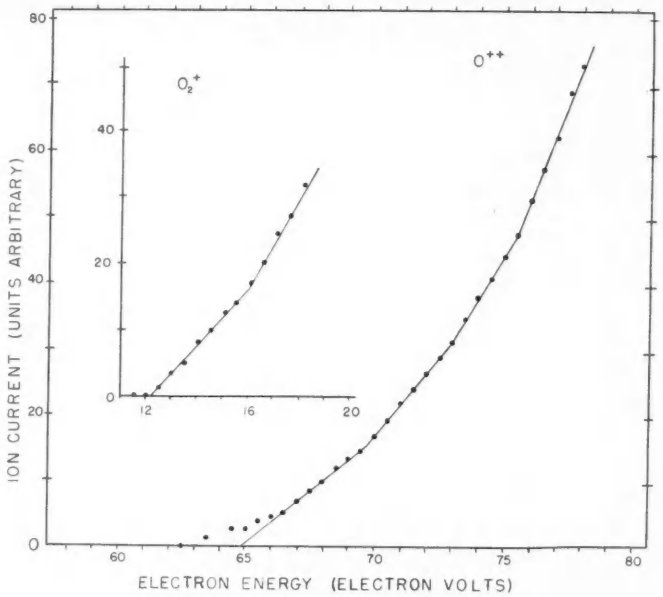

FIG. 4. Appearance potential curve for O^{++}.

A general reaction to cover this experimental fact would be

$$O_2 + e = O^{++*} + O^* + 3e. \qquad (D^*)$$

Here the starred species are in excited states. Experimental conditions preclude the possibility of the O_2 being in an excited state. There are several combinations of excited states for O^{++}, and O which satisfy (D*) (see Moore (1949) for values). However, the experimental errors (about 0.4 ev) in our appearance potential curves resulting from the use of a carbon filament do not permit us to select a combination with certainty. The following table gives one which

TABLE I

Suggested excited states for reaction (D*)

O^{++} state	O state	Appearance potential for (D*)	
		Observed	Reference
$2p^2\,{}^3P$	$3p\,{}^3P$	64.9 ev	64.8 ev
$2p^2\,{}^2D$	$3p\,{}^3P$	(Not observed)	67.3
$2p^2\,{}^1S$	$3p\,{}^3P$	69.4	70.2
$2p^3\,{}^5S$	$3p\,{}^3P$	72.3	72.3
$2p^3\,{}^3D$	$3p\,{}^3P$	79.0	79.7

has the virtue of postulating the O atom in a single state $3p\,{}^3P$ and the virtue of being relatively simple. The observed break at 74.5 ev is not accomodated by this scheme. A number of other schemes do fit it, and it may indicate a multiple process.

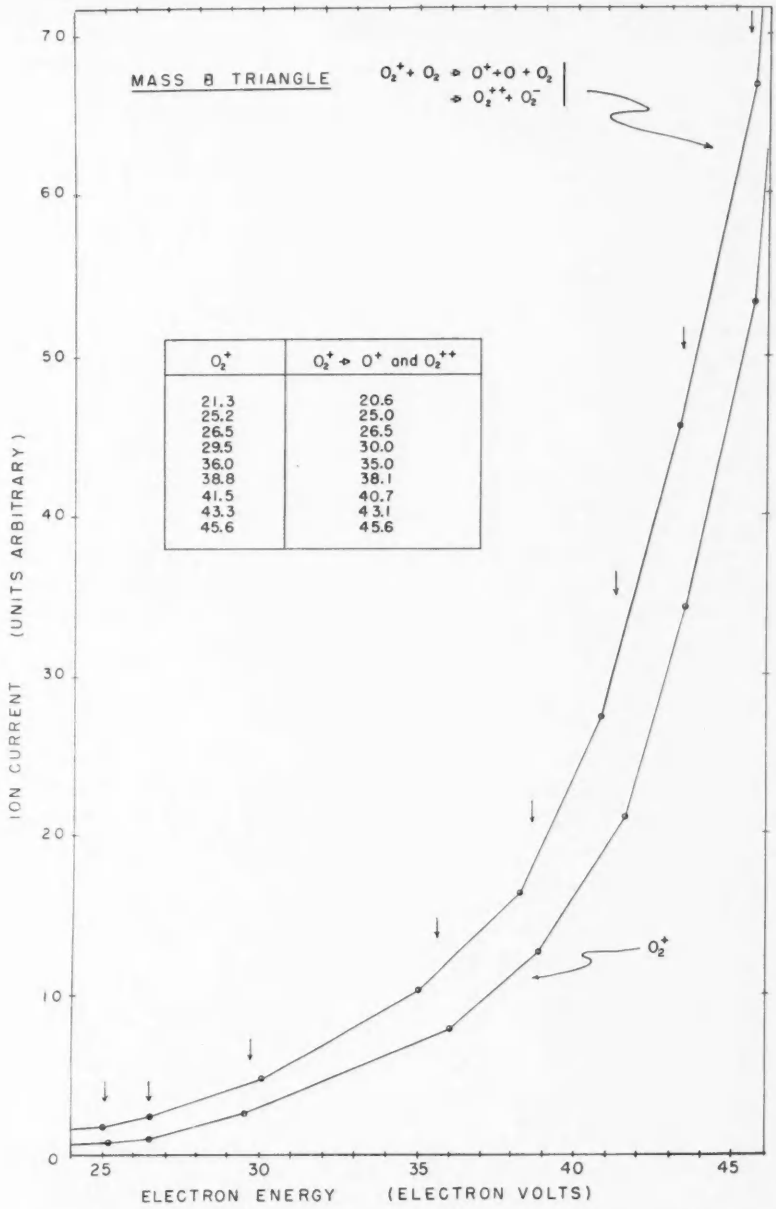

FIG. 5. Appearance potential curves for reactions (E) and (F) and for O_2^+.

Mass 8: Triangle

When the ion beam filter is adjusted to pass low-energy ions, and the electron energy is reduced to about 50 ev, the spur disappears, leaving the triangle. Thus the latter is formed by ions with a lower appearance potential, and having only a fraction of the initial ion beam energy. The spread of the peak is characteristic of Aston bands, as shown in Fig. 3*c*.

Appearance potential curves were obtained from the high-mass side, center, and low-mass side of the triangle, all being identical. An average curve is shown in Fig. 5, where it is compared with an appearance potential curve for O_2^+.

At low energies, breaks were found in the O_2^+ curve at 12.2 ev, 16.1 ev, and 18.2 ev (Fig. 4) corresponding to the ground level, $4\Sigma_g^-$ and $4\pi_u$ states of O_2^+ respectively (Herzberg 1950). These breaks have previously been observed by Herron and Schiff (1958), and Frost and McDowell (1958). These are not drawn in Fig. 5, but served to calibrate the energy scale. At higher energies, a series of breaks in the O_2^+ curve which have not been previously reported are shown. The correspondence of breaks in the triangle curve leaves little doubt that the O_2^+ is the source of the latter, as indicated by reactions (E) and (F). The O^+ and O_2^{++} ions forming the triangle according to these reactions would then result from the collision of an excited O_2^+ ion with an O_2 molecule.

The relative abundance of the triangle varies with pressure, as shown in Fig. 6. The initial linear part of the curve confirms that the process is a secondary one (e.g. reactions (E) and (F)). At higher pressures the O_2^+ beam is

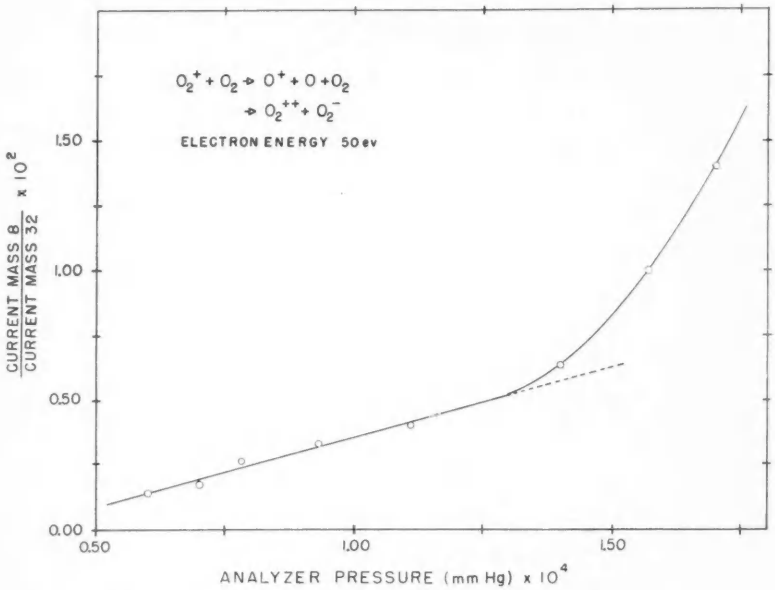

FIG. 6. Variation of abundance of mass 8 triangle with pressure.

scattered. In appropriate experiments where beam intensity was measured as a function of pressure, the O_2^+ maximum occurred at considerably lower pressure than that for mass 8. In a series of experiments to be reported later, the cross section for the sum of reactions (E) and (F) was found to be about 2×10^{-17} cm^2.

An analysis of the energy spread of the triangle ion beam was made using the energy filter. In Fig. 7 may be seen the successive appearances of the total

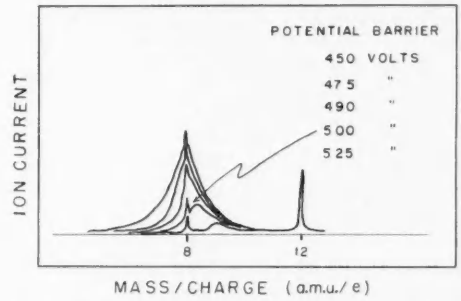

FIG. 7. Variation of appearance of mass 8 peak with barrier potential.

ion beam at mass 8 as the pass-level of the filter is lowered. Note that the spur component and the mass 12 peak remain unchanged. The total accelerating potential was 1000 volts. The high-energy component of the triangle is seen to appear first. The main energy level of the triangle is about one-half the main ion beam energy, confirming the postulated reactions (E) and (F). A small energy loss to the reaction has been consistently noted.

Mass 48: Ozone

The abundance of this ion was 0.05% of the O_2^+ peak at source pressure of 2×10^{-3} mm Hg, and using 100-ev bombarding electrons. No quantitative measurements other than this could be made on this small peak. At sensibly lower pressures the peak was negligible.

Mass 64

In this charge exchange reaction (H) the resulting O_2^+ ion appears at mass 64, and should have twice the energy of the main ion beam (since the parent O_2^{++} was accelerated with two charges). This was confirmed with the energy filter, the beam (0.05% of O_2^+ at 1.5×10^{-4} mm Hg) persisting after all others had been cut off until almost twice the main beam energy was applied. This eliminates the possibility of the peak being O_4^+ in our case. An O_4^+ abundance of less than 0.005% of O_2^+ would have been measurable. The cross section for this charge exchange reaction was established through reference to the peak at 16. If this is considered to be at least 90% O^+, then the cross section for reaction (H) is 1×10^{-16} cm^2. It is to be expected that the contribution of O_2^{++} to mass 16 is less than 10%, in which case the cross section for (H) will be larger. No precise measurements of the variation of this small peak with pressure were made.

An appearance potential curve measured for mass 64 (with 1800 volts potential barrier applied) gave an initial break at 46 ± 1.5 ev and a further well-defined break at 58 ± 1.5 ev. The reference value for the initial break (Herzberg 1944) is 47.2 ev. Now in Fig. 5, the various breaks in the appearance potential curve for the collision processes were seen to fit closely the breaks in the appearance potential curve of the parent O_2^+. The same correspondence should attain between the curve for mass 64 and the curve for the parent O_2^{++}. A thorough search for such breaks at mass 16 revealed none, indicating that the O_2^{++} was a very minor component of the peak at 16. Hagstrum and Tate (1941) on the other hand found a break in the mass 16 appearance potential curve at 50 ± 0.15 ev. The possible reaction

$$O_2^{++} + O_2 = 2O^+ + O_2, \qquad (J)$$

whose products appear at mass 16, might be a complicating factor. Further data on the portion of the mass 16 peak, which may be ascribed to O_2^{++} as discussed in the next section, leads to the conclusion that the cross section for reaction (H) is greater than 2×10^{-16} cm². This surprisingly large value will be discussed in a subsequent paper dealing with cross sections.

4. COMPLETE APPEARANCE POTENTIAL CURVES

In Fig. 8 are shown appearance potential curves for the species O^{++}, O_2^+, $O^+ + O_2^{++}$, and O_2^{++}. Salient characteristics of these curves are gathered in Table II.

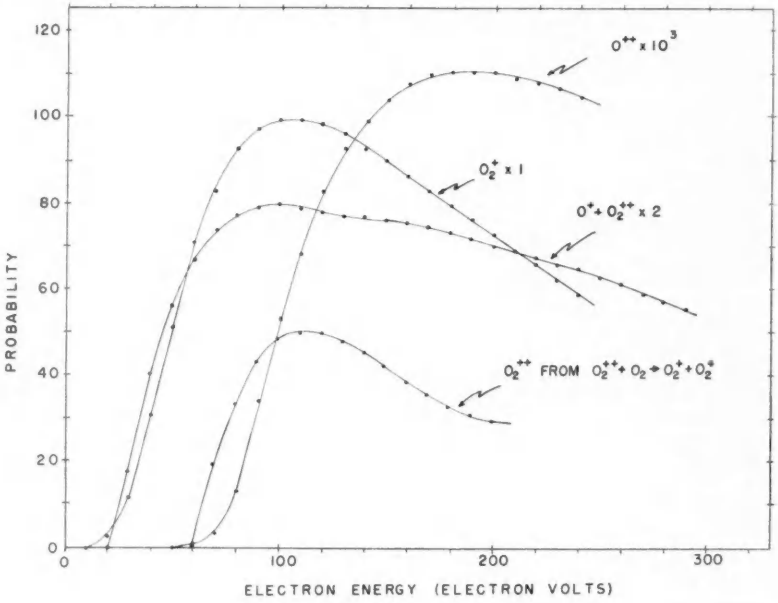

FIG. 8. Appearance potential curves.

TABLE II

Appearance potential characteristics from Fig. 8

Ion	Plot for σ_{max}, volts	95% width, volts	σ_{max} relative to O_2^+
O_2^+	100	45	100
$O^+ + O_2^{++}$	105	85	40
O^{++}	185	95	0.1
O_2^{++}	115	35	2

From Fig. 8, the 95% widths for the diatomic ions are seen to be about half the widths for the monoatomic ions. The curve labelled O_2^{++} only is taken from data on the mass 64 peak, at which point the products of the collision-induced dissociation appear. A similar curve would be found at mass 16, if it were possible to eliminate the O^+ ion. The actual curve measured at mass 16 is then a combination of those for O^+ and this O_2^{++}. From the curves in Fig. 8 it may be estimated that the O_2^{++} contributes less than 1/20 of the mass 16 curve, the subtraction of greater amounts than this from the composite curve leaving a very irregular curve which does not correspond to those usually observed. It is hoped to be able to initiate a search for negative ions which might throw further light on some of these processes.

ACKNOWLEDGMENTS

The authors are happy to acknowledge assistance in this research from Rev. Dr. Ernest Clarke, Paul Marmet, and Jean-Denis Carette. Helpful discussions were held with Dr. David Marsden.

This work is part of a program supported by the Centre de Recherches en Physique and National Research Council Grant BT-45, which assistance is acknowledged with pleasure.

REFERENCES

FROST, D. C. and McDOWELL, C. A. 1958. Joint Conference on Mass Spectrometry (The Institute of Petroleum Hydrocarbon Research, London).
GRUNDLAND, M. I. 1953. Compt. rend. **236**, 476.
HAGSTRUM, H. D. and TATE, J. T. 1941. Phys. Rev. **59**, 354.
HERRON, J. T. and SCHIFF, H. I. 1958. Can. J. Chem. **36**, 1159.
HERZBERG, G. 1944. Atomic spectra and atomic structure (Dover Publications, New York).
——— 1950. Spectra of diatomic molecules (D. Van Nostrand Co. Inc., New York).
HIPPLE, J. A., FOX, R. E., and CONDON, E. U. 1946. Phys. Rev. **69**, 347.
KERWIN, L., McELCHERAN, D. E., and COTTIN, M. 1957. Can. J. Phys. **35**, 783.
MATTAUCH, J. and LICHTBLAU, H. 1939. Z. Physik, **49**, 16.
MOORE, CHARLOTTE. 1949. Atomic energy levels. Bureau of Standards Circular No. 467 (U.S. Government Printing Office, Washington).

MEAN LIVES OF POSITRONS IN ALUMINUM AND THE ALKALI METALS[1]

R. E. BELL[2] AND M. H. JØRGENSEN

ABSTRACT

The time distribution of positron annihilations in the metals aluminum, lithium, sodium, potassium, and cesium have been measured with a fast time-to-amplitude converter. The decay curves appear to be complex, with about 5% of the events having a mean life of approximately 5×10^{-10} sec. The main (95%) components of the decay curves show the following mean lives, in units of 10^{-10} sec: Al, 1.9 ± 0.2; Li, 2.9 ± 0.2; Na, 3.15 ± 0.2; K, 4.0 ± 0.2; Cs, 4.3 ± 0.2. The results for the alkali metals disagree with the previously published measurements of De Benedetti and Richings (1952). These results are discussed, and the lifetimes for other metals are predicted roughly from them and from the angular correlation measurements of other workers.

INTRODUCTION

This paper reports new measurements of the lifetimes of positrons in aluminum and the alkali metals (except rubidium). The measurements were made by the delayed coincidence method using apparatus whose time resolution is good enough to allow the lifetime to be read directly from the logarithmic slopes of the resolution curves. All previous results for positron lifetimes in metals have been measured by the centroid-shift technique introduced by Bay (1950). This method, though statistically excellent, is subject to systematic errors that can completely upset the results. As an example, the total transit time of the pulse through a typical end-window photomultiplier (e.g. RCA 6342A) is about 3×10^{-8} sec; a drift of only one part in 10^3 in this transit time causes a spurious centroid shift of 3×10^{-11} sec. Similar effects can be caused by changes in pulse size distribution and counting rate. On the other hand the logarithmic slope of the resolution curves is insensitive to small changes of this kind.

The most quoted measurements of the mean life of positrons in aluminum are those of Bell and Graham (1953) and Gerholm (1956). Both results were obtained by the centroid-shift method, but with different experimental arrangements; they were $(1.5\pm0.3)\times10^{-10}$ sec and $(2.5\pm0.3)\times10^{-10}$ sec respectively. Other measurements have been made by Ferguson and Lewis (1953: $\tau = (1.6\pm0.6)\times10^{-10}$ sec), Minton (1954: $\tau = (2.9\pm0.3)\times10^{-10}$ sec), and Jones and Warren (1956: $\tau = (1.7\pm0.3)\times10^{-10}$ sec). A measurement of the mean life of positrons in lead by Sunyar (1957) gave the value $(1.6\pm0.15)\times10^{-10}$ sec, presumably supporting the shorter mean life values for aluminum. The present experiment gives a mean life lying among all these values, but somewhat favoring the shorter mean lives.

Measurements of positron mean lives in the alkali metals have been reported

[1]Manuscript received January 6, 1960.
Contribution from the Institute for Theoretical Physics, University of Copenhagen, Copenhagen, Denmark.
[2]Permanent address: Radiation Laboratory, McGill University, Montreal.

only by De Benedetti and Richings (1952). They measured the difference between the mean life in aluminum and the mean lives in lithium, sodium, and potassium, and found in every case that this difference was zero, with an experimental error of 0.7×10^{-10} sec. The results of the present measurements are in strong disagreement with this finding; for example the mean life in potassium exceeds that in aluminum by three times the assigned error of De Benedetti and Richings. An unpublished measurement of the mean life of positrons in cesium by Madansky is quoted as a footnote of a paper by Ferrell (1956). Madansky's value, $(3.7\pm0.6)\times10^{-10}$ sec, agrees within errors with the value found here.

EXPERIMENTAL PROCEDURE

(a) Apparatus

The measurements were made in the customary way with sources of Na^{22} immersed in the metal under test. Two diphenylacetylene gamma counters (2-cm diameter × 1.5 cm high), viewed by two RCA-6342A photomultipliers, were placed near the source, 90° apart. Of these counters, No. 1 was biased to accept the upper one-third of the Compton electron distribution of the 1.28 Mev nuclear gamma ray accompanying each positron from Na^{22}, and No. 2 was biased to accept the upper one-third of the Compton electron distribution of the annihilation radiation. The time distribution of positron annihilations in a metal was measured by analyzing the distribution of delays of counter 2 with respect to counter 1, using a fast time-to-amplitude converter and a 100-channel pulse analyzer. The instrumental time resolution was determined by replacing the positron source by a source of Co^{60}, without change in the counter biases. Ideally, such a pair of measurements yields the mean life of the positrons in the metal directly from the shift between the centroids of the two curves. In practice the errors already mentioned may make such a measurement untrustworthy, and we use the prompt Co^{60} curve only to demonstrate the time resolution of the apparatus.

The time-to-amplitude converter is similar to that described by Green and Bell (1958), but with a number of alterations. The actual conversion from time to amplitude in the apparatus of Green and Bell was made in a 6BN6 gated beam tube. We have found that several different devices will serve about equally well for this purpose; at present we are using a biased diode followed by an integrating condenser, as used earlier by Deutsch (unpublished) and Sunyar (1957). The choice was made mainly on the basis of convenience and simplicity. The instrumental time resolution curve for the conditions of the present experiment has a full width at half maximum of 5×10^{-10} sec, and logarithmic slopes of the sides of the curve corresponding to a half life of 6×10^{-11} sec (mean life $< 10^{-10}$ sec). Since the shortest mean life found in these measurements was 1.9×10^{-10} sec, it was always justifiable to read the mean life directly from the logarithmic slope of the measured time distribution curve.

The apparatus included a pile-up detector that rejected any coincidence event that was preceded or followed within 3 μsec by another pulse in either

counter. The pile-up detector had a resolving time of ~30 mμsec, that is, it recognized two pulses 30 mμsec apart as separate. Except for the loss of a few genuine events, the effect is the same as if all the amplifiers and pulse height selectors had resolving times of 30 mμsec.

The time-to-amplitude converter shows a residual effect of the pulse heights from the individual counters on the time analogue pulse. In the present apparatus this effect is cancelled to first order by adding a fraction of each of the individual counter pulses to the time analogue pulse; the fraction is adjustable in magnitude and sign. Such a device, correctly adjusted, widens the range of acceptable pulse heights from the individual counters without degrading the resolving time. The final effect is an increase in coincidence counting efficiency.

(b) Preparation of Samples

The samples of aluminum were prepared by depositing some drops of Na^{22} solution (as chloride) on a strip of household aluminum foil, and evaporating them to dryness. The strip of foil was then tightly rolled into a cylinder thick enough to prevent the escape of positrons. Household foil was chosen because it has been carefully degreased for domestic reasons. The source strength was usually chosen to be about 5 μc. With Na^{22} of reasonably high specific activity, positrons will annihilate only in aluminum, in such a sample.

The alkali metal samples were more difficult to prepare. In the case of lithium, the least reactive metal, it was sufficient simply to take two flat blocks of lithium metal, scrape their surfaces clean, and clamp them together over a Na^{22} source deposited on 2.5 mg/cm² aluminum foil. The whole assembly was then dipped in molten paraffin wax, in order to exclude air. In the cases of sodium and potassium, the Na^{22} activity was deposited on a 2.5 mg/cm² aluminum foil supported on a ring of stiff copper wire. This ring was held vertically in the bottom of a glass test tube just large enough to contain it, and the molten alkali metal was poured around it through a narrow heated funnel that retained the oxide layer. The alkali metal lumps that were melted for the purpose had been carefully scraped clean beforehand. All the dimensions were so chosen that no positrons could reach either the wire loop or the glass walls of the test tube. Molten paraffin was poured in on top of the alkali metal to seal it. The procedure for cesium metal was similar, but the whole process had to be carried out in a glove box filled with purified nitrogen. In addition, the melting point of cesium is lower than that of paraffin wax, and the seal could not be made in the usual way. Instead, a lucite test tube was used in place of the glass one, and a lucite stopper was cemented into it with acetone.

All the alkali metals, seen through the transparent walls of their containers, were perfectly bright and metallic in appearance, and remained so for periods of months. In all the samples, a few positrons, perhaps as many as 5% of the total, will annihilate in the aluminum support foil. The effect on the results will be very slight, and no correction has been made.

(c) Measuring Procedure

The measurement of a lifetime consisted of a run of some hours on the time-to-amplitude converter, using the sample in question, often immediately

preceded or followed by a shorter run made with a source of Co^{60} replacing the positron sample. The counting rates from the pulse height selectors were a few hundred counts per second, and the coincidence rate was around 200 counts per minute. The Co^{60} comparison source was selected to give similar single counting rates. The scale of the time-to-amplitude converter could be altered by changing the over-all gain of the system. It was calibrated by delaying the pulses from one counter with different lengths of RG 114/U coaxial cable ($Z_0 = 185\ \Omega$, $v/c = 0.88$). This calibration was always made by observing the shift of the centroid of the actual time distribution being measured, and it should be accurate within 2 or 3%. (The centroid shifts used for calibration are large, and the centroid-shift errors mentioned above are then negligible.) The calibration was stable within about 1% over periods of many days. The position of the centroid of a time distribution sometimes showed drifts of a few times 10^{-11} sec, or about one channel of the 100-channel analyzer. Whether these drifts were occurring in the time-to-amplitude apparatus or in the analyzer itself was never determined. Such drifts have almost no effect on our results, although they would be very serious in the centroid-shift method.

The chance coincidence rate was observed at large values of the delay, and was also calculated from the measured single counting rates. The two values were always consistent within statistical expectation. The chance rate to be subtracted was usually about 3×10^{-4} of the peak coincidence rate. All the conclusions of this experiment can be drawn from points having counting rates at least three times the chance rate.

In regions where the counting rate is low, the observed data have often been plotted with adjacent channels of the analyzer averaged to give a single plotted point. This step simplifies the appearance of the curves without essential change in their content, and also serves in many cases to remove zero values, which cannot be plotted on a logarithmic scale.

RESULTS

One of many measured time distributions for positrons in aluminum is shown in Fig. 1, with a Co^{60} prompt curve plotted to the same area. The fact that positrons in aluminum have an easily measurable mean life is clear in Fig. 1, but the decaying part of the curve (right-hand side) is not fitted by a single exponential. All our measured curves on aluminum and other metals show this "tail" effect in comparable degree; no such effect has ever been observed with an ordinary radioactive source, except in those rare cases where an actual mixture of two lifetimes was present.

The method of treating the data of Fig. 1 is to draw a reasonable straight line through the points of the tail, and subtract the component so found from the main curve. The line used for subtraction in Fig. 1 represents a component of mean life 3.85×10^{-10} sec with an intensity of 6.5%. These values are of course extremely rough. The remainder curve, representing $\sim$94% of all the annihilations, then shows a mean life of 1.93×10^{-10} sec. The same procedure, applied to a number of other runs with positrons in aluminum, gave values for the mean life ranging from 1.85 to 1.95×10^{-10} sec. We therefore quote the value $(1.9\pm0.2)\times10^{-10}$ sec. The assigned error is large enough to cover the

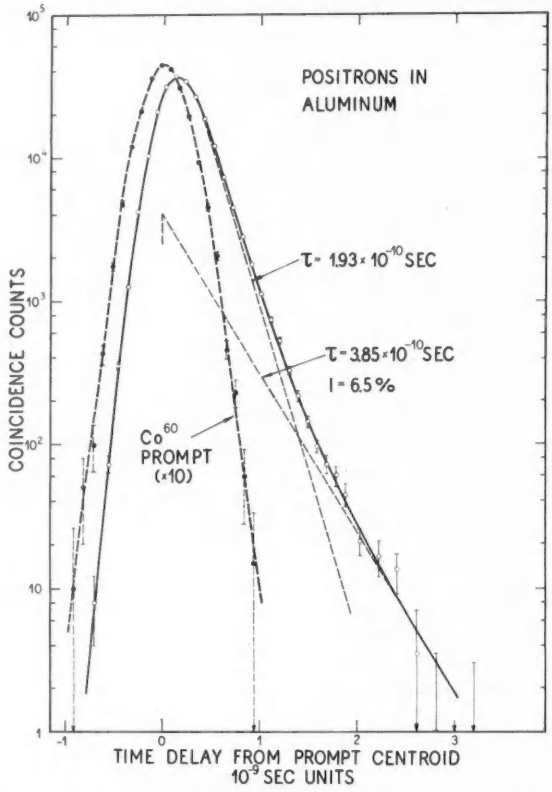

FIG. 1. One of several measured time distributions for positrons in aluminum, with a prompt curve (Co^{60}) for comparison.

mean life found by omitting the subtraction of the tail, and drawing a line through the steepest part of the curve (about 2.0×10^{-10} sec).

The results for lithium and sodium appear in Figs. 2 and 3. (The lithium result shows the effect of a drift of centroid between the recording of the prompt curve and the recording of the lithium curve.) Both lithium and sodium appear qualitatively similar to aluminum, but the mean lives found are $(2.9\pm0.2)\times10^{-10}$ sec for lithium, and $(3.15\pm0.2)\times10^{-10}$ sec for sodium. The tail effect in both lithium and sodium resembles that in aluminum. The curves for aluminum, lithium, and sodium were all recorded in one series of runs lasting 3 days, on the same scale of the time-to-amplitude converter. By the time we reach potassium and cesium, the mean life has lengthened enough to require a change of the time scale of the apparatus by a factor of about 1.5. Figure 4 shows the result for potassium, again with a Co^{60} curve for reference. The tail effect is now being lost under the longer main lifetime, and by the

time we reach cesium (Fig. 5) it is no longer distinguishable. Even for potassium, the subtraction of the tail makes no difference to the mean life of the main component. The mean lives of positrons in potassium and cesium are $(4.0\pm0.2)\times10^{-10}$ sec and $(4.3\pm0.2)\times10^{-10}$ sec respectively.

We now return to the weak tail of longer lifetime, as seen for example in aluminum (Fig. 1). Owing to its lifetime, this tail cannot be due to the accidental presence of oil or wax in the sample. Strenuous efforts were made to try to eliminate the effect, and thus to demonstrate that it was instrumental, but without success. One of these efforts was the installation of the pile-up detector already mentioned. This detector should reduce pile-up effects by a factor of the order of 20, and in fact it did clean up the left-hand side of the curve appreciably, but the effect on the right-hand side of the curve was negligible. Another attempt consisted of a measurement on an aluminum sample like the first, but having only 1/10 the Na^{22} activity in it, and hence giving 1/10 the relative pile-up effect. The result is shown in Fig. 6, and although the statistical accuracy is low, the tail effect is still present in the usual amount. This measurement was immediately followed by one using a source of Tb^{156} of strength equivalent to the Na^{22} in the aluminum. Tb^{156} has a gamma spectrum which, when viewed with an organic phosphor, is very similar to that of a source of Na^{22}. In the case of Tb^{156}, however, the higher energy radiations are delayed with respect to the $\sim$500 kev radiations by the half life of the 1507 kev excited state of Gd^{156}, 1.88×10^{-10} sec. The delay is thus in the opposite sense to that of a Na^{22} source. The result for the Tb^{156} source is also shown in Fig. 6. The exponential decay extending to the left is due to the half life just mentioned. (It was, in fact, this observation that prompted the present authors to make careful lifetime measurements of excited states of Gd^{156} (Bell and Jørgensen 1959).) The right-hand side of the Tb^{156} curve drops rapidly to zero, and remains identically zero for 60 consecutive channels of the analyzer, covering the entire region where the curve for positrons in aluminum is in question. This comparison of two weak sources that are closely identical in everything but lifetime strongly suggests that the tail effect seen with positrons in aluminum is real. Other attempts to eliminate it, involving different counter voltages, different pulse height selection, interchange of scintillation counters, different angular positions of counters, and lead shielding to reduce intercounter scattering, were all equally unsuccessful. The old aluminum curves of Bell and Graham (1953, Figs. 2 and 11), made with much worse time resolution in a different kind of apparatus, show signs of the tail. The aluminum curve of Green and Bell (1958*a*) made with somewhat worse time resolution in another time-to-amplitude converter, shows an effect that is statistically poor, but very similar. Gerholm (1956) found a tail of somewhat longer lifetime in aluminum, which he has since attributed at least in part to pile-up effects (private communication). We are informed by Dr. Gerholm, however, that he has never succeeded in observing a perfectly straight decay curve for positrons in aluminum. There is thus a good deal of precedent for finding the extra tail in aluminum, and it appears to be similar in the alkali metals. All the experimental results are collected in Table I.

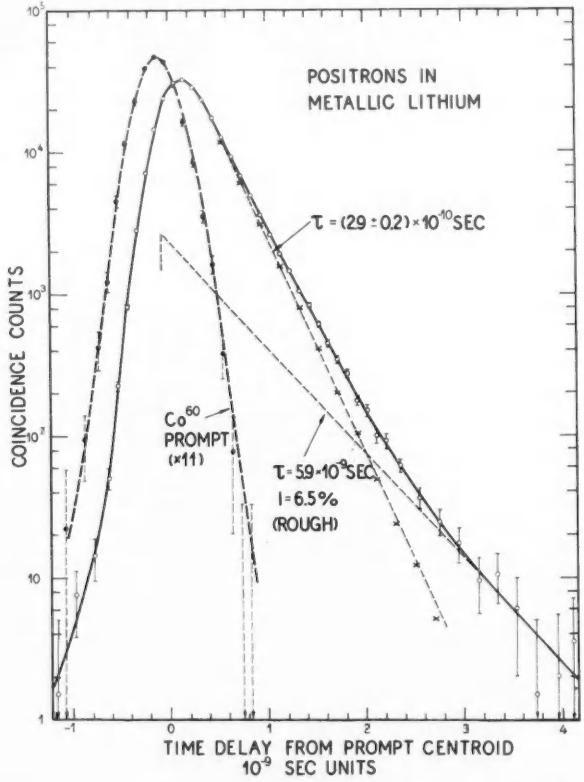

FIG. 2. Time distribution of positron annihilations in metallic lithium.

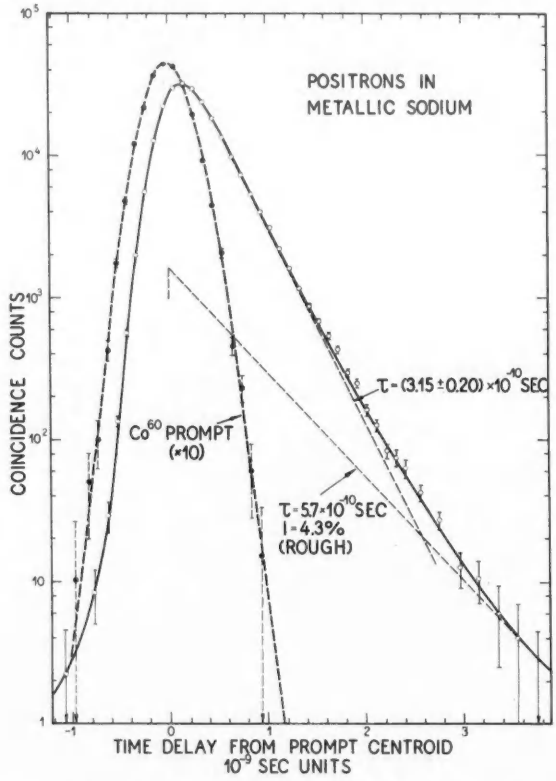

FIG. 3. Time distribution of positron annihilations in metallic sodium.

FIG. 2. Time distribution of positron annihilations in metallic lithium.

FIG. 3. Time distribution of positron annihilations in metallic sodium.

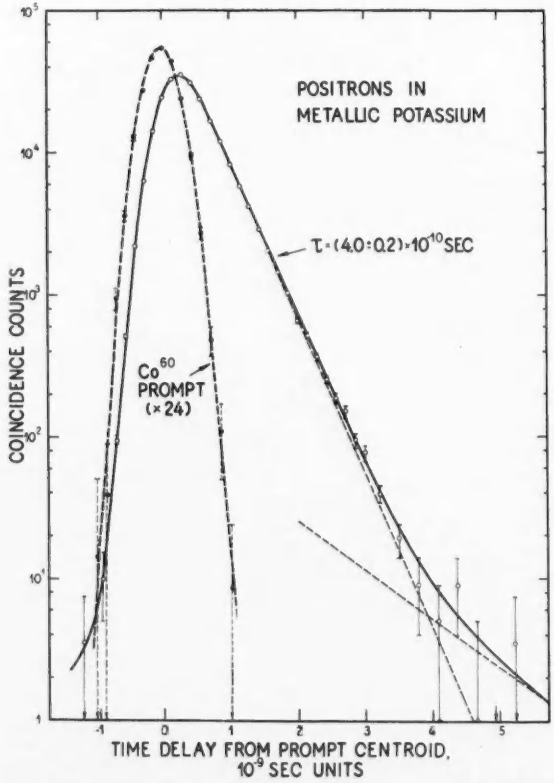

FIG. 4. Time distribution of positron annihilations in metallic potassium.

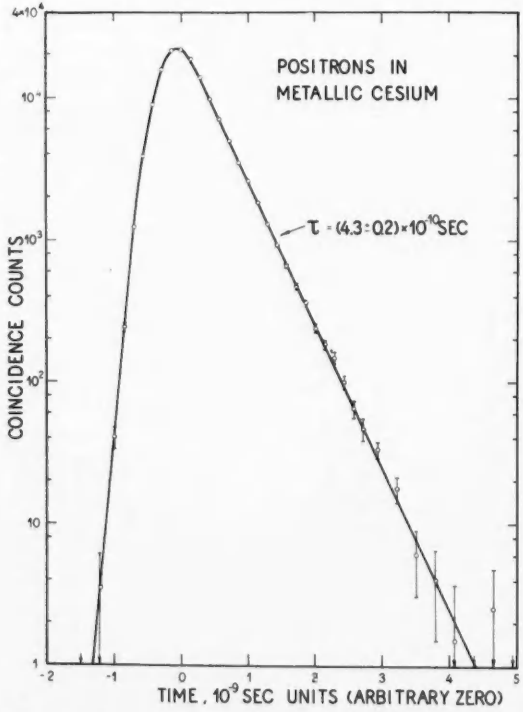

FIG. 5. Time distribution of positron annihilations in metallic cesium.

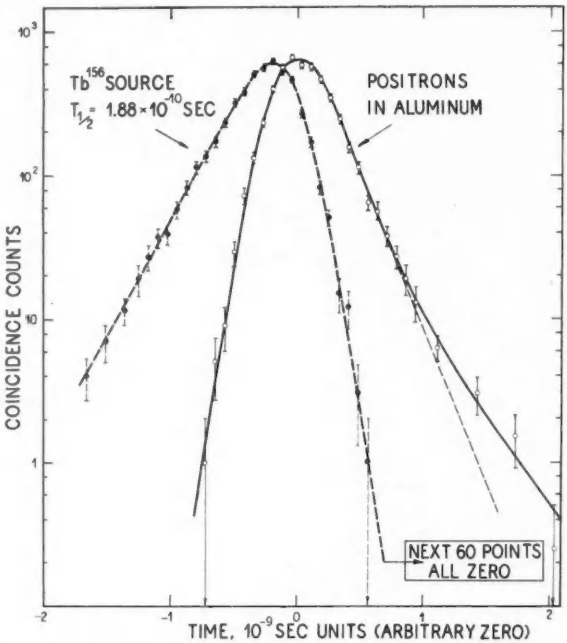

FIG. 6. Comparison of a weak source of positrons in aluminum (right-hand curve) with an equal source of Tb^{156} (left-hand curve).

TABLE I

Results of lifetime measurements on aluminum and the alkali metals

	Main component	Tail component	
Metal	τ (10^{-10} sec)	τ (10^{-10} sec)	Intensity (%)
Al	1.9±0.2	3.85	6.5
Li	2.9±0.2	5.9	6.5
Na	3.15±0.2	5.7	4.3
K	4.0±0.2	—	—
Cs	4.3±0.2	—	—

DISCUSSION

The main parts of the decay curves of aluminum and the alkali metals will be discussed first. We plot in Fig. 7 the experimental annihilation rates λ ($\equiv \tau^{-1}$) as a function of the dimensionless parameter r_s. (This parameter is the radius, in units of the Bohr radius, of the sphere whose volume equals the volume occupied by each valence electron in the metal. It is therefore proportional to the inverse cube root of the density of valence electrons. The valence number is taken as 3 for aluminum and 1 for the alkali metals.) Within their assigned errors, the experimental points lie on a smooth curve,

although there is no reason to expect this smoothness to be perfect. The broken curve at the left in Fig. 7 shows the value of λ calculated on the basis of a Sommerfeld free electron gas, using the Dirac annihilation cross section without Coulomb effect. A second broken curve in Fig. 7 is from the work of Ferrell (1956), in which a rough allowance is made for the enhancement in λ due to the Coulomb attraction between the positron and the electrons. Ferrell expected his curve to be unreliable at low electron densities (r_s greater than about 4), and he suggested that in this region the annihilation rate should approach that of the positronium negative ion, 3.06×10^9 sec^{-1}, shown at the right in Fig. 7. In fact the experimental curve approaches more nearly the value for the spin-averaged positronium atom, 2.0×10^9 sec^{-1}, also shown at the right in Fig. 7. Nevertheless the experimental results support Ferrell's qualitative idea.

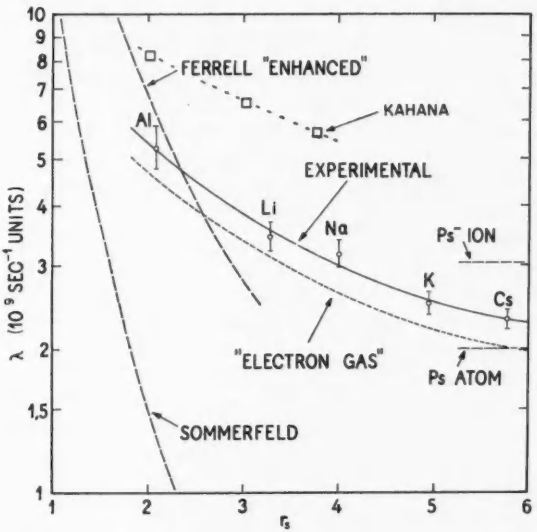

FIG. 7. Plot of λ (= positron annihilation probability) as a function of the dimensionless parameter r_s. The experimental points are shown with a solid curve drawn through them. The broken curve marked "electron gas" is 15% below the experimental curve. For the significance of this and the other curves and points, see the text.

The final curve shown in Fig. 7 is the dotted one labelled "electron gas", and it is derived from the experimental curve in the following way. Aluminum and the alkali metals are members of a large class of metals in which the measured angular correlation of the annihilation photons near 180° consists mainly of an inverted parabola (Green and Stewart 1955; Stewart 1957; Lang, De Benedetti, and Smoluchowski 1955; Lang and De Benedetti 1957). The parabolas have the shape and width expected for the Fermi momentum distribution corresponding to a simple Sommerfeld model of the metals concerned, together with a momentum-independent annihilation rate. In each such case

the parabola is superimposed on a low distribution extending to higher momenta. In the cases of aluminum and the alkali metals, this higher-momentum tail contains about 15% of the events. The tail is attributed by De Benedetti, Cowan, Konneker, and Primakoff (1950), and by Ferrell (1956), to the excluded-volume effect of the metallic ions, but Berko and Plaskett (1958) argue strongly that it is mainly due to annihilation of positrons with the outer electrons of the metallic ions ("core annihilation"). We take the view that it is an effect in addition to the annihilations of positrons with the electron gas. In that case an electron gas alone would have an annihilation rate about 15% smaller than that of the experimental curve in Fig. 7, as indicated by the dotted curve so labelled. This electron gas curve approaches the positronium atom value of λ very closely at large r_s.

A first goal of a theoretical treatment of positron annihilation in metals presumably is to produce a curve close to the electron gas curve. The details that distinguish a real metal could be added later. Ferrell's enhanced curve is a step in this direction; he also made a less successful calculation by another method. The experimental lifetimes show that the enhancement of the electron density at the position of the positron is very large, but the degree of enhancement must be nearly independent of electron momentum in order not to spoil agreement with the angular results. This remark eliminates the simple Coulomb enhancement factor appropriate to a heavy positron and a single electron,

$$(2\pi\alpha c/v)/\{1-\exp(-2\pi\alpha c/v)\}$$

(Heitler 1944), because it introduces a factor $1/v$ (v = electron velocity) into the annihilation rate, at low velocities. (Nevertheless, a detailed computation using this factor was made by Karpman and Fisher (1956).) Ferrell's discussion suggests that a reasonably complete theory will not have difficulty on this point. In a recent paper, Kahana (1960) has attacked the problem on the basis of the Bethe–Goldstone equation (1957), first developed for nucleons. Both the Pauli principle and electron screening are included, but the computations contain a number of approximations. Kahana's three computed points are shown as open squares in Fig. 7. They display the correct sort of variation of λ with r_s, but lie about a factor of 2 too high. It is not clear whether this discrepancy is due to the approximations used, or to the model. Kahana also shows that the annihilation rate varies very little with electron momentum, as required in a correct theory.

Turning to the weak component of longer lifetime, we may summarize the results by saying that about 5% of the positrons have a mean life of about 5×10^{-10} sec in the metals where the effect is distinguishable. These properties are consistent with what would be observed if about 5% of the positrons formed positronium atoms in the metal, and these positronium atoms underwent rapid triplet $\leftrightarrow$ singlet exchange. In that case a mean life a little less than 5×10^{-10} sec would be observed (Garwin 1953; Green and Bell 1958*a*). Moreover, it has recently been shown by Bég and Stehle (1959) that slow positrons in an electron gas have a capture rate for electrons of the order of

10^{15} sec^{-1}, the mechanism being the modified Auger effect first mentioned by Garwin (1953). Unfortunately this explanation is contradicted by the results on angular correlation of annihilation quanta. In amorphous materials, where positronium is formed, a narrow component appears in the angular distribution, corresponding to annihilation of positrons in slow-moving positronium atoms with the electrons to which they are bound (Stewart 1955; Page *et al.* 1955). This effect has been carefully sought, for a different reason, in the case of aluminum by Berko and Plaskett (1958), without result. Judging by their published curves, they would have detected as little as 1/10 as much narrow component as we have been discussing. If positronium atoms in a metal are thermalized or nearly so, the absence of the narrow component seems conclusive, and the 5% tail remains unexplained. Further work is needed.

The statement of Bell and Graham (1953) that the mean lives of positrons in metals appeared to be independent of the metal chosen within ±25% was based on the work of De Benedetti and Richings (1952), so far as the alkali metals were concerned. The general validity of the statement is now destroyed, although it still presumably applies to most metals. The electron gas curve of Fig. 7, and the angular correlation results, enable us to predict roughly the experimental mean lives to be expected for other metals. We calculate r_s for each metal from its valence, and read its electron gas annihilation rate, or inverse mean life τ_g^{-1}, from Fig. 7. We then turn to the angular correlation results, and read out roughly the fraction f of all the annihilations that lie in the parabolic part. This quantity can be found for some metals from Lang and De Benedetti (1957, their Table II), and for others by sketching and measuring areas on the curves of Stewart (1957). The predicted experimental mean life is $f\tau_g$. Some results of this procedure are shown in Table II. The metals in this table have been selected to show a wide variation in r_s (i.e. in electron density), so that τ_g in the table varies from 2.04 to 3.62×10^{-10} sec. On the other hand $f\tau_g$ varies only from 1.43 to 2.17×10^{-10} sec, lying in the correct range of absolute values, and having a reduced spread that easily fits within the ±25% range suggested by Bell and Graham (1953). Many metals (notably the transition metals and the metals around gold and platinum) have such

TABLE II

Rough prediction of the experimental mean life $f\tau_g$ to be expected in several metals, on the basis of the mean life τ_g from the "electron gas" curve of Fig. 7, and the fraction f derived from the angular correlation results

Metal	r_s	τ_g (10^{-10} sec)	f	$f\tau_g$ (10^{-10} sec)
Be	1.88	2.04	0.94	1.92
C (graphite)	1.92	2.08	0.74	1.54
Cu	2.67	2.70	0.53	1.43
Zn	2.30	2.39	0.68	1.62
Ag	3.01	3.00	0.58	1.74
Ba	3.74	3.62	0.60	2.17
Hg	3.40	3.33	0.47	1.57
Tl	3.58	3.47	0.53	1.84
Pb	2.30	2.39	0.75	1.79

complex angular distribution curves that it is scarcely possible to evaluate f for them at all. Nevertheless a theoretical calculation of an electron gas curve resembling that in Fig. 7, taken together with the existing discussions of the angular correlation data (especially Ferrell 1956; Berko and Plaskett 1958), would give us a good initial understanding of positron annihilation in metals.

We wish to thank Professor N. Bohr for the excellent working conditions in his Institute, and Professor A. Bohr and ing. O. B. Nielsen for their helpful interest. One of us (R. E. B.) is grateful for the hospitality of the Institute for a year.

REFERENCES

BAY, Z. 1950. Phys. Rev. **77**, 419.
BÉG, M. A. B. and STEHLE, P. M. 1959. Phys. Rev. **113**, 1345.
BELL, R. E. and GRAHAM, R. L. 1953. Phys. Rev. **90**, 644.
BELL, R. E. and JØRGENSEN, M. H. 1959. Nuclear Physics, **12**, 413.
BERKO, S. and PLASKETT, J. S. 1958. Phys. Rev. **112**, 1877.
BETHE, H. A. and GOLDSTONE, J. 1957. Proc. Roy. Soc. A, **239**, 551.
DE BENEDETTI, S. and RICHINGS, H. J. 1952. Phys. Rev. **85**, 377.
DE BENEDETTI, S., COWAN, C. E., KONNEKER, W. R., and PRIMAKOFF, H. 1950. Phys. Rev. **77**, 205.
FERGUSON, A. T. G. and LEWIS, G. M. 1953. Phil. Mag. **44**, 1339.
FERRELL, R. A. 1956. Revs. Modern Phys. **28**, 308.
GARWIN, R. L. 1953. Phys. Rev. **91**, 1571.
GERHOLM, T. R. 1956. Arkiv Fysik, **10**, 523.
GREEN, R. E. and BELL, R. E. 1958. Nuclear Instr. **3**, 127.
——— 1958*a*. Can. J. Phys. **36**, 1684.
GREEN, R. E. and STEWART, A. T. 1955. Phys. Rev. **98**, 486.
HEITLER, W. 1944. The quantum theory of radiation (Oxford University Press), p. 84.
JONES, G. and WARREN, J. B. 1956. Can. J. Phys. **34**, 1033.
KAHANA, S. 1960. Phys. Rev. **117**, 123.
KARPMAN, V. I. and FISHER, I. Z. 1956. Doklady Akad. Nauk S.S.S.R. **111**, 1212.
LANG, G. and DE BENEDETTI, S. 1957. Phys. Rev. **108**, 914.
LANG, G., DE BENEDETTI, S., and SMOLUCHOWSKI, R. 1955. Phys. Rev. **99**, 596.
MINTON, G. H. 1954. Phys. Rev. **94**, 758.
PAGE, L. A., HEINBERG, M., WALLACE, J., and TROUT, T. 1955. Phys. Rev. **98**, 206.
STEWART, A. T. 1955. Phys. Rev. **99**, 594.
——— 1957. Can. J. Phys. **35**, 168.
SUNYAR, A. W. 1957. Bull. Am. Phys. Soc. **2** (1), 37.

AN HYPOTHESIS CONCERNING TURBULENT DIFFUSION[1]

R. BOURRET

ABSTRACT

It is shown that the Goldstein equation for turbulent diffusion implies diffusion currents dependent upon the history of the concentration gradient. An analysis of the stochastic model upon which the Goldstein equation is based reveals that the hereditary function, by which the history is weighted, is the ensemble autocorrelation function of velocity. Heuristic arguments and an appeal to the theory of irreversible thermodynamic processes lead to the postulation of an integro-differential equation for turbulent diffusion involving the velocity autocorrelations of the diffusate particles.

I. THE GOLDSTEIN EQUATION

In order to consider a proposed extension of the theory of diffusion as developed by Taylor (1921) and Goldstein (1951) and extended by Michelson (1954) and Davies *et al.* (1954), a brief review of Goldstein's analysis is presented first. His notation has been altered slightly.

Consider a one-dimensional random flight approximated, as in Fig. 1, with discrete intervals of space η and of time τ. If the probabilities of occupation

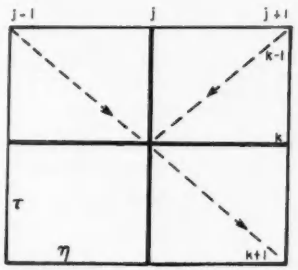

FIG. 1. Diagram of diffusive movements described by Goldstein's analysis.

of all the sites are known at an initial time, what are these probabilities at a later time? This is the problem to be solved by specific assumptions about the site-to-site transition probabilities. In these transitions, it is assumed that the diffusing particle moves with a constant velocity, $v = \eta/\tau$, either to the right or to the left. The probability that the ith site will be occupied at time k by a leftward- or a rightward-moving particle is designated by L_{ik} and R_{ik}, respectively. The total probability for the occupation of the site is then

$$P_{ik} = L_{ik} + R_{ik}. \tag{1}$$

[1]Manuscript received December 29, 1959.
Contribution from the Research Laboratories, Hughes Aircraft Company, Culver City, California. An abstract of this paper was given at the International Oceanographic Congress held in New York, 31 August–11 September 1959.

If p_+ and p_- are the respective probabilities for unaltered and reversed motion in unit time, then it can be inferred from Fig. 1 that

$$R_{i+1,\,k+1} = p_+R_{ik}+p_-L_{ik} \tag{2a}$$

and similarly that

$$L_{i-1,\,k+1} = p_+L_{ik}+p_-R_{ik}. \tag{2b}$$

These difference equations become differential equations when we explicitly introduce the time interval τ and the space interval η, expand to first order, and take the limit $\tau \to 0$. Thus, from (2) it is seen that

$$\begin{aligned} R(x+\eta, t+\tau) &= p_+(\tau)R(x, t)+p_-(\tau)L(x, t) \\ L(x-\eta, t+\tau) &= p_-(\tau)R(x, t)+p_+(\tau)L(x, t). \end{aligned} \tag{3}$$

Performing the expansion, dividing by τ, and taking the limit yields

$$\frac{\partial R}{\partial t}+v\frac{\partial R}{\partial x} = r_+R+r_-L \tag{4a}$$

and

$$\frac{\partial L}{\partial t}-v\frac{\partial L}{\partial x} = r_-R+r_+L. \tag{4b}$$

It has been stated that $v = \lim_{\tau\to 0}(\eta/\tau)$, and r_+ and r_- have been defined as follows:

$$r_+ = \lim_{\tau\to 0}\left[\frac{p_+(\tau)-1}{\tau}\right], \qquad r = \lim_{\tau\to 0}\left[\frac{p_-(\tau)}{\tau}\right]. \tag{5}$$

By the use of (1), the following equation can be obtained for P alone:

$$\frac{\partial^2 P}{\partial x^2}-\frac{1}{D}\frac{\partial P}{\partial t}-\frac{1}{v^2}\frac{\partial^2 P}{\partial t^2} = 0, \tag{6}$$

where the "diffusivity" is defined by

$$D = \frac{v^2}{r_--r_+} = \frac{v^2}{2r_-}; \tag{7}$$

the latter equality holds by virtue of the definitions (5). This modified diffusion equation, originally stated by Goldstein, has a very interesting feature to which attention seems not to have been called. Using the equation of continuity with $\mathbf{J}$ representing the diffusive flux, i.e.

$$\frac{\partial P}{\partial t}+\nabla\cdot\mathbf{J} = 0, \tag{8}$$

the three-dimensional form* of (6) may be expressed as

*This is the three-dimensional form given by naive induction from (6). The strict generalization to more than one dimension is somewhat involved. The case of two and three dimensions has been developed by the author and will be described elsewhere.

$$\nabla \cdot \left(\nabla P + \frac{1}{D} \mathbf{J} + \frac{1}{v^2} \frac{\partial \mathbf{J}}{\partial t} \right) = 0 \tag{9}$$

and hence it can be inferred that

$$\frac{\partial \mathbf{J}}{\partial t} + \frac{v^2}{D} \mathbf{J} = -v^2 \nabla P + \mathbf{H}(t) + \nabla \times \mathbf{G}(\mathbf{r}, t). \tag{10}$$

Since the functions $\mathbf{G}(\mathbf{r}, t)$ and $\mathbf{H}(t)$ have no physical significance in the present inquiry, they are neglected here. It is clear that in the steady state (10) reduces to Fick's law. The general solution, however, may be written in the form

$$\mathbf{J}(\mathbf{r}, t) = -D \nabla P_{\text{ret}}(\mathbf{r}, t) + \mathbf{J}(\mathbf{r}, 0) e^{-t/\tau_0}, \tag{11}$$

where

$$\tau_0 = \frac{D}{v^2}$$

and

$$P_{\text{ret}}(\mathbf{r}, t) = \int_0^t \frac{1}{\tau_0} e^{-t'/\tau_0} P(r, t - t') dt'. \tag{12}$$

This result is a consequence of the non-Markovian character (in the coordinates) of the Goldstein process in which persistence effects are introduced. In the difference equation from which (6) is obtained (for this equation see Goldstein (1951)), values of P at time k depend upon the previous values of P at time $k-2$, and if the dependence extends beyond $k-1$, the process is no longer Markovian. The stochastic process for the velocity, however, is Markovian, since the L and the R in (2) depend only upon the values at the immediately preceding time. By a general theorem of Doob (1942), it is known that the autocorrelation function for a Markov process must be of the form $e^{-\alpha|t|}$. This suggests that the hereditary function in (12) may have something to do with the velocity autocorrelation, and in fact, the exact relation will be demonstrated in the next section.

II. ENSEMBLE VELOCITY AUTOCORRELATION

Consider the velocity autocorrelation

$$R(t_2, t_1) = \langle v(t_1)\, v(t_2) \rangle \tag{13}$$

in which the braces indicate an average over the ensemble. This average may be expressed in terms of the second probability distribution, $W(v_1, t_1 | v_2, t_2)$:

$$R(t_2, t_1) = \int\int v_1 v_2 W(v_1, t_1 | v_2, t_2) dv_1 dv_2. \tag{14}$$

This distribution is the probability (density) of a measurement of velocity v_1 at time t_1 and of a measurement v_2 at the later time t_2. The velocity is associated with the same diffusing particle. In the present model, that of

Goldstein, we consider velocities of v and $-v$ only. In this case, for example, $W(v, t_1|v, t_2)$ means the residual rightward-moving fraction at time t_2 of the original rightward-moving fraction at time t_1. For simplicity, the total number is assumed to be unity so that fractional number and probability may be used more or less interchangeably. Employing the notation $N_R(t)$ and $N_L(t)$ for rightward- and leftward-moving fractions at time t, respectively, the second probability distribution in terms of delta functions may be written as follows:

$$(15)\quad W(v_1, t_1|v_2, t_2) = \delta(v_1+v)\delta(v_2+v)N_L(t_1)N_L(t_2)+\delta(v_1-v)\delta(v_2-v)N_R(t_1)N_R(t_2) +\delta(v_1+v)\delta(v_2-v)N_L(t_1)N_R(t_2)+\delta(v_1-v)\delta(v_2+v)N_R(t_1)N_L(t_2).$$

Substituting (15) into (14) gives the result

$$(16)\quad R(t_2, t_1) = v^2[N_R(t_1)N_R(t_2)+N_L(t_1)N_L(t_2)-N_R(t_1)N_L(t_2)-N_L(t_1)N_R(t_2)].$$

This expression can be explicitly evaluated from an examination of (4). The Laplace–Fourier transforms of the dependent variables R and L are introduced by

$$(17)\quad \begin{pmatrix} R_F^L(k, p) \\ L_F^L(k, p) \end{pmatrix} = \int_{-\infty}^{+\infty} dx \int_0^{+\infty} dt \begin{pmatrix} R(x, t) \\ L(x, t) \end{pmatrix} e^{ikx-pt}$$

with the inversion formula

$$(18)\quad \begin{pmatrix} R(x, t) \\ L(x, t) \end{pmatrix} = \frac{-i}{(2\pi)^2} \int_{-\infty}^{+\infty} dk \int_{-i\infty}^{+i\infty} dp \begin{pmatrix} R_F^L(k, p) \\ L_F^L(k, p) \end{pmatrix} e^{-ikx+pt}.$$

As may be seen from (18), the rightward- and leftward-moving fractions are readily expressed in terms of the transforms as shown below:

$$(19)\quad N_R(t) = \int_{-\infty}^{+\infty} R(x, t)dx = \frac{-i}{2\pi} \int_{-i\infty}^{+i\infty} R_F^L(0, p)e^{pt}dp.$$

$N_L(t)$ may be similarly expressed. The transform version of (4) is

$$(20)\quad \begin{aligned} (p-ikv-r_+)R_F^L(k, p)-r_-L_F^L(k, p) &= R_F(k, 0) \\ (p+ikv-r_+)L_F^L(k, p)-r_-R_F^L(k, p) &= L_F(k, 0), \end{aligned}$$

where the right-hand terms are just the Fourier transforms of the initial distributions. Solving these equations algebraically and using the short cut given by (19), it is found that

$$(21)\quad \begin{aligned} N_R(t) &= e^{r_+t}[N_R(0)\cosh r_-t+N_L(0)\sinh r_-t] \\ N_L(t) &= e^{r_+t}[N_R(0)\sinh r_-t+N_L(0)\cosh r_-t]. \end{aligned}$$

If at $t_1 = 0$ there were, for example, rightward-moving particles only, then $N_R(0) = 1$ and $N_L(0) = 0$.* From (21), then, the velocity autocorrelation is simply

$$(22)\quad R(t) = v^2e^{-v^2t/D},$$

*In terms of the Lagrangian analysis of the motion of an individual particle we would say: at time $t_1 = 0$ its motion was certainly to the right (or, alternatively, certainly to the left).

and neglecting the transient term, (11) may be written in the one-dimensional form

$$J(x,t) = -\frac{\partial}{\partial x}\int_0^t R(t')P(x,t-t')dt'. \tag{23}$$

Before considering generalizations of (23), it is instructive to inquire how the thermodynamics of irreversible processes leads to a similar result.

III. DIFFUSION AS AN IRREVERSIBLE THERMODYNAMIC PROCESS

For an ideal gas of like particles, a result equivalent to (23) can be derived under very reasonable assumptions.

The first law of thermodynamics leads to an expression for the entropy change in a reversible process which may be written

$$dS = \frac{dU}{T}+\frac{p}{T}dV. \tag{24}$$

The first term here is a measure of the change of entropy, caused by a diffusion of molecules, for example, in momentum space. This term corresponds to a process in which there is diminishing localizability of the molecules in momentum space. The second term corresponds to the spatial spreading of the molecules, and may represent, when positive, a loss of information as to the whereabouts of the system in configuration space. Now, the total mean entropy for a system may be expressed in the form (to some extent, the view of entropy proposed by Jaynes (1957) is adopted here)

$$S(t) = -\int\int P(\mathbf{p},\mathbf{r}) \ln P(\mathbf{p},\mathbf{r})d^3p\,d^3x, \tag{25}$$

where we note that, in general, the entropy is time dependent. Utilizing the additive property of the entropy function,

$$S(t) = S_r+S_p = -\int P_1(\mathbf{r}) \ln P_1(\mathbf{r})d^3x-\int P_2(\mathbf{p}) \ln P_2(\mathbf{p})d^3p. \tag{26}$$

In what is called an isothermal process, the second of these terms is constant. In the slow diffusion of a thermally isolated quantity of gas, there is a process of this kind. The slowness of the process ensures that the momentum distribution will at all times be in equilibrium. Therefore, it may be said that all entropy changes are due to changes in the first term of (26) that represent configurational entropy. Taking the time derivative of (26) and observing the constant normalization of the position-dependent concentration $P_1(\mathbf{r})$, it is seen that

$$\frac{dS}{dt} = -\int\frac{\partial P_1}{\partial t} \ln P_1(\mathbf{r})d^3x. \tag{27}$$

Henceforth, the subscript will be dropped, since it is no longer needed. Employing the equation of continuity (8) and vector identities gives

$$\frac{dS}{dt} = -\int_{\text{vol}} \mathbf{J}\cdot\boldsymbol{\nabla} \ln P\, d^3x+\int_{\text{surf}} (\ln P)\mathbf{J}\cdot d\boldsymbol{\Sigma}. \tag{28}$$

As is usual in the thermodynamic theory of irreversible processes, we examine the rate of entropy production per unit volume. The contributions of the surface integral in (28) may therefore be neglected. Writing $\dot{S}_0$ for entropy production per unit volume gives

$$P\,\dot{S}_0 = \mathbf{J}.\mathbf{X}, \tag{29}$$

where the abbreviation

$$\mathbf{X} = -\nabla P \tag{30}$$

is used, and $\mathbf{X}$ is called the "force" or "affinity" associated with the "flux" $\mathbf{J}$. Ordinarily one finds, or assumes, that the fluxes and the affinities are related by equations of the form

$$J_\alpha = D_{\alpha\beta}X_\beta \text{ (summation on repeated indices).} \tag{31}$$

The Onsager theory demonstrates the symmetry of the $D_{\alpha\beta}$ on a basis which appears inapplicable to the present problem. This demonstration includes treating the J_α as being due to fluctuations in the number of particles per unit volume. This may be illustrated simply by integrating the equation of continuity over a very small spherical volume to obtain the number of particles, N, contained therein. This is written

$$\frac{dN}{dt} = \mathbf{J}\cdot\boldsymbol{\Sigma} = D{:}\mathbf{X}\cdot\boldsymbol{\Sigma}, \tag{32}$$

where $\boldsymbol{\Sigma}$ represents the surface normal and the double dot represents the inner product of the diad D with the affinity vector $\mathbf{X}$ corresponding to (31). This rate of change, however, must be expressed more rigorously by

$$\frac{1}{\tau}\langle N(t+\tau)-N(t)\rangle_E = D{:}\mathbf{X}\cdot\boldsymbol{\Sigma}, \tag{33}$$

where E means ensemble average and τ does not approach zero but must be small compared with the time required to reach configurational equilibrium and yet large compared with the time required to reach momentum, or flux, equilibrium. If the latter has a relaxation time of the order τ_0, then $\tau > \tau_0$ is required. For convenience, the more definite stipulation that $\tau = 2\tau_0$ is made. It can now be seen that the fluxes have time to attain their prescribed values (31) in relation to the affinities. Expanding the expression in braces to second order in τ and allowing τ to assume its limiting value gives

$$\left\langle \frac{dN}{dt}+\tau_0\frac{d^2N}{dt^2}\right\rangle = -\mathbf{J}\cdot\boldsymbol{\Sigma}. \tag{35}$$

Using the first equality in (32), the average values of the fluxes can be written as

$$\frac{\partial\mathbf{J}}{\partial t}+\frac{1}{\tau_0}\mathbf{J} = \frac{1}{\tau_0}D{:}\mathbf{X}. \tag{36}$$

This has the solution (a generalization of (31))

$$\mathbf{J}(t) = \int_0^t \frac{1}{\tau_0} e^{-t'/\tau_0} D{:}\mathbf{X}(t-t')dt', \tag{37}$$

which is of the same form as the expression given in equation (23) for the Goldstein equation. The assumption that the system is always in a state of momentum equilibrium and that the entropy production rate, due to a changing flux distribution, is negligible is justified precisely by the retention of rate-of-change differentials of higher order, either as in equation (36) or as stipulated in equation (33). This point is discussed from a similar standpoint by De Groot (1952).

If the system under consideration is an ideal gas, it is reasonable to consider the velocity changes to be governed by a Markov process. This is because the dynamics of a particle may be described by a Langevin equation in which the fluctuating (driving) force is caused by collisions with other particles. For an ideal gas there are no "distant encounters," and so the collisions will produce intense, short impulses whose power spectrum is essentially white. The power spectrum of the resulting particle motions corresponds (by the Wiener–Khinchine theorem) to an exponential velocity autocorrelation function with a correlation time equal to the mean time between collisions. It is well known that the time between collisions is approximately equal to the time of relaxation of the velocities to the Maxwell distribution; hence, the appropriate velocity autocorrelation function for the ideal gaseous system is exactly the hereditary function appearing in (37) above.

IV. PROPOSED GENERALIZATION

An examination of (23) and (37) leads to a formally straightforward generalization involving the velocity cross-correlation matrix defined by

$$R_{ik}(t') = \langle v_i(t) v_k(t+t') \rangle, \tag{38}$$

where, as before, the average is to be taken over an ensemble of similar systems. The generalization of Fick's law now reads

$$J_i(\mathbf{r}, t) = -\frac{\partial}{\partial x^k} \int_0^t R_{ik}(t') P(\mathbf{r}, t-t')dt'. \tag{39}$$

Taking the divergence of this relation and employing the equation of continuity yields the postulated equation for turbulent diffusion:

$$\frac{\partial P}{\partial t} = \frac{\partial^2}{\partial x^i \partial x^k} \int_0^t R_{ik}(t') P(\mathbf{r}, t-t')dt'. \tag{40}$$

Since the velocity correlations need not be of the simple exponential form, this constitutes a significant generalization of the Goldstein equation. It is interesting to note that Batchelor and Townsend (1956) remark that a satisfactory theory of turbulent diffusion might be expected to take the form of an integral equation because of the persistence of motions.

The postulated equation leads to a well-known kinematical result, deducible independently of any diffusion equation, and due originally to Kampé de Fériet (1939). This relation expresses the mean square deviation of diffusing particles in terms of the velocity autocorrelation. This result is obtained by multiplying equation (40) by the square of the radius vector and integrating it over all space. After interchanging the order of the differentiation and integration, it is seen that

$$\frac{d}{dt}\langle r^2\rangle = \int d^3x \int_0^t r^2 \frac{\partial^2}{\partial x^i \partial x^k} R_{ik}(t')P(\mathbf{r}, t-t')dt'. \tag{41}$$

By a number of partial integrations coupled with the assumption that the concentration and its gradiant diminish at large distances according to

$$rP \to 0 \quad \text{and} \quad r^2 \frac{\partial P}{\partial r} \to 0 \quad \text{as} \quad r \to \infty, \tag{42}$$

the desired relation is obtained:

$$\frac{d}{dt}\langle r^2\rangle = 2\sum_{k=1}^{3} \int_0^t R_{kk}(t')dt'. \tag{43}$$

It is required here, too, that the turbulence be statistically homogeneous, i.e., that the $R_{ik}(t')$ be independent of position. It should be pointed out that this result is strictly correct only if the source functions are sufficiently well behaved. For example, an impulse point-source solution to the Goldstein equation has, in addition to the well-behaved wake solution, a wave-front solution with delta-function character. This latter contributes an additional transient term to the quantity given by (43).

It is interesting to compare (40) with another diffusion equation, also involving velocity autocorrelation functions, which has been given by Pai (1957). He derives

$$\frac{\partial P}{\partial t} = D_{ik}(t) \frac{\partial^2 P}{\partial x^i \partial x^k}, \tag{44}$$

where the diffusion tensor is given by

$$D_{ik}(t) = \frac{1}{2}\int_{t_0}^{t} \langle v_i(t')v_k(t) + v_i(t)v_k(t')\rangle \, dt'. \tag{45}$$

Pai's equation may be written with $t_0 = 0$.

$$\frac{\partial P}{\partial t} = \int_0^t R_{ik}dt \frac{\partial^2 P}{\partial x^i \partial x^k}. \tag{46}$$

Pai's analysis assumes a normal distribution of displacements per unit time. This is essentially an assumption regarding the form of the "propagation function" for the diffusing particle and completely determines the result. It is also an assumption which has the same validity as the central limit theorem and, like the latter, applies only to the results of a large number of independent

events. Specifically, Pai's assumption is valid in the present context only for times that are long compared with a characteristic time of the diffusion process. In gaseous diffusion, this would mean the average time between collisions; here it is of the order of the relaxation time, or time scale of the turbulence, and is given by

$$\tau_0 = \frac{1}{v^2}\int_0^\infty R(t')dt'. \tag{47}$$

V. DIFFERENTIAL FORM OF PROPOSED EQUATION

The proposed description (40) can be cast in purely differential form whenever the autocorrelation functions have Laplace transforms expressible as a ratio of polynomials. The transform is defined by

$$\Phi_{ik}(s) = \int_0^\infty R_{ik}(t)e^{-st}dt. \tag{48}$$

Writing formally,

$$R_{ik}(t) = (2\pi i)^{-1}\int_{-i\infty}^{+i\infty} e^{st}\Phi_{ik}(s)ds = (2\pi i)^{-1}\Phi_{ik}\left(\frac{\partial}{\partial t}\right)\int_{-i\infty}^{+i\infty} e^{st}ds \tag{49}$$

$$= \Phi_{ik}\left(\frac{\partial}{\partial t}\right)\delta(t).$$

Substituting this operational result into (40) gives

$$\frac{\partial P}{\partial t} = \frac{\partial^2}{\partial x^i \partial x^k}\int_0^t \left[\Phi_{ik}\left(\frac{\partial}{\partial t'}\right)\delta(t')\right] P(\mathbf{r}, t-t')dt' + \delta(\mathbf{r})\delta(t), \tag{50}$$

where an impulse point source at the origin has been added to the original equation. Finally, from the properties of the delta function,

$$\frac{\partial P}{\partial t} = \frac{\partial^2}{\partial x^i \partial x^k}\Phi_{ik}\left(\frac{\partial}{\partial t}\right)P + \delta(\mathbf{r})\delta(t). \tag{51}$$

When Φ_{ik} can be expressed as a ratio of polynomials, we may write

$$\Phi_{ik} = \psi_{ik}/\chi, \tag{52}$$

where χ is the least common denominator of the Φ_{ik}. Operating on both sides of the preceding equation with χ yields

$$\chi\left(\frac{\partial}{\partial t}\right)\frac{\partial P}{\partial t} = \frac{\partial^2}{\partial x^i \partial x^k}\psi_{ik}\left(\frac{\partial}{\partial t}\right)P + \delta(\mathbf{r})\chi\left(\frac{\partial}{\partial t}\right)\delta(t). \tag{53}$$

This is the differential form of the equation for turbulent diffusion. The point-source term may be omitted in applications but has been included here because of the unusual form it takes in the differential equation (though not in the integro-differential equation).

The solution of the above equation, with the singular source terms, corresponds physically to the diffusion of unit amount of diffusate released instantaneously at the origin at time zero. The Green's function solution, however,

must be distinguished from this one. The Green's function is the solution of the above equation with the source function replaced by one in which the operator χ does not appear. The physical solution corresponding to a unit-impulse point source then can be obtained from the Green's function solution by multiplying by the $\chi(\partial/\partial t)$ operator.

Some examples of the turbulent autocorrelation functions, their transforms, and the polynomial operators ψ_{ik} and χ will be shown below.

A. The Classical Case of Fickian Diffusion

$$R_{ik}(t) = D\,\delta_{ik}\,\delta_+(t) \tag{54}$$

$$\Phi_{ik}(s) = D\,\delta_{ik} \tag{55}$$

$$\psi_{ik} = D\,\delta_{ik} \tag{56}$$

$$\chi = 1 \tag{57}$$

where $\delta_+(t)$ is so defined that

$$\int_0^t \delta_+(t)dt = 1 \qquad t > 0 \tag{58}$$

and δ_{ik} is the Kronecker delta.

B. The Case Reducing to the Goldstein–Michelson Equation

$$R_{ik}(t) = \langle v_k^2\rangle\,\delta_{ik}e^{-|t|/\tau_0} \tag{59}$$

$$\Phi_{ik}(s) = \tau_0\langle v_k^2\rangle\delta_{ik}/(1+\tau_0 s) \tag{60}$$

$$\psi_{ik} = \delta_{ik}\langle v_k^2\rangle\tau_0 \tag{61}$$

$$\chi = 1+\tau_0\frac{\partial}{\partial t}. \tag{62}$$

C. The "Phenomenological" Case (given by Frenkiel (1958, 1953) and applicable with suitable parameter values to a variety of turbulent regimes)

$$R_{ik}(t) = \delta_{ik}\langle v_k^2\rangle e^{-|t|/\tau_k}\cos\omega_k t \tag{63}$$

$$\Phi_{ik}(s) = \tau_k\delta_{ik}\langle v_k^2\rangle(s\tau_k+1)/[(\tau_k\omega_k)^2+(s\tau_k+1)^2] \tag{64}$$

$$\psi_{ik} = \tau_k\langle v_k^2\rangle\delta_{ik}\left(1+\tau_k\frac{\partial}{\partial t}\right) \tag{65}$$

$$\chi = \left(1+\tau_k\frac{\partial}{\partial t}\right)^2+(\omega_k\tau_k)^2. \tag{66}$$

D. The Case Corresponding to the Turbulence Described by von Karman–Howarth (1938)

$$R_{11}(t) = v\langle{}^2_{[1]}\rangle\, e^{-\beta|t|} \tag{67}$$

$$R_{22}(t) = R_{33}(t) = \langle v_\perp^2 \rangle e^{-\beta|t|}(1-\tfrac{1}{2}\beta|t|) \tag{68}$$

with cross-correlations vanishing.

$$\Phi_{11} = \langle v_{||}^2 \rangle/(s+\beta) \tag{69}$$

$$\Phi_{22} = \Phi_{33} = \langle v_\perp^2 \rangle(s+\tfrac{1}{2}\beta)/(s+\beta)^2 \tag{70}$$

$$\psi_{11} = \langle v_{||}^2 \rangle \left(\frac{\partial}{\partial t}+\beta\right) \tag{71}$$

$$\psi_{22} = \psi_{33} = \langle v_\perp^2 \rangle \left(\frac{\partial}{\partial t}+\frac{\beta}{2}\right) \tag{72}$$

$$\chi = \left(\frac{\partial}{\partial t}+\beta\right)^2. \tag{73}$$

VI. DISCUSSION

The diffusion equation given here was originally conceived, and has been presented, in a purely inductive fashion. However, since the first draft of this material was prepared, the author has learned that J. M. Richardson* has obtained, on very general deductive grounds, a quasi-differential diffusion equation, for the case of negligible spatial velocity correlations, that is equivalent to (40). The absence of any spatial correlation term in our equation is conspicuous; consequently, use of the new formulation is probably justified only in application to regimes in which the spatial coherence is negligible in comparison with the time coherence. In particular, application to plasmas with collective excitations may be precluded for this reason. From a consideration of the form of the equations of Richardson and from results obtained in a rigorous extension of the Goldstein model to two and three dimensions (to be presented elsewhere), it appears that the equation proposed here is valid providing at least one of the following two conditions are met:

(1) the spatial velocity correlations are negligible;

(2) space derivatives higher than the second are negligible.

Applications of the diffusion equation proposed here to systems satisfying one of these criteria will be presented in subsequent reports. The effects of spatial velocity correlations will also be discussed.

REFERENCES

BATCHELOR, G. K. and TOWNSEND, A. A. 1956. *In* Surveys in mechanics, *edited by* G. K. Batchelor and R. M. Davies (Cambridge University Press, New York).

DAVIES, R. W., DIAMOND, R. J., and SMITH, T. B. 1954. American Institute of Aerological Research, OSR-TN-54-62.

DE GROOT, S. R. 1952. Thermodynamics of irreversible processes (Interscience Publishers, Inc., New York), pp. 222–223.

DOOB, J. L. 1942. Ann. Math. **43**(2), 351.

FRENKIEL, F. N. 1958. NACA Technical Memorandum. 1436.

——— 1953. *In* Advances in applied mechanics III, *edited by* R. von Mies and T. von Karman (Academic Press, New York), pp. 62–106.

GOLDSTEIN, S. 1951. Quart. J. Mech. and Appl. Math. **4**(2), 129.

*Private communication.

JAYNES, E. T. 1957. Phys. Rev. **106**(4), 620.
KAMPÉ DE FÉRIET, J. 1957. Ann. soc. sci. Bruxelles, **59**, Ser. I, 145.
VON KÁRMÁN, T. and HOWARTH, L. 1938. Proc. Roy. Soc. A, **164**, 192.
MICHELSON, I. 1954. American Institute of Aerological Research, AF 18(600)-476.
PAI, SHIH-I. 1957. Viscous flow theory, II, turbulent flow (D. Van Nostrand Co., Inc., New York), pp. 181–182.
RICHARDSON, J. M. Hughes Research Laboratories. Private communication.
TAYLOR, G. I. 1921. Proc. London Math. Soc. **20**, 196.

THE THIRD SPECTRUM OF COBALT (Co III)[1]

A. G. SHENSTONE

ABSTRACT

A nearly complete analysis of the third spectrum of Co (Co III) is given, based chiefly on observations in the vacuum ultraviolet region. The chief structures found are $3d^7$, $3d^6\,4s$, $3d^6\,4p$, and $3d^6\,4d$. The last of these is not commonly found in third spectra and it is here very incomplete. Some cases of unusual intensities in intersystem combinations are pointed out, especially ones in which the intensity in the combinations with the central of three J values is zero or very small. The complete line list is given.

During the nineteen-thirties when there were many laboratories engaged in the analysis of atomic spectra, the third and fourth spectra of the metals of the first long period were neglected in favor of the lower and much higher ionizations. After the war we started at Princeton to fill this lacuna by extending the analyses of third spectra which had been partially analyzed and by making analyses as complete as possible of the ones which had been passed over. In 1950 we started the observation of Ni III and in 1951 Co III. The preliminary term tables derived from those analyses appeared in Atomic Energy Levels, Vol. II, in 1952. A more complete description of Ni III was published in 1954 (Shenstone 1954), and additions to it were made in Professor Catalan's laboratory in Madrid (Garcia-Riquelme 1955). Recently I have returned to the spectrum Co III and have been able to make such considerable additions to it that I believe it is now in as complete a state as is possible with the present observations. A description of the sources and instruments used in this investigation is given in some detail in the paper on Ni III (Shenstone 1954) to which reference should be made.

The spectrum of Co III is somewhat more complex than that of Ni III and its description is not quite as complete in spite of the fact that the isoelectronic spectrum Fe II (A.E.L. 1952) has been very thoroughly analyzed, whereas Co II, which is isoelectronic with Ni III, has not. Mn I is also isoelectronic with Co III but many of its important electron structures are of a different character involving two excited electrons.

In Fe II and Co III, the chief structures are $3d^7$, $3d^6\,4s$, $3d^6\,4p$, $3d^6\,5s$, $3d^6\,4d$, all of which are of considerable complexity. The main multiplets are those arising from the transition $3d^6(^5D)4s$–$3d^6(^5D)4p$. In Fe II they fall in the region 2700 Å to 2300 Å where observations of all kinds, including Zeeman effect, can be made with great accuracy, giving a consequent certainty in the analysis even though many other multiplets from the same electron transition are mixed with them. In Co III all of these multiplets are at shorter wavelengths, 2000 Å to 1800 Å, where resolving power and accuracy of measurement are considerably poorer. There is a consequent overlapping of lines, with the result that several have to be assigned to more than one transition. On the

[1]Manuscript received January 26, 1960.
Contribution from the Palmer Physical Laboratory, Princeton University, Princeton, N.J.

TABLE I

Even levels of Co III

Electron structure	Designation	J	Value	Intervals
$3d^7$	$a\ ^4F$	$4\frac{1}{2}$	0.0	
		$3\frac{1}{2}$	841.2	−841.2
		$2\frac{1}{2}$	1451.3	−610.1
		$1\frac{1}{2}$	1866.8	−415.5
$3d^7$	$a\ ^4P$	$2\frac{1}{2}$	15201.9	
		$1\frac{1}{2}$	15428.2	−226.3
		$\frac{1}{2}$	15811.4	−383.2
$3d^7$	$a\ ^2G$	$4\frac{1}{2}$	16977.6	
		$3\frac{1}{2}$	17766.2	−788.6
$3d^7$	$a\ ^2P$	$1\frac{1}{2}$	20194.9	
		$\frac{1}{2}$	20918.5?	−723.6
$3d^7$	$a\ ^2H$	$5\frac{1}{2}$	22720.3	
		$4\frac{1}{2}$	23434.3	−714.0
$3d^7$	$a\ ^2D$	$2\frac{1}{2}$	23058.8	
		$1\frac{1}{2}$	24236.8	−1178.0
$3d^7$	$a\ ^2F$	$3\frac{1}{2}$	37021.0	
		$2\frac{1}{2}$	37316.5	−295.5
$3d^6(^5D)4s$	$a\ ^6D$	$4\frac{1}{2}$	46438.3	
		$3\frac{1}{2}$	47003.1	−564.8
		$2\frac{1}{2}$	47415.4	−412.3
		$1\frac{1}{2}$	47698.6	−283.2
		$\frac{1}{2}$	47864.8	−166.2
$3d^6(^5D)4s$	$a\ ^4D$	$3\frac{1}{2}$	55729.2	
		$2\frac{1}{2}$	56373.8	−644.6
		$1\frac{1}{2}$	56794.8	−421.0
		$\frac{1}{2}$	57036.8	−242.0
$3d^6(^3P)4s$	$b\ ^4P$	$2\frac{1}{2}$	70934.1	
		$1\frac{1}{2}$	72341.9	−1407.8
		$\frac{1}{2}$	73214.5	−872.6
$3d^6(^3H)4s$	$a\ ^4H$	$6\frac{1}{2}$	71623.1	
		$5\frac{1}{2}$	71873.7	−250.6
		$4\frac{1}{2}$	72083.3	−209.6
		$3\frac{1}{2}$	72270.5	−187.2
$3d^6(^3F)4s$	$b\ ^4F$	$4\frac{1}{2}$	73286.0	
		$3\frac{1}{2}$	73540.2	−254.2
		$2\frac{1}{2}$	73726.6	−186.4
		$1\frac{1}{2}$	73861.8	−135.2
$3d^6(^3G)4s$	$a\ ^4G$	$5\frac{1}{2}$	76518.9	
		$4\frac{1}{2}$	77121.1	−602.2
		$3\frac{1}{2}$	77383.1	−262.0
		$2\frac{1}{2}$	77472.3	−89.2
$3d^6(^3P)4s$	$b\ ^2P$	$1\frac{1}{2}$	76791.1	
		$\frac{1}{2}$	78434.3	−1643.2
$3d^6(^3H)4s$	$b\ ^2H$	$5\frac{1}{2}$	77411.6	
		$4\frac{1}{2}$	77622.9	−211.3
$3d^6(^3F)4s$	$b\ ^2F$	$3\frac{1}{2}$	78927.8	
		$2\frac{1}{2}$	79425.3	−497.5
$3d^6(^3G)4s$	$b\ ^2G$	$4\frac{1}{2}$	82363.3	
		$3\frac{1}{2}$	82920.7	−557.4
$3d^6(^3D)4s$	$b\ ^4D$	$3\frac{1}{2}$	83938.9	
		$2\frac{1}{2}$	83799.6	+139.3
		$1\frac{1}{2}$	83773.4	+26.2
		$\frac{1}{2}$	83789.3	−15.9
$3d^6(^1I)4s$	$a\ ^2I$	$6\frac{1}{2}$	85474.1	
		$5\frac{1}{2}$	85517.3	−43.2
$3d^6(^1G)4s$	$c\ ^2G$	$4\frac{1}{2}$	86283.8	
		$3\frac{1}{2}$	86327.1	−43.3
$3d^6(^1D)4s$	$b\ ^2D$	$2\frac{1}{2}$	91715.1?	
$3d^6(^5D)4d$	$e\ ^6F$	$5\frac{1}{2}$	168012.7	
		$4\frac{1}{2}$	168211.5	−198.8
		$3\frac{1}{2}$	168449.6	−238.1
		$2\frac{1}{2}$	168688.9	−239.3
		$1\frac{1}{2}$	168885.5	−196.6
		$\frac{1}{2}$	169011.2	−125.7
$3d^6(^5D)4d$	$e\ ^6D$	$4\frac{1}{2}$	169527.7	
		$3\frac{1}{2}$	169595.9	−68.2
		$2\frac{1}{2}$	169770.3	−174.4
		$1\frac{1}{2}$	169996.0	−225.7
		$\frac{1}{2}$	170194.7	−198.7
$3d^6(^5D)4d$	$e\ ^6P$	$3\frac{1}{2}$	169591.0?	
		$2\frac{1}{2}$	170355.5?	−764.5
		$1\frac{1}{2}$	170804.6	−449.1
$3d^6(^5D)5s$	$f\ ^6D$	$4\frac{1}{2}$	170535.2	
		$3\frac{1}{2}$	171079.3	−544.1
		$2\frac{1}{2}$	171466.6	−387.3
		$1\frac{1}{2}$	171740.4	−273.8
		$\frac{1}{2}$	171941.5	−201.1
$3d^6(^5D)4d$	$e\ ^6G$	$6\frac{1}{2}$	170725.7	
		$5\frac{1}{2}$	171028.9	−303.2
		$4\frac{1}{2}$	171269.1	−240.2
		$3\frac{1}{2}$	171527.6	−258.5
		$2\frac{1}{2}$	171729.6	−202.0
		$1\frac{1}{2}$	171825.8	−96.2
$3d^6(^5D)4d$	$e\ ^4F$	$4\frac{1}{2}$	171942.6	
		$3\frac{1}{2}$	172377.0	−434.4
		$2\frac{1}{2}$	172802.7	−425.7
		$1\frac{1}{2}$	173133.5	−330.8
$3d^6(^5D)5s$	$f\ ^4D$	$3\frac{1}{2}$	172583.6	
		$2\frac{1}{2}$	173194.9	−611.3
		$1\frac{1}{2}$	173609.3	−414.4
		$\frac{1}{2}$	173851.1	−242.8
$3d^6$	^5D		270200	Limit

TABLE II

Odd levels of Co III

Electron structure	Designation	J	Value	Intervals
$3d^6(^5D)4p$	$z\,^6D$	$4\frac{1}{2}$	98290.3	
		$3\frac{1}{2}$	98545.6	−255.3
		$2\frac{1}{2}$	98823.2	−277.6
		$1\frac{1}{2}$	99043.5	−220.3
		$\frac{1}{2}$	99182.2	−138.7
$3d^6(^5D)4p$	$z\,^6F$	$5\frac{1}{2}$	103245.0	
		$4\frac{1}{2}$	103386.7	−141.7
		$3\frac{1}{2}$	103501.7	−115.0
		$2\frac{1}{2}$	103593.7	−92.0
		$1\frac{1}{2}$	103655.7	−62.0
		$\frac{1}{2}$	103690.8	−35.1
$3d^6(^5D)4p$	$z\,^6P$	$3\frac{1}{2}$	105008.7	
		$2\frac{1}{2}$	105965.1	−956.4
		$1\frac{1}{2}$	106591.9	−626.8
$3d^6(^5D)4p$	$z\,^4D$	$3\frac{1}{2}$	106489.2	
		$2\frac{1}{2}$	106954.7	−365.5
		$1\frac{1}{2}$	107297.0	−342.3
		$\frac{1}{2}$	107507.6	−210.6
$3d^6(^5D)4p$	$z\,^4F$	$4\frac{1}{2}$	106764.9	
		$3\frac{1}{2}$	107530.1	−765.2
		$2\frac{1}{2}$	108052.9	−522.8
		$1\frac{1}{2}$	108403.4	−350.5
$3d^6(^5D)4p$	$z\,^4P$	$2\frac{1}{2}$	110371.2	
		$1\frac{1}{2}$	110961.5	−590.3
		$\frac{1}{2}$	111283.1	−321.6
$3d^6(^3P)4p$	$z\,^4S$	$1\frac{1}{2}$	123123.1	
$3d^6(^3H)4p$	$z\,^4G$	$5\frac{1}{2}$	124765.9	
		$4\frac{1}{2}$	125012.4	−246.5
		$3\frac{1}{2}$	125227.0	−214.6
		$2\frac{1}{2}$	125369.1	−142.1
$3d^6(^3P)4p$	$y\,^4P$	$2\frac{1}{2}$	125003.3	
		$1\frac{1}{2}$	126381.8?	−1378.5
		$\frac{1}{2}$	127224.7?	−842.9
$3d^6(^3H)4p$	$z\,^4H$	$6\frac{1}{2}$	125276.2	
		$5\frac{1}{2}$	125296.2	−20.0
		$4\frac{1}{2}$	125421.6	−125.4
		$3\frac{1}{2}$	125690.5	−268.9
$3d^6(^3P)4p$	$z\,^2D$	$2\frac{1}{2}$	125992.7	
		$1\frac{1}{2}$	127458.1	−1465.4
$3d^6(^3H)4p$	$z\,^4I$	$7\frac{1}{2}$	126119.0	
		$6\frac{1}{2}$	126475.5	−356.5
		$5\frac{1}{2}$	126501.3	−25.8
		$4\frac{1}{2}$	126239.4	+261.9
$3d^6(^3P)4p$	$y\,^4D$	$3\frac{1}{2}$	126549.3	
		$2\frac{1}{2}$	128085.2	−1535.9
		$1\frac{1}{2}$	128423.1	−337.9
		$\frac{1}{2}$	128536.3	−113.2
$3d^6(^3F)4p$	$y\,^4F$	$4\frac{1}{2}$	126998.1	
		$3\frac{1}{2}$	126892.1	+106.0
		$2\frac{1}{2}$	126870.9	+21.2
		$1\frac{1}{2}$	126987.6	−116.7
$3d^6(^3H)4p$	$z\,^2G$	$4\frac{1}{2}$	127050.8	
		$3\frac{1}{2}$	127317.7	−266.9
$3d^6(^3H)4p$	$z\,^2I$	$6\frac{1}{2}$	127672.9	
		$5\frac{1}{2}$	128258.9	−586.0
$3d^6(^3F)4p$	$x\,^4D$	$3\frac{1}{2}$	128017.7	
		$2\frac{1}{2}$	128524.9	−507.2
		$1\frac{1}{2}$	128804.9	−280.0
		$\frac{1}{2}$	128937.4	−132.5
$3d^6(^3F)4p$	$y\,^4G$	$5\frac{1}{2}$	129556.0	
		$4\frac{1}{2}$	129592.3	−36.3
		$3\frac{1}{2}$	129706.9	−114.6
		$2\frac{1}{2}$	129747.3	−40.4
$3d^6(^3F)4p$	$z\,^2F$	$3\frac{1}{2}$	130183.8	
		$2\frac{1}{2}$	130407.8	−224.0
$3d^6(^3P)4p$	$z\,^2P$	$1\frac{1}{2}$	130909.0	
		$\frac{1}{2}$	130799.5	+109.5
$3d^6(^3F)4p$	$y\,^2G$	$4\frac{1}{2}$	130801.9	
		$3\frac{1}{2}$	131279.9	−478.0
$3d^6(^3H)4p$	$z\,^2H$	$5\frac{1}{2}$	131054.2	
		$4\frac{1}{2}$	131538.3	−484.1
$3d^6(^3G)4p$	$x\,^4F$	$4\frac{1}{2}$	131098.2	
		$3\frac{1}{2}$	131581.6	−483.4
		$2\frac{1}{2}$	132489.0	−907.4
		$1\frac{1}{2}$	132592.4	−103.4
$3d^6(^3G)4p$	$x\,^4G$	$5\frac{1}{2}$	131371.1	
		$4\frac{1}{2}$	131887.1	−516.0
		$3\frac{1}{2}$	132277.1	−390.0
		$2\frac{1}{2}$	131883.9	+393.2
$3d^6(^3P)4p$	$z\,^2S$	$\frac{1}{2}$	132314.9	
$3d^6(^3G)4p$	$y\,^4H$	$6\frac{1}{2}$	132376.8	
		$5\frac{1}{2}$	132506.2	−129.4
		$4\frac{1}{2}$	132587.0	−80.8
		$3\frac{1}{2}$	132623.8	−36.8
$3d^6(^3F)4p$	$y\,^2D$	$2\frac{1}{2}$	133711.4	
		$1\frac{1}{2}$	134079.8	−368.4
$3d^6(^3G)4p$	$y\,^2H$	$5\frac{1}{2}$	134696.1	
		$4\frac{1}{2}$	135404.0	−707.9
$3d^6(^3G)4p$	$y\,^2F$	$3\frac{1}{2}$	136290.1	
		$2\frac{1}{2}$	136129.1	+61.0

TABLE II (*Concluded*)

Odd levels of Co III

Electron structure	Designation	J	Value	Intervals
$3d^6(^1I)4p$	$z\,^2K$	$7\frac{1}{2}$	138234.3	+871.3
		$6\frac{1}{2}$	137363.0	
$3d^6(^3G)4p$	$x\,^2G$	$5\frac{1}{2}$	137661.4	−151.0
		$4\frac{1}{2}$	137812.4	
$3d^6(^3D)4p$	$x\,^4P$	$2\frac{1}{2}$	138774.7	−195.8
		$1\frac{1}{2}$	138970.5	−343.7
		$\frac{1}{2}$	139314.2	
$3d^6(^1I)4p$	$x\,^2H$	$5\frac{1}{2}$	139137.5	+216.5
		$4\frac{1}{2}$	138921.0	
$3d^6(^3D)4p$	$w\,^4D$	$3\frac{1}{2}$	139818.7	+75.3
		$2\frac{1}{2}$	139743.4	+116.2
		$1\frac{1}{2}$	139627.2	−103.8
		$\frac{1}{2}$	139731.0	
$3d^6(^3D)4p$	$w\,^4F$	$4\frac{1}{2}$	140492.4	+266.6
		$3\frac{1}{2}$	140225.8	+14.2
		$2\frac{1}{2}$	140211.6	+11.5
		$1\frac{1}{2}$	140200.1	
$3d^6(^1G)4p$	$w\,^2G$	$4\frac{1}{2}$	140358.4	−24.5
		$3\frac{1}{2}$	140382.9	
$3d^6(^1G)4p$	$x\,^2F$	$3\frac{1}{2}$	140645.4	−141.9
		$2\frac{1}{2}$	140787.3	
$3d^6(^1G)4p$	$w\,^2H$	$5\frac{1}{2}$	141190.5	−156.8
		$4\frac{1}{2}$	141347.3	
$3d^6(^1I)4p$	$y\,^2I$	$6\frac{1}{2}$	141868.8	−5.0
		$5\frac{1}{2}$	141873.8	
$3d^6(^3D)4p$	$w\,^2F$	$3\frac{1}{2}$	143677.1?	
$3d^6(^1D)4p$	$v\,^2F$	$3\frac{1}{2}$	146815.6	
$3d^6(^1D)4p$	$x\,^2D$	$2\frac{1}{2}$	146950.7	
$3d^6(b^3P)4p$	$y\,^4S$	$1\frac{1}{2}$	155702.4	
$3d^6(b^3P)4p$	$w\,^4P$	$2\frac{1}{2}$	156291.4	+243.6
		$1\frac{1}{2}$	156047.8?	
?	$v\,^4P$	$2\frac{1}{2}$	161811.3	
$3d^6$	^5D		270200	Limit

other hand, the structure $3d^7$, which in Fe II is mixed with $3d^6\,4s$, is in Co III lower by over 40,000 cm^{-1}. It therefore produces a set of strong lines reaching down to 650 Å, completely separated from the main transitions. This is of considerable aid in the analysis, because the short wavelength lines must be transitions to one or another of the levels of $3d^7$.

The details of the analysis are contained in the tables. Tables I and II give the even and odd levels arranged in terms in order of decreasing J. Table III gives a resume of all the identified terms and Table IV is the list of lines from which the analysis was made. The latter includes all of the observed lines except for a few of doubtful origin or very low intensity and it will be seen that most of the lines have been assigned. There still remain unassigned, however, a number of moderately strong lines in the region 1300 Å to 1600 Å and a few even stronger lines between 1800 Å and 2000 Å. These groups require explanation.

The shorter of the two regions contains mainly lines from the transition $4p$–$5s$ and $4p$–$4d$. The higher structures involved, especially the $4d$, are very complex. Even $3d^6(^5D)4d$ alone yields 37 levels, of which 24 have been found. It seems, therefore, that the undiscovered levels of the complete structure can very easily account for all of the remaining unidentified lines of this group.

The longer wavelength group is in the region occupied by the $4s$–$4p$ transition and the lines are in all probability due to the unidentified higher levels of those two structures. The chief even levels not yet found are the high $d^7\,^2D$ and those

TABLE III

Observed terms of Co III

$1s^2 2s^2 2p^6 3p^6$	Observed terms																			
$3d^7$							$a\,^4P$			$a\,^4F$										
							$a\,^2P$	$a\,^2D$		$a\,^2F$	$a\,^2G$	$a\,^2H$								
	$ns\ (n>4)$						$np\ (n>4)$										$nd\ (n>4)$			
$3d^6(^5D)nx$		$a,f\,^6D$					$z\,^6P$	$z\,^6D$		$z\,^6F$							$e\,^6P$	$e\,^6D$	$e\,^6F$	$e\,^6G$
		$a,f\,^4D$					$z\,^4P$	$z\,^4D$		$z\,^4F$									$e\,^4F$	
(^3P)	$b\,^4P$					$z\,^4S$	$y\,^4P$	$y\,^4D$												
	$b\,^2P$					$z\,^2S$	$z\,^2P$	$z\,^2D$												
(^3H)				$a\,^4H$							$z\,^4G$	$z\,^4H$	$z\,^4I$							
				$b\,^2H$							$z\,^2G$	$z\,^2H$	$z\,^2I$							
(^3F)		$b\,^4F$						$x\,^4D$		$y\,^4F$	$y\,^4G$									
		$b\,^2F$						$y\,^2D$		$z\,^2F$	$y\,^2G$									
(^3G)			$a\,^4G$							$x\,^4F$	$x\,^4G$	$x\,^4H$								
			$b\,^2G$							$y\,^2F$	$x\,^2G$	$y\,^2H$								
(^1I)					$a\,^2I$							$x\,^2H$	$y\,^2I$	$z\,^2K$						
(^3D)	$b\,^4D$						$x\,^4P$	$w\,^4D$		$w\,^4F$										
										$w\,^2F$										
(^1G)			$c\,^2G$							$x\,^2F$	$w\,^2G$	$w\,^2H$								
(^1D)	$b\,^2D$							$x\,^2D$	$v\,^2F$											
$(b\,^2P)$						$y\,^4S$	$w\,^4P$													

TABLE IV

Observed lines of Co III

λ (vac.)	I	ν		λ (vac.)	I	ν	
649.342	1	154002.1		770.192	1	129837.8	$a\ ^2G_{4\frac{1}{2}}$–$v\ ^2F_{3\frac{1}{2}}$
651.323	0	153533.7		770.723	2	129748.3	
666.271	5	150089.1		770.967	0	129707.2	$a\ ^4F_{4\frac{1}{2}}$–$y\ ^4G_{3\frac{1}{2}}$
668.867	3	149506.6		771.638	10	129594.4	$a\ ^4F_{4\frac{1}{2}}$–$y\ ^4G_{4\frac{1}{2}}$
681.867	0	146639.4		771.868	30	129555.8	$a\ ^4F_{4\frac{1}{2}}$–$y\ ^4G_{5\frac{1}{2}}$
682.084	5	146609.5	$a\ ^4P_{2\frac{1}{2}}$–$v\ ^4P_{2\frac{1}{2}}$	773.125	1	129343.7	$a\ ^4F_{3\frac{1}{2}}$–$z\ ^2F_{3\frac{1}{2}}$
683.140	3	146382.9	$a\ ^4P_{1\frac{1}{2}}$–$v\ ^4P_{2\frac{1}{2}}$	775.446	2	128958.0	$a\ ^4F_{2\frac{1}{2}}$–$z\ ^2F_{2\frac{1}{2}}$
708.767	15	141090.1	$a\ ^4P_{2\frac{1}{2}}$–$w\ ^4P_{2\frac{1}{2}}$	775.992	10	128867.3	$a\ ^4F_{3\frac{1}{2}}$–$y\ ^4G_{3\frac{1}{2}}$
709.912	10	140862.5	$a\ ^4P_{1\frac{1}{2}}$–$w\ ^4P_{2\frac{1}{2}}$	776.688	20	128751.8	$a\ ^4F_{3\frac{1}{2}}$–$y\ ^4G_{4\frac{1}{2}}$
709.996	15	140845.9		776.794	5	128734.3	$a\ ^4F_{2\frac{1}{2}}$–$z\ ^2F_{3\frac{1}{2}}$
710.592	0	140727.7		779.436	3	128297.9	$a\ ^4F_{2\frac{1}{2}}$–$y\ ^4G_{2\frac{1}{2}}$
711.002	0	140646.6	$a\ ^4F_{4\frac{1}{2}}$–$x\ ^2F_{3\frac{1}{2}}$	779.683	20	128257.3	$a\ ^4F_{2\frac{1}{2}}$–$y\ ^4G_{3\frac{1}{2}}$
711.741	5	140500.5	$a\ ^4P_{2\frac{1}{2}}$–$y\ ^4S_{1\frac{1}{2}}$	780.287	0	128158.0	
712.193	0?	140411.3		781.130	20	128019.7	$a\ ^4F_{4\frac{1}{2}}$–$x\ ^4D_{3\frac{1}{2}}$
712.890	2	140274.1	$a\ ^4P_{1\frac{1}{2}}$–$y\ ^4S_{1\frac{1}{2}}$	781.250	3	128000.0	
714.836	0	139892.2	$a\ ^4P_{\frac{1}{2}}$–$y\ ^4S_{1\frac{1}{2}}$	781.983	15	127880.0	$a\ ^4F_{1\frac{1}{2}}$–$y\ ^4G_{2\frac{1}{2}}$
715.125	0	139835.7		783.179	10	127684.7	$a\ ^4F_{3\frac{1}{2}}$–$x\ ^4D_{2\frac{1}{2}}$
716.055	2	139654.1	$a\ ^4F_{3\frac{1}{2}}$–$w\ ^4F_{4\frac{1}{2}}$	785.034	0	127383.0	
717.490	1	139374.8	$a\ ^4F_{3\frac{1}{2}}$–$w\ ^4F_{2\frac{1}{2}}$ and $w\ ^4F_{2\frac{1}{2}}$	785.207	10	127355.0	$a\ ^4F_{2\frac{1}{2}}$–$x\ ^4D_{1\frac{1}{2}}$
				785.426	1	127319.4	$a\ ^4F_{4\frac{1}{2}}$–$z\ ^2G_{4\frac{1}{2}}$
735.720	0	135921.3		785.677	1	127278.8	
738.066	2	135489.2		785.883	15	127245.4	$a\ ^4F_{3\frac{1}{2}}$–$y\ ^4D_{2\frac{1}{2}}$
741.032	1	134946.9		786.958	8	127071.6	$a\ ^4F_{1\frac{1}{2}}$–$x\ ^4D_{\frac{1}{2}}$
745.762	0	134091.0		787.406	5	126999.3	$a\ ^4F_{4\frac{1}{2}}$–$y\ ^4F_{4\frac{1}{2}}$
745.939	0	134059.2		787.562	8	126974.1	$a\ ^4F_{2\frac{1}{2}}$–$y\ ^4D_{1\frac{1}{2}}$
747.375	0	133801.6		788.057	8	126894.4	$a\ ^4F_{4\frac{1}{2}}$–$y\ ^4F_{3\frac{1}{2}}$
748.019	1	133686.4		788.693	2	126792.0	
748.419	0	133615.0		788.815	0	126772.4	
752.485	0	132893.0		789.447	30	126670.9	$a\ ^4F_{1\frac{1}{2}}$–$y\ ^4D_{\frac{1}{2}}$
752.759	3	132844.6		789.662	2	126636.5	$a\ ^4F_{2\frac{1}{2}}$–$y\ ^4D_{2\frac{1}{2}}$
754.795	2*h*	132486.3		790.197	50	126550.7	$a\ ^4F_{4\frac{1}{2}}$–$y\ ^4D_{3\frac{1}{2}}$
755.253	5	132405.0		790.268	3?	126539.4	
755.512	0	132360.6		790.688	25	126472.1	$a\ ^4F_{3\frac{1}{2}}$–$z\ ^2G_{3\frac{1}{2}}$?
755.972	1	132280.2	$a\ ^4F_{4\frac{1}{2}}$–$x\ ^4G_{3\frac{1}{2}}$	791.440	3?	126352.0	
756.064	1	132263.9	$a\ ^4F_{2\frac{1}{2}}$–$y\ ^2D_{2\frac{1}{2}}$	792.661	5	126157.3	$a\ ^4F_{3\frac{1}{2}}$–$y\ ^4F_{4\frac{1}{2}}$
756.338	5	132216.0	$a\ ^4F_{1\frac{1}{2}}$–$y\ ^2D_{1\frac{1}{2}}$	792.833	5	126130.0	
758.212	20	131889.2	$a\ ^4F_{4\frac{1}{2}}$–$x\ ^4G_{4\frac{1}{2}}$	793.600	2	126008.1	$a\ ^4F_{2\frac{1}{2}}$–$z\ ^2D_{1\frac{1}{2}}$
759.592	3	131649.6	$a\ ^4F_{3\frac{1}{2}}$–$x\ ^4F_{2\frac{1}{2}}$	794.493	1	125866.4	$a\ ^4F_{2\frac{1}{2}}$–$z\ ^2G_{3\frac{1}{2}}$
759.644	3	131640.6		795.475	5	125711.1	$a\ ^4F_{3\frac{1}{2}}$–$y\ ^4D_{3\frac{1}{2}}$
759.970	0	131584.1	$a\ ^4F_{4\frac{1}{2}}$–$x\ ^4F_{3\frac{1}{2}}$	797.166	2	125444.4	$a\ ^4F_{2\frac{1}{2}}$–$y\ ^4F_{3\frac{1}{2}}$
760.211	1	131542.4	$a\ ^4F_{4\frac{1}{2}}$–$z\ ^2H_{4\frac{1}{2}}$	797.312	2	125421.4	$a\ ^4F_{2\frac{1}{2}}$–$y\ ^4F_{2\frac{1}{2}}$
760.825	30	131436.3	$a\ ^4F_{3\frac{1}{2}}$–$x\ ^4G_{3\frac{1}{2}}$	799.034	0	125151.1	$a\ ^4F_{3\frac{1}{2}}$–$z\ ^2D_{2\frac{1}{2}}$
761.202	1	131371.2	$a\ ^4F_{4\frac{1}{2}}$–$x\ ^4G_{5\frac{1}{2}}$	799.237	2	125119.3	$a\ ^4F_{1\frac{1}{2}}$–$y\ ^4F_{1\frac{1}{2}}$
762.038	1	131227.1		799.361	0	125099.9	$a\ ^4F_{2\frac{1}{2}}$–$y\ ^4D_{3\frac{1}{2}}$
762.529	3	131142.6	$a\ ^4F_{2\frac{1}{2}}$–$x\ ^4F_{1\frac{1}{2}}$	799.919	10*h*	125012.7	$a\ ^4F_{1\frac{1}{2}}$–$z\ ^4G_{4\frac{1}{2}}$
762.694	0	131114.2		800.445	2	124930.5	$a\ ^4F_{2\frac{1}{2}}$–$y\ ^4P_{1\frac{1}{2}}$
762.775	50	131100.3	$a\ ^4F_{4\frac{1}{2}}$–$x\ ^4F_{4\frac{1}{2}}$	801.493	30	124767.2	$a\ ^4F_{4\frac{1}{2}}$–$z\ ^4G_{5\frac{1}{2}}$
763.013	0	131059.4	$a\ ^4F_{4\frac{1}{2}}$–$z\ ^2H_{5\frac{1}{2}}$	802.434	1*h*	124620.8	$a\ ^4P_{2\frac{1}{2}}$–$w\ ^4D_{3\frac{1}{2}}$
763.131	25	131039.1	$a\ ^4F_{2\frac{1}{2}}$–$y\ ^4F_{2\frac{1}{2}}$	802.943	3	124541.8	$a\ ^4P_{2\frac{1}{2}}$–$w\ ^4D_{2\frac{1}{2}}$
764.229	0	130850.8		803.942	5	124387.1	$a\ ^4F_{3\frac{1}{2}}$–$z\ ^4G_{3\frac{1}{2}}$
764.363	2	130827.9	$a\ ^4F_{2\frac{1}{2}}$–$x\ ^4G_{3\frac{1}{2}}$	804.495	1*h*	124301.6	$a\ ^4P_{1\frac{1}{2}}$–$w\ ^4D_{\frac{1}{2}}$
764.418	2	130818.5		805.345	20	124170.4	$a\ ^4F_{3\frac{1}{2}}$–$z\ ^4G_{4\frac{1}{2}}$
764.866	10	130741.9	$a\ ^4F_{3\frac{1}{2}}$–$x\ ^4F_{3\frac{1}{2}}$	805.379	3	124165.1	$a\ ^4F_{3\frac{1}{2}}$–$y\ ^4P_{2\frac{1}{2}}$
764.959	20	130726.0	$a\ ^4F_{1\frac{1}{2}}$–$x\ ^4F_{1\frac{1}{2}}$	806.962	3*h*	123921.6	$a\ ^4P_{\frac{1}{2}}$–$w\ ^4D_{\frac{1}{2}}$
765.104	3*h*	130701.2	$a\ ^4F_{3\frac{1}{2}}$–$z\ ^2H_{4\frac{1}{2}}$	807.156	1	123891.8	
765.561	3	130623.2	$a\ ^4F_{1\frac{1}{2}}$–$y\ ^4F_{2\frac{1}{2}}$	807.910	15	123776.2	$a\ ^4F_{2\frac{1}{2}}$–$z\ ^4G_{3\frac{1}{2}}$
766.667	10*h*	130434.7	$a\ ^4F_{2\frac{1}{2}}$–$x\ ^4G_{2\frac{1}{2}}$	808.033	3	123757.3	$a\ ^2D_{2\frac{1}{2}}$–$v\ ^2F_{3\frac{1}{2}}$
767.703	20	130258.7	$a\ ^4F_{2\frac{1}{2}}$–$x\ ^4F_{4\frac{1}{2}}$	808.612	5	123668.7	$a\ ^2G_{4\frac{1}{2}}$–$x\ ^2F_{3\frac{1}{2}}$
767.770	15	130247.3		809.221	15	123575.6	$a\ ^4P_{2\frac{1}{2}}$–$x\ ^4P_{2\frac{1}{2}}$
768.458	20	130131.1	$a\ ^4F_{2\frac{1}{2}}$–$x\ ^4F_{3\frac{1}{2}}$	809.609	10	123516.4	$a\ ^2G_{4\frac{1}{2}}$–$w\ ^4F_{4\frac{1}{2}}$
769.128	10	130017.4	$a\ ^4F_{1\frac{1}{2}}$–$x\ ^4G_{2\frac{1}{2}}$	809.706	15	123501.9	$a\ ^4F_{1\frac{1}{2}}$–$z\ ^4G_{2\frac{1}{2}}$
769.343	5	129981.0		809.844	2	123480.6	
769.459	3	129961.4	$a\ ^4F_{3\frac{1}{2}}$–$y\ ^2G_{4\frac{1}{2}}$	810.502	15	123380.3	$a\ ^2G_{4\frac{1}{2}}$–$w\ ^2G_{4\frac{1}{2}}$

TABLE IV (*Continued*)

Observed lines of Co III

λ (vac.)	I	ν	λ (vac.)	I	ν
810.716	10	123347.8 $a\ ^4P_{1\frac{1}{2}}$–$x\ ^4P_{2\frac{1}{2}}$	910.415	0	109841.2 $a\ ^2D_{1\frac{1}{2}}$–$y\ ^2D_{1\frac{1}{2}}$
811.951	10	123160.1 $a\ ^4P_{\frac{1}{2}}$–$x\ ^4P_{1\frac{1}{2}}$	910.721	0	109803.1 $a\ ^4P_{2\frac{1}{2}}$–$y\ ^4P_{2\frac{1}{2}}$
812.869	10	123021.1 $a\ ^2G_{3\frac{1}{2}}$–$x\ ^2F_{2\frac{1}{2}}$	912.817	2	109551.0 $a\ ^2G_{3\frac{1}{2}}$–$z\ ^2G_{3\frac{1}{2}}$
814.066	1	122840.2 $a\ ^2G_{4\frac{1}{2}}$–$w\ ^4D_{3\frac{1}{2}}$	913.239	2	109500.4 $a\ ^2F_{3\frac{1}{2}}$–$v\ ^2F_{3\frac{1}{2}}$
814.649	2*h*	122752.3	916.714	1	109085.3
815.555	25	122615.9 $a\ ^2G_{3\frac{1}{2}}$–$w\ ^2G_{3\frac{1}{2}}$	918.233	1	108904.8
816.407	0	122487.9	920.371	2	108651.8 $a\ ^2H_{5\frac{1}{2}}$–$x\ ^4G_{5\frac{1}{2}}$
816.617	10	122456.4 $a\ ^2G_{3\frac{1}{2}}$–$w\ ^4F_{2\frac{1}{2}}$	923.075	10	108333.6 $a\ ^2H_{5\frac{1}{2}}$–$z\ ^2H_{5\frac{1}{2}}$
816.864	1	122419.4	925.045	8	108102.8 $a\ ^2H_{4\frac{1}{2}}$–$z\ ^2H_{4\frac{1}{2}}$
817.937	1	122258.8	925.230	0	108081.2 $a\ ^2H_{5\frac{1}{2}}$–$y\ ^2G_{4\frac{1}{2}}$
818.600	20	122159.8 $a\ ^2G_{4\frac{1}{2}}$–$x\ ^2H_{5\frac{1}{2}}$	926.591	0	107922.5 $a\ ^4P_{2\frac{1}{2}}$–$z\ ^4S_{1\frac{1}{2}}$
820.066	3	121941.4 $a\ ^2G_{4\frac{1}{2}}$–$x\ ^2H_{4\frac{1}{2}}$	927.224	5	107848.8 $a\ ^2D_{2\frac{1}{2}}$–$z\ ^2P_{1\frac{1}{2}}$
821.771	0	121688.4	929.970	5	107530.4 $a\ ^4F_{4\frac{1}{2}}$–$z\ ^4F_{3\frac{1}{2}}$
825.403	15	121152.9 $a\ ^2G_{3\frac{1}{2}}$–$x\ ^2H_{4\frac{1}{2}}$	932.733	3	107211.8 $a\ ^4F_{3\frac{1}{2}}$–$z\ ^4F_{2\frac{1}{2}}$
828.608	1	120684.3 $a\ ^2G_{4\frac{1}{2}}$–$x\ ^2G_{4\frac{1}{2}}$	935.003	3	106951.5 $a\ ^4F_{2\frac{1}{2}}$–$z\ ^4F_{1\frac{1}{2}}$
829.072	10	120616.8 $a\ ^2D_{2\frac{1}{2}}$–$w\ ^2F_{3\frac{1}{2}}$	936.639	30	106764.7 $a\ ^4F_{4\frac{1}{2}}$–$z\ ^4F_{4\frac{1}{2}}$
832.050	5	120185.1	937.310	20	106688.3 $a\ ^4F_{3\frac{1}{2}}$–$z\ ^4F_{3\frac{1}{2}}$
836.128	1	119598.9	938.077	10	106601.1 $a\ ^4F_{2\frac{1}{2}}$–$z\ ^4F_{2\frac{1}{2}}$
837.330	1	119427.2	938.647	5	106536.3 $a\ ^4F_{1\frac{1}{2}}$–$z\ ^4F_{1\frac{1}{2}}$
838.133	25	119312.8 $a\ ^2G_{4\frac{1}{2}}$–$y\ ^2F_{3\frac{1}{2}}$	939.060	30	106489.5 $a\ ^4F_{4\frac{1}{2}}$–$z\ ^4D_{3\frac{1}{2}}$
839.284	30	119149.2 $a\ ^2H_{5\frac{1}{2}}$–$y\ ^2I_{6\frac{1}{2}}$	941.756	0	106184.6 $a\ ^4F_{1\frac{1}{2}}$–$z\ ^4F_{2\frac{1}{2}}$
844.097	20	118469.8 $a\ ^2H_{5\frac{1}{2}}$–$w\ ^2H_{5\frac{1}{2}}$	942.051	0	106151.4
844.310	8	118439.9 $a\ ^2H_{4\frac{1}{2}}$–$y\ ^2I_{5\frac{1}{2}}$	942.388	20	106113.4 $a\ ^4F_{3\frac{1}{2}}$–$z\ ^4D_{2\frac{1}{2}}$
844.411	1	118425.7 $a\ ^2G_{4\frac{1}{2}}$–$y\ ^2H_{4\frac{1}{2}}$	942.696	1	106078.7 $a\ ^4F_{2\frac{1}{2}}$–$z\ ^4F_{3\frac{1}{2}}$
844.866	10	118362.0 $a\ ^2G_{3\frac{1}{2}}$–$y\ ^2F_{2\frac{1}{2}}$	944.084	1	105922.8 $a\ ^4F_{2\frac{1}{2}}$–$z\ ^4F_{4\frac{1}{2}}$
845.793	1	118232.2	944.768	20	105846.1 $a\ ^4F_{2\frac{1}{2}}$–$z\ ^4D_{1\frac{1}{2}}$
848.088	30	117912.3 $a\ ^2H_{4\frac{1}{2}}$–$w\ ^2H_{4\frac{1}{2}}$	945.198	0	105797.9 $a\ ^2P_{1\frac{1}{2}}$–$z\ ^2D_{2\frac{1}{2}}$
849.210	0	117756.5 $a\ ^2H_{4\frac{1}{2}}$–$w\ ^2H_{5\frac{1}{2}}$	946.526	10	105649.5 $a\ ^4F_{3\frac{1}{2}}$–$z\ ^4D_{3\frac{1}{2}}$
849.485	5	117718.4 $a\ ^2G_{4\frac{1}{2}}$–$y\ ^2H_{5\frac{1}{2}}$	946.594	20	105641.9 $a\ ^4F_{4\frac{1}{2}}$–$z\ ^4D_{4\frac{1}{2}}$
850.067	3	117637.8 $a\ ^2G_{3\frac{1}{2}}$–$y\ ^2H_{4\frac{1}{2}}$	947.838	10	105503.3 $a\ ^4F_{2\frac{1}{2}}$–$z\ ^4D_{2\frac{1}{2}}$
850.424	3	117588.4 $a\ ^2D_{2\frac{1}{2}}$–$x\ ^2F_{3\frac{1}{2}}$	948.501	5	105429.5 $a\ ^4F_{1\frac{1}{2}}$–$z\ ^4D_{1\frac{1}{2}}$
850.965	0	117513.6	951.264	0	105123.3 $a\ ^4F_{3\frac{1}{2}}$–$z\ ^6P_{2\frac{1}{2}}$
858.663	1	116460.1	952.279	2	105011.2 $a\ ^4F_{4\frac{1}{2}}$–$z\ ^6P_{3\frac{1}{2}}$
858.975	15	116418.4 $a\ ^2H_{5\frac{1}{2}}$–$x\ ^2H_{5\frac{1}{2}}$	952.812	2	104952.4 $a\ ^2H_{5\frac{1}{2}}$–$z\ ^2I_{6\frac{1}{2}}$
865.567	0	115531.2 $a\ ^2G_{4\frac{1}{2}}$–$y\ ^4H_{5\frac{1}{2}}$	953.977	2	104824.2 $a\ ^2H_{4\frac{1}{2}}$–$z\ ^2I_{5\frac{1}{2}}$
865.898	0	115487.0 $a\ ^2H_{4\frac{1}{2}}$–$x\ ^2H_{4\frac{1}{2}}$	989.169	1	101094.8
870.007	15	114941.6 $a\ ^2H_{5\frac{1}{2}}$–$x\ ^2G_{4\frac{1}{2}}$	992.145	5	100791.4 $a\ ^2F_{2\frac{1}{2}}$–$x\ ^2G_{3\frac{1}{2}}$
874.294	10	114378.0 $a\ ^2H_{4\frac{1}{2}}$–$x\ ^2G_{3\frac{1}{2}}$	996.558	8	100345.4 $a\ ^2F_{3\frac{1}{2}}$–$x\ ^2G_{4\frac{1}{2}}$
876.594	5	114077.9 $a\ ^2G_{4\frac{1}{2}}$–$z\ ^2H_{5\frac{1}{2}}$	1008.997	2	99108.3 $a\ ^2F_{2\frac{1}{2}}$–$y\ ^2F_{2\frac{1}{2}}$
877.881	0	113910.7	1030.280	0	97062.0 $a\ ^2F_{2\frac{1}{2}}$–$y\ ^2D_{1\frac{1}{2}}$
878.080	0	113884.8 $a\ ^2P_{1\frac{1}{2}}$–$y\ ^2D_{1\frac{1}{2}}$	1037.174	0	96394.5 $a\ ^2F_{3\frac{1}{2}}$–$y\ ^2D_{2\frac{1}{2}}$
878.543	10	113824.8 $a\ ^2G_{4\frac{1}{2}}$–$y\ ^2G_{4\frac{1}{2}}$	1043.243	15	95854.9 $a\ ^4P_{1\frac{1}{2}}$–$z\ ^4P_{\frac{1}{2}}$
878.963	5	113770.4 $a\ ^2G_{3\frac{1}{2}}$–$z\ ^2H_{4\frac{1}{2}}$	1044.281	20	95759.7 $a\ ^4P_{2\frac{1}{2}}$–$z\ ^4P_{1\frac{1}{2}}$
879.480	0	113703.6	1046.760	3	95532.9 $a\ ^4P_{1\frac{1}{2}}$–$z\ ^4P_{1\frac{1}{2}}$
880.950	10	113513.8 $a\ ^2G_{3\frac{1}{2}}$–$x\ ^4G_{3\frac{1}{2}}$	1047.471	2	95467.9 $a\ ^4P_{\frac{1}{2}}$–$z\ ^4P_{\frac{1}{2}}$?
882.025	0	113375.5 $a\ ^4P_{1\frac{1}{2}}$–$x\ ^4D_{1\frac{1}{2}}$	1048.879	3	95339.9
883.154	5	113230.5 $a\ ^2D_{2\frac{1}{2}}$–$y\ ^2F_{3\frac{1}{2}}$	1050.762	20	95169.0 $a\ ^4P_{2\frac{1}{2}}$–$z\ ^4P_{2\frac{1}{2}}$
883.345	1	113206.1 $a\ ^2G_{4\frac{1}{2}}$–$z\ ^2F_{3\frac{1}{2}}$	1050.977	10	95149.6 $a\ ^4P_{\frac{1}{2}}$–$z\ ^4P_{1\frac{1}{2}}$
883.703	2	113160.2 $a\ ^2P_{\frac{1}{2}}$–$y\ ^2D_{1\frac{1}{2}}$	1053.257	10	94943.6 $a\ ^4P_{1\frac{1}{2}}$–$z\ ^4P_{2\frac{1}{2}}$
883.960	0	113127.8 $a\ ^4P_{\frac{1}{2}}$–$x\ ^4D_{\frac{1}{2}}$	1064.568	0	93934.8
884.192	2	113097.6 $a\ ^4P_{1\frac{1}{2}}$–$x\ ^4D_{2\frac{1}{2}}$	1077.530	2	92804.8
885.011	0	112992.9 $a\ ^4P_{\frac{1}{2}}$–$x\ ^4D_{1\frac{1}{2}}$	1078.127	2	92749.2
886.378	5	112818.7 $a\ ^4P_{2\frac{1}{2}}$–$x\ ^4D_{3\frac{1}{2}}$	1079.098	2	92670.0
887.777	0	112640.9 $a\ ^2G_{3\frac{1}{2}}$–$z\ ^2F_{2\frac{1}{2}}$	1088.486	1	91870.7 $a\ ^4P_{1\frac{1}{2}}$–$z\ ^4D_{1\frac{1}{2}}$
887.988	0	112614.1 $a\ ^4P_{\frac{1}{2}}$–$y\ ^4D_{1\frac{1}{2}}$	1089.899	1	91751.6 $a\ ^4P_{2\frac{1}{2}}$–$z\ ^4D_{2\frac{1}{2}}$
891.902	5	112120.0 $a\ ^2P_{1\frac{1}{2}}$–$z\ ^2S_{\frac{1}{2}}$	1090.554	0	91696.5 $a\ ^4P_{\frac{1}{2}}$–$z\ ^4D_{\frac{1}{2}}$
893.045	15	111976.4 $a\ ^2H_{5\frac{1}{2}}$–$y\ ^2H_{5\frac{1}{2}}$	1090.668	0	91686.9
893.095	8	111970.2 $a\ ^2H_{4\frac{1}{2}}$–$y\ ^2H_{4\frac{1}{2}}$	1092.581	10	91526.4 $a\ ^4P_{1\frac{1}{2}}$–$z\ ^4D_{2\frac{1}{2}}$
893.713	8	111892.7 $a\ ^2D_{1\frac{1}{2}}$–$y\ ^2F_{2\frac{1}{2}}$	1093.066	5	91485.8 $a\ ^4P_{\frac{1}{2}}$–$z\ ^4D_{1\frac{1}{2}}$
897.686	1	111397.5 $a\ ^2P_{\frac{1}{2}}$–$z\ ^2S_{\frac{1}{2}}$	1095.443	15	91287.3 $a\ ^4P_{2\frac{1}{2}}$–$z\ ^4D_{3\frac{1}{2}}$
899.025	1	111231.6	1114.405	1	89734.0 $a\ ^2F_{3\frac{1}{2}}$–$z\ ^2G_{4\frac{1}{2}}$
903.730	5	110652.5 $a\ ^2D_{2\frac{1}{2}}$–$y\ ^2D_{2\frac{1}{2}}$	1270.646	2	78700.1
908.491	5	110072.6 $a\ ^2G_{4\frac{1}{2}}$–$z\ ^2G_{4\frac{1}{2}}$	1272.416	3	78590.7

TABLE IV (*Continued*)

Observed lines of Co III

λ (vac.)	I	ν	
1286.626	2	77722.7	
1308.850	1	76402.9	
1371.419	2	72917.2	$z\,^6D_{2\frac{1}{2}}$–$f\,^6D_{1\frac{1}{2}}$
1371.779	3	72898.0	$z\,^6D_{1\frac{1}{2}}$–$f\,^6D_{\frac{1}{2}}$
1372.536	0	72857.8	
1376.576	0	72644.0	$z\,^6D_{2\frac{1}{2}}$–$f\,^6D_{2\frac{1}{2}}$
1378.208	2	72558.0	$z\,^6D_{\frac{1}{2}}$–$f\,^6D_{1\frac{1}{2}}$
1378.665	10	72533.9	$z\,^6D_{3\frac{1}{2}}$–$f\,^6D_{2\frac{1}{2}}$
1380.775	5	72423.1	$z\,^6D_{1\frac{1}{2}}$–$f\,^6D_{2\frac{1}{2}}$
1383.971	20	72255.8	$z\,^6D_{2\frac{1}{2}}$–$f\,^6D_{3\frac{1}{2}}$
1384.187	50	72244.6	$z\,^6D_{1\frac{1}{2}}$–$f\,^6D_{4\frac{1}{2}}$
1389.079	10	71990.1	$z\,^6D_{3\frac{1}{2}}$–$f\,^6D_{4\frac{1}{2}}$
1396.210	2	71622.5	$z\,^6D_{\frac{1}{2}}$–$e\,^6P_{1\frac{1}{2}}$
1402.415	10	71305.6	$z\,^6D_{1\frac{1}{2}}$–$e\,^6D_{2\frac{1}{2}}$
1403.755	5	71237.5	$z\,^6D_{4\frac{1}{2}}$–$e\,^6D_{4\frac{1}{2}}$
1404.009	10	71224.6	$z\,^6D_{3\frac{1}{2}}$–$e\,^6D_{3\frac{1}{2}}$
1405.032	5	71172.8	$z\,^6D_{2\frac{1}{2}}$–$e\,^6D_{1\frac{1}{2}}$
1405.451	1	71151.5	$z\,^6D_{1\frac{1}{2}}$–$e\,^6D_{\frac{1}{2}}$
1408.808	5	70982.0	$z\,^6D_{3\frac{1}{2}}$–$e\,^6D_{4\frac{1}{2}}$
1409.340	50	70955.2	
1412.012	5	70820.9	$a\,^4D_{3\frac{1}{2}}$–$y\,^4D_{3\frac{1}{2}}$
1412.974	10	70772.7	$z\,^6D_{2\frac{1}{2}}$–$e\,^6D_{3\frac{1}{2}}$
1413.884	10	70727.2	$z\,^6D_{1\frac{1}{2}}$–$e\,^6D_{2\frac{1}{2}}$
1425.329	1	70159.2	$z\,^6D_{4\frac{1}{2}}$–$e\,^6F_{4\frac{1}{2}}$
1425.650	3	70143.4	$z\,^6D_{3\frac{1}{2}}$–$e\,^6F_{2\frac{1}{2}}$
1425.984	1	70127.0	
1427.308	2	70062.0	$z\,^6D_{2\frac{1}{2}}$–$e\,^6F_{1\frac{1}{2}}$
1428.331	2	70011.8	
1429.236	0	69967.5	$z\,^6D_{1\frac{1}{2}}$–$e\,^6F_{\frac{1}{2}}$
1429.324	0	69963.1	$a\,^4D_{3\frac{1}{2}}$–$z\,^4H_{3\frac{1}{2}}$?
1430.177	30	69921.4	$z\,^6D_{4\frac{1}{2}}$–$e\,^6F_{4\frac{1}{2}}$
1430.530	30	69904.2	$z\,^6D_{3\frac{1}{2}}$–$e\,^6F_{3\frac{1}{2}}$
1431.323	30	69865.4	$z\,^6D_{2\frac{1}{2}}$–$e\,^6F_{2\frac{1}{2}}$
1431.800	10	69842.2	$z\,^6D_{1\frac{1}{2}}$–$e\,^6F_{1\frac{1}{2}}$
1431.065	10	69829.2	$z\,^6D_{\frac{1}{2}}$–$e\,^6F_{\frac{1}{2}}$
1432.556	10	69805.3	
1434.259	200	69722.4	$z\,^6D_{4\frac{1}{2}}$–$e\,^6F_{5\frac{1}{2}}$
1434.642	1	69703.8	$z\,^6D_{\frac{1}{2}}$–$e\,^6F_{1\frac{1}{2}}$
1435.426	100	69665.7	$z\,^6D_{3\frac{1}{2}}$–$e\,^6F_{4\frac{1}{2}}$
1435.840	5	69645.6	$z\,^6D_{1\frac{1}{2}}$–$e\,^6F_{2\frac{1}{2}}$
1436.236	20	69626.4	$z\,^6D_{2\frac{1}{2}}$–$e\,^6F_{3\frac{1}{2}}$
1445.427	2	69183.7	
1447.216	3	69098.2	
1448.890	1	69018.4	
1463.037	3	68350.9	
1463.936	2	68309.0	
1464.733	2	68271.8	
1464.932	2	68262.5	
1465.101	2	68254.7	
1465.558	3	68233.4	
1466.579	5	68185.9	
1466.919	3	68170.1	$z\,^6F_{\frac{1}{2}}$–$e\,^6G_{1\frac{1}{2}}$
1467.394	10*h*	68148.0	$z\,^6F_{2\frac{1}{2}}$–$f\,^6D_{1\frac{1}{2}}$
1467.663	10	68135.5	$z\,^6F_{\frac{1}{2}}$–$e\,^6G_{1\frac{1}{2}}$
1468.010	2*h*	68119.4	
1468.992	10	68073.9	$z\,^6F_{1\frac{1}{2}}$–$e\,^6G_{2\frac{1}{2}}$
1470.282*C*?	1	68014.2	
1470.700	1	67994.8	
1471.140	2	67974.5	
1471.328	2	67965.8	$z\,^6F_{3\frac{1}{2}}$–$f\,^6D_{2\frac{1}{2}}$
1471.575	1	67954.4	$a\,^4H_{3\frac{1}{2}}$–$w\,^4F_{3\frac{1}{2}}$?
1472.019	20	67933.9	$z\,^6F_{2\frac{1}{2}}$–$e\,^6G_{3\frac{1}{2}}$
1472.756	3	67899.9	
1473.303	2*h*	67874.7	$z\,^6F_{2\frac{1}{2}}$–$f\,^6F_{2\frac{1}{2}}$
1473.528	5	67864.3	
1474.278	3	67829.8	
1474.953	3	67798.8	
1475.266	1	67784.4	$z\,^6F_{5\frac{1}{2}}$–$e\,^6G_{5\frac{1}{2}}$
1475.635	20	67767.4	$z\,^6F_{3\frac{1}{2}}$–$e\,^6G_{4\frac{1}{2}}$
1476.366	5	67733.9	
1476.895	5	67709.6	
1477.260	2	67692.9	$z\,^6F_{4\frac{1}{2}}$–$f\,^6D_{3\frac{1}{2}}$
1478.367	50	67642.2	$z\,^6F_{4\frac{1}{2}}$–$e\,^6G_{5\frac{1}{2}}$
1478.858	2	67619.7	
1479.393	3	67595.3	
1479.880	2	67573.0	
1481.905	100	67480.7	$z\,^6F_{5\frac{1}{2}}$–$e\,^6G_{6\frac{1}{2}}$
1483.363	10	67414.4	
1483.800	20	67394.5	
1484.565	1	67359.8	$b\,^4F_{4\frac{1}{2}}$–$x\,^2F_{3\frac{1}{2}}$
1484.780	1	67350.1	
1485.170	15	67332.4	
1485.510	2	67316.9	
1487.962	2*h*	67206.0	$b\,^4F_{4\frac{1}{2}}$–$w\,^4F_{4\frac{1}{2}}$
1488.174	5	67196.4	
1488.465	1	67183.3	
1488.753	2	67170.3	
1488.975	1	67160.3	
1489.243	0	67148.2	$z\,^6F_{4\frac{1}{2}}$–$f\,^6D_{4\frac{1}{2}}$
1489.550	1	67134.4	
1489.899	20	67118.6	
1490.511	1	67091.1	
1491.273	10	67056.8	
1492.528	5	67000.4	
1493.152	20	66972.4	$b\,^4P_{1\frac{1}{2}}$–$x\,^4P_{\frac{1}{2}}$
1493.595	3*H*	66952.6	$b\,^4F_{3\frac{1}{2}}$–$w\,^4F_{4\frac{1}{2}}$?
1497.700	10	66769.0	
1498.144	2	66749.3	$a\,^4D_{2\frac{1}{2}}$–$z\,^4S_{1\frac{1}{2}}$
1498.830	20*H*	66718.7	
1499.124	50	66705.6	$z\,^4D_{3\frac{1}{2}}$–$f\,^4D_{2\frac{1}{2}}$
1499.877	5	66672.1	$b\,^4F_{3\frac{1}{2}}$–$w\,^4F_{2\frac{1}{2}}$
1500.269	20	66654.7	$z\,^4D_{2\frac{1}{2}}$–$f\,^4D_{1\frac{1}{2}}$
1502.531	5	66554.4	$z\,^4D_{1\frac{1}{2}}$–$f\,^4D_{\frac{1}{2}}$
1504.362	3	66473.4	$b\,^4F_{2\frac{1}{2}}$–$w\,^4F_{1\frac{1}{2}}$
1505.249	10	66434.2	$b\,^4P_{1\frac{1}{2}}$–$x\,^4P_{2\frac{1}{2}}$?
1508.683	1	66283.0	$z\,^6F_{5\frac{1}{2}}$–$e\,^6D_{4\frac{1}{2}}$
1510.489	2	66203.7	$b\,^4F_{3\frac{1}{2}}$–$w\,^4D_{2\frac{1}{2}}$ and $z\,^6F_{4\frac{1}{2}}$–$e\,^6P_{3\frac{1}{2}}$?
1511.404	5	66163.6	
1511.730	3	66159.4	
1511.920	5	66141.1	$z\,^6F_{4\frac{1}{2}}$–$e\,^6D_{4\frac{1}{2}}$
1512.997	5	66094.0	$z\,^6F_{3\frac{1}{2}}$–$e\,^6D_{3\frac{1}{2}}$ and $z\,^4D_{3\frac{1}{2}}$–$f\,^4D_{3\frac{1}{2}}$
1513.706	5	66063.0	
1515.027	50	66005.4	
1515.638	2	65978.8	
1515.776	2	65972.8	
1515.982	3	65963.8	
1517.070	2	65916.5	
1517.153	2	65912.9	
1517.482	15	65898.6	
1517.724	10	65888.1	$z\,^4D_{3\frac{1}{2}}$–$e\,^4F_{3\frac{1}{2}}$
1518.636	1	65848.6	$z\,^4D_{2\frac{1}{2}}$–$e\,^4F_{2\frac{1}{2}}$
1519.326	15	65818.7	$z\,^4F_{4\frac{1}{2}}$–$f\,^4D_{3\frac{1}{2}}$

TABLE IV (*Continued*)

Observed lines of Co III

λ (vac.)	I	ν	
1522.049	3	65700.9	
1522.885	20	65664.8	$z\ ^4F_{3\frac{1}{2}}$–$f\ ^4D_{2\frac{1}{2}}$
1523.153	10*d*?	65653.3	
1524.113	15	65611.9	$z\ ^4F_{4\frac{1}{2}}$–$e\ ^4F_{3\frac{1}{2}}$
1524.472	3	65596.5	
1524.942	2*h*	65576.3	$a\ ^4H_{4\frac{1}{2}}$–$x\ ^2G_{4\frac{1}{2}}$?
1525.163	2*h*	65566.8	
1525.407	15	65556.3	$z\ ^4F_{2\frac{1}{2}}$–$f\ ^4D_{1\frac{1}{2}}$
1526.734	30	65499.3	
1527.780	20	65454.5	$z\ ^4F_{3\frac{1}{2}}$–$e\ ^4F_{4\frac{1}{2}}$?
1527.948	3	65447.3	$z\ ^4F_{1\frac{1}{2}}$–$f\ ^4D_{\frac{1}{2}}$
1530.385	3	65343.0	
1530.906	10*h*	65320.8	$z\ ^6F_{\frac{1}{2}}$–$e\ ^6F_{1\frac{1}{2}}$
1531.068	15*h*	65313.9	
1532.032	10	65272.8	$z\ ^4F_{3\frac{1}{2}}$–$e\ ^4F_{2\frac{1}{2}}$
1534.268	200	65177.7	$z\ ^4F_{4\frac{1}{2}}$–$e\ ^4F_{4\frac{1}{2}}$
1536.554	5	65080.7	$z\ ^4F_{2\frac{1}{2}}$–$e\ ^4F_{1\frac{1}{2}}$
1536.955	5	65063.7	$z\ ^6F_{4\frac{1}{2}}$–$e\ ^6F_{3\frac{1}{2}}$
1539.255	2	64966.5	$z\ ^6F_{5\frac{1}{2}}$–$e\ ^6F_{4\frac{1}{2}}$
1539.458	20	64957.9	
1542.094	100	64846.9	$z\ ^4F_{3\frac{1}{2}}$–$e\ ^4F_{3\frac{1}{2}}$
1542.616	10	64824.9	$z\ ^6F_{4\frac{1}{2}}$–$e\ ^6F_{4\frac{1}{2}}$
1543.981	30	64767.6	$z\ ^6F_{3\frac{1}{2}}$–$e\ ^6F_{3\frac{1}{2}}$
1544.129	3	64761.4	$z\ ^6P_{3\frac{1}{2}}$–$e\ ^6D_{2\frac{1}{2}}$
1544.411	30	64749.6	$z\ ^4F_{2\frac{1}{2}}$–$e\ ^4F_{2\frac{1}{2}}$ and $b\ ^2F_{3\frac{1}{2}}$–$w\ ^2F_{2\frac{1}{2}}$
1544.880	40	64730.0	$z\ ^4F_{1\frac{1}{2}}$–$e\ ^4F_{1\frac{1}{2}}$
1547.309	5	64628.3	
1548.413	20	64582.3	$z\ ^6P_{3\frac{1}{2}}$–$e\ ^6P_{3\frac{1}{2}}$
1549.940	20	64518.6	$z\ ^6P_{3\frac{1}{2}}$–$e\ ^6D_{4\frac{1}{2}}$
1551.536	5	64452.3	$b\ ^2G_{4\frac{1}{2}}$–$v\ ^2F_{3\frac{1}{2}}$
1553.015	5	64390.9	$z\ ^6P_{2\frac{1}{2}}$–$e\ ^6P_{2\frac{1}{2}}$
1557.328	5	64212.6	$z\ ^6P_{1\frac{1}{2}}$–$e\ ^6P_{1\frac{1}{2}}$
1561.746	2	64030.9	$z\ ^6P_{2\frac{1}{2}}$–$e\ ^6D_{1\frac{1}{2}}$
1563.158	5	63973.1	$a\ ^4G_{5\frac{1}{2}}$–$w\ ^4F_{4\frac{1}{2}}$
1564.090	2	63934.9	$b\ ^2H_{5\frac{1}{2}}$–$w\ ^2H_{4\frac{1}{2}}$
1567.173	3	63809.2	
1567.917	0	63778.9	$b\ ^2H_{5\frac{1}{2}}$–$w\ ^2H_{5\frac{1}{2}}$
1568.308	1	63763.0	$z\ ^6P_{1\frac{1}{2}}$–$e\ ^6P_{2\frac{1}{2}}$
1569.264	1	63724.1	$b\ ^2H_{4\frac{1}{2}}$–$w\ ^2H_{4\frac{1}{2}}$
1572.266	1	63602.5	$z\ ^6P_{1\frac{1}{2}}$–$e\ ^6D_{\frac{1}{2}}$
1573.921	10*h*	63535.6	
1576.025	2	63450.8	
1578.093	0	63367.6	$a\ ^6D_{3\frac{1}{2}}$–$z\ ^4P_{2\frac{1}{2}}$
1580.619	0	63266.4	
1580.735	0	63261.7	$a\ ^6D_{1\frac{1}{2}}$–$z\ ^4P_{1\frac{1}{2}}$ and $a\ ^4G_{4\frac{1}{2}}$–$w\ ^2G_{3\frac{1}{2}}$
1581.502	5	63231.0	
1582.044	3	63209.4	
1584.663	1	63104.9	$a\ ^4G_{4\frac{1}{2}}$–$w\ ^4F_{3\frac{1}{2}}$
1586.180	15	63044.6	
1587.186	10	63004.6	$b\ ^4F_{4\frac{1}{2}}$–$y\ ^2F_{2\frac{1}{2}}$
1588.642	10	62946.8	$b\ ^2H_{5\frac{1}{2}}$–$w\ ^2G_{4\frac{1}{2}}$
1593.446	10	62757.1	
1594.182	0	62728.1	$a\ ^4G_{2\frac{1}{2}}$–$w\ ^4F_{1\frac{1}{2}}$
1594.953	10	62697.8	$a\ ^4G_{4\frac{1}{2}}$–$w\ ^4D_{3\frac{1}{2}}$
1601.903	3	62425.8	
1603.563	15	62361.1	$a\ ^4G_{3\frac{1}{2}}$–$w\ ^4D_{2\frac{1}{2}}$
1607.410	5	62211.9	
1608.777	5	62159.0	
1608.864	5	62155.7	$a\ ^4G_{2\frac{1}{2}}$–$w\ ^4D_{1\frac{1}{2}}$
1608.950	5	62152.3	
1618.491	5	61785.9	
1620.051	2	61726.5	$b\ ^2H_{5\frac{1}{2}}$–$x\ ^2H_{5\frac{1}{2}}$
1620.254	3	61718.7	$b\ ^2F_{3\frac{1}{2}}$–$x\ ^2F_{3\frac{1}{2}}$
1622.923	3	61617.2	
1629.157	1	61381.4	
1629.666	5	61362.3	$b\ ^2F_{2\frac{1}{2}}$–$x\ ^2F_{2\frac{1}{2}}$
1635.521	5	61142.6	$a\ ^4G_{5\frac{1}{2}}$–$x\ ^2G_{4\frac{1}{2}}$
1645.986	30	60753.9	$a\ ^4H_{6\frac{1}{2}}$–$y\ ^4H_{6\frac{1}{2}}$
1647.100	1	60712.8	$a\ ^4H_{5\frac{1}{2}}$–$y\ ^4H_{4\frac{1}{2}}$
1649.153	5	60637.2	$a\ ^6D_{2\frac{1}{2}}$–$z\ ^4F_{2\frac{1}{2}}$
1649.265	200*d*	60633.0	$a\ ^4H_{\frac{1}{2}}$–$y\ ^4H_{\frac{1}{2}}$
1651.783	0	60540.6	$a\ ^4H_{4\frac{1}{2}}$–$y\ ^4H_{3\frac{1}{2}}$
1652.024	5	60531.8	$c\ ^2G_{4\frac{1}{2}}$–$v\ ^2F_{3\frac{1}{2}}$
1652.182	5	60526.0	$a\ ^6D_{3\frac{1}{2}}$–$z\ ^4F_{3\frac{1}{2}}$
1652.791	10	60503.7	$a\ ^4H_{3\frac{1}{2}}$–$y\ ^4H_{4\frac{1}{2}}$
1659.757	10	60249.8	$b\ ^4P_{1\frac{1}{2}}$–$x\ ^4F_{1\frac{1}{2}}$ and $b\ ^2H_{5\frac{1}{2}}$–$x\ ^2G_{4\frac{1}{2}}$
1661.422	10	60189.4	$b\ ^2H_{4\frac{1}{2}}$–$x\ ^2G_{3\frac{1}{2}}$
1663.500	3	60114.2	$a\ ^6D_{2\frac{1}{2}}$–$z\ ^4F_{3\frac{1}{2}}$
1665.269	50	60050.4	$a\ ^6D_{4\frac{1}{2}}$–$z\ ^4D_{3\frac{1}{2}}$
1668.032	5	59950.9	$a\ ^6D_{3\frac{1}{2}}$–$z\ ^4D_{2\frac{1}{2}}$
1672.133	2	59803.9	$a\ ^4H_{4\frac{1}{2}}$–$x\ ^4G_{4\frac{1}{2}}$
1673.325	10	59761.3	$a\ ^6D_{3\frac{1}{2}}$–$z\ ^4F_{4\frac{1}{2}}$
1673.679	20	59748.6	$a\ ^4H_{6\frac{1}{2}}$–$x\ ^4G_{5\frac{1}{2}}$
1677.901	15	59598.3	$a\ ^6D_{1\frac{1}{2}}$–$z\ ^4D_{1\frac{1}{2}}$
1679.481	5	59542.2	$b\ ^4P_{1\frac{1}{2}}$–$x\ ^4G_{2\frac{1}{2}}$
1679.578	20	59538.8	$a\ ^6D_{2\frac{1}{2}}$–$z\ ^4D_{2\frac{1}{2}}$
1680.734	1	59497.8	$a\ ^4H_{5\frac{1}{2}}$–$x\ ^4G_{5\frac{1}{2}}$
1681.074	10	59485.8	$a\ ^6D_{3\frac{1}{2}}$–$z\ ^4D_{3\frac{1}{2}}$
1683.180	1	59411.4	
1687.910	5	59244.9	
1689.283	3	59196.7	$a\ ^4H_{4\frac{1}{2}}$–$x\ ^4G_{3\frac{1}{2}}$
1689.858	100	59176.6	$a\ ^6D_{2\frac{1}{2}}$–$z\ ^6P_{1\frac{1}{2}}$
1690.399	5	59157.6	
1693.085	30	59063.8	
1695.090	1	58993.9	
1696.008	1000	58962.0	$a\ ^6D_{3\frac{1}{2}}$–$z\ ^6P_{2\frac{1}{2}}$
1696.875	5	58931.9	
1696.980	5	58928.2	$a\ ^4H_{5\frac{1}{2}}$–$y\ ^2G_{4\frac{1}{2}}$
1697.988	800	58893.2	$a\ ^6D_{1\frac{1}{2}}$–$z\ ^6P_{1\frac{1}{2}}$
1699.880	1	58827.7	$b\ ^2G_{4\frac{1}{2}}$–$w\ ^2H_{5\frac{1}{2}}$
1701.770	1	58762.3	$b\ ^4F_{2\frac{1}{2}}$–$x\ ^4F_{2\frac{1}{2}}$
1702.506	3	58736.9	$b\ ^4F_{1\frac{1}{2}}$–$x\ ^4G_{2\frac{1}{2}}$
1702.790	500	58727.1	$a\ ^6D_{\frac{1}{2}}$–$z\ ^6P_{1\frac{1}{2}}$
1704.817	5	58657.3	$a\ ^4G_{2\frac{1}{2}}$–$y\ ^2F_{2\frac{1}{2}}$
1705.306	0	58640.5	
1707.348	1000	58570.4	$a\ ^6D_{4\frac{1}{2}}$–$z\ ^6P_{3\frac{1}{2}}$
1707.951	500	58549.7	$a\ ^6D_{2\frac{1}{2}}$–$z\ ^6P_{2\frac{1}{2}}$
1709.395	3	58500.2	
1711.531	5	58427.2	$b\ ^2G_{3\frac{1}{2}}$–$w\ ^2H_{4\frac{1}{2}}$
1712.489	2	58394.5	
1715.768	2	58282.9	$a\ ^4G_{4\frac{1}{2}}$–$y\ ^2H_{4\frac{1}{2}}$ and $b\ ^2G_{4\frac{1}{2}}$–$x\ ^2F_{3\frac{1}{2}}$
1716.251	200	58266.5	$a\ ^6D_{1\frac{1}{2}}$–$z\ ^6P_{2\frac{1}{2}}$
1718.887	2	58177.2	$a\ ^4G_{5\frac{1}{2}}$–$y\ ^2H_{5\frac{1}{2}}$
1719.383	3	58160.4	
1720.068	20	58137.2	$a\ ^4H_{3\frac{1}{2}}$–$z\ ^2F_{2\frac{1}{2}}$
1721.151	10	58100.7	$a\ ^4H_{4\frac{1}{2}}$–$z\ ^2F_{3\frac{1}{2}}$
1721.678	3	58082.9	
1722.911	1	58041.3	$b\ ^4F_{3\frac{1}{2}}$–$x\ ^4F_{3\frac{1}{2}}$

TABLE IV (*Continued*)

Observed lines of Co III

λ (vac.)	I	ν	
1723.327	1	58027.3	
1723.536	1	58020.3	$a\ ^4G_{3\frac{1}{2}}$–$y\ ^2H_{4\frac{1}{2}}$
1723.970	500	58005.6	$a\ ^6D_{3\frac{1}{2}}$–$z\ ^6P_{3\frac{1}{2}}$
1726.134	100	57932.9	$a\ ^4H_{6\frac{1}{2}}$–$y\ ^4G_{5\frac{1}{2}}$
1726.726	15	57913.1	$a\ ^4H_{3\frac{1}{2}}$–$z\ ^2F_{3\frac{1}{2}}$
1728.091	3	57867.3	$b\ ^2G_{3\frac{1}{2}}$–$x\ ^2F_{2\frac{1}{2}}$
1729.724	5	57812.7	$b\ ^4F_{1\frac{1}{2}}$–$x\ ^4F_{1\frac{1}{2}}$
1730.669	250	57781.1	$b\ ^2H_{4\frac{1}{2}}$–$y\ ^2H_{4\frac{1}{2}}$
1732.358	0	57724.8	$b\ ^2G_{3\frac{1}{2}}$–$x\ ^2F_{3\frac{1}{2}}$
1732.545	200	57718.6	$a\ ^4H_{5\frac{1}{2}}$–$y\ ^4G_{4\frac{1}{2}}$
1733.635	10	57682.3	$a\ ^4H_{5\frac{1}{2}}$–$y\ ^4G_{5\frac{1}{2}}$
1735.400	50	57623.6	$a\ ^4H_{4\frac{1}{2}}$–$y\ ^4G_{3\frac{1}{2}}$
1736.312	250	57593.3	$a\ ^6D_{2\frac{1}{2}}$–$z\ ^6P_{3\frac{1}{2}}$
1736.856	3	57575.0	$a\ ^4G_{4\frac{1}{2}}$–$y\ ^2H_{5\frac{1}{2}}$
1737.523	3	57553.2	$b\ ^4F_{2\frac{1}{2}}$–$x\ ^4G_{3\frac{1}{2}}$
1738.653	1	57515.8	$b\ ^4F_{4\frac{1}{2}}$–$y\ ^2G_{4\frac{1}{2}}$
1739.833	30	57476.8	$a\ ^4H_{3\frac{1}{2}}$–$y\ ^4G_{2\frac{1}{2}}$
1741.057	5	57436.4	$a\ ^4H_{3\frac{1}{2}}$–$y\ ^4G_{3\frac{1}{2}}$
1742.372	2	57393.0	$c\ ^2G_{4\frac{1}{2}}$–$w\ ^2F_{3\frac{1}{2}}$
1743.212	10	57365.4	
1743.311	30	57362.1	$b\ ^2F_{3\frac{1}{2}}$–$y\ ^2F_{3\frac{1}{2}}$
1744.529	2	57322.1	$a\ ^4H_{3\frac{1}{2}}$–$y\ ^4G_{4\frac{1}{2}}$
1745.674	400	57284.5	$b\ ^2H_{5\frac{1}{2}}$–$y\ ^2H_{5\frac{1}{2}}$
1746.131	0	57269.5	
1746.369	20	57261.7	$b\ ^4F_{3\frac{1}{2}}$–$y\ ^2G_{4\frac{1}{2}}$
1746.853	5	57245.8	
1749.728	25	57151.7	$b\ ^4P_{2\frac{1}{2}}$–$y\ ^4D_{2\frac{1}{2}}$
1751.037	100	57109.0	
1751.854	200	57082.4	$b\ ^4P_{2\frac{1}{2}}$–$x\ ^4D_{3\frac{1}{2}}$
1754.761	0	56987.8	$b\ ^4D_{2\frac{1}{2}}$–$x\ ^2F_{2\frac{1}{2}}$
1755.979	500	56948.3	$a\ ^6D_{4\frac{1}{2}}$–$z\ ^6F_{4\frac{1}{2}}$
1756.851	30	56920.0	$b\ ^2P_{1\frac{1}{2}}$–$y\ ^2D_{2\frac{1}{2}}$
1757.531	15	56898.0	$b\ ^4F_{4\frac{1}{2}}$–$z\ ^4F_{3\frac{1}{2}}$
1758.454	0	56868.1	$b\ ^4F_{3\frac{1}{2}}$–$z\ ^2F_{2\frac{1}{2}}$
1759.144	5	56845.8	$b\ ^4D_{2\frac{1}{2}}$–$x\ ^2F_{3\frac{1}{2}}$
1760.354	5000	56806.8	$a\ ^6D_{4\frac{1}{2}}$–$z\ ^6F_{5\frac{1}{2}}$
1761.082	1	56783.3	
1761.367	10	56774.1	$b\ ^2G_{4\frac{1}{2}}$–$x\ ^2H_{5\frac{1}{2}}$
1763.465	100	56706.5	$b\ ^4D_{3\frac{1}{2}}$–$x\ ^2F_{3\frac{1}{2}}$
1763.533	15	56704.4	$b\ ^2F_{2\frac{1}{2}}$–$y\ ^2F_{2\frac{1}{2}}$
1765.414	0	56643.9	$b\ ^4F_{3\frac{1}{2}}$–$z\ ^2F_{3\frac{1}{2}}$
1765.566	1	56639.1	
1767.084	30	56590.4	$a\ ^6D_{2\frac{1}{2}}$–$z\ ^8F_{2\frac{1}{2}}$
1767.308	50	56583.2	$b\ ^4D_{2\frac{1}{2}}$–$w\ ^2G_{3\frac{1}{2}}$
1768.003	5*H*	56561.0	
1768.238	200	56553.5	$b\ ^4D_{3\frac{1}{2}}$–$w\ ^4F_{4\frac{1}{2}}$
1768.471	100	56546.0	$b\ ^4F_{4\frac{1}{2}}$–$z\ ^2F_{4\frac{1}{2}}$
1769.495	10	56513.3	
1769.957	500	56498.5	$a\ ^6D_{3\frac{1}{2}}$–$z\ ^6F_{3\frac{1}{2}}$
1770.500	10	56481.2	
1771.259	100	56457.0	$b\ ^4F_{2\frac{1}{2}}$–$z\ ^2G_{3\frac{1}{2}}$
1771.854	200	56438.1	$b\ ^4D_{1\frac{1}{2}}$–$w\ ^4F_{2\frac{1}{2}}$
1772.233	300	56426.0	$b\ ^4D_{1\frac{1}{2}}$–$w\ ^4F_{1\frac{1}{2}}$ and $b\ ^4D_{2\frac{1}{2}}$–$w\ ^4F_{2\frac{1}{2}}$
1772.438	200	56419.5	$b\ ^4D_{3\frac{1}{2}}$–$w\ ^2G_{4\frac{1}{2}}$
1772.549	50	56415.9	
1772.671	100	56412.0	$b\ ^4D_{\frac{1}{2}}$–$w\ ^4F_{1\frac{1}{2}}$ and $b\ ^4D_{2\frac{1}{2}}$–$w\ ^4F_{2\frac{1}{2}}$
1773.215	500	56394.7	$a\ ^2I_{6\frac{1}{2}}$–$y\ ^2I_{6\frac{1}{2}}$
1773.568	5000	56383.5	$a\ ^6D_{3\frac{1}{2}}$–$z\ ^6F_{4\frac{1}{2}}$
1774.418	500	56356.5	$a\ ^2I_{5\frac{1}{2}}$–$y\ ^2I_{5\frac{1}{2}}$
1774.577	10	56351.5	$a\ ^2I_{5\frac{1}{2}}$–$y\ ^2I_{6\frac{1}{2}}$
1776.630	1	56286.3	$b\ ^4D_{2\frac{1}{2}}$–$w\ ^4F_{3\frac{1}{2}}$
1777.145	1000	56270.0	$b\ ^4F_{4\frac{1}{2}}$–$y\ ^4G_{5\frac{1}{2}}$
1778.091	100	56240.1	$a\ ^6D_{2\frac{1}{2}}$–$z\ ^6F_{1\frac{1}{2}}$
1779.536	20	56194.4	$b\ ^4P_{1\frac{1}{2}}$–$y\ ^4D_{\frac{1}{2}}$
1779.896	3	56183.1	$b\ ^4P_{1\frac{1}{2}}$–$x\ ^4D_{2\frac{1}{2}}$
1780.046	2000	56178.3	$a\ ^6D_{2\frac{1}{2}}$–$z\ ^6F_{2\frac{1}{2}}$
1780.686	0	56158.1	
1782.195	5	56110.6	
1782.966	3000	56086.3	$a\ ^6D_{2\frac{1}{2}}$–$z\ ^6F_{3\frac{1}{2}}$
1784.055	500	56052.1	$b\ ^4F_{3\frac{1}{2}}$–$y\ ^4G_{4\frac{1}{2}}$
1784.790	30	56029.0	
1784.944	3	56022.6	
1785.116	20	56018.8	$b\ ^4D_{2\frac{1}{2}}$–$w\ ^4D_{3\frac{1}{2}}$
1785.705	5	56000.3	$b\ ^2G_{3\frac{1}{2}}$–$y\ ^2H_{4\frac{1}{2}}$
1785.965	50	55992.1	$a\ ^6D_{1\frac{1}{2}}$–$z\ ^6F_{\frac{1}{2}}$
1786.342	200	55980.3	$b\ ^4F_{2\frac{1}{2}}$–$y\ ^4G_{2\frac{1}{2}}$
1786.679	50	55969.8	$b\ ^4D_{1\frac{1}{2}}$–$w\ ^4D_{2\frac{1}{2}}$
1787.082	1000	55957.1	$a\ ^6D_{1\frac{1}{2}}$–$z\ ^6F_{1\frac{1}{2}}$ and $b\ ^4D_{1\frac{1}{2}}$–$w\ ^4D_{\frac{1}{2}}$
1787.502	50	55944.0	$b\ ^4D_{2\frac{1}{2}}$–$w\ ^4D_{2\frac{1}{2}}$
1787.575	30	55941.7	$b\ ^4D_{\frac{1}{2}}$–$w\ ^4D_{\frac{1}{2}}$
1788.627	50	55908.8	
1789.070	1000	55895.0	$a\ ^6D_{1\frac{1}{2}}$–$z\ ^6F_{2\frac{1}{2}}$
1789.373	100	55885.5	$b\ ^4F_{1\frac{1}{2}}$–$y\ ^4G_{2\frac{1}{2}}$
1789.549	100	55880.0	$b\ ^4D_{3\frac{1}{2}}$–$w\ ^4D_{3\frac{1}{2}}$
1790.258	500	55857.9	$a\ ^4G_{5\frac{1}{2}}$–$y\ ^4H_{6\frac{1}{2}}$
1790.389	50	55853.5	$b\ ^4D_{1\frac{1}{2}}$–$w\ ^4D_{1\frac{1}{2}}$
1790.892	25	55838.1	$b\ ^4D_{\frac{1}{2}}$–$w\ ^4D_{1\frac{1}{2}}$
1791.153	300	55830.0	$a\ ^2I_{5\frac{1}{2}}$–$w\ ^2H_{4\frac{1}{2}}$
1791.277	500	55826.1	$a\ ^6D_{\frac{1}{2}}$–$z\ ^6F_{\frac{1}{2}}$
1792.144	100	55799.1	$a\ ^4H_{5\frac{1}{2}}$–$z\ ^2I_{6\frac{1}{2}}$
1792.410	300	55790.8	$a\ ^6D_{\frac{1}{2}}$–$z\ ^6F_{1\frac{1}{2}}$
1793.924	200	55743.7	$b\ ^4P_{1\frac{1}{2}}$–$y\ ^4D_{2\frac{1}{2}}$
1794.804	100	55716.4	$a\ ^2I_{6\frac{1}{2}}$–$w\ ^2H_{5\frac{1}{2}}$
1795.426	2	55697.1	$b\ ^2P_{1\frac{1}{2}}$–$x\ ^4F_{2\frac{1}{2}}$
1796.200	10	55673.1	$a\ ^2I_{5\frac{1}{2}}$–$w\ ^2H_{5\frac{1}{2}}$
1796.664	5	55658.7	
1797.095	10	55645.4	$b\ ^2P_{\frac{1}{2}}$–$y\ ^2D_{1\frac{1}{2}}$
1798.064	500	55615.4	$b\ ^4P_{2\frac{1}{2}}$–$y\ ^4D_{3\frac{1}{2}}$
1798.876	5	55590.5	$b\ ^4P_{\frac{1}{2}}$–$x\ ^4D_{1\frac{1}{2}}$
1800.469	50	55541.1	$b\ ^4D_{1\frac{1}{2}}$–$x\ ^4P_{\frac{1}{2}}$
1800.974	25	55525.5	$b\ ^4D_{\frac{1}{2}}$–$x\ ^4P_{\frac{1}{2}}$
1801.030	25	55523.8	$b\ ^2P_{1\frac{1}{2}}$–$z\ ^2S_{\frac{1}{2}}$
1801.940	0	55495.8	
1802.917	1	55465.7	$a\ ^4G_{4\frac{1}{2}}$–$y\ ^4H_{4\frac{1}{2}}$
1805.535	500	55385.2	$a\ ^4G_{4\frac{1}{2}}$–$y\ ^4H_{5\frac{1}{2}}$
1806.096	10	55368.0	$a\ ^4G_{5\frac{1}{2}}$–$x\ ^4G_{4\frac{1}{2}}$
1806.350	10	55360.3	
1806.492	5	55355.9	
1808.384	300	55298.0	$b\ ^2G_{4\frac{1}{2}}$–$x\ ^2G_{4\frac{1}{2}}$
1809.233	40	55272.0	
1809.904	5	55251.5	
1810.464	15	55234.5	$a\ ^4H_{4\frac{1}{2}}$–$z\ ^2G_{3\frac{1}{2}}$
1811.317	100	55208.4	$b\ ^4P_{\frac{1}{2}}$–$y\ ^4D_{1\frac{1}{2}}$
1811.466	400	55203.9	$a\ ^4G_{3\frac{1}{2}}$–$y\ ^4H_{4\frac{1}{2}}$
1811.694	3	55197.0	$b\ ^4D_{1\frac{1}{2}}$–$x\ ^4P_{1\frac{1}{2}}$
1812.336	5	55177.4	$a\ ^4H_{5\frac{1}{2}}$–$z\ ^2G_{4\frac{1}{2}}$
1812.550	50	55170.9	$b\ ^4D_{2\frac{1}{2}}$–$x\ ^4P_{1\frac{1}{2}}$
1813.044	50	55155.9	$a\ ^4G_{4\frac{1}{2}}$–$x\ ^4G_{3\frac{1}{2}}$
1813.186	300	55151.5	$a\ ^4G_{2\frac{1}{2}}$–$y\ ^4H_{3\frac{1}{2}}$
1814.084	10	55124.2	$a\ ^4H_{4\frac{1}{2}}$–$y\ ^4F_{4\frac{1}{2}}$

TABLE IV (*Continued*)

Observed lines of Co III

λ (vac.)	I	ν	
1814.219	100	55120.1	$a\ {}^4G_{2\frac{1}{2}}$–$x\ {}^4F_{1\frac{1}{2}}$
1814.573	2	55109.4	
1814.683	100	55106.0	$a\ {}^4G_{2\frac{1}{2}}$–$x\ {}^4F_{2\frac{1}{2}}$
1814.865	100	55100.5	$b\ {}^2D_{2\frac{1}{2}}$–$v\ {}^2F_{3\frac{1}{2}}$
1815.063	20	55094.5	$b\ {}^2H_{5\frac{1}{2}}$–$y\ {}^4H_{5\frac{1}{2}}$
1815.596	200	55078.3	$b\ {}^4F_{2\frac{1}{2}}$–$x\ {}^4D_{1\frac{1}{2}}$
1815.686	200	55075.6	$b\ {}^4F_{1\frac{1}{2}}$–$x\ {}^4D_{\frac{1}{2}}$
1816.084	5	55063.5	$c\ {}^2G_{4\frac{1}{2}}$–$w\ {}^2H_{4\frac{1}{2}}$
1816.250	10	55058.5	$b\ {}^4P_{2\frac{1}{2}}$–$z\ {}^2D_{2\frac{1}{2}}$
1816.617	20	55047.4	$a\ {}^4H_{2\frac{1}{2}}$–$z\ {}^2G_{2\frac{1}{2}}$
1817.518	100	55020.1	$c\ {}^2G_{3\frac{1}{2}}$–$w\ {}^2H_{4\frac{1}{2}}$
1817.626	100	55016.8	$a\ {}^4G_{2\frac{1}{2}}$–$x\ {}^4F_{2\frac{1}{2}}$
1817.750	20	55013.1	
1818.684	200	54984.8	$b\ {}^4F_{3\frac{1}{2}}$–$x\ {}^4D_{2\frac{1}{2}}$
1819.009	2	54975.0	$b\ {}^4D_{2\frac{1}{2}}$–$x\ {}^4P_{2\frac{1}{2}}$
1819.070	1	54973.1	$b\ {}^4F_{4\frac{1}{2}}$–$z\ {}^2I_{5\frac{1}{2}}$
1819.261	30	54967.4	$a\ {}^4H_{4\frac{1}{2}}$–$z\ {}^2G_{4\frac{1}{2}}$
1819.330	200	54965.3	$b\ {}^2H_{5\frac{1}{2}}$–$y\ {}^4H_{6\frac{1}{2}}$
1819.733	100	54953.1	
1820.064	100	54943.1	$b\ {}^4F_{1\frac{1}{2}}$–$x\ {}^4D_{1\frac{1}{2}}$
1821.004	1	54914.8	$a\ {}^4H_{4\frac{1}{2}}$–$y\ {}^4F_{4\frac{1}{2}}$
1821.262	400	54907.0	$c\ {}^2G_{4\frac{1}{2}}$–$w\ {}^2H_{5\frac{1}{2}}$
1821.688	400	54894.1	$a\ {}^4G_{3\frac{1}{2}}$–$x\ {}^4G_{3\frac{1}{2}}$
1821.766	400	54891.8	$b\ {}^2G_{3\frac{1}{2}}$–$x\ {}^2G_{3\frac{1}{2}}$
1822.046	100	54883.4	$b\ {}^4P_{1\frac{1}{2}}$–$y\ {}^4P_{\frac{1}{2}}$ and $b\ {}^2H_{4\frac{1}{2}}$–$y\ {}^4H_{5\frac{1}{2}}$
1822.215	1?	54878.3	$a\ {}^4H_{6\frac{1}{2}}$–$z\ {}^4I_{5\frac{1}{2}}$
1823.079	1000	54852.3	$a\ {}^4H_{5\frac{1}{2}}$–$z\ {}^4I_{6\frac{1}{2}}$ and $a\ {}^4G_{5\frac{1}{2}}$–$x\ {}^4G_{5\frac{1}{2}}$
1823.414	100	54842.2	$a\ {}^2I_{5\frac{1}{2}}$–$w\ {}^2G_{4\frac{1}{2}}$?
1823.622	150	54835.9	$b\ {}^4D_{3\frac{1}{2}}$–$x\ {}^4P_{2\frac{1}{2}}$
1824.874	100	54798.3	$b\ {}^4F_{2\frac{1}{2}}$–$x\ {}^4D_{2\frac{1}{2}}$
1825.365	400	54783.6	$b\ {}^2F_{3\frac{1}{2}}$–$y\ {}^2D_{2\frac{1}{2}}$
1825.464	300	54780.6	$a\ {}^4H_{3\frac{1}{2}}$–$z\ {}^2G_{4\frac{1}{2}}$
1825.947	750	54766.1	$a\ {}^4G_{4\frac{1}{2}}$–$x\ {}^4G_{4\frac{1}{2}}$
1826.716	1	54743.0	
1827.094	300	54731.7	$b\ {}^4F_{4\frac{1}{2}}$–$x\ {}^4D_{3\frac{1}{2}}$
1829.392	5	54663.0	$b\ {}^4F_{1\frac{1}{2}}$–$x\ {}^4D_{2\frac{1}{2}}$
1829.674	200	54654.5	$b\ {}^2F_{2\frac{1}{2}}$–$y\ {}^2D_{1\frac{1}{2}}$
1830.093	2000	54642.0	$a\ {}^4D_{3\frac{1}{2}}$–$z\ {}^4P_{2\frac{1}{2}}$
1830.581	300	54627.5	$a\ {}^4H_{5\frac{1}{2}}$–$z\ {}^4I_{5\frac{1}{2}}$
1830.780	20?	54621.5	$a\ {}^4H_{3\frac{1}{2}}$–$y\ {}^4F_{3\frac{1}{2}}$
1830.870	150	54618.8	
1831.439	2000	54601.9	$a\ {}^4H_{5\frac{1}{2}}$–$z\ {}^4I_{6\frac{1}{2}}$
1831.916	750	54587.7	$a\ {}^4D_{2\frac{1}{2}}$–$z\ {}^4P_{1\frac{1}{2}}$
1832.201	400	54579.2	$a\ {}^4G_{5\frac{1}{2}}$–$x\ {}^4F_{4\frac{1}{2}}$
1832.784	1	54561.8	$b\ {}^4F_{1\frac{1}{2}}$–$y\ {}^4D_{1\frac{1}{2}}$
1833.876	50	54529.3	$b\ {}^4P_{1\frac{1}{2}}$–$y\ {}^4F_{2\frac{1}{2}}$
1834.840	75	54500.7	$a\ {}^4G_{3\frac{1}{2}}$–$x\ {}^4G_{2\frac{1}{2}}$
1835.000	5000	54495.9	$a\ {}^4H_{6\frac{1}{2}}$–$z\ {}^4I_{7\frac{1}{2}}$
1835.255	100	54488.3	$a\ {}^4D_{1\frac{1}{2}}$–$z\ {}^4P_{\frac{1}{2}}$
1835.617	150	54477.6	$b\ {}^4F_{3\frac{1}{2}}$–$x\ {}^4D_{3\frac{1}{2}}$
1835.687	20	54475.5	$b\ {}^2H_{5\frac{1}{2}}$–$x\ {}^2G_{4\frac{1}{2}}$
1836.200	300	54460.3	$a\ {}^4G_{4\frac{1}{2}}$–$x\ {}^4F_{3\frac{1}{2}}$ and $c\ {}^2G_{3\frac{1}{2}}$–$x\ {}^2F_{2\frac{1}{2}}$
1837.630	1000	54417.9	$a\ {}^4H_{4\frac{1}{2}}$–$z\ {}^4I_{5\frac{1}{2}}$
1837.840	100	54411.7	$a\ {}^4G_{2\frac{1}{2}}$–$x\ {}^4G_{2\frac{1}{2}}$
1838.659	2	54387.5	
1839.535	50	54361.6	$c\ {}^2G_{4\frac{1}{2}}$–$x\ {}^2F_{3\frac{1}{2}}$
1839.636	20	54358.6	$b\ {}^4F_{2\frac{1}{2}}$–$y\ {}^4D_{2\frac{1}{2}}$
1841.582	5	54301.1	
1841.924	15	54291.0	$b\ {}^4F_{2\frac{1}{2}}$–$x\ {}^4D_{3\frac{1}{2}}$
1842.109	1	54285.6	$b\ {}^2F_{2\frac{1}{2}}$–$y\ {}^2D_{2\frac{1}{2}}$
1843.332	2	54249.6	$a\ {}^4G_{4\frac{1}{2}}$–$x\ {}^4G_{5\frac{1}{2}}$
1843.443	200	54246.3	$a\ {}^4D_{\frac{1}{2}}$–$z\ {}^4P_{\frac{1}{2}}$
1843.532	200	54243.7	$b\ {}^4P_{\frac{1}{2}}$–$z\ {}^2D_{1\frac{1}{2}}$
1843.960	75	54231.1	
1844.684	30	54209.8	
1844.726	50	54208.6	$c\ {}^2G_{4\frac{1}{2}}$–$w\ {}^4F_{4\frac{1}{2}}$
1845.074	100	54198.4	$a\ {}^4G_{3\frac{1}{2}}$–$x\ {}^4F_{3\frac{1}{2}}$
1845.636	2	54181.9	
1846.050	20?	54169.7	
1846.157	500	54166.6	$a\ {}^4D_{1\frac{1}{2}}$–$z\ {}^4P_{1\frac{1}{2}}$
1846.514	50*d*	54156.1	$a\ {}^4H_{4\frac{1}{2}}$–$z\ {}^4I_{4\frac{1}{2}}$ and $a\ {}^4G_{2\frac{1}{2}}$–$z\ {}^2H_{4\frac{1}{2}}$
1847.300	125	54133.1	
1847.825	125	54117.7	$b\ {}^2P_{1\frac{1}{2}}$–$z\ {}^2P_{1\frac{1}{2}}$
1848.030	25	54111.7	
1849.299	150	54074.5	$c\ {}^2G_{4\frac{1}{2}}$–$w\ {}^2G_{4\frac{1}{2}}$
1849.464	300	54069.7	$b\ {}^4P_{2\frac{1}{2}}$–$y\ {}^4P_{2\frac{1}{2}}$
1849.932	200	54056.0	$c\ {}^2G_{3\frac{1}{2}}$–$w\ {}^2G_{3\frac{1}{2}}$
1850.503	300	54039.4	$b\ {}^4P_{1\frac{1}{2}}$–$y\ {}^4P_{1\frac{1}{2}}$
1850.780	10	54031.3	$b\ {}^4F_{4\frac{1}{2}}$–$z\ {}^2G_{3\frac{1}{2}}$ and $c\ {}^2G_{3\frac{1}{2}}$–$w\ {}^2G_{4\frac{1}{2}}$
1851.509	50	54010.0	$b\ {}^4P_{\frac{1}{2}}$–$y\ {}^4P_{\frac{1}{2}}$ and $b\ {}^2P_{1\frac{1}{2}}$–$z\ {}^2P_{\frac{1}{2}}$?
1851.937	200	53997.5	$a\ {}^4D_{2\frac{1}{2}}$–$z\ {}^4P_{2\frac{1}{2}}$
1852.645	20	53976.9	$a\ {}^4G_{4\frac{1}{2}}$–$x\ {}^4F_{4\frac{1}{2}}$
1852.919	500	53968.9	$a\ {}^4H_{3\frac{1}{2}}$–$z\ {}^4I_{4\frac{1}{2}}$
1853.266	10	53958.8	$b\ {}^2H_{5\frac{1}{2}}$–$x\ {}^2G_{5\frac{1}{2}}$
1853.841	10	53942.1	$c\ {}^2G_{4\frac{1}{2}}$–$w\ {}^4F_{3\frac{1}{2}}$
1854.194	125	53931.8	$a\ {}^4G_{4\frac{1}{2}}$–$y\ {}^2H_{5\frac{1}{2}}$
1854.393	400	53926.0	$a\ {}^4D_{\frac{1}{2}}$–$z\ {}^4P_{1\frac{1}{2}}$ and $b\ {}^2G_{4\frac{1}{2}}$–$y\ {}^2F_{3\frac{1}{2}}$
1854.763	400	53915.2	$b\ {}^2H_{4\frac{1}{2}}$–$z\ {}^2H_{4\frac{1}{2}}$
1855.331	25	53898.7	$c\ {}^2G_{3\frac{1}{2}}$–$w\ {}^4F_{3\frac{1}{2}}$
1855.954	50	53880.6	$b\ {}^2P_{\frac{1}{2}}$–$z\ {}^2S_{\frac{1}{2}}$
1857.657	50	53831.3	
1858.487	50	53807.2	$a\ {}^4G_{2\frac{1}{2}}$–$x\ {}^4G_{2\frac{1}{2}}$
1859.510	50	53777.6	$b\ {}^4F_{3\frac{1}{2}}$–$z\ {}^2G_{2\frac{1}{2}}$
1860.428	1	53751.1	
1860.866	2	53738.4	
1861.775	1000	53712.2	$b\ {}^4F_{4\frac{1}{2}}$–$y\ {}^4F_{4\frac{1}{2}}$
1862.660	100	53686.7	$b\ {}^2H_{5\frac{1}{2}}$–$x\ {}^4F_{4\frac{1}{2}}$
1863.134	5	53673.0	$a\ {}^4H_{6\frac{1}{2}}$–$z\ {}^4H_{5\frac{1}{2}}$
1863.467	200	53663.4	$a\ {}^2I_{6\frac{1}{2}}$–$x\ {}^2H_{5\frac{1}{2}}$
1863.615	20	53659.2	$b\ {}^2F_{3\frac{1}{2}}$–$y\ {}^4H_{4\frac{1}{2}}$
1863.826	2000	53653.1	$a\ {}^4H_{6\frac{1}{2}}$–$z\ {}^4H_{6\frac{1}{2}}$
1864.187	400	53642.7	$b\ {}^2H_{5\frac{1}{2}}$–$z\ {}^2H_{5\frac{1}{2}}$
1864.519	50	53633.1	
1865.424	100	53607.1	$a\ {}^4H_{4\frac{1}{2}}$–$z\ {}^4H_{3\frac{1}{2}}$
1865.456	100	53606.2	$b\ {}^4F_{4\frac{1}{2}}$–$y\ {}^4F_{3\frac{1}{2}}$
1866.497	20	53576.3	$a\ {}^4D_{1\frac{1}{2}}$–$z\ {}^4P_{2\frac{1}{2}}$
1866.615	100	53572.9	
1867.490	50	53547.8	$a\ {}^4H_{5\frac{1}{2}}$–$z\ {}^4H_{4\frac{1}{2}}$
1867.930	30	53535.2	$c\ {}^2G_{4\frac{1}{2}}$–$w\ {}^4D_{3\frac{1}{2}}$
1868.796	30	53510.4	$b\ {}^4F_{3\frac{1}{2}}$–$z\ {}^2G_{4\frac{1}{2}}$
1870.012	30	53475.6	$b\ {}^2H_{4\frac{1}{2}}$–$x\ {}^2G_{5\frac{1}{2}}$
1870.634	75	53457.8	$b\ {}^4F_{3\frac{1}{2}}$–$y\ {}^4F_{4\frac{1}{2}}$

TABLE IV (*Continued*)

λ (vac.)	I	ν	
1871.870	500	53422.5	$a\ ^4H_{5\frac{1}{2}}$–$z\ ^4H_{5\frac{1}{2}}$
1871.952	300	53420.2	$a\ ^4H_{3\frac{1}{2}}$–$z\ ^4H_{3\frac{1}{2}}$
1872.532	200	53403.6	$a\ ^2I_{5\frac{1}{2}}$–$x\ ^2H_{4\frac{1}{2}}$
1872.575	300	53402.4	$a\ ^4H_{5\frac{1}{2}}$–$z\ ^4H_{6\frac{1}{2}}$
1873.014	1	53389.9	$b\ ^2H_{5\frac{1}{2}}$–$y\ ^2G_{4\frac{1}{2}}$
1874.355	100	53351.7	$b\ ^4F_{3\frac{1}{2}}$–$y\ ^4F_{3\frac{1}{2}}$
1874.822	300	53338.4	$a\ ^4H_{4\frac{1}{2}}$–$z\ ^4H_{4\frac{1}{2}}$
1875.094	200	53330.7	$b\ ^4F_{3\frac{1}{2}}$–$y\ ^4F_{2\frac{1}{2}}$
1875.609	0	53316.0	
1877.464	50	53263.3	$b\ ^4F_{4\frac{1}{2}}$–$y\ ^4D_{3\frac{1}{2}}$
1877.544	50	53261.1	$b\ ^4F_{2\frac{1}{2}}$–$y\ ^4F_{1\frac{1}{2}}$
1879.170	10	53215.9	$b\ ^4F_{4\frac{1}{2}}$–$z\ ^4I_{5\frac{1}{2}}$
1879.244	300	53212.9	$a\ ^4H_{4\frac{1}{2}}$–$z\ ^4H_{5\frac{1}{2}}$
1879.385	100	53208.9	$b\ ^2G_{3\frac{1}{2}}$–$y\ ^2F_{2\frac{1}{2}}$
1879.753	50	53198.5	$b\ ^2F_{2\frac{1}{2}}$–$y\ ^4H_{3\frac{1}{2}}$
1880.321	50	53182.4	
1880.449	30	53178.8	$b\ ^2H_{4\frac{1}{2}}$–$y\ ^2G_{4\frac{1}{2}}$
1880.912	50	53165.7	$b\ ^4F_{2\frac{1}{2}}$–$y\ ^4F_{3\frac{1}{2}}$
1881.080	150	53161.0	$a\ ^4G_{4\frac{1}{2}}$–$z\ ^2F_{3\frac{1}{2}}$?
1881.427	150	53151.1	$a\ ^4H_{5\frac{1}{2}}$–$z\ ^4H_{4\frac{1}{2}}$
1881.702	1000	53143.4	$a\ ^4H_{6\frac{1}{2}}$–$z\ ^4G_{5\frac{1}{2}}$ and $a\ ^4H_{4\frac{1}{2}}$–$z\ ^4G_{3\frac{1}{2}}$ and $b\ ^4F_{2\frac{1}{2}}$–$y\ ^4F_{2\frac{1}{2}}$
1881.867	300	53138.7	$a\ ^4H_{5\frac{1}{2}}$–$z\ ^4G_{4\frac{1}{2}}$
1882.323	150	53125.8	$b\ ^4F_{1\frac{1}{2}}$–$y\ ^4F_{1\frac{1}{2}}$
1883.286	200	53098.7	$a\ ^4H_{3\frac{1}{2}}$–$z\ ^4G_{2\frac{1}{2}}$
1884.532	3	53063.6	$b\ ^2F_{2\frac{1}{2}}$–$x\ ^4F_{2\frac{1}{2}}$
1885.476	15h	53037.0	$a\ ^4G_{5\frac{1}{2}}$–$y\ ^4G_{5\frac{1}{2}}$
1886.469	50	53009.1	$b\ ^4F_{3\frac{1}{2}}$–$y\ ^4D_{3\frac{1}{2}}$? and $b\ ^4F_{1\frac{1}{2}}$–$y\ ^4F_{2\frac{1}{2}}$
1886.742	200	53001.4	
1888.345	10	52956.4	$a\ ^4H_{3\frac{1}{2}}$–$z\ ^4G_{3\frac{1}{2}}$ and $b\ ^2F_{3\frac{1}{2}}$–$x\ ^4G_{2\frac{1}{2}}$
1888.451	10	52954.5	$b\ ^4F_{4\frac{1}{2}}$–$z\ ^4I_{4\frac{1}{2}}$?
1889.090	10	52935.5	$a\ ^4G_{2\frac{1}{2}}$–$z\ ^2F_{2\frac{1}{2}}$
1889.321	20	52929.1	$a\ ^4H_{4\frac{1}{2}}$–$z\ ^4G_{4\frac{1}{2}}$
1890.642	2	52892.1	$a\ ^4H_{3\frac{1}{2}}$–$z\ ^4G_{5\frac{1}{2}}$
1892.011	150	52853.8	$c\ ^2G_{4\frac{1}{2}}$–$x\ ^2H_{5\frac{1}{2}}$
1893.095	20	52823.6	$b\ ^4F_{2\frac{1}{2}}$–$y\ ^4D_{3\frac{1}{2}}$
1893.911	5	52800.8	$a\ ^4G_{3\frac{1}{2}}$–$z\ ^2F_{3\frac{1}{2}}$
1895.368	500	52760.2	$a\ ^2I_{6\frac{1}{2}}$–$z\ ^2K_{7\frac{1}{2}}$
1895.495	30	52756.7	
1896.031	1	52741.8	$a\ ^4H_{3\frac{1}{2}}$–$z\ ^4G_{4\frac{1}{2}}$
1897.560	5	52699.3	$b\ ^4F_{3\frac{1}{2}}$–$z\ ^4I_{4\frac{1}{2}}$
1899.183	5	52654.2	$b\ ^2F_{3\frac{1}{2}}$–$x\ ^4F_{3\frac{1}{2}}$
1899.795	50	52637.3	$c\ ^2G_{4\frac{1}{2}}$–$x\ ^2H_{4\frac{1}{2}}$
1900.763	50	52610.5	$b\ ^2F_{3\frac{1}{2}}$–$z\ ^2H_{4\frac{1}{2}}$
1901.357	300	52594.0	$c\ ^2G_{3\frac{1}{2}}$–$x\ ^2H_{4\frac{1}{2}}$
1903.199	5	52543.1	
1905.354	300	52483.7	$b\ ^2G_{3\frac{1}{2}}$–$y\ ^2H_{4\frac{1}{2}}$
1905.674	20	52474.9	$b\ ^2P_{\frac{1}{2}}$–$z\ ^2P_{1\frac{1}{2}}$
1905.810	5	52471.1	$a\ ^4G_{4\frac{1}{2}}$–$y\ ^4G_{4\frac{1}{2}}$
1906.265	30	52458.6	$b\ ^2F_{2\frac{1}{2}}$–$x\ ^4G_{2\frac{1}{2}}$
1907.458	30	52425.8	
1909.666	150	52365.2	$b\ ^2P_{\frac{1}{2}}$–$z\ ^2P_{\frac{1}{2}}$
1910.151	1	52351.9	$b\ ^2F_{3\frac{1}{2}}$–$x\ ^4G_{3\frac{1}{2}}$
1910.840	300	52333.0	$b\ ^2G_{4\frac{1}{2}}$–$y\ ^2H_{5\frac{1}{2}}$
1911.174	20	52323.9	$a\ ^4D_{3\frac{1}{2}}$–$z\ ^4F_{2\frac{1}{2}}$ and $a\ ^4G_{3\frac{1}{2}}$–$y\ ^4G_{3\frac{1}{2}}$
1912.465	10	52288.5	
1912.952	30	52275.2	$a\ ^4G_{2\frac{1}{2}}$–$y\ ^4G_{2\frac{1}{2}}$
1916.112	50	52189.0	$b\ ^4P_{2\frac{1}{2}}$–$z\ ^4S_{1\frac{1}{2}}$
1917.321	20	52156.1	$b\ ^2F_{2\frac{1}{2}}$–$x\ ^4F_{3\frac{1}{2}}$
1919.120	500	52107.2	$a\ ^6D_{4\frac{1}{2}}$–$z\ ^6D_{3\frac{1}{2}}$
1919.980	5	52083.9	$b\ ^2H_{4\frac{1}{2}}$–$y\ ^4G_{3\frac{1}{2}}$
1922.000	1	52029.1	$a\ ^4D_{2\frac{1}{2}}$–$z\ ^4F_{1\frac{1}{2}}$
1923.801	2	51980.4	
1924.529	50	51960.8	$b\ ^2D_{2\frac{1}{2}}$–$w\ ^2F_{3\frac{1}{2}}$?
1924.722	10	51955.6	
1925.260	20h	51941.0	$b\ ^4F_{4\frac{1}{2}}$–$z\ ^4G_{3\frac{1}{2}}$
1925.513	5	51934.2	
1925.563	15	51932.9	$b\ ^2H_{4\frac{1}{2}}$–$y\ ^4G_{5\frac{1}{2}}$
1925.910	1	51923.5	
1926.365	1	51911.2	
1926.659	2	51903.3	
1927.198	5	51888.8	$a\ ^2I_{6\frac{1}{2}}$–$z\ ^2K_{6\frac{1}{2}}$
1927.740	200	51874.2	$b\ ^2F_{3\frac{1}{2}}$–$y\ ^2G_{4\frac{1}{2}}$
1928.490	100	51854.0	$b\ ^2F_{2\frac{1}{2}}$–$y\ ^2G_{3\frac{1}{2}}$
1928.570	500	51851.9	$a\ ^6D_{4\frac{1}{2}}$–$z\ ^6D_{4\frac{1}{2}}$
1928.802	200	51845.7	$a\ ^2I_{5\frac{1}{2}}$–$z\ ^2K_{6\frac{1}{2}}$
1929.756	300	51820.0	$a\ ^6D_{3\frac{1}{2}}$–$z\ ^6D_{2\frac{1}{2}}$
1930.479	50	51800.6	$a\ ^4D_{3\frac{1}{2}}$–$z\ ^4F_{3\frac{1}{2}}$
1932.442	5h	51748.0	$b\ ^2P_{1\frac{1}{2}}$–$y\ ^4D_{1\frac{1}{2}}$?
1932.766	1	51739.3	$a\ ^4G_{5\frac{1}{2}}$–$z\ ^2I_{5\frac{1}{2}}$
1933.250	50	51726.4	$b\ ^4F_{4\frac{1}{2}}$–$z\ ^4G_{4\frac{1}{2}}$
1933.742	1	51713.2	
1934.274	50	51699.0	
1934.734	50	51686.7	$b\ ^4F_{3\frac{1}{2}}$–$z\ ^4G_{3\frac{1}{2}}$
1935.023	100	51679.0	$a\ ^4D_{2\frac{1}{2}}$–$z\ ^4F_{2\frac{1}{2}}$
1936.392	20	51642.2	$b\ ^4F_{2\frac{1}{2}}$–$z\ ^4G_{2\frac{1}{2}}$
1936.784	5	51632.0	$b\ ^2P_{1\frac{1}{2}}$–$y\ ^4D_{1\frac{1}{2}}$
1936.933	300	51628.0	$a\ ^6D_{2\frac{1}{2}}$–$z\ ^6D_{1\frac{1}{2}}$
1937.661	100	51608.6	$a\ ^4D_{1\frac{1}{2}}$–$z\ ^4F_{1\frac{1}{2}}$
1940.147	500	51542.5	$a\ ^6D_{3\frac{1}{2}}$–$z\ ^6D_{3\frac{1}{2}}$
1941.460	50	51507.6	$b\ ^4F_{4\frac{1}{2}}$–$z\ ^4G_{5\frac{1}{2}}$
1941.730	100	51500.5	$b\ ^4F_{2\frac{1}{2}}$–$z\ ^4G_{3\frac{1}{2}}$
1942.369	200	51483.5	$a\ ^6D_{1\frac{1}{2}}$–$z\ ^6D_{\frac{1}{2}}$ and $b\ ^2F_{2\frac{1}{2}}$–$z\ ^2P_{1\frac{1}{2}}$
1942.497	100	51480.1	$b\ ^4F_{4\frac{1}{2}}$–$z\ ^4G_{5\frac{1}{2}}$
1942.796	100	51472.2	$b\ ^4F_{3\frac{1}{2}}$–$z\ ^4G_{4\frac{1}{2}}$
1945.234	200	51407.7	$a\ ^6D_{2\frac{1}{2}}$–$z\ ^6D_{2\frac{1}{2}}$
1946.792	300	51366.6	$a\ ^4D_{\frac{1}{2}}$–$z\ ^4F_{1\frac{1}{2}}$
1947.626	5	51344.6	$a\ ^6D_{1\frac{1}{2}}$–$z\ ^6D_{1\frac{1}{2}}$
1948.655	100	51317.4	$a\ ^6D_{\frac{1}{2}}$–$z\ ^6D_{\frac{1}{2}}$
1949.006	20	51308.2	
1949.533	30	51294.3	$b\ ^2P_{1\frac{1}{2}}$–$y\ ^4D_{2\frac{1}{2}}$
1949.805	200	51287.2	$a\ ^6D_{3\frac{1}{2}}$–$z\ ^6D_{4\frac{1}{2}}$
1950.668	2	51264.5	
1950.911	400	51258.1	$a\ ^4D_{1\frac{1}{2}}$–$z\ ^4F_{2\frac{1}{2}}$
1950.961	50	51256.8	$b\ ^2F_{3\frac{1}{2}}$–$z\ ^2F_{3\frac{1}{2}}$
1952.158	200	51225.4	$a\ ^4D_{3\frac{1}{2}}$–$z\ ^4D_{2\frac{1}{2}}$
1953.942	500	51178.6	$a\ ^6D_{\frac{1}{2}}$–$z\ ^6D_{1\frac{1}{2}}$
1954.791	300	51156.4	$a\ ^4D_{2\frac{1}{2}}$–$z\ ^4F_{3\frac{1}{2}}$
1954.876	100	51154.1	$a\ ^4G_{5\frac{1}{2}}$–$z\ ^2I_{6\frac{1}{2}}$
1955.505	30	51137.7	$a\ ^4G_{4\frac{1}{2}}$–$z\ ^2I_{5\frac{1}{2}}$
1955.793	200	51130.2	$a\ ^6D_{2\frac{1}{2}}$–$z\ ^6D_{3\frac{1}{2}}$
1956.011	200	51124.5	$a\ ^6D_{1\frac{1}{2}}$–$z\ ^6D_{2\frac{1}{2}}$
1956.770	0	51104.6	
1958.590	30	51057.1	
1959.414	500	51035.7	$a\ ^4D_{3\frac{1}{2}}$–$z\ ^4F_{4\frac{1}{2}}$
1961.450	50	50982.7	$b\ ^2F_{2\frac{1}{2}}$–$z\ ^2F_{2\frac{1}{2}}$
1963.243	3	50936.1	

TABLE IV (*Continued*)

Observed lines of Co III

λ (vac.)	I	ν	
1963.743	100	50923.2	$a\ {}^4D_{2\frac{1}{2}}$–$z\ {}^4D_{1\frac{1}{2}}$
1964.765	3	50896.7	$a\ {}^4G_{4\frac{1}{2}}$–$x\ {}^4D_{3\frac{1}{2}}$
1966.029	2	50863.9	
1966.680	3	50847.1	$b\ {}^2H_{5\frac{1}{2}}$–$z\ {}^2I_{5\frac{1}{2}}$
1969.312	20	50779.2	$b\ {}^2F_{3\frac{1}{2}}$–$y\ {}^4G_{3\frac{1}{2}}$
1970.054	300	50760.0	$a\ {}^4D_{3\frac{1}{2}}$–$z\ {}^4D_{3\frac{1}{2}}$
1971.889	100	50712.8	$a\ {}^4D_{1\frac{1}{2}}$–$z\ {}^4D_{\frac{1}{2}}$
1973.667	5	50667.1	$b\ {}^2P_{1\frac{1}{2}}$–$z\ {}^2D_{1\frac{1}{2}}$
1973.767	10	50664.5	$b\ {}^2F_{3\frac{1}{2}}$–$y\ {}^4G_{4\frac{1}{2}}$
1974.003	2	50658.5	
1974.883	200	50635.9	$b\ {}^2H_{4\frac{1}{2}}$–$z\ {}^2I_{5\frac{1}{2}}$
1977.031	200	50580.9	$a\ {}^4D_{2\frac{1}{2}}$–$z\ {}^4D_{2\frac{1}{2}}$
1978.948	50	50531.9	$a\ {}^4G_{5\frac{1}{2}}$–$z\ {}^2G_{4\frac{1}{2}}$
1980.113	200	50502.2	$a\ {}^4D_{1\frac{1}{2}}$–$z\ {}^4D_{1\frac{1}{2}}$
1981.000	1	50479.6	$a\ {}^4G_{5\frac{1}{2}}$–$y\ {}^4F_{4\frac{1}{2}}$
1981.345	100	50470.8	$a\ {}^4D_{\frac{1}{2}}$–$z\ {}^4D_{\frac{1}{2}}$
1982.049	1	50452.8	
1982.361	1	50444.9	
1984.324	30	50395.0	$b\ {}^2H_{4\frac{1}{2}}$–$x\ {}^4D_{3\frac{1}{2}}$
1986.704	3	50334.6	
1987.197	30	50322.1	$b\ {}^2F_{2\frac{1}{2}}$–$y\ {}^4G_{2\frac{1}{2}}$
1987.952	10	50303.0	
1988.806	5	50281.4	$b\ {}^2F_{2\frac{1}{2}}$–$y\ {}^4G_{3\frac{1}{2}}$
1989.598	400	50261.4	$b\ {}^2H_{5\frac{1}{2}}$–$z\ {}^2I_{6\frac{1}{2}}$
1989.645	100	50260.2	$a\ {}^4D_{\frac{1}{2}}$–$z\ {}^4D_{1\frac{1}{2}}$
1990.841	10	50230.0	
1991.929	1	50202.6	
1992.158	10	50196.8	$a\ {}^4G_{4\frac{1}{2}}$–$z\ {}^2G_{3\frac{1}{2}}$
1993.625	100	50159.9	$a\ {}^4D_{1\frac{1}{2}}$–$z\ {}^4D_{2\frac{1}{2}}$
1995.397	50	50115.3	$a\ {}^4D_{2\frac{1}{2}}$–$z\ {}^4D_{3\frac{1}{2}}$
1999.913	3	50002.2	
2000.447	20	49988.8	$b\ {}^2P_{\frac{1}{2}}$–$y\ {}^4D_{1\frac{1}{2}}$
2000.702	0	49982.5	$a\ {}^4G_{\frac{1}{2}}$–$z\ {}^4I_{\frac{1}{2}}$
2001.735	100	49956.7	$a\ {}^4G_{5\frac{1}{2}}$–$z\ {}^4I_{6\frac{1}{2}}$
2002.559	0	49936.1	$a\ {}^4G_{3\frac{1}{2}}$–$z\ {}^2G_{3\frac{1}{2}}$?
2003.437	0	49914.2	$b\ {}^2G_{4\frac{1}{2}}$–$x\ {}^4G_{3\frac{1}{2}}$
2004.555	5	49886.4	
2004.939	3	49876.8	$a\ {}^4G_{4\frac{1}{2}}$–$y\ {}^4F_{4\frac{1}{2}}$
2006.194	20	49845.6	$a\ {}^4G_{2\frac{1}{2}}$–$z\ {}^2G_{3\frac{1}{2}}$
2011.252	50	49720.3	$a\ {}^4G_{3\frac{1}{2}}$–$z\ {}^4I_{4\frac{1}{2}}$
2012.266	200	49695.2	$b\ {}^2H_{4\frac{1}{2}}$–$z\ {}^2G_{3\frac{1}{2}}$
2013.379	20	49667.7	$a\ {}^4G_{3\frac{1}{2}}$–$z\ {}^2G_{4\frac{1}{2}}$
2014.534	200	49639.3	$b\ {}^2H_{5\frac{1}{2}}$–$z\ {}^2G_{4\frac{1}{2}}$
2016.473	20	49591.5	$a\ {}^4D_{2\frac{1}{2}}$–$z\ {}^6P_{2\frac{1}{2}}$
2016.685	10	49586.3	$b\ {}^2H_{5\frac{1}{2}}$–$y\ {}^4F_{4\frac{1}{2}}$
2020.064	30	49503.4	
2020.775	50	49486.0	$a\ {}^4G_{3\frac{1}{2}}$–$y\ {}^4F_{2\frac{1}{2}}$
2025.118	30	49379.8	$a\ {}^4G_{4\frac{1}{2}}$–$z\ {}^4I_{5\frac{1}{2}}$
2029.229	50	49279.7	$a\ {}^4D_{3\frac{1}{2}}$–$z\ {}^6P_{3\frac{1}{2}}$
2031.331	2	49228.8	
2032.464	100	49201.4	$b\ {}^2P_{1\frac{1}{2}}$–$z\ {}^2D_{2\frac{1}{2}}$
2033.728	3	49170.8	$a\ {}^4D_{1\frac{1}{2}}$–$z\ {}^6P_{2\frac{1}{2}}$
2034.264	5	49157.8	$b\ {}^2F_{3\frac{1}{2}}$–$y\ {}^4D_{2\frac{1}{2}}$
2034.939	10	49141.5	
2039.820	50	49023.9	$b\ {}^2P_{\frac{1}{2}}$–$z\ {}^2D_{1\frac{1}{2}}$
2040.498	5	49007.6	$b\ {}^2G_{4\frac{1}{2}}$–$x\ {}^4G_{5\frac{1}{2}}$
2040.884	10*h*	48998.4	$b\ {}^2F_{2\frac{1}{2}}$–$y\ {}^4D_{1\frac{1}{2}}$
2043.700	2	48930.9	$b\ {}^2D_{2\frac{1}{2}}$–$x\ {}^2F_{3\frac{1}{2}}$
2044.882	5	48902.6	$a\ {}^4G_{5\frac{1}{2}}$–$z\ {}^4H_{4\frac{1}{2}}$
2046.817	10	48856.3	$a\ {}^4G_{3\frac{1}{2}}$–$z\ {}^4I_{4\frac{1}{2}}$
2048.019	30	48827.7	$b\ {}^2H_{5\frac{1}{2}}$–$z\ {}^4I_{4\frac{1}{2}}$
2048.409	3	48818.4	$b\ {}^4D_{1\frac{1}{2}}$–$x\ {}^4F_{1\frac{1}{2}}$
2049.093	5	48802.1	$b\ {}^4D_{\frac{1}{2}}$–$x\ {}^4F_{1\frac{1}{2}}$
2052.770	10	48714.7	$b\ {}^4D_{1\frac{1}{2}}$–$x\ {}^4F_{2\frac{1}{2}}$
2053.769	200	48691.0	$b\ {}^2G_{4\frac{1}{2}}$–$z\ {}^2H_{5\frac{1}{2}}$
2053.977	2	48686.0	$b\ {}^4D_{2\frac{1}{2}}$–$y\ {}^4H_{3\frac{1}{2}}$?
2056.869	100	48617.6	$b\ {}^2G_{3\frac{1}{2}}$–$z\ {}^2H_{4\frac{1}{2}}$
2062.825	10	48477.2	$b\ {}^4D_{2\frac{1}{2}}$–$x\ {}^4G_{3\frac{1}{2}}$
2072.67	5	48246.9	$a\ {}^4G_{5\frac{1}{2}}$–$z\ {}^4G_{5\frac{1}{2}}$
2073.91	3	48218.2	$a\ {}^4G_{2\frac{1}{2}}$–$z\ {}^4H_{3\frac{1}{2}}$
2074.18	3	48211.8	$b\ {}^2P_{1\frac{1}{2}}$–$y\ {}^4P_{2\frac{1}{2}}$
2075.78	0	48174.7	$a\ {}^4G_{4\frac{1}{2}}$–$z\ {}^4H_{5\frac{1}{2}}$
2078.01	1	48123.0	$b\ {}^2F_{3\frac{1}{2}}$–$z\ {}^2G_{4\frac{1}{2}}$
2080.40	10	48067.6	$b\ {}^2H_{4\frac{1}{2}}$–$z\ {}^4H_{3\frac{1}{2}}$
2081.67	2	48038.4	$a\ {}^4G_{3\frac{1}{2}}$–$z\ {}^4H_{4\frac{1}{2}}$
2081.90	2	48032.9	$b\ {}^2F_{2\frac{1}{2}}$–$z\ {}^2D_{1\frac{1}{2}}$
2082.91	0	48009.8	$b\ {}^2H_{5\frac{1}{2}}$–$z\ {}^4H_{4\frac{1}{2}}$
2084.89	1	47964.1	$b\ {}^2F_{3\frac{1}{2}}$–$y\ {}^4F_{4\frac{1}{2}}$
2085.61	2	47947.6	$b\ {}^2P_{\frac{1}{2}}$–$y\ {}^4P_{1\frac{1}{2}}$ and $b\ {}^4D_{3\frac{1}{2}}$–$x\ {}^4G_{4\frac{1}{2}}$
2088.06	1	47891.3	$a\ {}^4G_{4\frac{1}{2}}$–$z\ {}^4G_{4\frac{1}{2}}$
2089.24	15	47864.2	$b\ {}^2H_{5\frac{1}{2}}$–$z\ {}^4H_{6\frac{1}{2}}$
2090.09	0	47844.8	$a\ {}^4G_{3\frac{1}{2}}$–$z\ {}^4G_{3\frac{1}{2}}$
2091.17	10	47820.2	$b\ {}^2G_{4\frac{1}{2}}$–$z\ {}^2F_{3\frac{1}{2}}$
2092.88	0	47781.0	$b\ {}^4D_{2\frac{1}{2}}$–$x\ {}^4F_{2\frac{1}{2}}$
2097.62	3	47673.0	$b\ {}^2H_{4\frac{1}{2}}$–$z\ {}^4H_{5\frac{1}{2}}$
2098.30	10	47657.5	$a\ {}^4D_{3\frac{1}{2}}$–$z\ {}^6F_{4\frac{1}{2}}$
2105.84	3	47486.9	$b\ {}^2G_{3\frac{1}{2}}$–$z\ {}^2F_{2\frac{1}{2}}$
2111.82	1	47352.5	$b\ {}^2H_{5\frac{1}{2}}$–$z\ {}^4G_{5\frac{1}{2}}$?
2120.49	3	47158.9	$b\ {}^4D_{3\frac{1}{2}}$–$x\ {}^4F_{4\frac{1}{2}}$
2121.89	5	47127.9	$a\ {}^4D_{2\frac{1}{2}}$–$z\ {}^6F_{3\frac{1}{2}}$
2124.74	5	47064.6	$b\ {}^2F_{3\frac{1}{2}}$–$z\ {}^2D_{2\frac{1}{2}}$
2134.82	10	46842.3	
2135.55	2	46826.3	$b\ {}^2G_{3\frac{1}{2}}$–$y\ {}^4G_{2\frac{1}{2}}$
2136.81	3	46798.7	$a\ {}^4D_{1\frac{1}{2}}$–$z\ {}^6F_{2\frac{1}{2}}$
2137.98	5	46773.2	
2172.94	5	46020.5	$a\ {}^2I_{5\frac{1}{2}}$–$z\ {}^2H_{4\frac{1}{2}}$
2193.94	8	45580.1	$a\ {}^2I_{6\frac{1}{2}}$–$z\ {}^2H_{5\frac{1}{2}}$
λ (air)			
2267.910	5	44079.8	$b\ {}^4D_{3\frac{1}{2}}$–$x\ {}^4D_{3\frac{1}{2}}$
2321.67	2	43059.2	$b\ {}^4D_{3\frac{1}{2}}$–$y\ {}^4F_{4\frac{1}{2}}$
2348.80	1	42561.1	$a\ {}^4D_{3\frac{1}{2}}$–$z\ {}^6D_{4\frac{1}{2}}$
2438.76	3	40992.0	$c\ {}^2G_{3\frac{1}{2}}$–$z\ {}^2G_{3\frac{1}{2}}$
2452.16	10	40768.0	$c\ {}^2G_{4\frac{1}{2}}$–$z\ {}^2G_{4\frac{1}{2}}$
2481.67	5	40283.3	
2514.93	2	39750.6	
2534.98	2	39436.2	$b\ {}^4P_{2\frac{1}{2}}$–$z\ {}^4P_{2\frac{1}{2}}$
2539.65	2	39363.7	$c\ {}^2G_{4\frac{1}{2}}$–$z\ {}^4H_{5\frac{1}{2}}$
2569.35	2	39908.7	
2811.75	20	35554.6	$b\ {}^4P_{2\frac{1}{2}}$–$z\ {}^4D_{2\frac{1}{2}}$
2860.03	5	34954.5	$b\ {}^4P_{1\frac{1}{2}}$–$z\ {}^4D_{1\frac{1}{2}}$
2888.31	10	34612.2	$b\ {}^4P_{1\frac{1}{2}}$–$z\ {}^4D_{2\frac{1}{2}}$
2915.26	5	34292.2	$b\ {}^4P_{\frac{1}{2}}$–$z\ {}^4D_{\frac{1}{2}}$
2933.27	10	34081.7	$b\ {}^4P_{\frac{1}{2}}$–$z\ {}^4D_{1\frac{1}{2}}$
2954.11	1	33841.3	
2971.30	5	33645.5	$b\ {}^4F_{1\frac{1}{2}}$–$z\ {}^4D_{\frac{1}{2}}$
2973.68	1	33618.6	
2978.01	10	33569.7	$b\ {}^4F_{2\frac{1}{2}}$–$z\ {}^4D_{1\frac{1}{2}}$
2986.13	2	33478.4	$b\ {}^4F_{4\frac{1}{2}}$–$z\ {}^4F_{4\frac{1}{2}}$
2990.04	2	33434.6	$b\ {}^4F_{4\frac{1}{2}}$–$z\ {}^4D_{4\frac{1}{2}}$
2991.89	20	33414.0	$b\ {}^4F_{3\frac{1}{2}}$–$z\ {}^4D_{2\frac{1}{2}}$
3010.92	25	33202.8	$b\ {}^4F_{4\frac{1}{2}}$–$z\ {}^4D_{3\frac{1}{2}}$
3018.41	3	33120.4	
3024.92	2	33049.1	

TABLE IV (*Concluded*)
Observed lines of Co III

λ (air)	I	ν		λ (air)	I	ν	
3075.89	5	32501.5		3305.38	15	30245.1	$a\ ^4G_{5\frac{1}{2}}$–$z\ ^4F_{4\frac{1}{2}}$
3097.74	2	32272.3		3451.25	10	28966.7	
3116.68	10	32076.1		3526.24	2	28350.8	
3151.40	2	31722.8		3634.21	1	27508.5	$a\ ^4D_{1\frac{1}{2}}$–$z\ ^4P_{\frac{1}{2}}$
3180.64	2	31431.2		3636.31	1	27492.6	$a\ ^4D_{\frac{1}{2}}$–$z\ ^4P_{\frac{1}{2}}$
3232.11	20	30930.6	$a\ ^4G_{2\frac{1}{2}}$–$z\ ^4F_{1\frac{1}{2}}$	3667.52	2	27258.7	
3249.24	2	30767.6		3677.23	2	27186.7	$b\ ^4D_{1\frac{1}{2}}$–$z\ ^4P_{1\frac{1}{2}}$
3259.68	20	30669.1	$a\ ^4G_{3\frac{1}{2}}$–$z\ ^4F_{2\frac{1}{2}}$	3680.74	3	27160.8	$b\ ^4D_{2\frac{1}{2}}$–$z\ ^4P_{1\frac{1}{2}}$
3269.23	2	30579.5	$a\ ^4G_{2\frac{1}{2}}$–$z\ ^4F_{2\frac{1}{2}}$	3762.50	1	26570.6	$b\ ^4D_{2\frac{1}{2}}$–$z\ ^4P_{2\frac{1}{2}}$
3287.68	10	30407.8	$a\ ^4G_{4\frac{1}{2}}$–$z\ ^4F_{3\frac{1}{2}}$	3782.27	15	26431.7	$b\ ^4D_{3\frac{1}{2}}$–$z\ ^4P_{2\frac{1}{2}}$

based on the $3d^6$ terms ^3D(part), ^1S, ^1D(part), ^1F, $b\ ^3P$, $b\ ^3F$, $b\ ^1G$. It might seem that some of these levels could be found from the remaining lines, but a thorough search has been unsuccessful.

INTERSYSTEM LINES

The terms of different multiplicity are connected by the numerous combinations which are expected in a spectrum which shows evidence of j–j coupling. Some of the intensity of such lines is due to the sharing of properties by neighboring levels of the same J value but different origin as in the case of $w\ ^4D_{3\frac{1}{2}}$, $w\ ^4F_{3\frac{1}{2}}$, $w\ ^2G_{3\frac{1}{2}}$, and $x\ ^2F_{3\frac{1}{2}}$; but there are many for which such an explanation is not tenable. The intensities of the lines are also frequently very anomalous as in the following case (Table V).

TABLE V

	a^4H				b^4F				a^4G			
	$6\frac{1}{2}$	$5\frac{1}{2}$	$4\frac{1}{2}$	$3\frac{1}{2}$	$4\frac{1}{2}$	$3\frac{1}{2}$	$2\frac{1}{2}$	$1\frac{1}{2}$	$5\frac{1}{2}$	$4\frac{1}{2}$	$3\frac{1}{2}$	$2\frac{1}{2}$
$z^2G_{4\frac{1}{2}}$		5	30	100		30			50		20	
$3\frac{1}{2}$			15	20	20	50				10		20
$z^2F_{3\frac{1}{2}}$			10	15	15	0	100				5	
$2\frac{1}{2}$				20		00	100					10

On the evidence of these intensities alone $z^2G_{4\frac{1}{2}}$ might be $^4I_{4\frac{1}{2}}$ or $^4G_{4\frac{1}{2}}$ or $^4F_{4\frac{1}{2}}$ and $z^2G_{3\frac{1}{2}}$ could be $^4H_{3\frac{1}{2}}$ or $^4F_{3\frac{1}{2}}$. Likewise, z^2F could be given a number of different names. Especially difficult to understand is the not uncommon habit of intersystem combinations of missing the central of three levels of successive J.

Another curious example of intersystem combinations is given in (Table VI).

TABLE VI

	$b^2H_{5\frac{1}{2}}$	$4\frac{1}{2}$	$b^2F_{3\frac{1}{2}}$	$2\frac{1}{2}$
$y^4H_{6\frac{1}{2}}$	200			
$5\frac{1}{2}$	20	200		
$4\frac{1}{2}$			20	
$3\frac{1}{2}$				50

HIGH EVEN TERMS

In Fe II the high terms due to $5s$ and $4d$ are separated by over 4000 wavenumbers and they are therefore easily distinguished. In Co III these electrons have nearly the same energy so that terms due to them overlap completely. Each of the structures produces a ^6D term and both have now been found in Co III. These terms in Fe II make combinations of very different intensity, the $4s$ term giving strong lines, while the $4d\ ^6D$ is represented by a few levels giving very weak combinations. There are two ^6D terms in Co III having these characteristics and they were assigned to $5s$ and $4d$ by comparison with Fe II. It is regretted that the only high level reported to Mrs. Sitterly for inclusion in A.E.L. was wrongly identified as $3d^6(^5D)5s\ ^6D_{4\frac{1}{2}}$, whereas it is now with some certainty identified as the $5d\ ^6D_{4\frac{1}{2}}$ level. The term $e\ ^6G$ is based on single lines except for one satellite, but there seems little doubt of its reality. A comparison of the $4d$ and $5s$ terms of Fe II and Co III is given in Fig. 1.

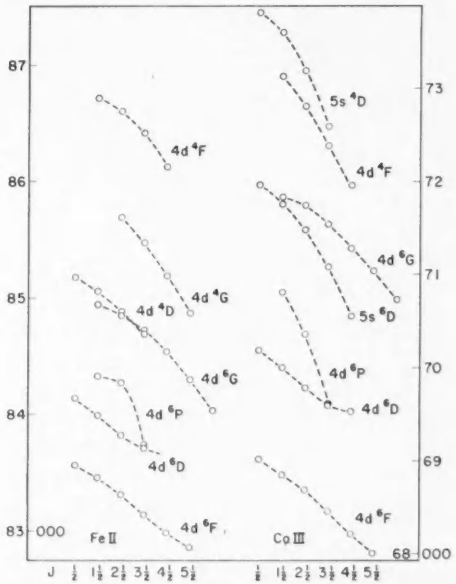

FIG. 1. $4d$ Levels of Fe II and Co III.

TWO-ELECTRON TERMS

In Ni III the observations of the short wavelength end of the spectrum made it possible to find several of the terms of $3d^6\ 4s(^6D)4p$ and subsequently Garcia-Riquelme identified two even levels as belonging to $3d^6\ 4s^2\ ^5D$ (Garcia-Riquelme 1958). Although none of the levels of $3d^5\ 4s\ 4p$ of Co III have been found, it is possible by a comparison such as is given in Catalan, Rohrlich, and Shenstone (1954) to place $3d^5\ 4s^2\ ^6S$ at about 132,000. Attempts to find such a term have been unsuccessful.

Observations of the pulsed cobalt hollow cathode have been made at Lund by Garcia-Riquelme and Velasco and they have kindly put the line list at my disposal. The wavelength range is 2308 Å to 3998 Å and the list includes most of the lines of Table III where the lists overlap. In the longer wavelength part, one might expect the lines due to the transition $4d$–$4f$, but I have been unsuccessful in a search for such combinations. The long wavelength observations probably must be made more complete before such a complicated structure as $3d^6\,4f$ can be identified.

In A. E. L. the value of the series limit $3d^6\,{}^5D$ is given as 270,200 cm^{-1}. The additions to the analysis given in this paper include no evidence on which to change that value and it is therefore to be accepted as the best available at present. The corresponding ionization potential is 33.49 volts.

REFERENCES

ATOMIC ENERGY LEVELS, Vol. II, page 55.
CATALAN, M. A., ROHRLICH, F., and SHENSTONE, A. G. 1954. Proc. Roy. Soc. A, **221**, 421.
GARCIA-RIQUELME, O. 1955. Ann. reale soc. Esp. (A), **51**, 59.
——— 1958. J. Opt. Soc. Am. **48**, 183.
SHENSTONE, A. G. 1954. J. Opt. Soc. of Am. **44**, 749.

ASYMMETRIES IN THE BETA DECAY OF POLARIZED NEUTRONS*

M. A. CLARK AND J. M. ROBSON

It has been shown by Jackson *et al.* (1957) how various asymmetries in the decay of polarized neutrons give important information about the nature of the interaction responsible for the decay. Allowing for failure both of parity conservation and of time reversal invariance, these workers showed that the angular distribution of the decay products includes the following terms:

$$A\frac{\mathbf{J}}{J}\cdot\frac{\mathbf{p}_e}{E_e}+B\frac{\mathbf{J}}{J}\cdot\frac{\mathbf{p}_\nu}{E_\nu}+D\frac{\mathbf{J}}{J}\cdot\left(\frac{\mathbf{p}_e}{E_e}\times\frac{\mathbf{p}_\nu}{E_\nu}\right)$$

using their notation. The terms A and B are non-zero only if parity is not conserved and D is non-zero only if time reversal invariance is violated. The coefficients depend in various ways on the coupling constants and thus measurements of A and B provide information about the nature of the interaction.

We report here a final value for our measurement of D, and also the results of a measurement of B.

We have continued our measurement of the coefficient D as already described elsewhere (Clark *et al.* 1958*a* and *b*) and we have obtained a final value of $D = -0.14\pm0.20$. For full violation of time reversal invariance one expects $D = 0.45$, using a mixture of vector and axial vector interactions, where $|C_A/C_V| = 1.19$. Our result is thus consistent with time reversal invariance in the neutron decay. (Burgy *et al.* (1958*b*) have reported $D = -.04\pm.07$.)

The principle of the measurement of the coefficient B in the neutron decay can be seen from Fig. 1 in which a neutron with spin "up" is assumed to decay with the proton going to the left, as indicated by the arrow "p". If the electron is detected in the direction $E1$, as shown in the left-hand diagram, then, by conservation of linear momentum, the antineutrino must go upwards. If, on the other hand, the electron is detected in the direction $E2$, as shown in the right-hand diagram, the antineutrino must go downwards and be approximately antiparallel to the neutron spin. Thus a comparison of the (p, $E1$) and (p, $E2$) coincidence rates will, after suitable corrections for geometry and electron energy, yield a value for B, the coefficient of the correlation between the neutron spin and the neutrino direction. We have used the apparatus already described (Clark *et al.* 1958*a* and *b*) for this measurement with only one modification. The two electron counters were remounted so that the plane defined by their axes was now perpendicular to the neutron beam direction, instead of containing it as in the time reversal experiment. With this arrangement, the axes of the proton and electron counters satisfy the conditions of

*Issued as A.E.C.L. No. 986.

Fig. 1. The same methods of beam purification and polarization were used for this experiment as for the time reversal experiment. As before, any effects of instrumental drifts were minimized by counting with hourly cycles of alternately polarized and unpolarized neutrons. These hourly cycles also served

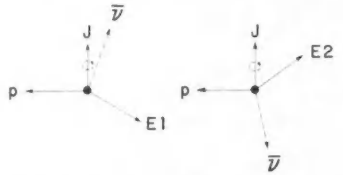

FIG. 1. A neutron with its spin "up" decays into an electron, E, a proton, p, and an antineutrino, $\bar{\nu}$. With the proton and electron detected as in the left diagram the antineutrino must, by momentum conservation, have travelled approximately parallel to the neutron spin direction. With the proton and electron detected as in the right diagram the antineutrino must have travelled approximately opposite to the neutron spin direction.

the useful purpose of providing a convenient monitor of the degree of neutron polarization. Daily checks were made of the range of energy sensitivity of the electron counting systems, and of the coincidence resolving time and of all other aspects of the electronics which could affect the observed number of coincidences. The neutron spins were turned over every few days by reversing the magnetic fields of the neutron polarizing and guide systems. Data were accumulated over several such cycles thus eliminating any asymmetries due to these fields or due to differences in the geometries of the two electron counters.

The measured coincidence asymmetry, after correction for detection geometry, electron energy, and polarization of the neutron beam gives $B = +0.96 \pm 0.40$. The corrections include the effect of the $A(\mathbf{J}/J).(\mathbf{p}_e/E_e)$ term in this measurement. For this latter correction which was small (-0.03) we have used the value of A determined experimentally by Burgy *et al.*

Since $B = 2x(x-1)/(1+3x^2)$ if $x = C_A/C_V$, our result implies a value of C_A/C_V either less than -0.3 or greater than $+6$. The latest value for C_{GT}^2/C_F^2 derived by Kistner and Rustad (1959) from the half-life measurement of Sosnovsky *et al.* (1959) is 1.42 ± 0.06. These data are shown in Fig. 2 and clearly establish opposite phase for the V and A interactions in the neutron decay, a conclusion which has been reached independently by Burgy *et al.* (1958*a*). An interaction of the form V–A is in agreement with the electron–neutrino angular correlation results (Allen *et al.* 1959; Robson 1958; Trebukhovskii *et al.* 1959).

We are grateful to Dr. R. Nathans for assistance in the production of the polarized beam, to Dr. B. N. Brockhouse, who suggested the use of a crystalline quartz filter for beam purification, and to Mr. G. C. Dixon for his assistance in constructing, testing, and using the experimental apparatus.

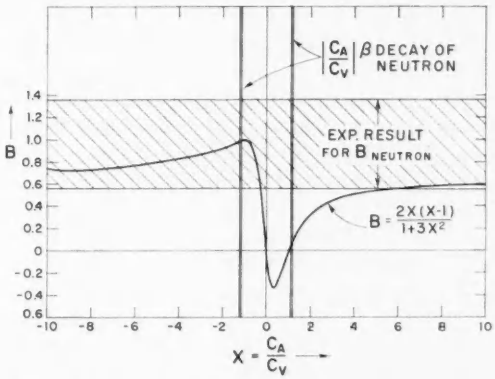

FIG. 2. Comparison of theory and experiment for the B coefficient. B is plotted as ordinate and $x = C_A/C_V$ as abscissa. The curve gives the theoretical dependence of B on x. The vertical lines show the value of $|C_A/C_V|$ as determined from the neutron decay (Sosnovsky *et al.* 1959). The sectioned region encloses our experimental value for B allowing for the error quoted in the text.

ALLEN, J. S., BURMAN, R. L., HERRMANNSFELDT, W. B., STÄHELIN, P., and BRAID, T. H. 1959. Phys. Rev. **116**, 134.
BURGY, M. T., EPSTEIN, R. J., KROHN, V. E., NOVEY, T. B., RABOY, S., RINGO, G. R., and TELEGDI, V. L. 1957. Phys. Rev. **107**, 1731.
BURGY, M. T., KROHN, V. E., NOVEY, T. B., RINGO, G. R., and TELEGDI, V. L. 1958*a*. Phys. Rev. **110**, 1214.
——— 1958*b*. Phys. Rev. Letters, **1**, 324.
CLARK, M. A., ROBSON, J. M., and NATHANS, R. 1958*a*. Phys. Rev. Letters, **1**, 100.
——— 1958*b*. Proceedings of the Second International Conference on the Peaceful Uses of Atomic Energy, Geneva, Vol. 30, P/196, 290.
JACKSON, J. D., TREIMAN, S. B., and WYLD, H. W., Jr. 1957. Phys. Rev. **106**, 517.
KISTNER, O. C. and RUSTAD, B. M. 1959. Phys. Rev. **114**, 1329.
PLEASANTON, F., JOHNSON, C. H., and SNELL, A. H. 1959. Bull. Am. Phys. Soc. II, **4**, 78.
ROBSON, J. M. 1958. Can. J. Phys. **36**, 1450.
SOSNOVSKY, A. N., SPIVAK, P. E., PROKOFIEV, YU. A., KUTIKOV, I. E., and DOBRININ, YU. P. 1959. Nuclear Physics, **10**, 395.
TREBUKHOVSKII, YU. V., VLADIMIRSKII, V. V., GRIGOR'EV, V. K., and ERGAKOV, V. A. 1959. J. Exptl. Theoret. Phys. (USSR) **36**, 1314.

RECEIVED FEBRUARY 8, 1960.
PHYSICS DIVISION,
ATOMIC ENERGY OF CANADA LIMITED,
CHALK RIVER, ONTARIO.

THE SPECIFIC HEAT OF CRYSTALLINE QUARTZ BETWEEN 2° K AND 4° K

G. H. S. Jones and A. C. Hollis Hallett

In 1956 a theoretical analysis of the lattice vibrations of natural quartz was made by Betts *et al.* and a value of 555.8° K was obtained for its Debye temperature. This value is considerably greater than the values of 166° K and 204° K deduced respectively by Anderson (1936) and by Saksena (1941) from experimental results, and it was of interest to measure the specific heat of natural quartz at low temperatures where there is reason to hope that the specific heat of quartz would obey the Debye T^3 law thus enabling the Debye temperature to be determined from the measurements.

Previous measurements at low temperatures have been made by Nernst (1911), Anderson (1936), and others and a compilation of these has been given by Sosman (1927). The lowest temperature at which measurements had been made was 25° K (by Nernst) and even at this temperature it was necessary to express the temperature variation of the specific heat of quartz as the sum of a Debye function plus a variety of Einstein functions; in Saksena's (1941) analysis there are given 24 Einstein functions corresponding to a variety of frequencies discovered by spectroscopic methods. In all cases the Debye contribution to the specific heat was considered small compared with the Einstein functions, and there is probably considerable uncertainty in the values 166° K (Anderson) and 204° K (Saksena) given for the Debye temperature.

Accordingly, measurements have been made at Toronto on a natural quartz crystal in the range of temperature from 2° K to 4° K and it has been found that the Debye T^3 law is well followed by the results and a value of 470° K with an uncertainty of less than 10° K is deduced for the Debye temperature of quartz. This value is much closer to the theoretical estimate of 555.8° K (Betts *et al.* 1956) than were the previous estimates from experimental results, but it would appear that some discrepancy still exists.

The specimen used in this investigation was a piece of natural quartz crystal chosen for its freedom from internal defects as judged by visual inspection of its clarity. Its surface was not, however, perfect since the ends were somewhat chipped and one face was marked by a small roughened area. Another face had a complex step structure, the size of the steps being of the order of a few thousandths of an inch. It was approximately 4 cm long and was roughly 1 cm by 1 cm in section and had a mass of 10.926 g. To the specimen were bonded the "addenda" comprising a heater and carbon thermometer. The heater consisted of about 9 feet of Formel-coated Manganin wire of diameter 0.002 in. and had a resistance of about 600 ohms. This was wrapped around the crystal and cemented to it with a small quantity of shellac which was subsequently baked. The thermometer was a nominal 25-ohm, $\frac{1}{2}$-watt commercial radio resistor (Ohmite) whose outer casing had been ground away to reveal the carbon. This was attached to the specimen using a small quantity of cold-setting araldite. The total mass of the addenda, i.e. the heater, thermometer, and bonding agents, was 0.567 g.

The specimen was suspended within a brass chamber by means of fine nylon threads. These threads were secured to metal springs so that they were in tension, and the specimen hung freely in the center of the chamber without touching the walls or supports. The electrical leads from the thermometer and heater, coiled near the specimen, passed through a lead-in seal at the top of the chamber and through the liquid helium bath in which the chamber was immersed. This lead-in seal was a commercial seal of the type which had a number of fine tubes sealed in ceramic. It was soft-soldered into a hole bored in the top of the chamber, and the leads were passed through the tubes without join. The tubes and the socket for the seal were then filled with cold-setting araldite. The seal was vacuum tight even when immersed in helium II.

The chamber was supported at the bottom of the cryostat by a thin-walled monel tube which served as a pumping tube for the chamber and was connected to a pressure gauge, a liquid air trap, and diffusion and backing pumps, all outside the cryostat. A baffle inserted into the pumping tube near its lower end served to reduce the stray heat input into the chamber due to gas currents and to radiation. The resulting temperature drift of the specimen was somewhat variable depending primarily upon the efficiency of removal of the exchange gas within the chamber and upon the difference of temperature between the sample and the outside helium bath. For all the results reported here, however, the drift rate was sufficiently small compared with the deliberate heating that corrections for it could be determined readily and reliably.

The experiment consisted essentially of supplying a measured amount of power for a measured time to the heater, and observing the resulting change of temperature. The powers used varied between 3.7 and 0.22 microwatts and the heating times varied between 15 and 60 seconds. The power was determined by measuring the current flowing through the heater with a sensitive meter and the potential drop across the heater with a potentiometer. The change of temperature was observed as a change of resistance of the carbon thermometer using another potentiometer connected across it. These changes were measured either by observing the off-balance deflections of the potentiometer's galvanometer or by balancing the potentiometer manually, depending upon the rate at which the temperature changed. The thermometer was calibrated against the vapor pressure of the helium bath using the 1948 scale of temperature. Recalculation of the results in terms of the more recent 1955L scale did not produce changes which were significant when compared with the random scatter of the results.

The calculation of the heat capacity from the observed variation of temperature with time before, during, and after the heating period followed standard methods. For those measurements at 4° K and above, good thermal isolation of the specimen was achieved and the temperature drift rates before and after heating were negligible. Thus in this region the heat capacity was calculated from the measured heat input and the difference between the initial and final temperatures. For measurements below about 2.5° K, good

thermal isolation could not be achieved and the temperature drift rates before and after heating were appreciable. However, the rates of change of temperature with time before and after heating were constant and equal, and the temperature change due to the heating could be determined readily. Between about 2.5° K and 4° K the temperature drift before heating was made very small by maintaining the outside helium bath temperature very close to the initial temperature of the specimen. The rate of cooling of the specimen after the heating period was not constant in this temperature range, and the method used to calculate the heat capacity was that described by Kouvel (1956). In all cases the temperature of measurement was taken to be the mean of the initial and final temperatures. It is felt that in general the accuracy achieved in measuring the heat capacity was about 2%, and the mean temperatures are known within about 2 millidegrees.

The heat capacity measured by this procedure was the sum of the desired heat capacity of the quartz and the heat capacity of the addenda, comprising the heater, carbon thermometer, and bonding material. Although attempts to measure the heat capacity of the addenda directly were not successful, an indirect determination was made by measuring the heat capacity of another specimen consisting of a rod of pure copper fitted with addenda as similar as possible in appearance to that on the quartz. Since the heat capacity of the copper alone was well known from the work of Corak *et al.* (1955), the heat capacity of the addenda could be determined by subtraction. This heat capacity was surprisingly large, of the order of 40% of the heat capacity of the quartz alone, and was proportional to T^3 within the errors of measurement. This last fact was used to calculate the heat capacity of the addenda at each of the temperatures at which measurements were made on the quartz specimen, and values of the heat capacity of the quartz alone were obtained by subtraction.

The results obtained, expressed as the heat capacity of the quartz per gram, are plotted against the cube of the temperature in Fig. 1. It can be seen that the results lie reasonably well on a straight line and that therefore

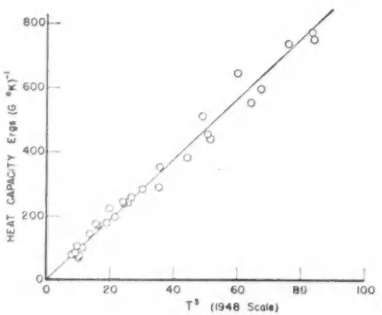

FIG. 1. The heat capacity of the natural quartz specimen plotted against the cube of the absolute temperature. The slope of the straight line corresponds to a Debye temperature, Θ, of 469° K.

the specific heat of quartz is proportional to T^3 in accordance with the Debye theory. Thus, assuming that this quartz can be represented by the chemical formula SiO_2, it was possible to determine an effective Debye temperature, $\Theta = 469°$ K, corresponding to this temperature range, and the straight line drawn in Fig. 1 has a slope corresponding to this value of Θ. The scatter of the individual points around this straight line might be considered as a variation of Θ with temperature, but since the departures of the individual results from the drawn line are more random than systematic, it is felt that these results give no definite information regarding a possible variation of Θ with temperature. In view of the large contribution to the total heat capacity made by the addenda, it is difficult to estimate a figure for the uncertainty in the value 469° K quoted for Θ. However, with all effects considered, the uncertainty in Θ should not be greater than 10° K.

Comparison of the present results with those obtained by Nernst (1911) and Anderson (1936) is shown in Fig. 2. Here the specific heat of natural crystalline quartz in calories per gram formula weight per degree has been plotted, using a logarithmic scale, against T/Θ also on a logarithmic scale assuming $\Theta = 469°$ K from the present measurements. The full curve drawn in Fig. 2 is the Debye theoretical curve for an atomic solid equivalent in atomic

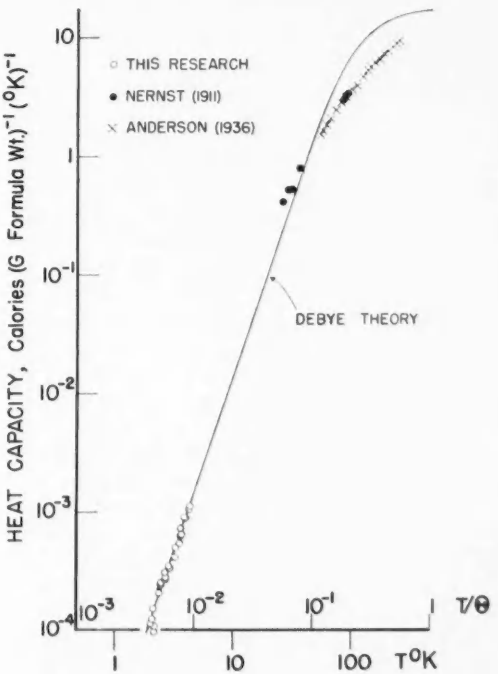

FIG. 2. Comparison of the results of this research with those of Nernst (1911) and Anderson (1936) and with the Debye theory (full curve).

mass and total number of atoms to the quartz. The full curve fits the present results since the value of Θ was derived from them. An exact fit with the results of Nernst and Anderson is clearly not present, but an exact fit could hardly be expected in view of the nature and structure of quartz. Figure 2 does, however, show that the present results are in line with the earlier measurements, and also indicate to some extent the deviations of the behavior of quartz from the Debye theory.

ACKNOWLEDGMENTS

The authors are indebted to the National Research Council of Canada and to the Ontario Research Foundation for their grants-in-aid of research which made this work possible. One of us, G. H. S. J., is indebted to the California Research Corporation for financial assistance.

ANDERSON, C. T. 1936. J. Am. Chem. Soc. **58**, 568.
BETTS, D. D., BHATIA, A. B., and HORTON, G. K. 1956. Phys. Rev. **104**, 43.
CORAK, W. S., GARFUNKEL, M. P., SATTERTHWAITE, C. B., and WEXLER, A. 1955. Phys. Rev. **98**, 1699.
KOUVEL, J. S. 1956. J. Appl. Phys. **27**, 639.
NERNST, W. 1911. Ann. Phys. **36**, 395.
SAKSENA, B. D. 1941. Proc. Indian Acad. Sci. A, **12**, 93.
SOSMAN, R. B. 1927. Properties of silica (The Chemical Catalog Co. Inc., New York). *See also* International Critical Tables, **5**, 105; **4**, 21.

RECEIVED JANUARY 30, 1960.
DEPARTMENT OF PHYSICS,
UNIVERSITY OF TORONTO,
TORONTO, ONTARIO.

ON THE AXIAL SYMMETRY OF THE NILSSON MODEL NUCLEUS*

T. D. NEWTON

The strong coupling approximation for Bohr's collective model (1952) of the nucleus, particularly when the single particle states are realized as Nilsson (1955) functions, has had many successes (e.g. Mottelson and Nilsson 1955; Gove and Litherland 1958). It is usual to determine the best shape of the potential well of the single-particle Hamiltonian by seeking the minimum energy of the assigned number of particles as the well shape is modified. In the references quoted above it is always assumed that the nucleus possesses an axis of symmetry. It is therefore of some interest to inquire whether or not the spheroidal shape of the Nilsson (1955) single-particle model nucleus is intrinsically stable; that is, does the minimum energy of a given number of fermions in an anisotropic oscillator potential with Nilsson spin-orbit coupling always correspond to a potential with axial symmetry?

A modification of the Bohr strong coupling model has recently been proposed by Davydov and Filippov (1958). In this model the collective motions

*Issued as A.E.C.L. No. 991.

are represented entirely by rotations but the nuclear shape is permitted to be aspheroidal. This Davydov–Filippov model provides a simpler description of the states of even–even nuclei than does Bohr's original form of the theory, although its application to other types of nuclei has not yet been fully worked out (cf. Davydov 1959). It is, therefore, also of interest for applications of this model to know what shape of oscillator potential will provide the minimum energy of a system of single particles.

The energy levels and eigenfunctions of a completely anisotropic oscillator have been computed (Newton 1960). The single-particle Hamiltonian is

$$H = -\frac{\hbar^2}{2\mu^*}\nabla^2+\tfrac{1}{2}\mu^*(\omega_x{}^2x^2+\omega_y{}^2y^2+\omega_z{}^2z^2)+C\bar{l}_t\,.\,\bar{s}+D\bar{l}_t{}^2. \tag{1}$$

Here the l_t are the infinitesimal pseudorotation operators; that is, if we define

$$\xi^2 = \frac{\mu^*\omega_x}{\hbar}x^2, \qquad \eta^2 = \frac{\mu^*\omega_y}{\hbar}y^2, \qquad \zeta^2 = \frac{\mu^*\omega_z}{\hbar}z^2 \tag{2}$$

then the l_t are the infinitesimal rotations in (ξ,η,ζ) space. C and D are constants. The mass parameter μ^* is the single-particle effective mass (Newton 1959) of a nucleon in the nucleus.

Since we wish to discuss (1) in cases in which ω_x, ω_y, and ω_z are all different, the single distortion parameter used by Nilsson is not sufficient and we have chosen to use parameters more nearly equivalent to those of Bohr (1952). We write

$$\omega_x = \omega_0.1_x{}^{-1}, \qquad \omega_y = \omega_0.1_y{}^{-1}, \qquad \omega_z = \omega_0.1_z{}^{-1}, \tag{3a}$$

$$\hbar^3\omega_x\omega_y\omega_z = 1, \tag{3b}$$

$$A_x = 1-\sqrt{5/4\pi}\,\beta\cos(\gamma+\pi/3), \tag{4a}$$

$$A_y = 1-\sqrt{5/4\pi}\,\beta\cos(\gamma-\pi/3), \tag{4b}$$

$$A_z = 1+\sqrt{5/4\pi}\,\beta\cos\gamma. \tag{4c}$$

The frequencies ω_x, ω_y, ω_z are thus inversely proportional to the axial intercepts of the distorted nuclear surface defined by Bohr (1952). Equation (3*b*) ensures constant nuclear volume and defines the energy scale. When $\gamma = 0$ or $\gamma = \pi/3$, equations (3) and (4) reduce to the Nilsson (1955) case, and the parameter β can then be related to Nilsson's parameters δ and ϵ,

$$\begin{aligned}\beta &= 1.0569(2\delta+3\sqrt{[1+(2/3)\delta][1-(4/3)\delta]}-3)/(1-2\delta)\\ &\approx 1.0569\delta(1-(3/2)\delta-\tfrac{1}{2}\delta^2-(13/24)\delta^3)/(1-2\delta)\end{aligned}$$

and

$$\beta = 1.0569\epsilon/(1-\epsilon/3)$$

for spheroidal systems.

Having determined the single-particle energies, the total energy of a model

nucleus can be obtained. It is the sum over all occupied levels of the quantity

$$\epsilon_k = \tfrac{1}{2}(1+\tfrac{1}{2}\mu^*/M)E_k-(\tfrac{1}{4}\mu^*/M)\langle C\bar{l}_t.\bar{s}+D\bar{l}_t^2\rangle_k \tag{5}$$

in which the subscript k labels a single-particle state of energy E_k and $\langle f\rangle_k$ represents the expectation value of the operator f in the state k. M is the true nucleon mass. In the model, neutrons and protons are not differentiated; two particles of each kind are allowed in each state k.

The Hamiltonian (1) is so constructed (Nilsson 1955, Appendix A) that the set of states of a given principal oscillator number $N = n_x+n_y+n_z$ is closed under H. The eigenvalues E_k have been computed for $N \leqslant 4$, 35 states in all, for each of 46 values of the parameters $\beta = -0.5$ (0.1) to 0.5 and $\gamma = 0$ ($\pi/24$) to $\pi/6$. At $\beta = 0$, γ is irrelevant. This provides positions for 70 particles of one kind, but since at large distortions some of the $N \geqslant 5$ levels may be brought very low in energy we have not attempted to discuss systems containing more than 50 particles of one kind.

The terms $C\bar{l}_t.\bar{s}+D\bar{l}_t^2$ in (1) are primarily postulated for the purpose of adjusting the order of levels and making major shells of the model close at the true particle number. Nilsson considers the values

$$C = -2\kappa\hbar\omega^0{}_0, \tag{6a}$$

$$D = -\kappa\mu_N\hbar\omega^0{}_0. \tag{6b}$$

On our energy scale $\hbar\omega^0{}_0 = 1$. The parameter μ_N varies with the principal quantum number. Nilsson (1955) suggests $\mu_0 = \mu_1 = \mu_2 = 0$, $\mu_3 = 0.035$, $\mu_4 = 0.045$, and $\kappa = 0.05$. We have used the Nilsson values of D, but have varied C independently of D.

We use the term "preferred shape" of a model nucleus containing Z protons and N neutrons to designate the potential of the form (1) for which the ground state energy is minimal under variation of β and γ. The preferred shape can be specified by the values β_0 and γ_0 at the minimum.

It is clear that the values of C and D affect the preferred shape. Consider a system of 40 nucleons of one kind. If $C = 0$, $D = 0$ we have a pure oscillator potential and 40 particles just fill the $N = 3$ shell. The preferred shape is spherical. If still with $C = 0$, $D = 0$ we consider 50 particles, we find the preferred shape is aspherical because of the partly filled $N = 4$ shell. However, an acceptable shell model must include spin-orbit coupling with $C < 0$ in order to make the shell closure occur at 50 particles. This term makes the greatest decrease in energy when the nucleus is spherical, and so as C decreases from 0 the preferred shape for 50 particles tends towards the spherical form. The preferred shape is not spherical at $C = -0.1$, but it has become spherical at $C = -0.3$.

In Figs. 1 and 2 we show the approximate preferred values of $(\beta_0\gamma_0)$ for even sets of one kind of nucleon with $C = -0.1$ (Fig. 1) and $C = -0.3$ (Fig. 2). These shapes possess the minimum energy, $\epsilon = \Sigma\epsilon_k$, from among the 46 calculated shapes. In Fig. 3 we show the way the energy of the systems of 28 and of 50 nucleons varies with distortion when $C = -0.3$. It should be noted that for these calculations C was changed without changing D and

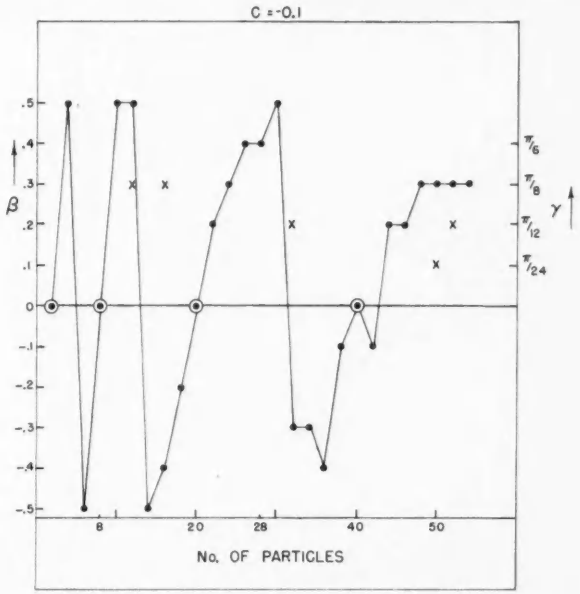

FIG. 1. The preferred distortion parameters with spin-orbit coupling $C = -0.1$ of systems containing an even number of one kind of fermion. The solid circles indicate the value of β shown on the left ordinate scale; the crosses indicate the non-zero values of γ_0 shown on the scale on the right side. If no cross appears for a given even number of particles the corresponding value γ_0 is zero, i.e. the system prefers axial symmetry.

the large value is not necessarily one which provides a good shell model level order. It is almost certainly too large to use in the shells of higher N. The purpose here is to indicate the form of the energy minimum near the spherical shape for these "magic numbers" when the spin-orbit coupling is considerably increased. $\mu^*/M = 0.609$ (Newton 1959) was used in computing ϵ_k. This parameter has no very large effect on the properties now under discussion.

The remaining figures illustrate our main point. They are "energy maps" of the ground state of five model nuclei. The systems illustrated are not particularly significant. The same general behavior is observable in greater or less degree in every system we have studied.

The maps show the variation of the energy ϵ of the ground state as a function of β and γ; the minimum of ϵ marks the preferred shape. It is more illuminating to restrict β to positive values and to represent the deformation $(-\beta,\gamma)$ by the equivalent parameters $(+\beta, \pi/3-\gamma)$. Curves are drawn for each of the computed values of γ, and are labelled p (for $\gamma = 0$, prolate) 1, 2, . . . , 7, σ (for $\gamma = \pi/3$, oblate). At some points the variation of ϵ with γ at fixed β is plotted as an insert. Between calculated points the curves are smoothly interpolated by eye. The contours are actually composed from arcs with discontinuities of slope at the points where the lowest state changes

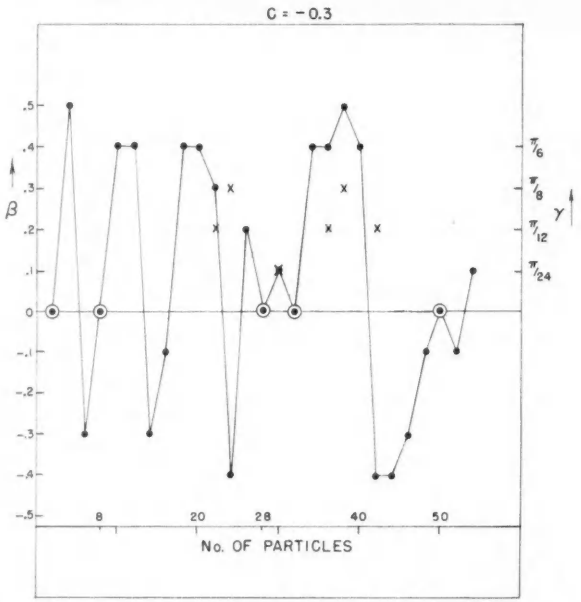

FIG. 2. The preferred distortion parameters with spin-orbit coupling $C = -0.3$. The meaning of the figure is otherwise the same as Fig. 1.

from one configuration to another. Consequently the interpolations may be somewhat inaccurate. The general features of the energy surfaces are, however, well established by the calculated values.

The salient feature of the energy surfaces is the marked changes which occur with changing spin-orbit coupling. With $C = 0$ the preferred shape is usually fairly well defined but as C is decreased from zero the energy minima are broader. The preferred value β_0 usually remains relatively well marked but the value of γ_0 is often ill defined. If one requires that the closed shells of 28 and 50 particles should be spherical, then the spin-orbit coupling in the $N = 3$ and $N = 4$ states should be negative and greater in magnitude than the value $-0.1\ \hbar\omega^0_0$.

Our few examples suffice to show also that the preferred shape for some sets of particles is not axially symmetric. One can see from Figs. 4*a*–4*e* that the energy of the system of independent particles may be decreased by 10 to 15% of $\hbar\omega^0_0$ by the change from axial symmetry to a non-axial shape. This energy change is comparable to the energy of a collective mode of excitation. Consequently the effects of departure from axial symmetry in Bohr's (1952) strong coupling theory cannot properly be treated by perturbation methods.

Finally we remark that the preferred shape is not always well defined, i.e. the ground state energy sometimes varies but little over a wide range of distortion parameters. Thus it is difficult to justify the concept of an asymmetrical top with unvarying principal moments of inertia.

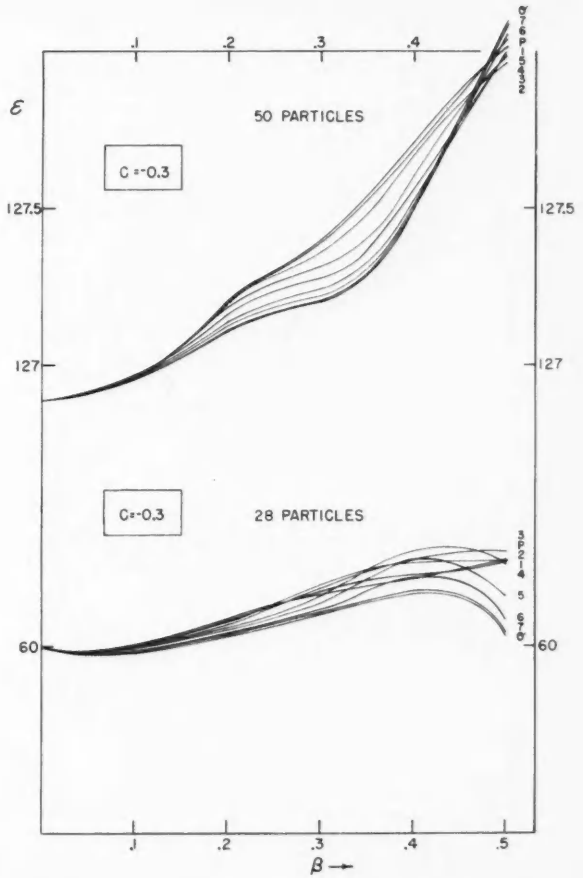

FIG. 3. The ground state energy of systems of 28 and of 50 particles of one kind when $C = -0.3$ as a function of distortion. The abscissa is the parameter β and the function $E(\beta)$ is drawn for each available value of γ from $\gamma = 0$ (prolate shape, curve p) to $\gamma = \pi/3$ (oblate shape, curve o) in steps $\gamma = \pi/24$.

In fact in the region of the light nuclei both the Bohr strong coupling approximation (e.g. Litherland, Paul, Bartholomew, and Gove 1956) and the Davydov–Filippov model (e.g. Litherland 1960) describe well some of the features of the excited states but both approximations have some disagreements with experiment, usually in predicting transition probabilities. The present calculation indicates some of the difficulties in the justification of these models, which may be the reason for their incomplete agreement with experiment.

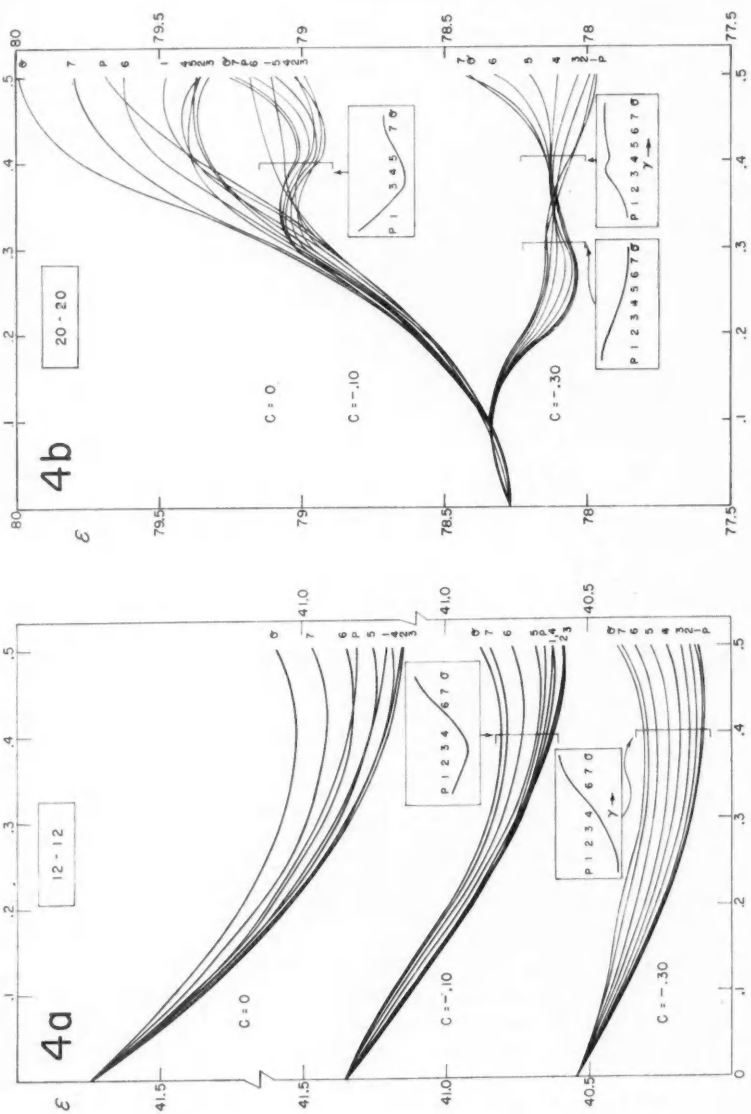

FIGS. 4*a* AND 4*b*.

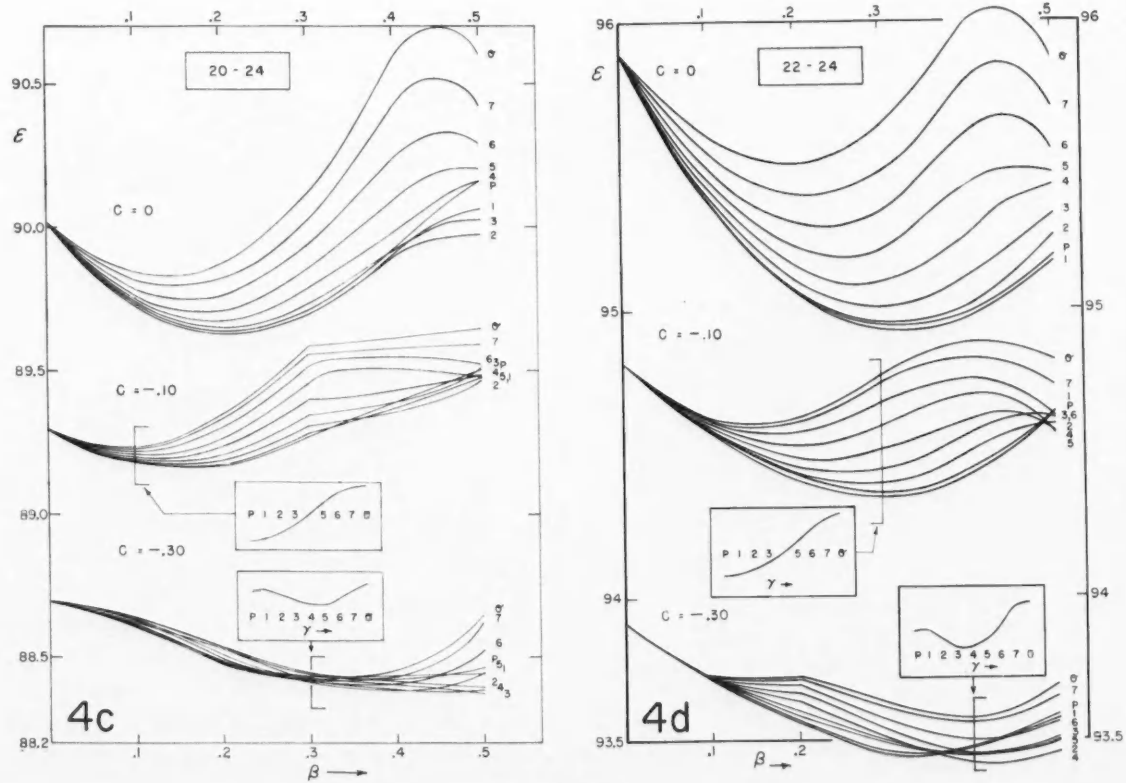

FIGS. 4c AND 4d.

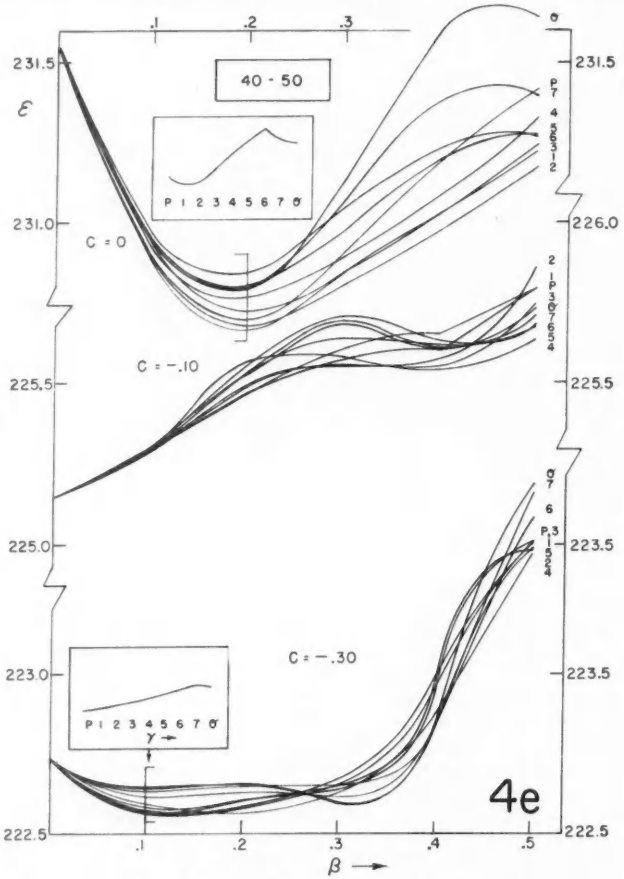

FIG. 4. The ground state energy of various systems of two kinds of particle as a function of the distortion. Each energy map is shown for three values of the spin-orbit coupling constant C. The parametrization is the same as in Fig. 3.

BOHR, A. 1952. Kgl. Danske Videnskab, Selskab, Mat.-fys. Medd. **26**, No. 14.
DAVYDOV, A. S. 1959. J. Exptl. Theoret. Phys. **36**, 1103.
DAVYDOV, A. S. and FILIPPOV, G. F. 1958. Nuclear Phys. **8**, 237.
GOVE, H. E. and LITHERLAND, A. E. 1958. Phys. Rev. **113**, 1078.
LITHERLAND, A. E. 1960. Nuclear Phys. To be published.
LITHERLAND, A. E., PAUL, E. B., BARTHOLOMEW, G. A., and GOVE, H. E. 1956. Phys. Rev. **102**, 208.
MOTTELSON, B. R. and NILSSON, S. G. 1955. Phys. Rev. **99**, 1615.
NEWTON, T. D. 1959. Can. J. Phys. **37**, 944.
——— 1960. Chalk River Report CRT-886.
NILSSON, S. G. 1955. Kgl. Danske Videnskab. Selskab, Mat.-fys. Medd. **29**, No. 16.

RECEIVED FEBRUARY 5, 1960.
THEORETICAL PHYSICS DIVISION,
ATOMIC ENERGY OF CANADA LIMITED,
CHALK RIVER, ONTARIO.

ON THE CONDENSATION COEFFICIENT IN THE GROWTH OF SILVER FROM THE VAPOR PHASE

R. A. RAPP,* J. P. HIRTH,† AND G. M. POUND‡

Chandra and Scott (1958) have recently reported condensation coefficients which were appreciably less than unity for the growth of gold, silver, and copper from the vapor at high beam fluxes. For silver at fluxes of about 10^{16} atoms/cm² sec, the condensation coefficients reported by Chandra and Scott ranged between 0.982 at −28° C and 0.879 at 171° C. Frauenfelder (1950) and Devienne (1953) had previously reported condensation coefficients for silver to be 0.3 to 0.8 and 0.9 to 1.0, respectively. Yang, Simnad, and Pound (1954) have determined the condensation coefficient for silver to be 1.0 at low fluxes of 10^{11} atoms/cm² sec at 192° C. Although different silver fluxes were used in the separate investigations, these data are still contradictory.

In view of this contradiction, the present authors determined condensation coefficients for silver at relatively high fluxes of $1.3–4.5\times10^{14}$ atoms/cm² sec and temperatures between 45° C and 440° C. In these experiments, the residual gas pressure in the vacuum system was varied between 4.4×10^{-5} and 6×10^{-10} mm Hg in order to determine whether the adsorption of gaseous impurities on the growing silver substrate affects the value of the condensation coefficient. The apparatus, shown in Fig. 1, is similar to that used by Chandra

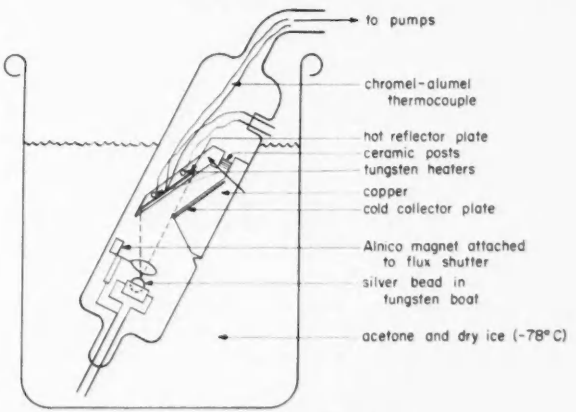

FIG. 1. Silver condensation chamber.

and Scott. A glass cover slide, 25 mm square and 0.15 mm thick, was held snugly in a copper jig which was heated by tungsten filaments. The temperatures of the copper block holding the "hot plate" (referred to as the "reflector

*Max-Planck Institut für Physikalische Chemie, Göttingen.
†Metals Research Laboratory, Carnegie Institute of Technology, Pittsburgh, Pennsylvania.
‡Department of Metallurgy, Sheffield University, Sheffield, England.

plate" by Chandra and Scott) were measured with a chromel–alumel thermocouple and are reported in Table I. The actual "front face" temperatures of the glass hot plates may have been somewhat lower than these listed temperatures. For a copper supporting block temperature of 200° C, calculations showed that the heat from radiation sources alone will maintain the silver deposit on the hot plate at 140° C. Since the amount of heat received by conduction from the copper block cannot be estimated (exact area of contact is unknown), one must conclude that the temperature of the silver deposit was between 140° C and 200° C. However, the indeterminacy of the substrate temperature does not affect the calculated condensation coefficients or the conclusions from this investigation. A silver bead which was held in a tungsten foil boat and heated to 900 to 950° C served as the source of silver vapor for deposition on the hot plate. Facing the hot plate, but not the silver beam, was another identical glass plate called the "cold plate" (referred to as the "collector plate" by Chandra and Scott). A "cold plate" temperature of approximately −78° C was maintained by contact between the plate and a copper block held at −78° C. The function of the cold plate was to collect even the smallest flux of silver atoms which might reflect or re-evaporate from the growing silver substrate (hot plate). In some experiments, the initial glass hot plate was gold-plated to insure rapid initial nucleation of the silver on the hot plate. Maintenance of all the surfaces of the system, except the hot plate, at −78° C precluded re-evaporation of any silver atoms to the cold plate from these extraneous surfaces. This was a notable departure from the radiation chamber apparatus of Chandra and Scott.

For the ultra-high vacua experiments, cleanliness of the substrates from condensable impurities was insured by a 3-cycle bake out of the system at 450° C, double-trapping of the Octoil pump with liquid nitrogen, and the cold bath (−78° C) surrounding the condensation chamber. For the two higher pressure experiments, a single liquid nitrogen trap and the surrounding cold bath were used.

Prior to an experiment, a flux shutter operated by a magnet outside of the vacuum system shielded the hot plate from metal vapor flux while the silver source was outgassing. When the residual gas pressure and the temperatures of the hot plate, cold plate, and silver source had become steady, the shutter was rotated, and silver was allowed to deposit on the hot plate. Only about 10 seconds was required to deposit a monolayer of silver on the hot plate for a flux of 1.3×10^{14} atoms/cm² sec. Hence the condensation on the hot plate was essentially silver on silver for an experiment of 1-hour duration.

The value of the condensation coefficient was determined by quantitative chemical analyses of the silver deposits on both the hot and cold plates. A calculated geometric factor related these data to the amounts of silver which would have been found on infinitely large parallel plates. The calculated geometric factor for our arrangement of plates was 0.29. The condensation coefficient was calculated from the formula

(1) α = wt. Ag hot plate/ wt. Ag hot plate + (wt. Ag cold plate/0.29).

TABLE I

Condensation coefficients for silver

Initial hot plate substrate*	Substrate temperature, °C	Reridual gas pressure, mm Hg	Silver flux atoms/cm² sec $\times 10^{-14}$	Silver supersaturation†	J_{Ag}/J_s‡	Wt. on hot plate, g$\times 10^6$	Wt. on cold plate (uncorrected), g$\times 10^6$	α	Estimated error in α	Maximum error in α
Glass	45	10^{-8}	1.3	$\sim 10^{21}$	1.2	2.82	2.74	0.99	±0.01	±0.02
Glass	205	4×10^{-6}	3.0	$\sim 10^{16}$	0.014	13.40	1.64	1.00	±0.01	±0.01
Gold	199	7×10^{-6}	4.3	$\sim 10^{16}$	0.014	19.00	2.69	1.00	±0.01	±0.01
Gold	202	6×10^{-10}	4.5	$\sim 10^{16}$	1600	20.40	2.48	1.00	±0.01	±0.01
Gold	440	3×10^{-9}	1.3	$\sim 10^{6}$	110	5.38	5.24	0.98	±0.01	±0.02

*Cold plate substrates were the same as the hot plate substrates except for the run at 205° C, for which a gold cold plate substrate was used.
†The supersaturation is the ratio of the actual silver flux to the equilibrium silver flux that would obtain at the substrate temperature.
‡J_{Ag}/J_s is the ratio of the flux of Ag atoms striking the hot plate to the flux of molecules of the residual gas striking the hot plate.

A description of the analytical methods is given by Sandell (1944). The small amounts of silver which were found on the cold plates were determined by using a Beckman D. U. spectrophotometer.

The results of this investigation are presented in Table I. In this table, the error in the hot plate weight determination is $\pm 2 \times 10^{-7}$ g. In a set of blank runs it was found that on the average both plates picked up 1.6×10^{-6} g of silver during bake out. This weight was subtracted from both hot and cold plates for the baked out tests at 45°, 202°, and 440° C and α values determined from the weights thus corrected. The estimated error includes only the uncertainties in the original weights of silver. The maximum error includes the error in original weights and the factor 1.6×10^{-6} g for the cases where this latter factor was subtracted from the raw data. Because of the necessity for the bake out each test was 1 week in duration. Hence insufficient tests could be performed to determine the reproducibility of the data.

In the experiments at 200° C the condensation coefficient was unity within experimental error. In all cases, the small amount of silver found on the cold plate is felt to represent silver re-evaporated from the hot plate in the initial portion of a run prior to or during nucleation of the first silver layers on the hot plate. Thus the apparent values of α for the tests at 45° C and 440° C are lower than the values at 200° C only because of the smaller weights deposited on the hot plate. The adsorption of residual gases at 199° C and 205° C did not decrease the value of the condensation coefficient from unity. Although the experimental conditions of these experiments were greatly different from those of Yang, Simnad, and Pound, our data are in agreement with the results of their investigation. Our data are in disagreement with the results of Chandra and Scott, and Frauenfelder. Explanations for the low condensation coefficients reported by these authors can only be speculative, but, as a result of our work, we would suggest that the seemingly re-evaporated atoms in the other investigations were from some source other than the growing silver substrate.

This work was sponsored by the U.S. Office of Naval Research, and is based on a portion of a thesis submitted by R. A. Rapp in partial fulfillment of the requirements for the degree of Doctor of Philosophy to the Graduate Faculty, Carnegie Institute of Technology.

Chandra, S. and Scott, G. D. 1958. Can. J. Phys. **36**, 1148.
Devienne, F. M. 1953. Vacuum, **3**, 392.
Frauenfelder, H. 1950. Helv. Phys. Acta, **23**, 347.
Sandell, E. B. 1944. Colorimetric determination of traces of metals, Vol. 3 (Interstate Publishers, Inc., New York), p. 395.
Yang, L., Simnad, M. T., and Pound, G. M. 1954. Acta Met. **2**, 470.

Received December 9, 1959.
Metals Research Laboratory,
Carnegie Institute of Technology,
Schenley Park,
Pittsburgh 13, Pa.

LETTERS TO THE EDITOR

Under this heading brief reports of important discoveries in physics may be published. These reports should not exceed 600 words and, for any issue, should be submitted not later than six weeks previous to the first day of the month of issue. No proof will be sent to the authors.

Frequency Measurement of Standard Frequency Transmissions[1,2]

Measurements are made at Ottawa, Canada, using N.R.C. caesium-beam frequency resonator as reference standard (with an assumed frequency of 9 192 631 770 c.p.s.). Frequency deviations from nominal are quoted in parts per 10^{10}. A negative sign indicates that the frequency is below nominal.

Date, February 1960	MSF, 60 kc/s	GBR, 16 kc/s		KK2XEI, 60 kc/s
		7½-hour average*	24-hour average	
1	−177	−173	−177	N.M.
2	−179	−177	−175	−89
3	−174	−175	−176	−88
4	−171	−174	−175	−89
5	N.M.	−173	−174	−88
6	−173	−179	−176	N.M.
7	−184	−179	−180	N.M.
8	−198	−178	−179	−87
9	N.M.	N.M.	N.M.	−96
10	−187	N.M.	N.M.	−97
11	−190	N.M.	N.M.	N.M.
12	−171	N.M.	N.M.	−105
13	N.M.	N.M.	N.M.	N.M.
14	−182	N.M.	N.M.	N.M.
15	−173	N.M.	N.M.	−94
16	N.M.	−178	N.M.	−101
17	−189	−175	−178	−92
18	−185	−182	−177	−93
19	−170	−182	−180	−94
20	−183	−178	−183	N.M.
21	−186	−183	−176	N.M.
22	−186	−183	−183	N.M.
23	−189	−179	−183	−96
24	−175	−184	−183	−94
25	N.M.	−183	−184	−96
26	N.M.	−186	−186	−36
27	−195	−194	−188	N.M.
28	−197	−193	−193	N.M.
29	N.M.	−190	−192	−45
Midmonthly mean	−183	−180	−180	−88
Midmonthly mean of WWV	−165			

NOTE: N.M. no measurement.
*Time of observations: 00.00 to 07.30 U.T.

RECEIVED MARCH 17, 1960.
S. N. KALRA
DIVISION OF APPLIED PHYSICS,
NATIONAL RESEARCH COUNCIL,
OTTAWA, CANADA.

[1]Issued as N.R.C. No. 5679.
[2]Cf. Kalra, S.N. 1959. Can. J. Phys. **37**, 1328.

THE PHYSICAL SOCIETY

MEMBERSHIP of the Society is open to all who are interested in Physics.

FELLOWS pay an Entrance Fee of £1 1*s*. ($3.15) and an Annual Subscription of £2 2*s*. ($6.00).

STUDENTS: A candidate for Studentship must be between the ages of 18 and 26, and pays an Annual Subscription of 5*s*. ($0.75).

MEETINGS: Fellows and Students may attend all Meetings of the Society including the annual Exhibition of Scientific Instruments and Apparatus.

PUBLICATIONS include the *Proceedings of the Physical Society*, published monthly, £12 12*s*. ($36.00) per annum, and *Reports on Progress in Physics*, published annually. Volume XXII, 1959, is now available (price £3 3*s*. ($9.45)). Members are entitled to receive any of the Publications at a reduced rate.

Further information can be obtained from:

THE PHYSICAL SOCIETY
1, LOWTHER GARDENS, PRINCE CONSORT ROAD
LONDON, S.W.7, ENGLAND

NOTES TO CONTRIBUTORS

Canadian Journal of Physics

MANUSCRIPTS

General.—Manuscripts, in English or French, should be typewritten, double spaced, on paper 8½×11 in. **The original and one copy are to be submitted.** Tables and captions for the figures should be placed at the end of the manuscript. Every sheet of the manuscript should be numbered. Style, arrangement, spelling, and abbreviations should conform to the usage of recent numbers of this journal. Greek letters or unusual signs should be written plainly or explained by marginal notes. Characters to be set in boldface type should be indicated by a wavy line below each character. Superscripts and subscripts must be legible and carefully placed. Manuscripts and illustrations should be carefully checked before they are submitted. Authors will be charged for unnecessary deviations from the usual format and for changes made in the proof that are considered excessive or unnecessary.

Abstract.—An abstract of not more than about 200 words, indicating the scope of the work and the principal findings, is required, except in Notes.

References.—References should be listed **alphabetically by authors' names,** unnumbered, and typed after the text. The form of the citations should be that used in current issues of this journal; in references to papers in periodicals, titles should not be given and only initial page numbers are required. The names of periodicals should be abbreviated in the form given in the most recent *List of Periodicals Abstracted by Chemical Abstracts.* All citations should be checked with the original articles and each one referred to in the text by the authors' names and the year.

Tables.—Tables should be numbered in roman numerals and each table referred to in the text. Titles should always be given but should be brief; column headings should be brief and descriptive matter in the tables confined to a minimum. Vertical rules should not be used. Numerous small tables should be avoided.

ILLUSTRATIONS

General.—All figures (including each figure of the plates) should be numbered consecutively from 1 up, in arabic numerals, and each figure referred to in the text. The author's name, title of the paper, and figure number should be written in the lower left corner of the sheets on which the illustrations appear. Captions should not be written on the illustrations.

Line drawings.—Drawings should be carefully made with India ink on white drawing paper, blue tracing linen, or co-ordinate paper ruled in blue only; any co-ordinate lines that are to appear in the reproduction should be ruled in black ink. Paper ruled in green, yellow, or red should not be used. All lines must be of sufficient thickness to reproduce well. Decimal points, periods, and stippled dots must be solid black circles large enough to be reduced if necessary. Letters and numerals should be neatly made, preferably with a stencil (**do NOT use typewriting**) and be of such size that the smallest lettering will be not less than 1 mm high when the figure is reduced to a suitable size. Many drawings are made too large; originals should not be more than 2 or 3 times the size of the desired reproduction. Whenever possible two or more drawings should be grouped to reduce the number of cuts required. In such groups of drawings, or in large drawings, full use of the space available should be made; the ratio of height to width should conform to that of a journal page (4¼×7½ in.), but allowance must be made for the captions. **The original drawings and one set of clear copies (e.g. small photographs) are to be submitted.**

Photographs.—Prints should be made on glossy paper, with strong contrasts. They should be trimmed so that essential features only are shown and mounted carefully, with rubber cement, on white cardboard, with no space between those arranged in groups. In mounting, full use of the space available should be made. **Photographs are to be submitted in duplicate; if they are to be reproduced in groups one set should be mounted, the duplicate set unmounted.**

REPRINTS

A total of 100 reprints of each paper, without covers, are supplied free. Additional reprints, with or without covers, may be purchased at the time of publication.

Charges for reprints are based on the number of printed pages, which may be calculated approximately by multiplying by 0.6 the number of manuscript pages (double-spaced typewritten sheets, 8½×11 in.) and including the space occupied by illustrations. Prices and instructions for ordering reprints are sent out with the galley proof.

Contents

E. H. McLaren and E. G. Murdock—The freezing points of high purity metals as precision temperature standards. VI. Thermal analyses on five samples of lead with purities greater than 99.999+% - - - - - - - - - 577

R. W. Smith—The white tin → grey tin transition in tin-mercury alloys - 588

P. A. Forsyth—On the geometry of radio reflections from aurora - - - 593

J. M. Daniels and K. E. Rieckhoff—Spin lattice relaxation in neodymium ethylsulphate at liquid helium temperatures - - - - - - - - - 604

R. D. Russell and Frank Kollar—Transistorized power supplies for a mass spectrometer - - - - - - - - - - - - - - - - - - 616

B. K. Bhattacharyya—Correlation studies of radio aurora magnetic and earth-current disturbances - - - - - - - - - - - - - - - 624

I. B. McDiarmid and D. C. Rose—High-altitude cosmic ray measurements at Fort Churchill - - - - - - - - - - - - - - - - - 638

Wm. McGowan and Larkin Kerwin—Some oxygen ions formed at high pressure in a mass spectrometer - - - - - - - - - - - - - - 642

R. E. Bell and M. H. Jørgensen—Mean lives of positrons in aluminum and the alkali metals - - - - - - - - - - - - - - - - - 652

R. Bourret—An hypothesis concerning turbulent diffusion - - - - - - 665

A. G. Shenstone—The third spectrum of cobalt (Co III) - - - - - - 677

Notes:

M. A. Clark and J. M. Robson—Asymmetries in the beta decay of polarized neutrons - 693

G. H. S. Jones and A. C. Hollis Hallett—The specific heat of crystalline quartz between 2° K and 4° K - - - - - - - - - - - - - - 696

T. D. Newton—On the axial symmetry of the Nilsson model nucleus - - 700

R. A. Rapp, J. P. Hirth, and G. M. Pound—On the condensation coefficient in the growth of silver from the vapor phase - - - - - - - - 709

Letters to the Editor:

S. N. Kalra—Frequency measurement of standard frequency transmissions 713

Printed in Canada *by* University of Toronto Press